FINITE ELEMENT MODELING OF SINGLE SHEAR FASTENER JOINT SPECIMENS: A COMPARISON OF SIMPLIFIED JOINT MODELING TECHNIQUES

A Thesis by

Chandresh Zinzuwadia

Bachelor of Science, Wichita State University, 2010

Submitted to the Department of Aerospace Engineering
and the faculty of the Graduate School of
Wichita State University
in partial fulfillment of
the requirements for the degree of
Master of Science

December 2014

© Copyright 2014 by Chandresh Zinzuwadia

All Rights Reserved

FINITE ELEMENT MODELING OF SINGLE SHEAR FASTENER JOINT SPECIMENS: A COMPARISON OF SIMPLIFIED JOINT MODELING TECHNIQUES

The following faculty members have examined the final copy of this thesis for form and content, and recommend that it be accepted in partial fulfillment of the requirement for the degree of Master of Science with a major in Aerospace Engineering.

_____
Dr. Suresh Keshavanarayana, Committee Chair

_____
Dr. Juan Felipe Acosta, Committee Member

_____
Dr. Krishna Krishnan, Committee Member

DEDICATION

To my beloved Family and Friends

ACKNOWLEDGEMENTS

I am grateful to have Dr. Suresh Keshavanarayana as my advisor for my course of graduate studies and for my thesis. His vast experience and knowledge, and continuous support and guidance have been instrumental to the completion of my thesis. I would also like to extend by deepest gratitude to Dr. Juan Felipe Acosta. He is a role model and has been a source of knowledge, motivation and progress both in my academic and professional life. Together they have been the key to the completion of my thesis.

I thank Dr. Gerardo Olivares for his support and enthusiasm. He has provided valuable input to the thesis and equipped me with all the tools and facilities required for the completion of my thesis. I also thank Dr. Krishna Krishnan for review of my thesis and for valuable comments and suggestions.

I would also like to thank my colleagues Kranthi Pingili, Nilesh Dhole, Luis Gomez and Adrian Gomez for their expertise and help with testing and use of finite element software LS-DYNA.

I thank the NIAR Computational Mechanics Lab for providing the necessary tools for completion of this thesis and the Federal Aviation Administration (FAA) for providing funding to this project.

ABSTRACT

Simplified finite element joint models were compared to a detailed three-dimensional model at coupon level to study their performance. Simplification of bolted joints is warranted by the element size limitation present when using explicit time integration methods for studying large scale finite element models. Two simplified models which are the rigid beam element bolt model with hole (configuration 1) and the mesh independent spotweld beam model (configuration 2), and extensions to these models which are the mesh independent spotweld beam with an elastic patch model (configuration 3) and the rigid beam element bolt model with no hole (configuration 4) were explored in this study. The load transfer, failure modes, stresses and strains, energy levels and bolt loads were evaluated for each simplified technique using a single shear lap joint specimen and compared to the detailed model. In addition, the effect of friction (0 to 0.4), preload (0 to 2300 N) and material rate sensitivity (loading rate, 20 in/s, 50 in/s and 100 in/s) was also studied.

In comparison to the detailed model, the load transfer was up to 10% higher for configuration 1, 9% higher to 17% lower for configuration 2, 11% higher to 8% lower for configuration 3 and 3% higher to 10% lower for configuration 4. The simplified models captured load transfer but due to the joining methods and absence of fastener hole (weak point in a joint), the joint was in fact stiffer and resulted in large load carrying capability. Higher loading rates did not affect the load transfer but increased the load carrying capacity of the detailed model by 26% and simplified model by 5%. Preload affected the load transfer in detailed model but not in simplified models. Friction affected the detailed model by 4% and the simplified model by 1%.

The detailed finite element model used for comparison was successfully validated using experimental test data and can be used as a baseline for further studies.

TABLE OF CONTENTS

Chapter Page

1. INTRODUCTION 1

1.1 Bolt Modeling in FEM and the Need for Simplified Bolt Models 1
1.2 Single Shear Lap Joint Performance 5
1.2.1 Load Transfer 5
1.3 Factors Affecting Bolted Joints 6
1.3.1 Installation Parameters 6
1.3.2 Loading Parameters 7
1.3.3 Stress Concentrations 8
1.3.4 Secondary Bending 9
1.3.5 Fastener Rotation/ Bending 9
1.3.6 Failure Modes 9
1.4 FE Analysis of Joints 10
1.4.1 Bolt Modeling Techniques for FEM 10
1.4.2 Research on FE Bolt Modeling 16
1.5 Research on Experimental Testing of Bolted Joints 20
1.6 Objectives 21
1.7 Methodology 22
1.7.1 Definition of Coupon used for this Study 22
1.7.2 Approach 24
1.8 Thesis Structure 25

2. TESTING 26

2.1 Clamping Force Measurements 26
2.1.1 Description of the Hi-Lok® Fastener System [39][40] 27
2.1.2 Test Article 28
2.1.3 Test Setup 30
2.1.4 Test Procedure 31
2.1.5 Clamping Force Test Results 33
2.2 Material Characterization Tests 34
2.2.1 Test Specimen Geometry 35
2.2.2 Test Setup and Procedure 35
2.2.3 Test Results 37
2.3 Load Transfer Tests 40
2.3.1 Test Article 41
2.3.2 Test Setup and Procedure 41
2.3.3 Load Transfer Test Results 46

3. FINITE ELEMENT MODELING – DESCRIPTION OF MODELS AND METHODS 49

3.1 FE Model Setup 49

TABLE OF CONTENTS (continued)

Chapter Page

3.1.1 Detailed FE Model 50
3.1.2 Simplified Technique – RBE Bolt Model 53
3.1.3 Simplified Technique – Mesh Independent Spotweld Beam Model 55
3.1.4 Simplified Technique – Mesh Independent Spotweld Beam with Elastic Patch Model 58
3.1.5 Simplified Technique – RBE Bolt Model with No Hole 59
3.2 Element Definitions 61
3.2.1 3D Solid Elements 62
3.2.2 2D Shell Elements 63
3.2.3 1D Beam Elements 63
3.3 Boundary Conditions and Constraints 64
3.4 Contact Modeling 66
3.4.1 *CONTACT_SPOTWELD 68
3.4.2 *CONTACT_TIED_NODES_TO_SURFACE_OFFSET 69
3.5 Preload Modeling 70
3.5.1 Preload in Solid Bolt Model 70
3.5.2 Preload in Beam Bolt Model 71
3.6 Material Modeling 72
3.6.1 Material Strain Rate Dependency 74
3.7 FE Simulation Parameters Studied 76
3.8 Calculations 76
3.8.1 Load Transfer 76
3.8.2 Load Transfer by Bolt and by Friction 77

4. FINITE ELEMENT MODELING - RESULTS 78

4.1 Detailed FE Bolt Model 78
4.1.1 Validation of FE Model and FE Modeling Methods 79
4.1.2 Kinematic Frames 81
4.1.3 Stress and Strain Profiles 82
4.1.4 Bolt Loads 83
4.1.5 Energy 86
4.2 Simplified FE Bolt Models 86
4.2.1 Configuration 1 – RBE Bolt Model 87
4.2.2 Configuration 2 – Mesh Independent Spotweld Beam 98
4.2.3 Configuration 3 – Mesh Independent Spotweld Beam with Patch 119
4.2.4 Configuration 4 – RBE Bolt Model No Hole 129
4.3 Parametric Analysis of Selected Simplified Model 140
4.3.1 Strain Rates Effect 141
4.3.2 Effect of Preload 146
4.3.3 Effect of Friction 151

TABLE OF CONTENTS (continued)

Chapter Page

5. SUMMARY AND CONCLUSIONS 153

5.1 Experimental Testing 153
5.2 Validation of FE Modeling Methods 154
5.3 Comparison of Detailed Joint Model to Simplified Joint Models 155
5.4 Effect of Strain Rates, Friction and Preload 161
5.5 Recommendations and Future Work 162
5.5.1 Future Work 164

REFERENCES 166

APPENDICES 172

A. HI-LOK FASTENER [40] 173
B. PRELOAD APPLICATION IN A SOLID BOLT 175
C. ENERGY FOR HIGH RATE STUDY 185

LIST OF FIGURES

Figure Page

1. Energy Distribution in 10-ft Fuselage Section with Full Cargo (t=0.3sec) [13] 3
2. Single lap joint connected with a bolt and the corresponding forces 5
3. Static Force Distribution in Detailed 3D Joint Model 6
4. Plate with circular hole [24] 8
5. Failure modes in single shear lap joint [10] 10
6. FE Bolt Model by Gadekar et al. [18] 15
7. FE Bolt Model by U. Sonnenschein [37] 16
8. Normalized Values of Outputs for Bolt Models [36] 20
9. Load Transfer Test Specimen 23
10. Main Part [15] 23
11. Load Transfer Part [15] 24
12. Hi-Lok® Fastener System [39] 28
13. Test Specimen 28
14. LWO-2 Load Cell Specifications [41] 29
15. Plate Dimensions with List of Diameters Tested 30
16. Test Setup for Preload measurement using Load Cell 31
17. Applied Load versus Voltage from Load Cell tested on MTS machine 32
18. Bolt Condition after Preload Test 33
19. Clamping Force versus Torque for Clearance Fit Hole 34
20. Clamping Force versus Torque for Interference Fit Hole 34
21. Geometry of Specimen used for Material Characterization 35
22. Schematic of Servo-Hydraulic Test System 36
23. Specimen Prepared with Strain Gage for Material Characterization 37

LIST OF FIGURES (continued)

Figure Page

24. Material Characterization Test Setup 37

25. Stress versus Strain (Recorded from Strain Gage) for Aluminum 2024-T3 Clad at 0.05 in/min 39

26. Stress versus Strain (Recorded from Extensometer) for Aluminum 2024-T3 Clad at 0.05 in/min 40

27. Material Characterization Specimens Post Failure 40

28. Anti-Buckling Fixture for Load Transfer Tests 41

29. Load Transfer Test Setup 42

30. High Rate Servo Hydraulic MTS Testing Machine at NIAR 44

31. Schematic of Tension Testing showing Slack inducer Mechanism [45] 45

32. Strain Gage Locations 46

33. Load Transfer Test Results: (a) Strain Gage 1 (b) Strain Gage 2 (c) Strain Gage 3 and (d) % Load Transfer 47

34. Failure on Specimen for the Load Transfer Test 48

35. Detailed 3D FE Model Setup 51

36. FE Discretization of Hi-Lok® Bolt and Nut 52

37. FE Discretization of (a) Doubler and (b) Anti-buckling Fixture 52

38. FE Discretization of Main Part and Load Transfer Part 53

39. Model Setup of RBE Bolt Model 54

40. Variations of RBE Bolt Models 55

41. FE Model Setup of Mesh Independent Spotweld Beam Bolt Model 56

42. Variations of Mesh Independent Spotweld Beam Bolt Model – Same mesh on Main Part and Transfer Part 56

43. Variations of Mesh Independent Spotweld Beam Bolt Model – Different mesh on Main Part and Transfer Part 57

LIST OF FIGURES (continued)

Figure Page

44. FE Model Setup of Mesh Independent Spotweld Beam with Elastic Patch Model 59

45. Variations of Mesh Independent Spotweld Beam with Elastic Patch 59

46. FE Model Setup of RBE Bolt Model with No Hole 60

47. Variations of RBE Bolt Model with No Hole 61

48. 3D Solid Elements [49] 62

49. 2D Shell Elements [49] 63

50. 1D Beam Element [49] 64

51. FE Model Boundary Conditions 65

52. Constraint on the Anti-Buckling Fixture 66

53. Components of *CONTACT_SPOTWELD [51] 68

54. Shape Functions [51] 68

55. Preload on Solid Bolt Model 71

56. Preload on Beam Bolt Model 72

57. Comparison of Engineering Stress-Strain to Effective Stress vs. Effective Plastic Strain for Clad Aluminum 2024-T3 at Quasi-static Rate 74

58. Clad Aluminum 2024-T3 Material Data for Quasistatic and Strain Rate 187.5/s 75

59. Cross Section Plane Locations on Single Shear Specimen 77

60. Cross Section Plane Location on Bolt 77

61. Static Force Distribution in Detailed FE Model 80

62. Detailed FE model (sim-solid) vs Load Transfer Test Results: (a) Axial Strain at Strain Gage 1 (b) Axial Strain at Strain Gage 2 (c) Axial Strain at Strain Gage 1 and (d) % LT 81

63. Stress Concentration in Plates with Hole 82

64. Kinematic Frames for Solid Model 82

Figure Page

65. Clamping Stresses Due to Preload Application on Detailed FE Joint Model 83

66. VonMises Stress on Main Part: Solid Model 83

67. Load Transferred by bolt on Solid Model (a) Load on transfer part, (b) Shear force on bolt and (c) %LT by bolt 85

68. Axial Force on Bolt Solid Model 85

69. Energy levels from Solid Model (a) Energy Balance (b) Internal Energy Distribution 86

70. Static Force Distribution in RBE Bolt Model 87

71. Load Transfer Comparison of Configuration 1 – RBE Bolt Model to Solid Bolt Model 89

72. Kinematic Frames Comparing Solid model to RBE Bolt Models 90

73. Stresses due to Preload Application (a) Sim-Config 1 (b) Sim-Config 1A and (c) Sim-Config 1B 91

74. VonMises Stress Comparison on Main Part (a) Sim-Config 1 (b) Sim-Config 1A and (c) Sim-Config 1B 92

75. Axial Strain vs Remote Stress for RBE Bolt Models (a) Strain gage 1 (b) Strain Gage 1 (close-up) (c) Strain Gage 2 and (d) Strain Gage 3 93

76. Comparison of Loads transferred by bolt (a) Load on Transfer Part (b) Shear Force on Bolt and (c) % LT by Bolt 95

77. Comparion of Axial Force on Bolt – Solid vs Simplified Config 1 96

78. Energy Distribution in Configuration 1B (a) Energy Balance (b) Internal Energy 97

79. Comparison of Strain Energy per Volume in 1 in. long patch (a) Main Part (b) Transfer Part 98

80. Comparison of Strain Energy in Bolt Shank versus Remote Stress – Configuration 1 98

81. Static Force Distribution in Mesh Independent Spotweld Beam Model 99

82. Load Transfer Comparison of Config 2 Mesh Independent Spotweld Beam - Similar mesh on Main Part and Transfer Part 100

LIST OF FIGURES (continued)

Figure Page

83. Load Transfer Comparison of Config 2 Mesh Independent Spotweld - Beam Mesh different on Main Part and Transfer part 101

84. Configurations chosen for Further Analysis 102

85. Nodes and Elements affected by Contact Point on Load Transfer Part 102

86. %LT Comparison for Config 2B, 2L, 2M and 2N 103

87. Out of Plane displacements (mm) on Load Transfer Part of Config 2B, 2L, 2M & 2N 104

88. Kinematic Frames Comparison of Mesh Independent Spotweld Beam Config 2-2E. 105

89. Kinematic Frames Comparison of Mesh Independent Spotweld Beam Config 2L-2O 106

90. Stresses due to Bolt Preload (a) Sim-Config 2, (b) Sim-Config 2A, (c) Sim-Config 2B and (d) Sim-Config 2E 107

91. Stresses due to Bolt Preload (a) Sim-Config 2K, (b) Sim-Config 2L, (c) Sim-Config 2M and (d) Sim-Config 2O 108

92. Von-Mises Stresses on Main Part at Initiation of Failure (a) Sim-Config 2, (b) Sim-Config 2A, (c) Sim-Config 2B and (d) Sim-Config 2E 109

93. Von-Mises Stresses on Main Part at Initiation of Failure (a) Sim-Config 2K, (b) Sim-Config 2L, (c) Sim-Config 2M and (d) Sim-Config 2O 110

94. Axial Strain vs Remote Stress for Mesh Independent Spotweld Models Config 2-2E (a) Strain gage 1 (b) Strain Gage 1 (close-up) (c) Strain Gage 2 and (d) Strain Gage 3 .. 111

95. Axial Strain vs Remote Stress for Mesh Independent Spotweld Models Config 2K-2O (a) Strain gage 1 (b) Strain Gage 1 (close-up) (c) Strain Gage 2 and (d) Strain Gage 3 112

96. Comparison of Loads transferred by bolt (a) Load on Transfer Part (b) Shear Force on Bolt and (c) % LT by Bolt 113

97. Comparison of Loads transferred by bolt (a) Load on Transfer Part (b) Shear Force on Bolt and (c) % LT by Bolt 114

98. Comparison of Axial Force on bolt (a) Config 2-2E (b) Config 2K-2O 115

99. Energy Distribution in Config 2B (a) Energy Balance (b) Internal Energy 116

LIST OF FIGURES (continued)

Figure Page

100. Energy at Low Remote Loads (a) Detailed Model (b) Simplified Model Config 2B. 117

101. Strain Energy per Volume in 1 in. long patch, 2 -2E (a) Main Part (b) Transfer Part 118

102. Strain Energy per Volume in 1 in. long patch, 2K-2O (a) Main Part (b) Transfer Part 118

103. Comparison of Bolt Internal Energy (a) Config 2-2E (b) Config 2K-2O 119

104. Free Body Diagram for Config 3 119

105. % Load Transfer Comparison 121

106. Kinematic Frames for Config 3 122

107. Stresses due to Preload (a) Config 3 (b) Config 3A and (c) Config 3B 123

108. Von Mises Stresses on Main Part (a) Config 3 (b) Config 3A and (c) Config 3B 124

109. Axial Strain vs Remote Stress for Mesh Independent Spotweld with Elastic Patch Model (a) Strain gage 1 (b) Strain Gage 1 (close-up) (c) Strain Gage 2 and (d) Strain Gage 3 125

110. Comparison of Loads transferred by bolt (a) Load on Transfer Part (b) Shear Force on Bolt and (c) % LT by Bolt 126

111. Comparison of Axial Force on bolt 127

112. Energy Distribution in Config 3B (a) Energy Balance (b) Internal Energy 128

113. Comparison of Strain Energy per Volume in 1 in. long patch (a) Main Part (b) Transfer Part 129

114. Comparison of Bolt Internal Energy 129

115. Free Body Diagram Config 4 130

116. % Load Transfer Comparison 132

117. Kinematic Frame Comparison for Config 4 133

118. Stresses due to Preload (a) Config 4 (b) Config 4A (c) Config 4E and (d) Config 4G 134

Figure Page

119. von Mises Stress on Main Part (a) Config 4 (b) Config 4A (c) Config 4E and (d) Config 4G 135

120. Axial Strain vs Remote Stress for RBE No Hole Model (a) Strain gage 1 (b) Strain Gage 1 (close-up) (c) Strain Gage 2 and (d) Strain Gage 3 136

121. Comparison of Loads transferred by bolt (a) Load on Transfer Part (b) Shear Force on Bolt and (c) % LT by Bolt 137

122. Comparison of Axial Force on bolt 138

123. Energy Distribution in Config 4G (a) Energy Balance (b) Internal Energy 139

124. Comparison of Strain Energy per Volume in 1 in. long patch (a) Main Part (b) Transfer Part 140

125. Comparison of Bolt Internal Energy 140

126. Strain Rate Measuring Locations on Detailed FE Model 141

127. Strain Rates on Main Part of Detailed FE Model (a) SG 1 (b) Hole Area 142

128. Comparion of High Loading Rate on Detailed FE Model (a) Strain at SG 1 (b) Strain at SG 2 (c) Strain at SG 3 and (d) % Load Transfer 143

129. Strain Rate Measuring location on Simplified FE Model 144

130. Strain Rates on Main Part of Detailed FE Model (a) SG 1 (b) Hole Area 144

131. Comparion of High Loading Rate on Simplified FE Model (a) Strain at SG 1 (b) Strain at SG 2 (c) Strain at SG 3 and (d) % Load Transfer 145

132. % Load Transfer by Bolt on Detailed FE Model 147

133. Comparison of Preload in Detailed FE Model (a) Strain at SG 1 (b) Strain at SG 2 (c) Strain at SG 3 and (d) % Load Transfer 147

134. Effect of Preload in Simplified FE Model Config 2B (a) Strain at SG 1 (b) Strain at SG 2 (c) Strain at SG 3 and (d) % Load Transfer 149

135. Effect of Preload in Simplified FE Model Config 2A (a) Strain at SG 1 (b) Strain at SG 2 (c) Strain at SG 3 and (d) % Load Transfer 150

136. % Load Transfer by Bolt for Simplified FE Model Config 2B 150

Figure Page

137. Axial force in Bolt for Simplified FE Model Config 2B 151

138. Effect of Friction of Detailed FE Model 152

139. Effect of Friction of Simplified FE model Config 2B 152

LIST OF TABLES

Table Page

1. Bolt Modeling Techniques used in FEM 11
2. Summary of Material Properties of Aluminum 2024-T3 Clad from Testing 38
3. Torque on Bolt Installation on Load Transfer Test Coupons 43
4. Mesh Quality Criteria 50
5. Mechanical Properties of Materials Used in FE Model 73
6. Energy Distribution for High Strain Rate – Detailed Model 143
7. Energy Distribution for High Strain Rate – Simplified Model 146
8. Element Size and Run Time Summary of Detailed and Selected Simplified FE Models 156
9. Comparison of Remote Stress at Failure and Energy after Failure 157
10. Comparison of % Load Transfer 159

CHAPTER 1

INTRODUCTION

Fastener joints are extensively used is structural assemblies, such as airplanes, and are exposed to several different types of loading throughout its life. Although considered as secondary elements, fasteners play a major role in defining the crashworthiness behavior of a structure. This study is performed to support finite element modeling (FEM) of large structural models where fasteners have to be idealized due to several restrictions on model refinement and size as discussed later in this chapter. LS DYNA [1], a powerful FEM tool capable of non-linear explicit dynamics is used for this study.

1.1 Bolt Modeling in FEM and the Need for Simplified Bolt Models

Aircraft structures contain several sub-components, such as engines, seats, radome and more, that require extensive destructive testing for certification. In addition, aircraft structure also requires certification for events such as bird strike, lightning strike and survivable crash scenarios. Physical testing of different subcomponents and events such as bird strike can be expensive since several variations exist for each case. With the recent improvements in computing technology, such large structural models and complex phenomena can be handled by analytical tools such as FEM [2][3][4]. Thus there is significant effort from industry and researchers around the globe to convince the authorities to accept certification by analysis (CBA) and hence minimize expensive physical testing [5][6][7].

CBA offers a rapid and less expensive way to evaluate design concepts and design changes while minimizing the requirement for physical testing to baseline models or worst case scenarios. An example of CBA is the AC 20-146 [9] developed by the FAA for aircraft seat certification. As per the AC 20-146, FE models can replace physical testing when: 1)

demonstrating compliance to standard test requirements for changes to a baseline seat design, 2) establishing the critical seat installation/configuration in preparation for dynamic testing.

Although powerful computing capabilities are available today for FEM, several shortcomings still exist when it comes to modeling elemental structures such as fasteners in large models [8]. Fasteners can be classified as either bolts or rivets, and although both have significant differences in appearance, structure, and installation methods, they both serve the same purpose. Large structural assemblies use fasteners as the primary joining entity to facilitate slip resistance and load transfer between joined parts [10][11][12]. Fastener joints are also common sites for fatigue crack initiations arising at the hole boundary due to stress concentrations resulting from bypass and bearing loads [12]. During a crash, a structure and the associated joints are required to fail in a controlled manner to absorb energy and alleviate the effects of the impact loading on the occupants. The energy is absorbed by the plastic collapse of thin-walled structures, and often they contain fastener joints. Hence, it is important to understand the behavior of fastener joints for improving crashworthiness characteristics. Researchers have conducted several crash tests and generated FE models of large structural assemblies 0[1][4][5], to evaluate the survivability of the occupants, but little has been reported in terms on joint behavior and fastener failures.

In a recent narrow body transport crashworthiness study conducted at the NIAR [13], it was reported that approximately 22000 fasteners were utilized in connecting a 10-ft fuselage section FE model and more than 10^5 fasteners for the full narrow body transport aircraft FE model. It was also noted from the study that for a 10-ft fuselage section with cargo, 14% of the residual internal energy was stored in the fasteners. As shown in Figure 1, the energy stored in the fasteners is more than the energy stored in frames or skin of the fuselage section.

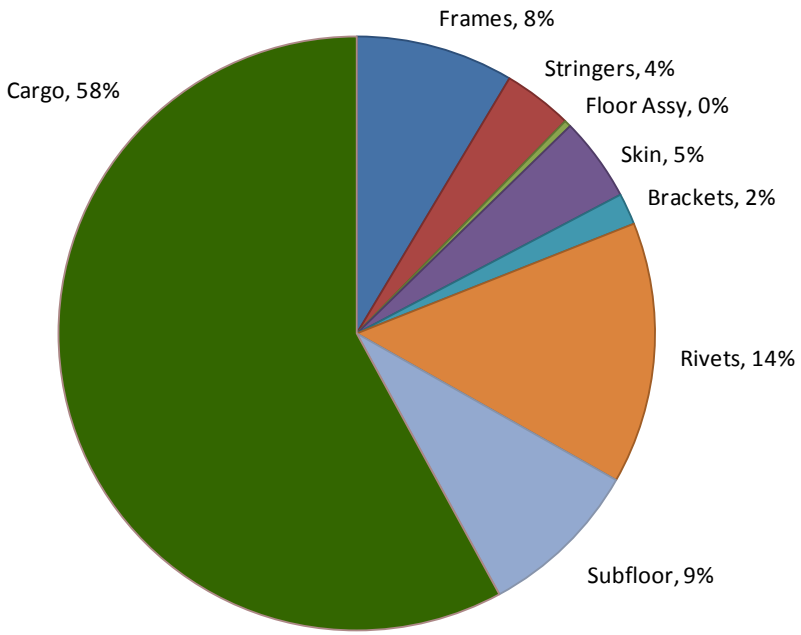

Figure 1. Energy Distribution in 10-ft Fuselage Section with Full Cargo (t=0.3sec) [13]

The study mentioned above was conducted using a powerful FEM tool, LS DYNA. The computational cost in LS DYNA is controlled by the size of the mesh, specifically the minimum element length [14]. In aircraft structures, the size of a rivet or bolt is considerably small compared to the full aircraft and when a FE model of such size is generated, it is not practical to accurately model the fasteners in order to control the computational cost. For example in LS-DYNA, the minimum time step (Δt) is calculated using the minimum element length (l) and the wave speed through the material (C) as shown in equation (1.1) [14]. This indicates that the smaller the element length, the smaller the time step and thus the higher the computational cost.

$$l = \Delta t \times C \text{ [14]} \tag{1.1}$$

In addition, modeling the fasteners in detail is a time consuming task as the discretization (meshing) of each component has to be controlled to ensure the mesh at fastener locations corresponds to the detailed fastener modeling method. Therefore, in the FE models of

the study mentioned here, holes for fastener joints were eliminated to control mesh size and the fasteners are idealized using beam elements.

The approximation of fasteners as beams can capture the simple mechanism of load transfer, in a bolted joint, to a certain extent. However, the underlying mechanisms of a joint are a lot more complex due to the presence of stress concentrations around the hole, clamp-up induced friction at faying surfaces, fastener rotations and end-fixity conditions on the fastener due to the presence of the head and nut [10][11][12][15]. In addition, at times crashworthiness analysis requires the consideration of strain rate effects which may also affect the behavior of the joint. Numerous studies, both experimental and analytical, have addressed these issues under fatigue and static loading conditions [15][16][17], but the consideration of high strain rates and dynamic loading is still open for exploration. To accurately simulate the effects of all mechanisms, a good quality finite element model capturing all geometrical features with 3D elements is necessary. While providing useful information, it has been shown [6][8] that such models are not practical when simulating large structural models. The idealization of fasteners with simplified techniques is the only practical solution that exists today for large FE models. With the advancement in CBA, increasing popularity of large models used for crashworthiness analysis, and the important role of fasteners in crash models, it is important to understand the limitations of simplified bolt modeling techniques under both static and dynamic loading conditions.

In a real world scenario, a fastener joint is likely to experience combined loading of tensile and shear loads. For detailed analysis, the focus of this study has been limited to shear loaded fastener joints, specifically bolts. In the following sections a summary of the literature

review detailing the factors affecting fastener joints, behavior of shear loaded joints and work done on FE analysis of joints and experimental testing of joints, is presented.

1.2 Single Shear Lap Joint Performance

When two plates are joined with a bolt, the bolt shank experiences pretension loads and thus opposing clamping forces are introduced on the plates by the bolt head and nut. When a longitudinal force is applied, shear forces develop in the fastener and bearing stresses and friction forces develop on the joined plates. Figure 2 shows the loads in a single shear lap joint [18].

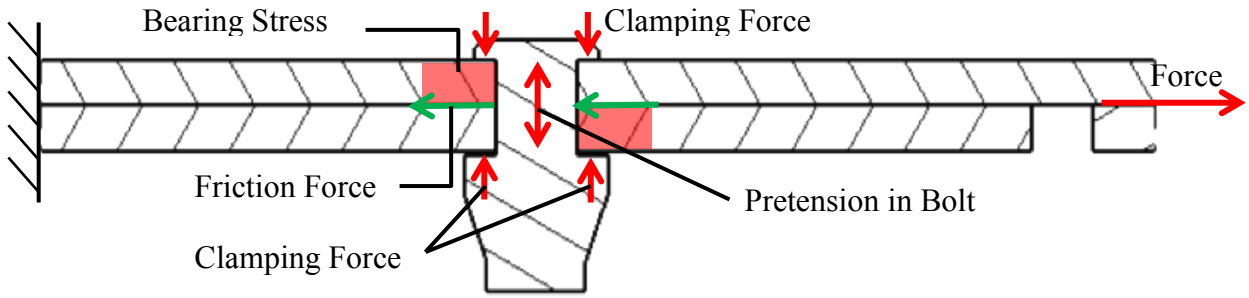

Figure 2. Single lap joint connected with a bolt and the corresponding forces

The primary objective of mechanically fastened joints is to facilitate load transfer [12]. In doing so many factors such as stress concentrations, secondary bending, fastener rotation and bending, clamp-up loads and friction affect the performance of the joint [12][15][25]. Many of these factors are also interrelated. A brief description of load transfer and factors that affect joint performance is provided in subsequent sections.

1.2.1 Load Transfer

In a single lap shear joint when a Force (F) is applied, due to the displacement compatibility between the main part and transfer part [12], F is divided into load transfer force ($F_{transfer)}$ and bypass force (F_{bypass}). F_{bypass} is the load that remains in the main part and $F_{transfer}$ is the load that is transmitted to the load transfer part. $F_{transfer}$ is generated from a bearing force

($F_{bearing}$) resulting from pressure exerted by the bolt shank on the hole surface and a friction force ($F_{friction}$) resulting from mating of the sheets. Due to bolt preload, friction effects are largely localized under the bolt head and nut surface where maximum clamping occurs.

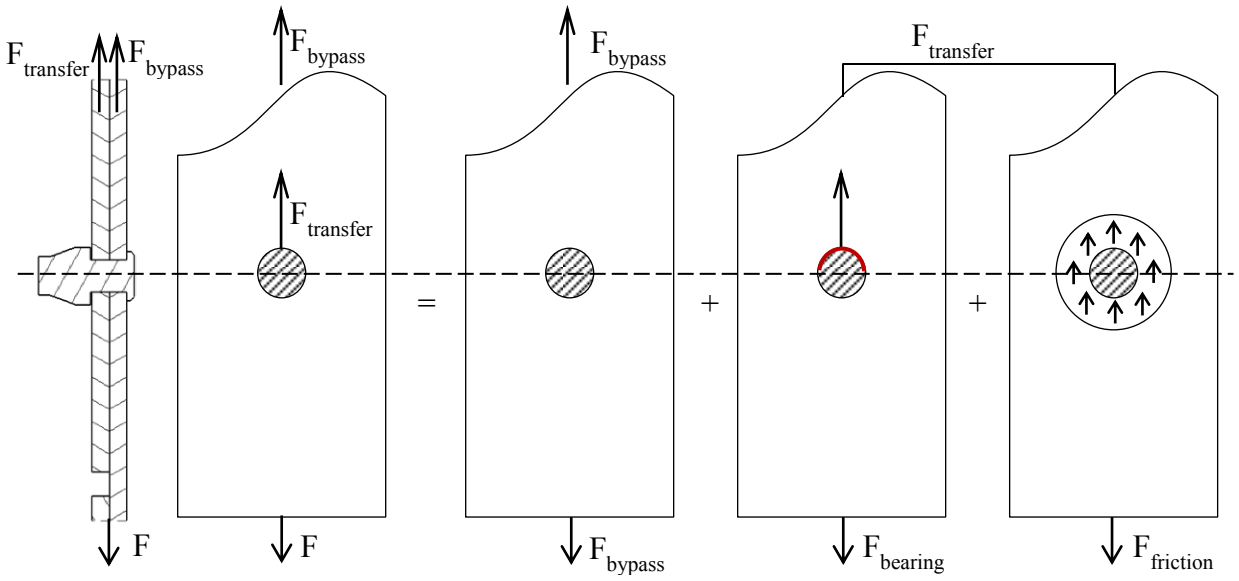

Figure 3. Static Force Distribution in Detailed 3D Joint Model

Figure 2 presents only a basic force distribution encountered by the specimen setup. It should be noted that load transfer is a rather complex phenomenon and factors such as the deformation of the hole, rotation of the joint, fastener bending, bolt clamp-up, hole preparation and friction level will affect the load transfer [15][19].

1.3 Factors Affecting Bolted Joints

The static, dynamic and fatigue performance of the joint under different loading conditions is affected by several parameters. Some of these parameters are discussed in this section.

1.3.1 Installation Parameters

The quality of the components that make up a joint, and the conditions induced on installation of these components have a significant effect on the performance on the joint [10]. In

addition, many of these installation conditions are interrelated. Some of the installation parameters are the surface condition and quality of the mating parts, fastener hole preparation (interference/ clearance), fastener type and finish, and clamping load.

The roughness of the surface dictates the friction on the faying surfaces of the joint. The strength of a shear joint is dependent on the friction of faying surfaces [10]. Initial residual stresses in the plates due to hole preparation or cold working also affect the strength of the joint.

Fastener hole preparation is also known to affect the strength and fatigue life of the joint. Interference fit fastener holes have shown improved fatigue life compared to clearance fit fastener holes [20].

Zeng L. and Haylock L. [21] have shown in their study that fastener coating and shear strength have an effect on the lap shear performance of the joint.

Clamping load is the load introduced to the fastened plates due to the tightening of the nut. Rivets have low clamping load compared to bolts, where it can be controlled. Studies have shown that higher clamping load increases the fatigue life of joints [22]. Higher clamping load decreases the stress concentrations around the fastener hole and increases the slip resistance [22].

1.3.2 Loading Parameters

A joint can be designed for pure shear loads, tensile loads or combined loading. In aircraft structures, combined and shear loading are common. The design of a joint can vary based on the principal load it experiences. The rate at which a joint is loaded also affects the strength of a joint. A study by Birch and Alves [23] shows that increasing pull velocity increased the mean load and the absorbed energy.

1.3.3 Stress Concentrations

Stress concentrations occur in loaded structures near section changes, that is holes, grooves, notches, sharp corners, cracks and others [24]. Due to the presence of bolt hole, stress concentrations are also expected in single lap shear joint specimen of this study. In mathematical terms, a stress concentration factor (K_T) is defined as the ratio of the maximum localized stress (σ_{max}) to the nominal stress in the member (σ_{nom}) as shown in equation (1.2) [24].

$$\sigma_{max} = K_T \times \sigma_{nom} \quad [24] \tag{1.2}$$

In a plate with a circular hole, as shown in Figure 4, it has been found that stress concentrations occur when $\theta = (1/2)\pi$ or $\theta = (3/2)\pi$ [24].

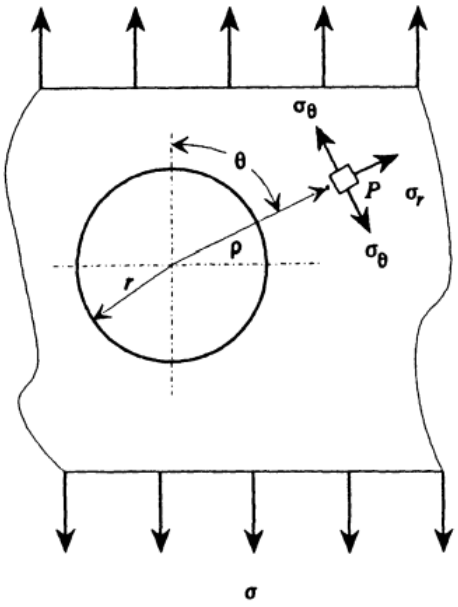

Figure 4. Plate with circular hole [24]

Studies have shown that tensile load passing through the hole, bearing loads and loads on the hole surface due to fastener bending and rotation contribute to the stress concentration factor of a fastener joint [16][17].

1.3.4 Secondary Bending

Secondary bending is a phenomena that occurs in single lap shear joints where the bolt and joint plates undergo bending due to loading eccentricities resulting in a non-uniform stress distribution through the thickness of the joined plates [19][25]. Experimentally, several ways of using strain gages to quantify secondary bending have been documented [15][26]. For this study, due to limited resources, these methods have not been employed.

Local load transfer, fastener diameter, plate thickness and clamping force are some of the parameters known to affect secondary bending [26][27][28][29]. Secondary bending is known to have a major effect on the fatigue life of single shear joints [30].

1.3.5 Fastener Rotation/ Bending

Fastener rotation/ bending or commonly known as fastener flexibility depends on the joint geometry, clamp up loads and the sheet and fastener materials [12]. It is an important parameter for determining the load transfer distribution in joints with multiple fastener rows [12]. Fastener rotation and bending are dependent on the end fixity provided by head and nut, clamp-up induced friction and material plasticity [19]. The joint compliance increases with excessive fastener rotation causing a decrease in load transfer.

1.3.6 Failure Modes

Failure modes depend on the strength of the joint members versus the strength of the bolt. It is also affected by the distance between the bolt and the edges [10]. In the case of single shear lap joint the following failure modes exist. These are also illustrated in Figure 5.

a. Tear out or marginal failure, where bolts are too close to an edge of the plate
b. Net section failure, where the plate is too thin, or soft compared to the bolt

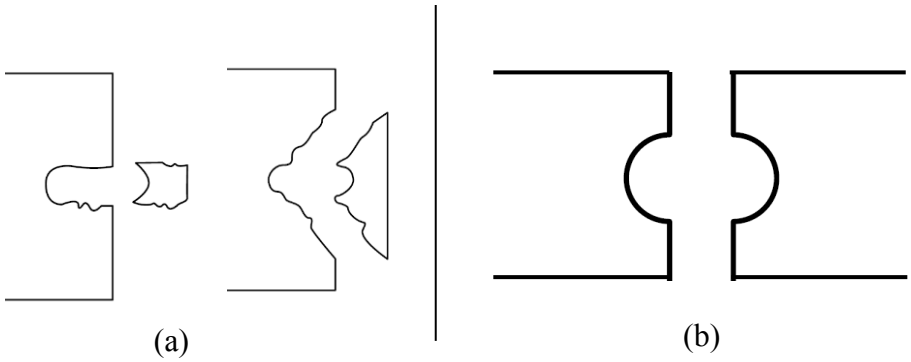

Figure 5. Failure modes in single shear lap joint [10]

1.4 FE Analysis of Joints

FEM is a numerical method often used to solve real-world problems that involve complicated physics, geometry and boundary conditions [31]. In terms of fastener joints, a great deal of research has already been conducted using FEM for detailed mechanical joint models [19][22][32] and simplified FE joint models [33][34][35][36], under various loading conditions. A summary of the different bolt modeling techniques and previous studies on bolted joints using FE analysis is presented in this section. Note that focus is directed to FE bolt modeling methods for the FEM tool LS DYNA.

1.4.1 Bolt Modeling Techniques for FEM

It has been shown that simplified bolt modeling techniques are necessary when using FEM for large structural models. A summary of some of the existing methods of modeling bolts for FE analysis are presented in Table 1 below. It should be noted that the methods shown in Table 1 are generic and show the basic entities required for the modeling technique. Several variations exist for some of the techniques and these variations can be found in the respective references.

TABLE 1
BOLT MODELING TECHNIQUES USED IN FEM

Technique	Illustration	Description	Advantages	Disadvantages	FE Modeling	REF
1. Solid Bolt Model	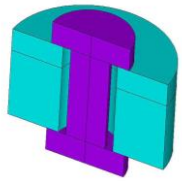	Head, Nut and bolt shank modeled with solid elements	- Provides best Accuracy - Allows transfer of tensile, bending and thermal loads -Complete Stress Distribution can be obtained - Allows Preload application - Failure can be modeled	- Requires contact definitions - Consists high number of elements - Not practical for large structural models	- Not practical for large structural models - Requires modeling of hole	[34]
2. Hybrid Bolt Model	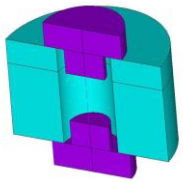	Head and Nut modeled with solid elements, Shank with beam element	- Allows transfer of tensile, bending and thermal loads -Complete Stress Distribution can be obtained - Allows Preload Application - Failure can be modeled	- Requires contact definitions - Consists high number of elements - Not practical for large structural models	- Not practical for large structural models - Requires modeling of hole	[34]
3. Spider Bolt Model	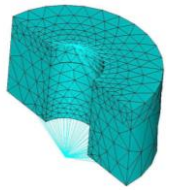	Head, Nut and bolt shank modeled with beam elements	- Allows transfer of tensile, bending and thermal loads - Requires small no. of elements and simplify process of extracting results - Failure can be modeled	- Requires contact definitions - Properties of beams have to be set to represent the head and nut moment of inertia and volume - Time consuming for large models	- Time consuming for large models - Requires modeling of hole	[34]

TABLE 1 (continued)

Technique	Illustration	Description	Advantages	Disadvantages	FE Modeling	REF
4. Coupled Bolt Model	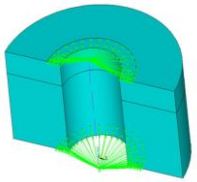	Only Bolt Shank modeled with beam element. DOF of surround nodes coupled with beam to represent head and nut. Many different Variations exist.	- One beam element to define bolt - Allows Preload application - Does not require contact definition - Can be modeled without hole - Failure can be modeled	- Only allows axial loads to be transfered through coupled nodes	- Time consuming setup for large models	[34]
5. Rigid Body Element (RBE) Bolt Model	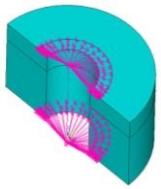	Only Bolt Shank modeled with beam element. Surrounding nodes of hole connected with beam using RBE to represent head and nut	- One beam element to define bolt - Allows Preload application - Does not require contact definition - Allows transfer of tensile, bending and thermal loads - Failure can be modeled	- Rigid elements do not account for stiffness	- Time consuming setup for large models - Requires modeling of hole	[34]
6. Rigid Body Element (RBE) Bolt Model with No hole	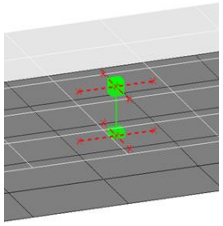	Only Bolt Shank modeled with beam element. Surrounding nodes connected with beam using RBE to represent head and nut - *Extension to model 5*	- One beam element to define bolt - Allows Preload application - Allows transfer of tensile, bending and thermal loads - Hole is not modeled - Failure can be modeled	- Requires contact definitions - Not practical for large structural models - Time consuming setup process - Several variations can exist with different results	- Time consuming setup	

TABLE 1 (continued)

Technique	Illustration	Description	Advantages	Disadvantages	FE Modeling	REF
7. Mesh Independent Spotweld Modeled with Beams	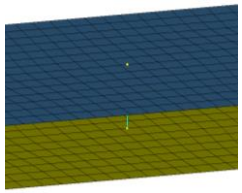	Head and Nut not modeled. Beam element represents bolt shank. Connected to parts using tied contact	- Allows transfer of tensile, bending and thermal loads - One beam element needed - Mesh independent therefore less preprocessing time - Failure can be modeled	- Requires contact definitions - Absence of fastener hole mitigates stress concentrations - Results Vary with position of beam relative to center of contact segment	- Practical for large models - Does not require modeling holes - Quick modeling	[35], [46]
8. Mesh Independent Spotweld Modeled with Beams and Elastic Patch to simulate hole	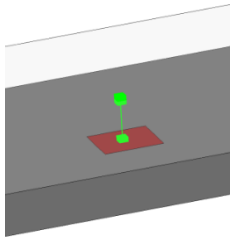	Head and Nut not modeled. Beam element represents bolt shank. Connected to parts using tied contact. A patch with elastic material properties modeled to simulate hole *Extension to model 7. Created in house.*	- One beam element to define bolt - Allows Preload application - Allows transfer of tensile, bending and thermal loads - Hole is not modeled - Failure can be modeled	- Requires contact definitions - Not practical for large structural models - Time consuming setup process - Several variations can exist with different results	- Time consuming setup as it is required to control mesh to ensure the element can simulate hole	

TABLE 1 (continued)

Technique	Illustration	Description	Advantages	Disadvantages	FE Modeling	REF
9. Massless Truss element Bolt	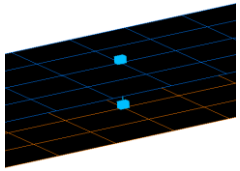	Head and Nut not modeled. Truss element represents bolt shank. Connected node to node. Type of a nodal constraint.	- One beam element to define bolt - Hole is not modeled - Does not require contact definition - Failure can be modeled	- Only transfers axial loads - Absence of fastener hole mitigates stress concentrations	-Time consuming setup process as mesh has to be controlled since connection is node to node	[35]
10. Massless Beam element Bolt	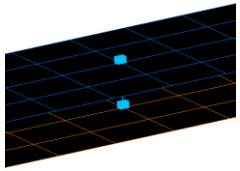	Head and Nut not modeled. Beam element represents bolt shank. Connected node to node. Type of a nodal constraint.	- One beam element to define bolt - Hole is not modeled - Does not require contact definition - Failure can be modeled	- Absence of fastener hole mitigates stress concentrations	-Time consuming setup process as mesh has to be controlled since connection is node to node	[35]
11. Shell Elements Bolt	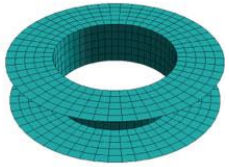	Shell elements used to model head nut and bolt shank	- Provides better Accuracy than beams - Allows transfer of tensile, bending and thermal loads - Allows Preload application - Failure can be modeled	- Requires contact definitions - Consists high number of elements - Not practical for large structural models	- Not practical for large structural models - Requires modeling of hole	[36]

In addition to the methods described in Table 1, researchers have developed more complex ways of representing a bolt using simplified elements. Gadekar et al. [18] developed and validated a bolt model, using LS DYNA, employing three different element types as shown in Figure 6. The bolt shank was modeled with a beam element and is connected to the periphery of the hole using contact springs. Shell element patches, representing the bolt head and nut, are modeled as rigid bodies. They found that under shear loading, stress patterns closely matched with realistic physical behavior for both configurations. The tensile and compressive behavior of the beam bolt model closely matched that of the solid model. The physical tensile test showed a softer response in the elastic region compared to simulation predictions. The frictional forces were also well predicted by the proposed models and they closely matched the physical test results. Gadekar et al [18] concluded that both approaches show good correlation with theoretical calculations and physical test results under shear and tensile loadings. The beam model is advantageous if failure forces for bolted joint are known under different loading conditions. Further detailed study is required using dynamic loading that occurs in crash applications.

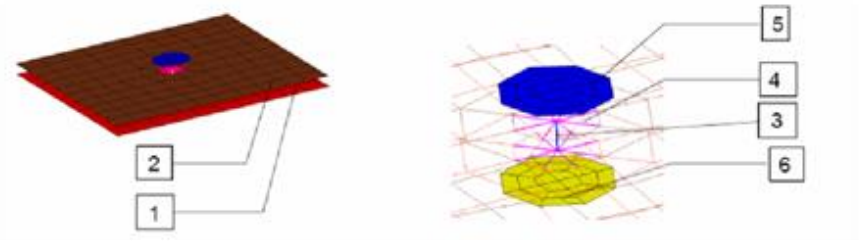

Component	Material	Element Type/ Thickness
1	MAT 24	SHELL, ELFORM16, 5mm
2		SHELL, ELFORM16, 5mm
3	MAT 100	BEAM, ELFORM9, 12mm
4	SDMAT6	CONTACT SPRING
5	MAT20 (CON1=0 CON2=7)	SHELL, ELFORM 2, 5mm
6	MAT20 (CON1=0 CON2=7)	SHELL, ELFORM 2, 5mm

Figure 6. FE Bolt Model by Gadekar et al. [18]

Figure 7 shows a bolt model generated by U. Sonnenschein [37]. This model consists of three different components. The bolt shank is modeled with a beam element and shell elements are used for the head and nut. Null beams are modeled around the periphery of the hole for contact purposes. The model showed good force characteristics and calculated bolt failure. Plastic deformations observed in the test were also reflected in the simulation.

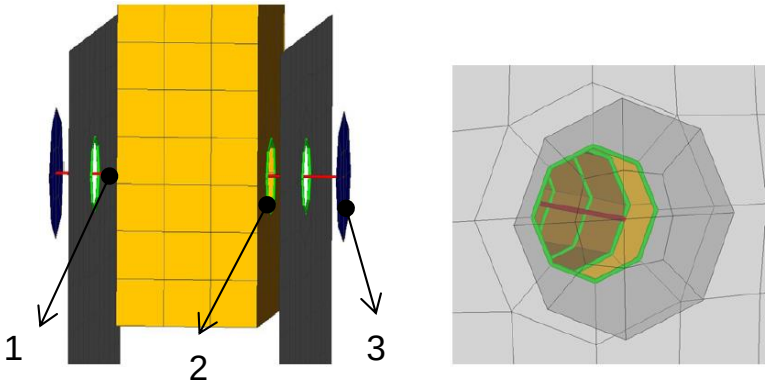

Component	Description
1	Elfrom 9, Spotweld Beams
2	Null beams for Contact
3	Shell Elements for Bolt Head and Nut

Figure 7. FE Bolt Model by U. Sonnenschein [37]

1.4.2 Research on FE Bolt Modeling

Factors that affect bolted joints and the mechanisms observed in bolted lap joints have been discussed in section 1.3 and 1.2. Some of these factors have been addressed in the following research conducted using FEM.

In the study performed by Ghods [19], a detailed three dimensional FE model of Hi-Lok® fastener joint system was used to investigate the effects of parameters such as clamp-up, friction coefficient, load transfer and plasticity on the structural response of the joint system. Medium, intermediate and low load transfer coupons were used to achieve different percentage

of load transfer. This study was conducted under quasi-static loading conditions with both tensile and compressive forces applied to the specimen by a cycle of loading and unloading.

Based on the study, Ghods concluded that friction coefficient, of all the parameters, had the most influence on load transfer, stress concentration factor and fastener rotation in all three geometries. In the presence of friction, the load transfer decreases non-linearly for both loading and unloading under both tensile and compressive conditions. It was also noted that load transfer is higher under loading than unloading for all scenarios. It was found that fastener rotation and stress concentration factors decrease with an increase in friction coefficient.

Ghods also found that fastener preload affects load transfer, stress concentration factors and fastener rotations only at low levels of applied loading. Load transfer increases with increasing fastener preload while the stress concentration factors decrease.

Material plasticity also had an influence on load transfer and stress concentrations. Elastic material models showed higher percentage of load transfer during tension compared to elastic-plastic material model. In addition, reduced stress concentration factors were observed in the presence of plasticity. Also, fastener rotations were slightly higher with plastic deformations.

Researchers have also looked into simplified bolt modeling techniques under both static and dynamic loading conditions. A summary of some of the key work and their conclusions are presented below.

Kang, Kim and Yoon [33] also conducted a comparison study between four of the bolt model types discussed in Table 1. They compared the solid model, spider model, coupled model and the no bolt model. They also used the bolt models for a structural analysis of a large marine diesel engine consisting of several parts. Pretension was applied to the four models by artificial coefficients of thermal expansion.

They used three different verification tests to compare the bolt models. First, they conducted a static experiment where a 10 N static load is applied at the free end of a lap joint and stresses and strains are measured at three locations on the surface of the specimen. Secondly, they conducted general loading tests where they subjected the bolt models to three different kinds of loading: two types of bending and shear. Finally they conducted a modal analysis to verify the bolt models for dynamic simulations.

The static test yielded similar overall stress distributions for all models but large discrepancies were observed in the region near the bolted joint. The general loading conditions yielded similar results as the static test. Major differences were seen around the hole for bending tests due to the absence of bolt head and nut on other models. For the case of shear loading, the results for the three models show very little variance since the analysis is largely dependent on the friction. From the modal analysis, natural frequencies for the different models were compared to experimental test. The three models yielded similar results to test and hence, are verified for dynamic analysis. From the test on the diesel engine, the solid bolt model predicted most accurately. From static analysis results, coupled bolt model and spider bolt model saved 62% and 49% of computational time and 21% and 19% of memory usage compared to solid bolt model.

Sonmez, Tanlak and Talay [36] studied detailed and simplified bolt models under impact loading. A plate was connected to two smaller, but thicker, sheets at each end by fasteners. This assembly was attached to a main frame. An impactor was dropped at the center of the plate to introduce the dynamic load. A full 3D model of the shell and plates was tested as the control and the plates were modeled with shell elements for comparing twelve different

simplified techniques. The following simplified techniques were studied (follows the order in Figure 8).

1) 3D bolt model with shell plates
2) Rigid shank with coupling constraints to represent head and nut
3) Deformable shell bolt
4) Rigid shell bolt
5) Timoshenko beam with coupling constraints
6) Timoshenko beam with coupling constraints without a hole
7) Tie constraint with hole
8) Tie constraint without hole
9) Cross coupling constraint with hole
10) Connector beam along the perimeter of the hole
11) Connector beam along the perimeter of the hole and the washers outer profile
12) Cross connector beams

The results of the study were then summarized in a table and normalized based on the detailed 3D model. Based on the results shown in Figure 8, Sonmez et al concluded that the simplified models resulted in computational time savings of 80% to 90% and among the simplified models, model 3 most accurately predicted the behavior of the structure for various loading cases and mesh densities. Note that model 3 consists of the fastener hole.

The model	Analysis time (s)	Plastic strain around the hole	von Mises stress around the hole	Plastic strain in the inner zone	von Mises stress in the inner zone	Central displacement
Full model	100.0	100.0	100.0	100.0	100.0	100.0
S.M. 1	73.4	86.2	100.4	174.9	106.6	97.9
S.M. 2	16.5	48.8	93.4	773.5	99.5	86.7
S.M. 3	13.0	94.8	102	154.2	108.2	99.9
S.M. 4	11.8	89.0	101.8	228.9	108.4	82.6
S.M. 5	15.2	47.6	91.8	745.2	101.9	86.8
S.M. 6	16.2	50.8	95.0	822.6	97.8	86.2
S.M. 7	14.3	56.8	96.6	1120.3	101.6	85.9
S.M. 8	15.8	62.8	97.0	1048.2	101.6	85.5
S.M. 9	14.5	47.0	96.6	1069.4	101.7	85.3
S.M. 10	15.4	933.1	274.7	157.0	102.2	98.7
S.M. 11	12.6	133.4	104.5	979.2	102.4	86.8
S.M. 12	14.5	894.1	125.0	272.3	99.5	95.0

Figure 8. Normalized Values of Outputs for Bolt Models [36]

1.5 **Research on Experimental Testing of Bolted Joints**

Physical testing is a key aspect for any structural development. It is used for validation, certification and documentation purposes. A variety of different tests have been performed on bolted joints including but not limited to fatigue, tension, compression, dynamic and torsion.

In an study performed by Keshavanarayana et al. [15], MLT specimens, same as the ones used for this study, were joined using Hi-Lok® and rivets and were subjected to cycle of tension and compression loading at a quasi-static loading rate. A clearance hole was used in the specimen with the Hi-Lok® fastener. The load transfer was measured for the tension compression cycle and the specimen with the Hi-Lok® fastener experienced an initial drop in the %LT after which the %LT stayed at slightly below 40% for the rest of the tensile loading phase.

Dynamic failure of structural joint system has been heavily studied by Birch and Alves [23]. Several single lap bolted specimens were tested at different loading rates. The specimens were divided into two sets: set-A specimens were connected using a bolt which had 3mm socket diameter and 5.3mm head diameter and no washer was used, while set-B specimens were connected using a 5mm diameter hexagon headed bolts with 9.7mm diameter steel washers. A high speed servo-hydraulic tensile test machine was used to test the specimens. The plates were constructed from cold rolled mild steel and were 1mm thick. In-plane shear load was introduced

and was measured using high frequency response piezoelectric load cell placed as close as possible to grip. Displacements were measured using LVDT transducer located on the hydraulic ram of the test machine.

Similar failure patterns for both set of specimens were observed. For set A, the head of the bolt was always pulled through the parent material. No change in failure mode with respect to pull velocity was observed. There was little bending across the lateral axis of the joined plates. The absorbed energy and mean loads increased significantly with respect to pull velocity. This could be attributed to material strain rate sensitivity.

1.6 **Objectives**

The understanding of the contributions and mechanisms of bolts is crucial to predict the behavior of a structure and to design of an efficient structure. For large FE models simplification of the fastener joint is necessary for cost effectiveness, due to the presence of thousands of such joints. In support to the CBA efforts, the following objectives are set for this study.

1. To generate experimental test data for single lap shear joints subjected to tensile loading and to quantify the load transfer.

2. To build a detailed FE model using 3D elements capable of capturing the effects of clamping force and friction accurately and to validate it against experimental testing results and to serve as baseline for comparison with simplified FE bolt models.

3. To investigate simplified FE bolt modeling methods in single lap shear joints subjected to tensile loading and to highlight their limitations and performance.

4. To study the effects of high rate loading on the behavior of single lap shear joints for both the detailed and simplified models.

1.7 Methodology

A summary of the steps taken for this study are summarized in this section along with the details of the component (specimen) used for the study.

1.7.1 Definition of Coupon used for this Study

The study is performed with a half dog-bone type single lap shear assembly as shown in Figure 9. The assembly consists of two parts connected using a Hi-Lok® fastener. A doubler was used to eliminate any eccentricity in loading the specimen. An illustration of the assembled specimen and the terminology used is shown in Figure 9. The specimen assembly used in this study has already been used by previous researchers [15][19].

The fastener used is a Hi-Lok® system with a HL-18 steel pin and a HL-70 aluminum nut. Details of the pin and the nut can be found in APPENDIX A. Hi-Lok® fastener system is widely used in aircraft structures [12].

The main part that carries the applied load has a full dog bone shape. The main part is gripped at the larger tab and a constant displacement is applied. Once the load is transferred, the remaining bypass load is carried by the bypass side, that is, the side after the fastener. The main part is constructed from Aluminum 2024-T3 Clad and its dimensions are detailed in Figure 10.

The load transfer part, sketched in Figure 11, has the shape of a half dog bone. Load is transferred from the main part to this part through the fastener and through friction between faying surfaces. The load transfer part and the main part are gripped and constrained at the bypass end. This part is constructed from Aluminum 2024-T3 Clad.

Note that this structural assembly consists of a bolt with a steel pin (Young's Modulus = approx. 200,000 MPa) connecting aluminum parts (Young's Modulus = approx. 70,000 MPa).

Thus the stiffness of the fastener is much greater than the stiffness of the plates it connects and therefore fastener failure will not occur.

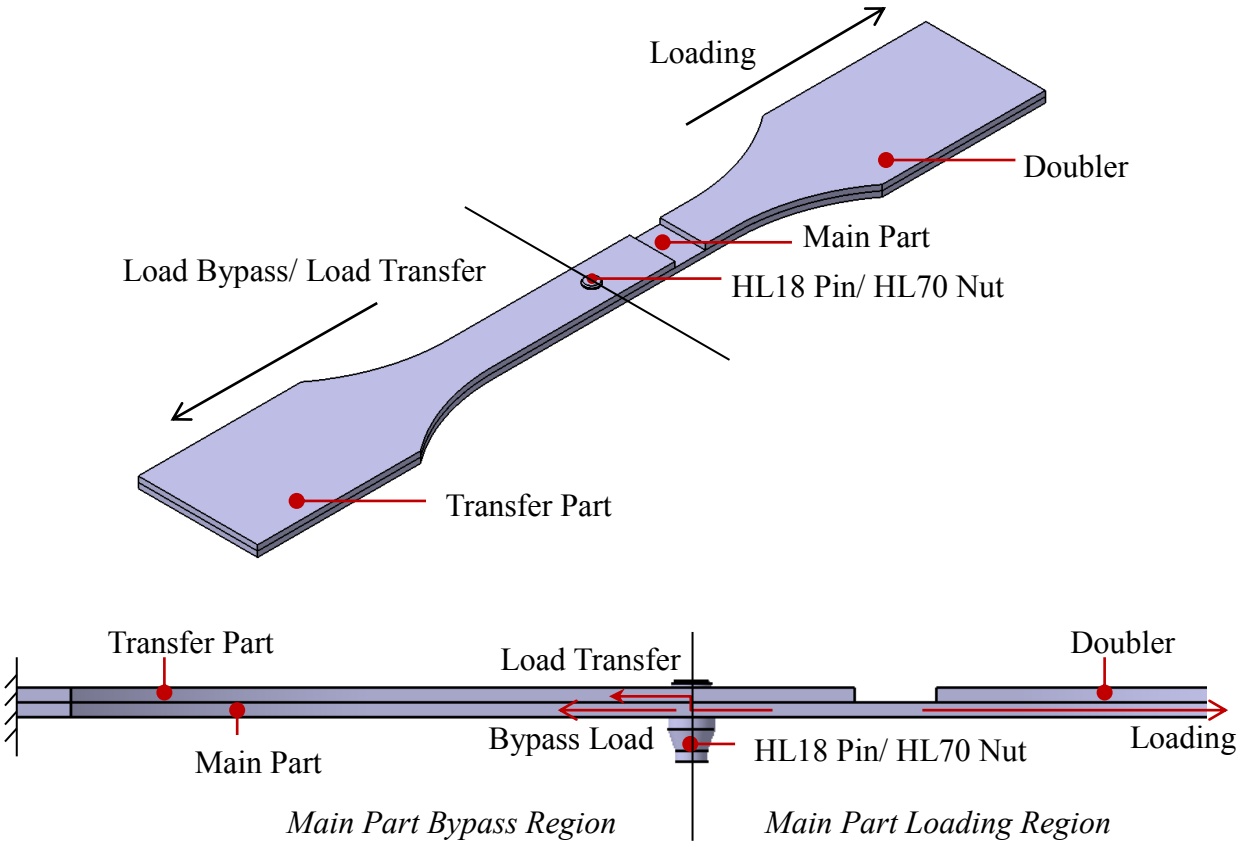

Figure 9. Load Transfer Test Specimen

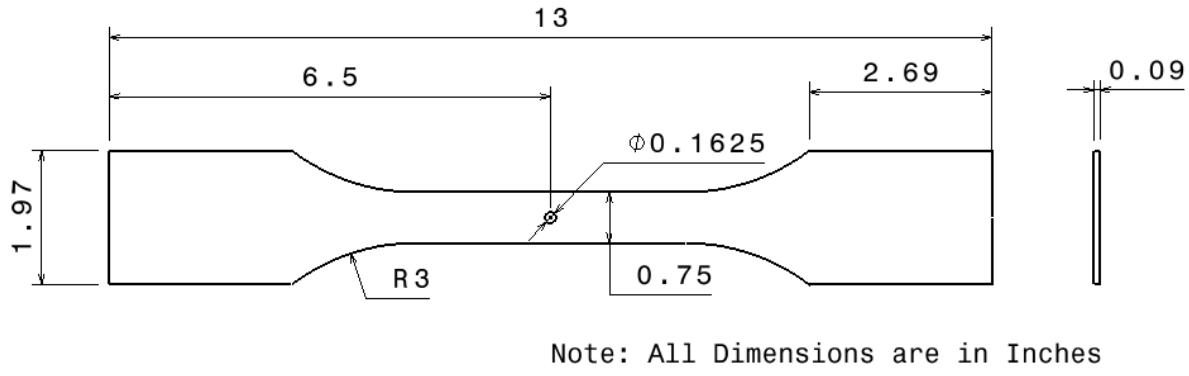

Figure 10. Main Part [15]

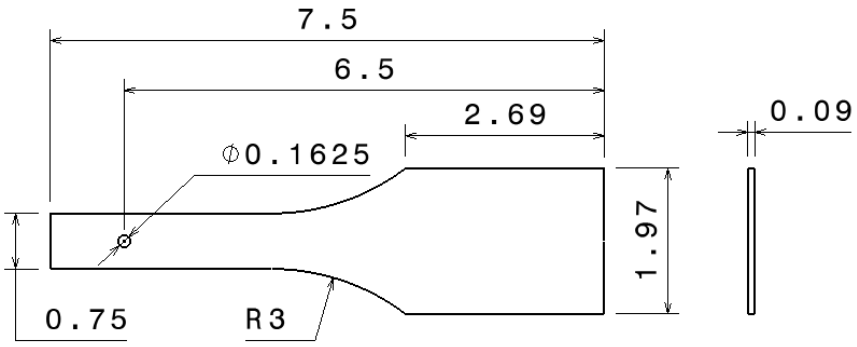

Figure 11. Load Transfer Part [15]

1.7.2 Approach

Several tests are performed on single lap Hi-Lok® fastener joint system. The repeatability of the tests is documented to verify the test results. A three dimensional finite element is modeled and validated against the test results.

Since this study is aimed to support crashworthiness of large structural models, several simplified FE bolt models are selected based on their applicability to such models. Simulations of large structural FE models require efficient element formulations with preferably large element length to control the time step. Thus simplified models chosen for comparison are models where the fastener hole is not accounted for. The fastener hole cannot be accurately captured with such large elements. In addition, such models generally consist of several parts connected together by a single bolt. Thus a simplified model capable of connecting parts irrespective of the mesh of individual components is desired. Without such capability, preprocessing of the model itself would become very costly. Keeping this in mind, a few simplified FE bolt models are compared to the validated solid model. The limitations and use of the simplified techniques are also discussed. A selected simplified technique is then subjected to

a preload and friction parametric study. Further an analysis of the selected model is performed at high loading rates using rate sensitive material properties.

Finally the results are discussed, conclusions and recommendations are drawn, and comments are made for future work.

1.8 **Thesis Structure**

The main focus of the thesis is to study simplified bolt modeling techniques for crash simulations and large FE models and to understand the effect of strain rate sensitivity, preload, friction and mesh on the simplified joint models.

Chapter 2 discusses the experimental tests performed to support this study. Three tests were performed: test to quantify preload, material characterization tests and the load transfer test (single lap shear). The apparatus, methodology, and the testing results are documented in this section.

Chapter 3 details the development of the finite element model of the system. The FE mesh, contacts, material cards and boundary conditions are detailed in this chapter.

Chapter 4 details the validation of the detailed finite element model and the comparison of simplified joint models to the detailed joint model. In addition the effect of material strain rate sensitivity, friction and preload on both detailed and simplified joint model is also presented.

Chapter 5 consists of a summary of the results from the study and conclusions drawn from this study. Recommendations for future work are also detailed in this chapter. References are then listed and other information sources and detailed results from the simulations have been presented in the Appendices.

CHAPTER 2

TESTING

Experimental testing is a key part of research used for studying the physical behavior of a system or a component. It can be used for generating mechanical properties of materials, for studying the performance of a component or a system, or to study the interaction and contribution of each component within a system. It is also used for verification and conformity of finite element models. For this study, three different experimental tests were conducted as detailed below. Test setup details, procedure and results for each test has been presented in the sections that follow.

1. Tests were conducted to quantify the clamping load introduced on the specimen when the Hi-Lok® fastener is installed. This was necessary for accurate FE models.

2. Tests were conducted to quantify the material properties for the specimens used in the load transfer tests. The material data is crucial for FE models. FE models perform only as good as the data that is input in the model.

3. Tests were conducted to study the load transfer characteristics of a one half dog bone single lap joint specimen. The results from the detailed FE model will be compared to this test data and further the limitations and performance of the simplified bolt modeling techniques will be evaluated based on the detailed FE model.

2.1 Clamping Force Measurements

This test was a preface to the tensile single shear joint tests. The test was designed to measure the preload for a Hi-Lok® Fastener system and evaluate the variability for a set of fasteners. Ghods [19] found that fastener preload affects load transfer, stress concentration factors and fastener rotations only at low levels of applied loading. He found that load transfer

increases with increasing fastener preload while the stress concentration factors decrease. Therefore, it is necessary to quantify the bolt preload for accurate finite element models.

Chakherlou, Vand and Oskouei [38] measured the clamping force of a bolted connection by placing a strain gage mounted steel bushing between the plate and nut. This was possible due to the large size of the bolt. The fastener type used for this study is a HL 18 pin and a HL 70 collar. The nominal diameter of the pin is 0.1625 in and due to such small size the preload could not be directly measured at the fastener shank using a strain gage or another instrument. In this experiment, the preload was calculated based on the clamping force of the fastener. The clamping force was measured using a washer load cell (LWO-2) that was placed in between two aluminum plates of the same thickness and material as the plates used for the load transfer test. The HL-18 fastener was inserted through the plates and the load cell and the assembly was clamped with a HL 70 nut. The clamping force, measured by the load cell when the fastener installation was complete, was recorded along with the torque.

The effect of fastener hole preparation was also studied through this test. Fastener holes can be machined for an interference fit or a clearance fit. Therefore, plates with these two configurations were used for the experiments.

2.1.1 Description of the Hi-Lok® Fastener System [39][40]

A Hi-Lok® fastener consists of a Pin and a Collar as shown in Figure 12 below. Hi-Lok®s are designed with a predefined range of preload, and to achieve that, the collar consists a hex nut that shears off at a certain range of torque. The process of fastening involves the use of a hex key that is inserted into the pin which prohibits the pin from spinning. The torque on the nut is applied while the pin is held using the hex key. Therefore this process requires the use of a box end head for the torque wrench. It is important to ensure that the pin does not spin so that all the

torque applied is used for fastening and not to overcome friction between the pin and the plates. An illustration of the Hi-Lok® fastening system is shown in Figure 12.

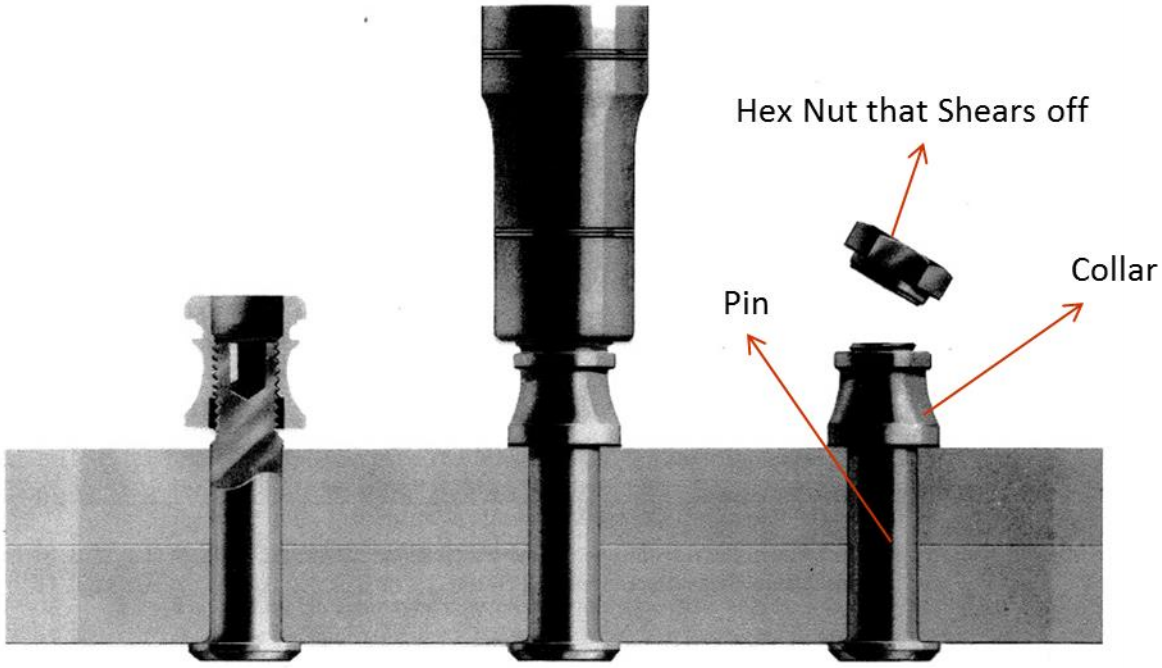

Figure 12. Hi-Lok® Fastener System [39]

2.1.2 Test Article

The test article assembly consisted of two aluminum plates, HL18 pin, HL 70 nut and a LWO-2 load cell [41]. The load cell was placed in between two plates and the pin and nut were used to clamp the plates and the load cell together. The specimen assembly is shown in Figure 13 below.

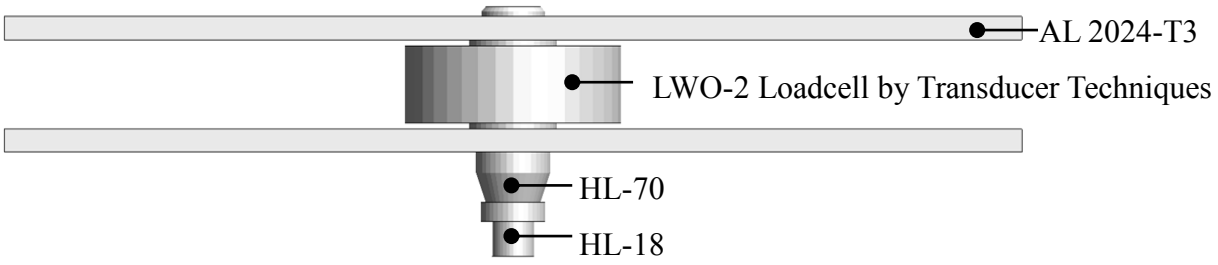

Figure 13. Test Specimen

2.1.2.1 LWO-2 Load Cell

The LWO series load cells are washer shaped, strain gage based load cells most commonly used in fastener testing and through hole load applications. The load cell LWO-2 used for this test is manufactured by transducer techniques [41] and has a load measuring range of up to 2400 lbs. Figure 14 below shows the geometry and specifications of the load cell.

Rated Output (R.O.):	2 mV/V nominal
Nonlinearity:	2.0% of R.O.
Hysteresis:	2.0% of R.O
Nonrepeatability:	1.0% of R.O.
Zero Balance:	1.0% of R.O.
Compensated Temp. Range:	60° to 160°F
Safe Temp. Range:	-65° to 200°F
Temp. Effect on Output:	0.005% of Load/°F
Temp. Effect on Zero:	0.01% of R.O./°F
Terminal Resistance:	350 ohms nominal
Excitation Voltage:	10 VDC
Safe Overload:	150% of R.O.
Deflection Inches:	0.001 @ R.O.

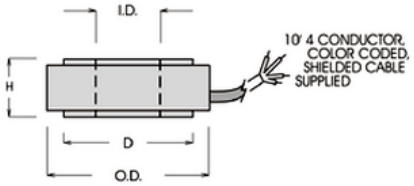

DIMENSIONS (INCHES)

MODEL	CAPACITY LBS.	O.D. DIA.	I.D. DIA.	D	H
LWO-2	2,400	.85	.192	.345	.350

Figure 14. LWO-2 Load Cell Specifications [41]

2.1.2.2 Plates

The plates were manufactured from the same material used for the single shear test coupons, which is clad Aluminum 2024-T3. Figure 15 below shows the dimensions of the plates. To study the effects of hole preparation the plates were prepared with two different hole diameters. One set was manufactured with hole diameter less than the nominal fastener diameter to obtain an interference fit and the other set was manufactured with diameter equal to the maximum fastener diameter for a clearance fit. The requirements specified in the Hi-Lok® fasteneing guide [39] were used to machine the interference fit. Each plate contained five holes and three sets of plates were used for each hole diameter configuration.

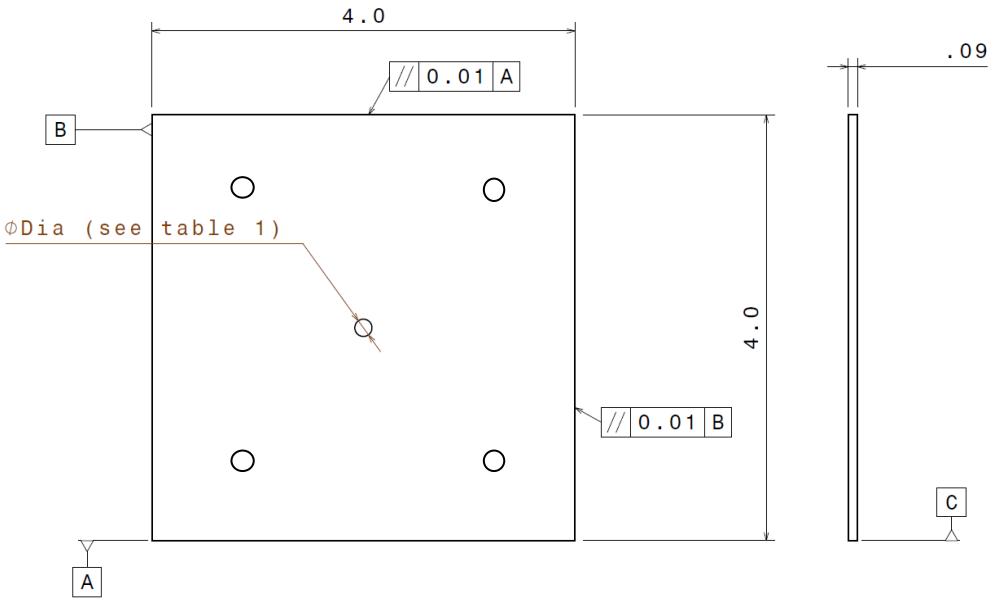

TABLE 1: Different Diameters Required

Specimen Type	Dia (Diameter)	Quantity
1	0.1610 + 0.001	6
2	0.1625 + 0.001	6

Note: All dimensions are in inches

Figure 15. Plate Dimensions with List of Diameters Tested

2.1.2.3 Hi-Lok® Fastener

The Hi-Lok® fastener consists of two parts, the pin and the collar. The fastener used for this test was the same fastener configuration as the load transfer tests. The fastener consisted of a HL 18 pin and a HL 70 nut (APPENDIX A).

2.1.3 Test Setup

To perform the test, the specimen assembly described above was set up as shown in Figure 16 below. The equipment used for the experiment was a vise, TMO-2 signal conditioner by trasducer techniques, voltmeter and a Tohnichi digital torque wrench [42]. The vise was used to clamp the specimen assembly. The load cell was connected to a signal conditioner and the voltage output from the signal conditioner was read by a voltmeter. The digital torque wrench

was used to torque the nut and the maximum torque reading from the wrench, the torque at which the hex portion of the nut sheared off, was recorded.

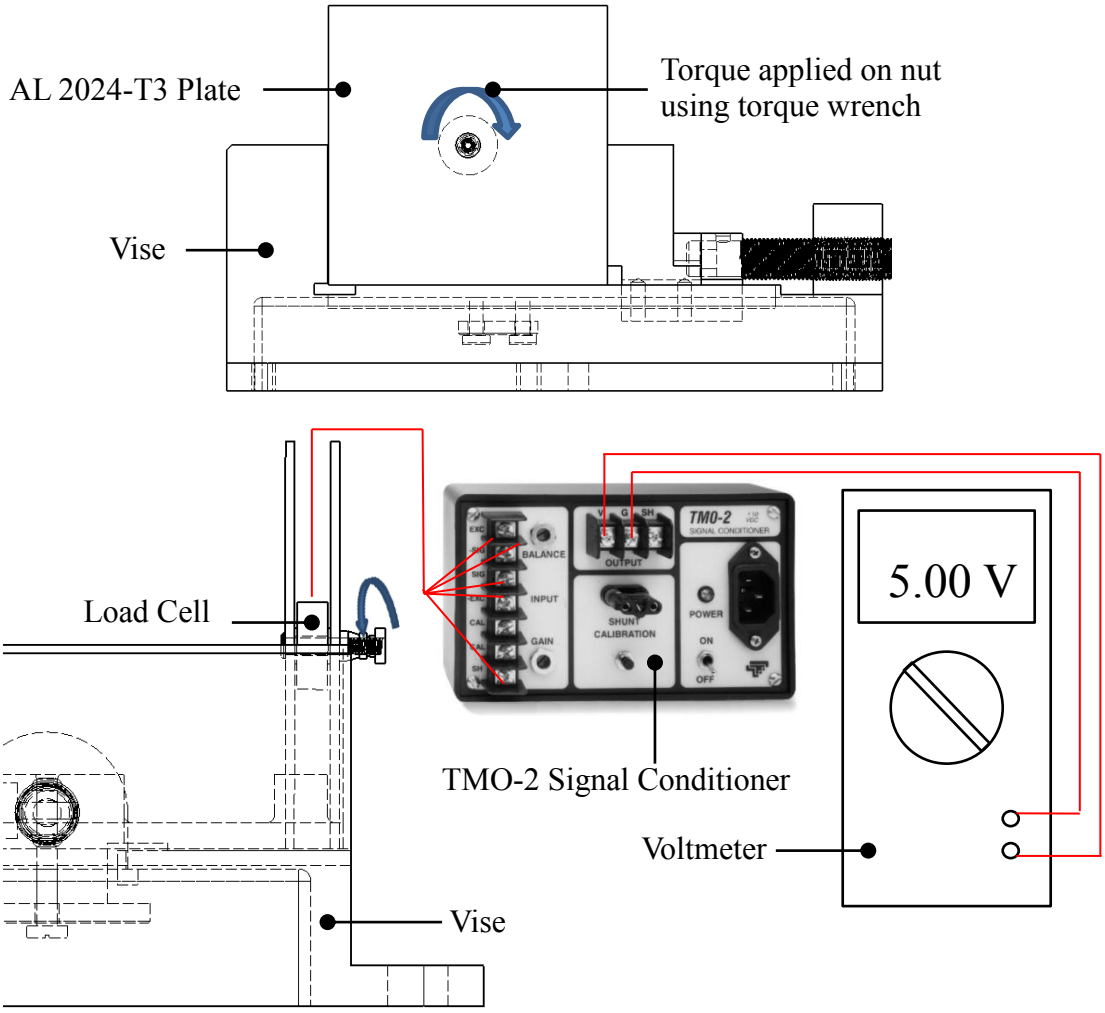

Figure 16. Test Setup for Preload measurement using Load Cell

2.1.4 Test Procedure

Before setting up the test, the specimen dimensions were noted. The specimen assembly described in section 2.1.2 was then clamped using a vise. The load cell was connected to a signal conditioner which was connected to a voltmeter for voltage output. The voltage corresponds to a clamping load. The nut was then tightened, using a torque wrench, until the hex portion of the nut sheared off as described in section 2.1.1. The torque at nut shear off and the corresponding

voltage from the voltmeter were recorded. The clamping force was then determined by look up on the voltage versus load plot which was generated as described below.

2.1.4.1 Load Cell Verification and Signal Conditioner Calibration

Prior to using the load cell, a compressive load was applied on the load cell using a 5 kip MTS test machine to verify the load cell readings and to set the gain on the signal conditioner. The load cell was connected to the signal conditioner and a volt meter and the maximum limit load of the load cell (2400 lbf) was applied using the MTS machine [43]. The gain on the signal conditioner was adjusted until the voltmeter read 10 V. After setting the gain a load versus voltage plot, shown in Figure 17, was generated by performing several loading cycles on the load cell. This plot was used to generate an equation (2.1) to convert the voltage recorded from the load cell to load value, as shown in the test set-up in section 2.1.3.

$$V = 0.000927F_{applied} + 0.168241 \tag{2.1}$$

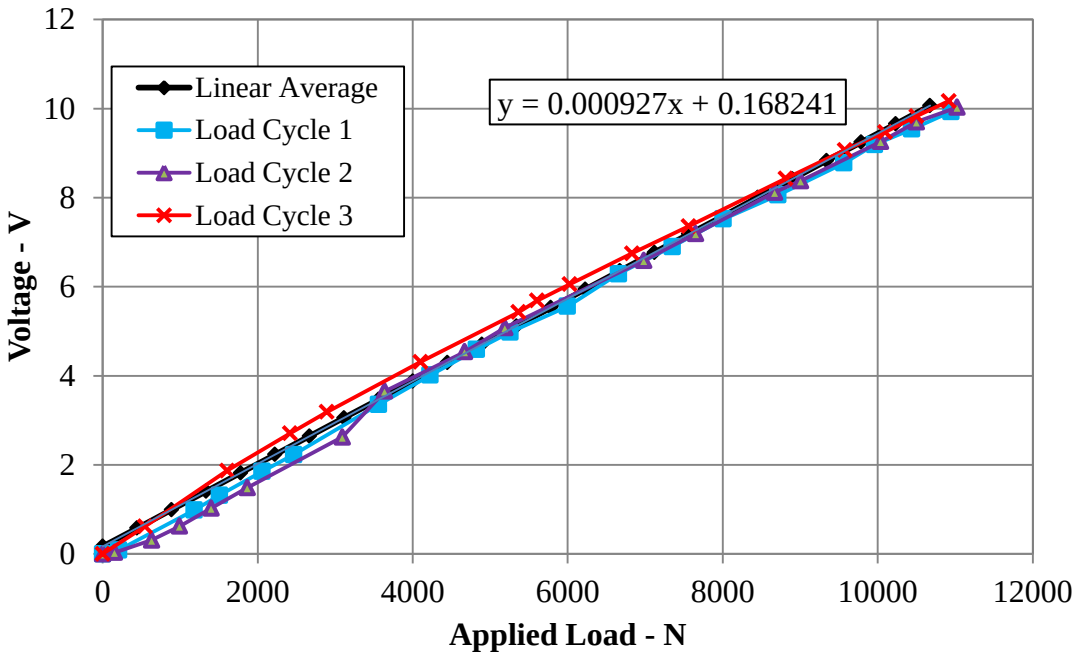

Figure 17. Applied Load versus Voltage from Load Cell tested on MTS machine

2.1.5 Clamping Force Test Results

A total of fifteen samples were collected for each hole diameter configuration. A linear curve fit was created to fit the data points. Results for clearance fit hole are shown in Figure 19 and those for interference fit hole are shown in Figure 20. Based on the results, clearance fit plates experienced higher overall clamping force compared to interference fit. During the test, it was noted that in the interference fit specimens, the coating (thin layer on the outside of the bolt) on the bolt was getting scrapped on the installation of the bolt to the plates, as shown in Figure 18. In addition, interference fit will cause higher friction values between the hole surfaces and the bolt shank. As a result, lower clamping force is seen on interference fit specimens since some load is required to overcome the friction between the pin and the inner surface of the holes. No particular trend in torque versus clamping load is seen in the results for both clearance and interference fit. Since the configuration of the load transfer test specimens was interference fit hole, equation (2.2), extracted by a linear fit of data in Figure 20, was used to evaluate the clamping force.

$$F_{clamp} = 1230.4T - 902.69 \tag{2.2}$$

Figure 18. Bolt Condition after Preload Test

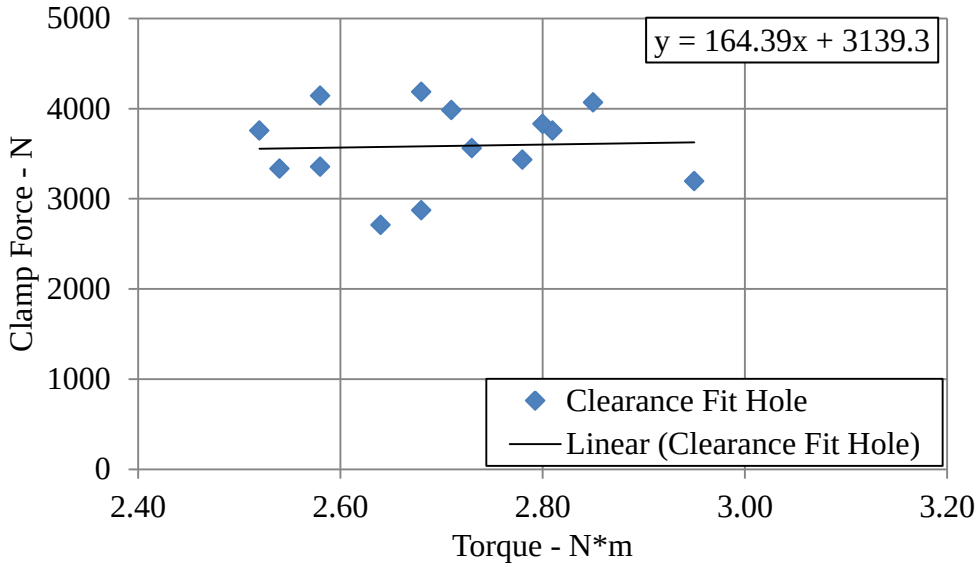

Figure 19. Clamping Force versus Torque for Clearance Fit Hole

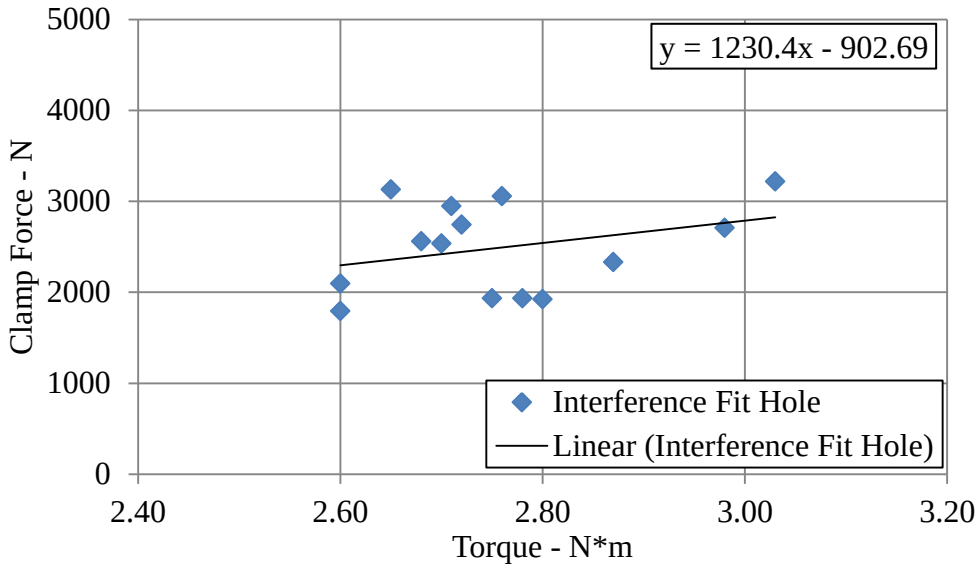

Figure 20. Clamping Force versus Torque for Interference Fit Hole

2.2 **Material Characterization Tests**

The FE model generated is only as good as the data that is input to the model. As discussed in section 1.7.1, the bolt is much stiffer than the plates and hence plastic deformations will occur on the plates. Thus, for capturing the plastic behavior of the plates in the FE model,

coupons were extracted from the plate material and quasi-static tests were conducted to obtain its stress-strain relationship.

2.2.1 Test Specimen Geometry

The specimens tested for material characterization were dog-bone shape with an extended tab [45] constructed from Aluminum 2024-T3 clad with a nominal thickness of 0.09 inches, which is the same material and thickness of the plate used for the load transfer tests. Nominal dimensions of the specimen, tested for material characterization, are shown in Figure 21.

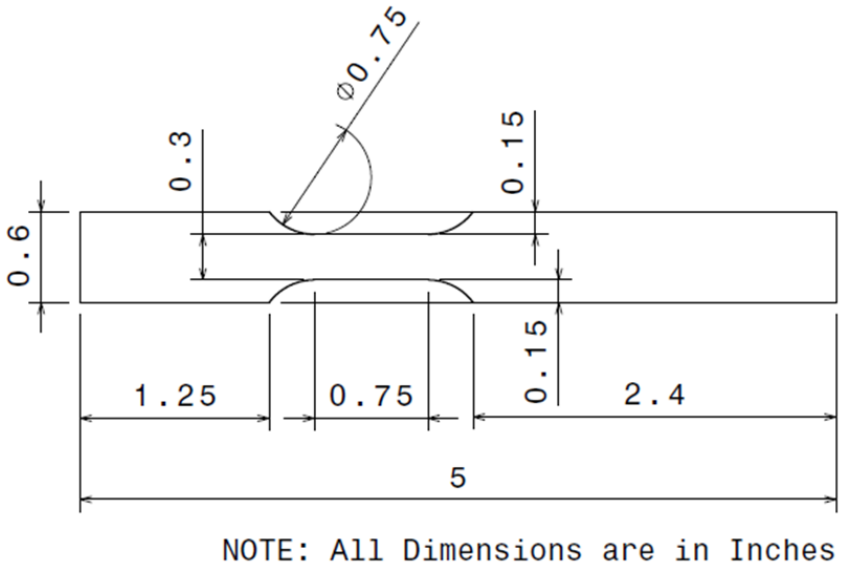

Figure 21. Geometry of Specimen used for Material Characterization

2.2.2 Test Setup and Procedure

A servo-hydraulic test system, shown in Figure 22, was used for this test. The test system was a 22-kip MTS system with fixed grips. A CEA-06-250UN-350/P2 Vishay strain gage [44] was mounted at the center of the gage section of five specimens as shown in Figure 23. Due to the limitation of maximum strain reading by the strain gage, a laser extensometer was used to

capture the deformations up to failure. The full test set-up with the laser extensometer is shown in Figure 24.

To ensure the repeatability of results, the following procedure was followed for five specimens. After mounting the strain gage, the specimen was first gripped at the top. The bottom actuator was then moved to grip the bottom half of the specimen. To set up the laser extensometer, two pieces of tape were placed on the specimen to mark the gage section. The extensometer was positioned to read the distance between the tapes. An initial load of approximately 20 lbf was introduced to the specimen to ensure that the strain gage and the extensometer are functioning. After the checks, a tensile load was applied to the specimen monotonically by displacing the actuator at a quasi-static rate of 0.05 in/min and the data (force, displacement, strain) was acquired at 10 Hz.

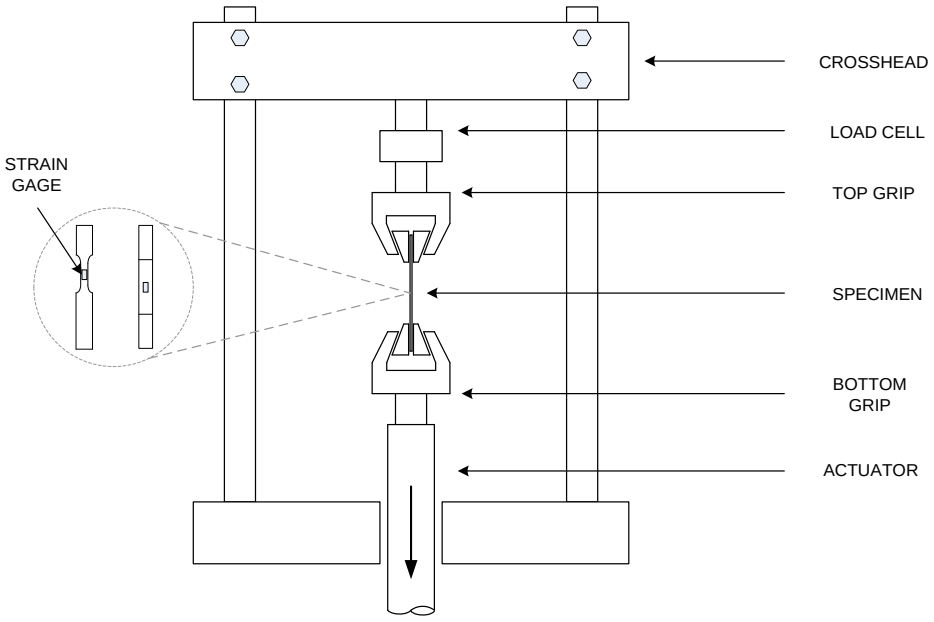

Figure 22. Schematic of Servo-Hydraulic Test System

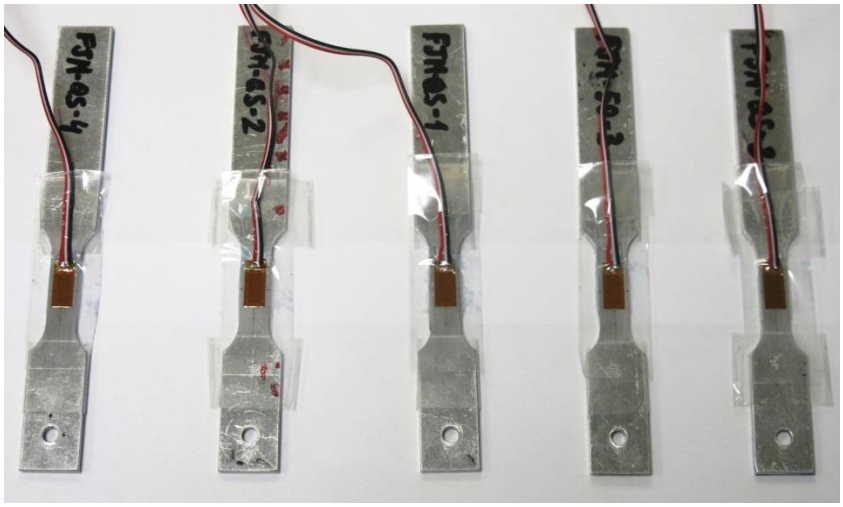

Figure 23. Specimen Prepared with Strain Gage for Material Characterization

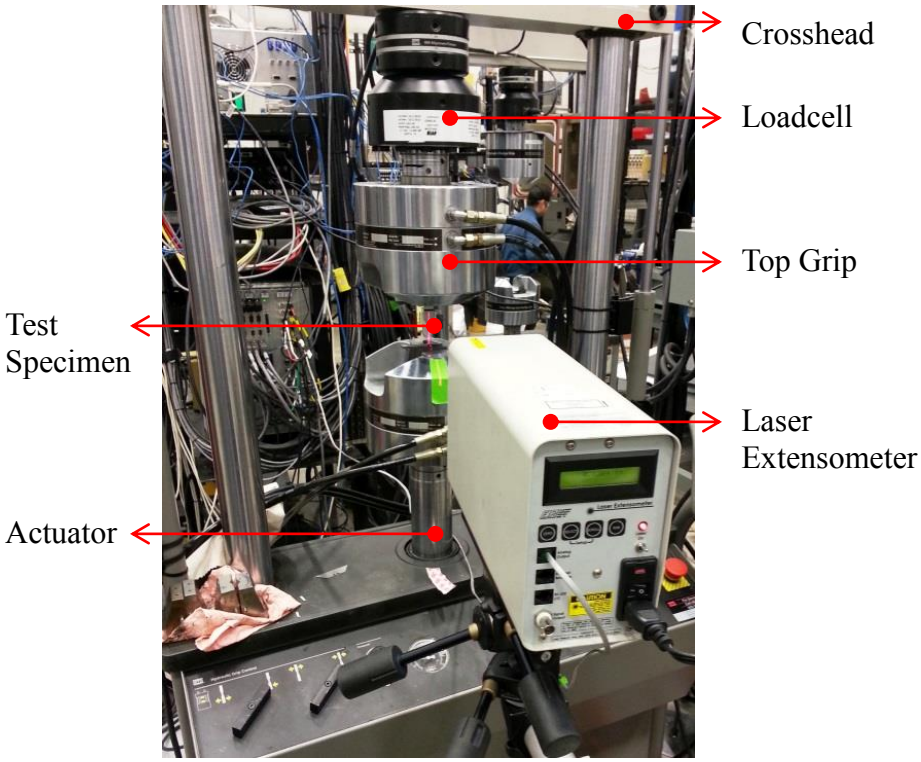

Figure 24. Material Characterization Test Setup

2.2.3 Test Results

Important material properties were extracted from the test data for all five specimens and are shown in Table 2. To evaluate the repeatability of the test, the average (x), standard

deviation (s) and the coefficient of variation (CV) have also been reported in Table 2. These parameters are evaluated using equations (2.3), (2.4) and (2.5) [45].

$$\bar{x} = \frac{\sum_{i=1}^{n} x_i}{n} \tag{2.3}$$

$$s = \sqrt{\frac{1}{n-1}\sum_{i=1}^{n}\left(x_i - \bar{x}\right)^2} \tag{2.4}$$

$$CV = \frac{s}{\bar{x}} \cdot 100 \tag{2.5}$$

Overall, except for the young's modulus calculated using extensometer data, all the evaluated material properties vary within 10%. Thus good repeatability of the test data was achieved through the tests.

TABLE 2
SUMMARY OF MATERIAL PROPERTIES OF ALUMINUM 2024-T3 CLAD FROM TESTING

	Youngs Modulus (Strain Gage)	Yield Stress (Strain Gage)	Youngs Modulus (Ext.)	Yield Stress (Ext.)	Ultimate Stress (Ext.)	Failure Strain (Ext.)
	MPa	**MPa**	**MPa**	**MPa**	**MPa**	**mm/mm**
FJM_QS_1	69019.27	329.76	61347.23	334.00	464.17	0.2122
FJM_QS_2	68622.34	327.33	76493.22	328.11	461.33	0.2329
FJM_QS_3	72866.73	331.97	55837.36	333.57	464.87	0.2066
FJM_QS_4	69010.77	331.29	50307.26	335.98	464.42	0.2255
FJM_50_3_QS	69513.27	331.58	58026.73	338.50	466.68	0.2298
Average (x)	**69806.48**	**330.38**	**60402.36**	**334.03**	**464.29**	**0.22**
Standard Deviation (s)	0.3	276.0	1.4	557.3	279.4	0.01
Coefficient of Variation (CV%)	2.5	0.6	16.3	1.2	0.4	5.2

Note: Ext. - Laser Extensometer

In addition to the material properties, the stress-strain profiles for the specimens were also extracted. Figure 25 shows the stress-strain profile generated using strain values recorded by the strain gage. Since the strain gage data was limited, a laser extensometer was also used to record the deformations. The stress-strain curve with strain extracted from extensometer data is shown in Figure 26. Stresses were evaluated using equation (2.6), where F is the force recorded by the load cell and A is the cross-sectional area at the gage section of the specimen. The strain data was extracted from the extensometer using equation (2.7), where L is the length and L_0 is the original length. Figure 27 shows the post failure condition of the specimens and it can be noted that, as expected, failure was consistently obtained at the gage section.

$$\text{Stress} = \frac{F}{A} \tag{2.6}$$

$$\text{Strain(Extensometer)} = \frac{L - L_0}{L_0} \tag{2.7}$$

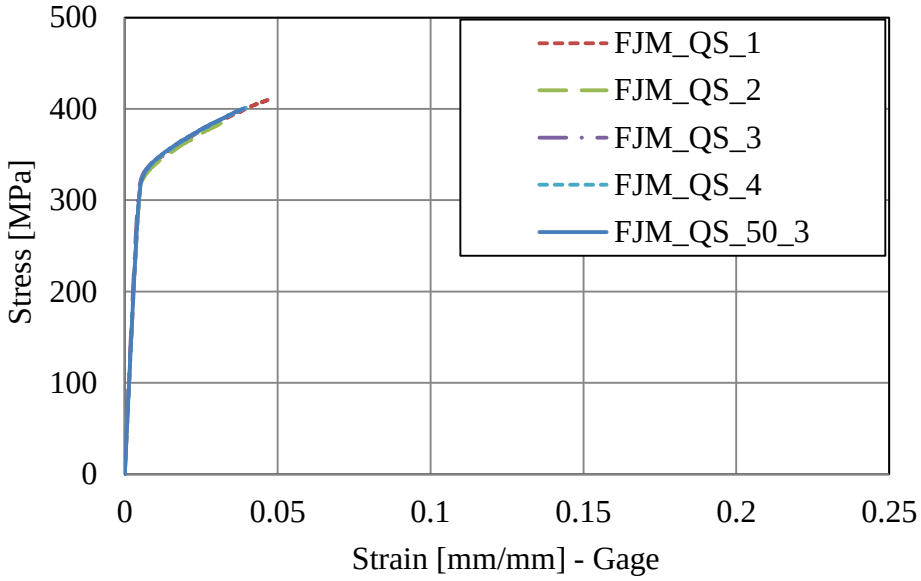

Figure 25. Stress versus Strain (Recorded from Strain Gage) for Aluminum 2024-T3 Clad at 0.05 in/min

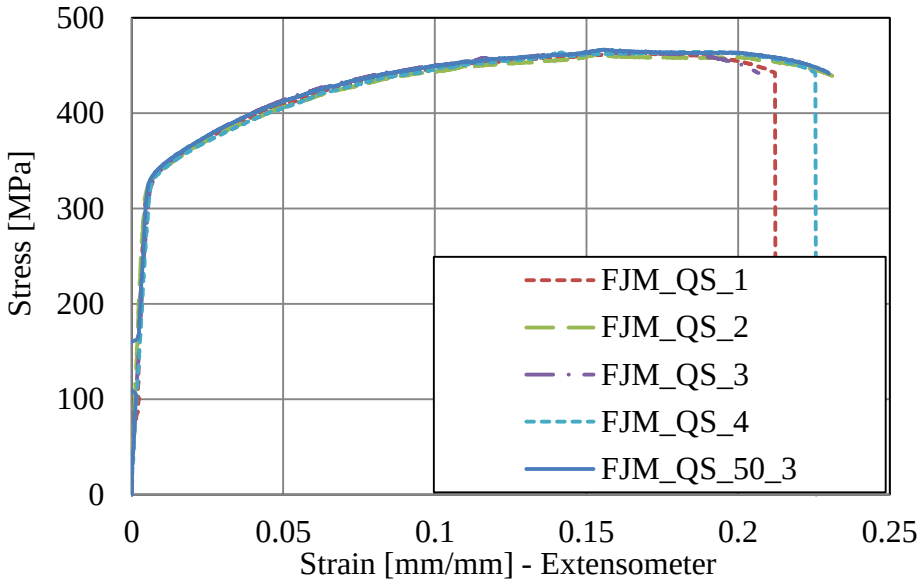

Figure 26. Stress versus Strain (Recorded from Extensometer) for Aluminum 2024-T3 Clad at 0.05 in/min

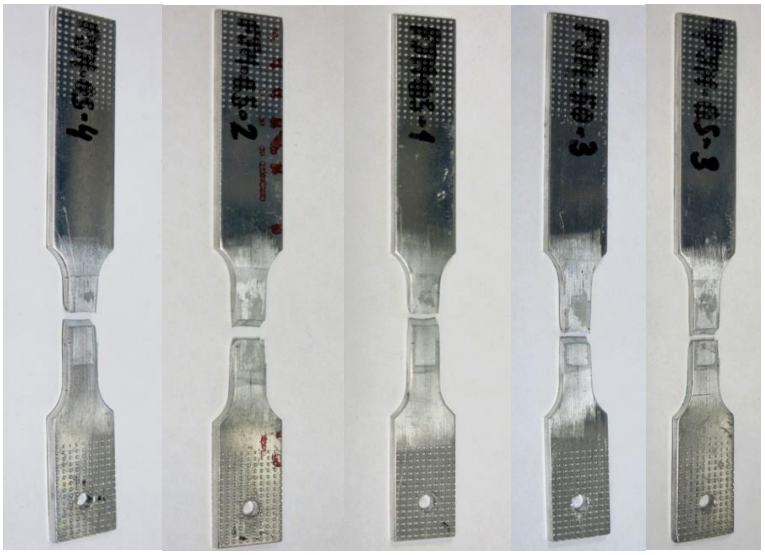

Figure 27. Material Characterization Specimens Post Failure

2.3 **Load Transfer Tests**

This test was designed to understand the load transfer characteristics of a single shear fastener joint specimen. A one half dog bone setup was used with three components which were the main part, transfer part and the fastener. For this experiment, both the main part and the

transfer part were manufactured from clad aluminum 2024-T3 and a Hi-Lok® fastener was used to connect the parts. Tensile load at quasi-static rate is introduced in the main part (loading region), and as the fastener gets engaged, the load gets transferred to the transfer part and some gets by-passed to the main part (by-pass region). The amount of load transfer was evaluated until failure was reached on the specimen.

2.3.1 Test Article

Description of the test article is provided in section 1.7.1. In addition to the coupon an anti-buckling fixture (ABF), with Teflon body and aluminum plates at the end, was also utilized to eliminate secondary bending of the specimen as shown in Figure 28. The aluminum plates were attached to the Teflon body to provide stiffness and to avoid bending in the fixture itself.

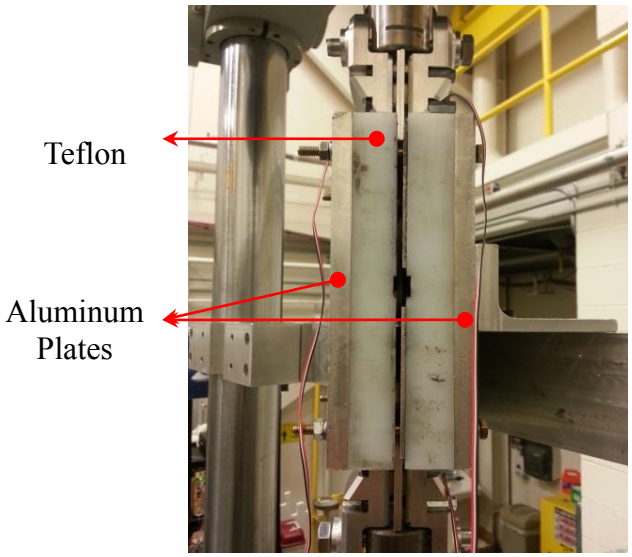

Figure 28. Anti-Buckling Fixture for Load Transfer Tests

2.3.2 Test Setup and Procedure

This test was also set up on a servo-hydraulic system as shown in Figure 22. The long term goal of this topic is to test the same specimen configuration under high strain rates and hence a high speed servo hydraulic MTS machine [43] was used to conduct the tests. Figure 29 shows the setup used for this test including the fixtures for constraining the anti-buckling.

Specifications of the high speed MTS machine are detailed in section 2.3.2.1. A tensile load on the specimen is introduced by displacing the actuator. For testing at high speeds, it was important to ensure that on the onset of loading, the actuator had reached the desired speed. To achieve this, a slack inducer system, designed and fabricated at WSU/NIAR (Wichita State University/ National Institute for Aviation Research) was utilized for the test. Details of the system have been discussed in section 2.3.2.2. Although the tests for this study are only at quasi-static rates, the setup used for the test is intended for high speed testing. This was done to reduce the variability when comparing the quasi-static testing results to the high speed data in the future.

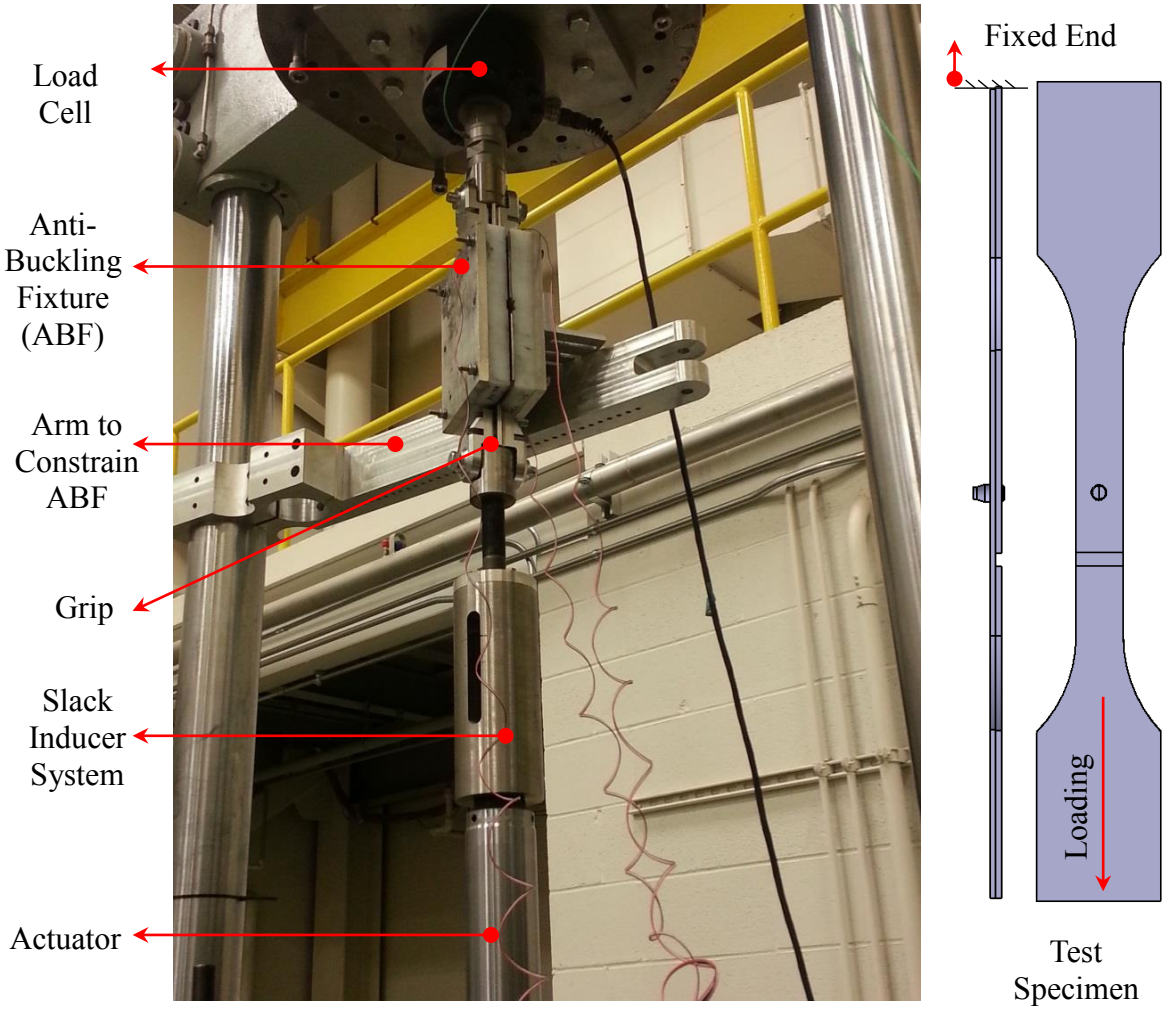

Figure 29. Load Transfer Test Setup

Several steps were taken to prepare the specimens for testing. First, three strain gages were mounted on the specimen. Two gages were mounted on the main part; one on the loading region and one on the by-pass region. The third strain gage was mounted on the load transfer part. Details of the strain gage used and a schematic of the gage placement are shown in section 2.3.2.3. After the installation of the gages, the Hi-Lok® fastener is installed and the torque at the hex shear off is recorded. To install the Hi-Lok® fastener, the specimen is constrained on a fixture and the fastener is installed following the guidelines for Hi-Lok® Installation [39]. The clamping force is calculated using equation (2.2), and the toque and clamping force data is presented in Table 3. This data is used for the detailed and simplified FE models. The anti-buckling fixture is then mounted on the specimen and the gages are connected to the data acquisition system to ensure there is no contact between the ABF and the gages. This is done by compressing the ABF at the gage locations and monitoring the strains. The specimen assembly is then mounted on the MTS test machine and the slack inducer is adjusted for quasi-static testing. To check the set-up, an initial load of approximately 20 lbf is applied to the system. After all checks, a tensile load is introduced by displacing the actuator at a quasi-static rate of 0.05 in/min. Displacement of the actuator, Load recorded by the load cell and strains from the three gages are recorded by the data acquisition system at 10 Hz.

TABLE 3
TORQUE ON BOLT INSTALLATION ON LOAD TRANSFER TEST COUPONS

Test #	Torque at Hex Breakoff (N.m)	Clamping force (N) (using eqn. 2.2)
1	2.32	1952
2	2.79	2530
3	2.62	2321
Average	**2.6**	**2296**

2.3.2.1 High Speed Servo Hydraulic MTS Machine

The tension testing was conducted at NIAR using a high stroke rate MTS servo hydraulic testing machine shown in Figure 30. The testing machine is capable of maximum speeds up to 500 inches/sec. The testing machine can apply sustained loads up to 5000 lbf at maximum speed and up to 9000 lbf sustained when the speed is reduced to quasi-static range (less than 1 inch/sec).

Figure 30. High Rate Servo Hydraulic MTS Testing Machine at NIAR

2.3.2.2 WSU/NIAR Slack Inducer System [45]

One of the possibilities in the future is to extend this testing for high loading rates for which the slack inducer system is required. That is because to reach a desired loading rate, a finite period of acceleration and a finite displacement is required. The amount of displacement is proportional to the loading rate required. By using the slack inducer system, the user can define a certain distance (or slack) to allow the actuator to reach the desired loading rate prior to loading

the specimen. The slack inducer mechanism was designed and fabricated at WSU/NIAR and is illustrated in Figure 31.

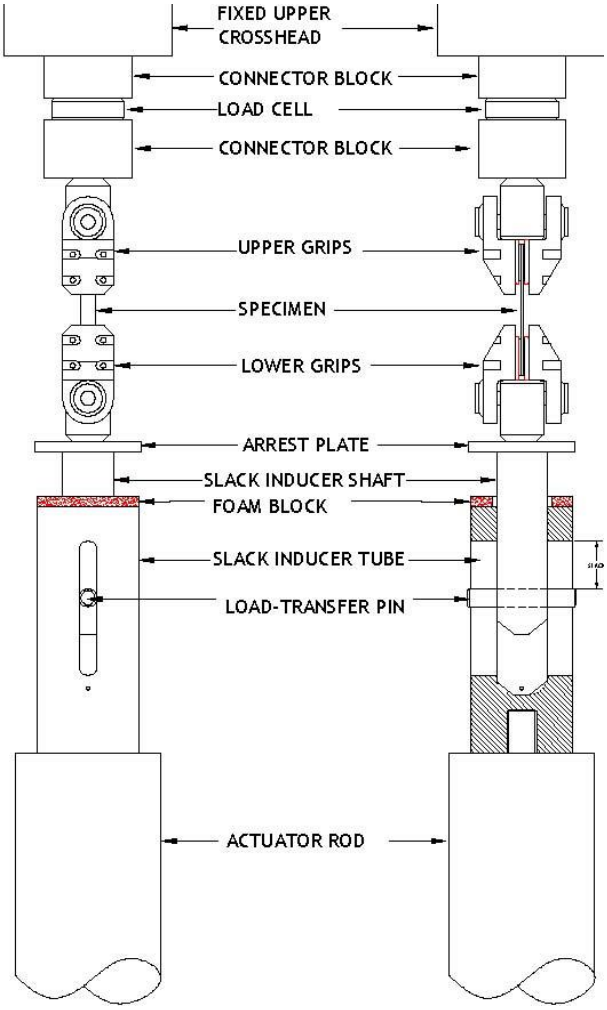

Figure 31. Schematic of Tension Testing showing Slack inducer Mechanism [45]

2.3.2.3 Strain Gage Installation

Three strain gages were placed on specimen. Two gages were placed on the main part on either sides of the bolt and one gage will be placed on the transfer part. All the gages were placed 1 inch away from the center of the hole. A schematic showing the strain gage positions is presented in Figure 32 below. Vishay CEA-06-250UN-350/P2 strain gages with a gage factor of 2.105 and resistance of 350 ohms were used for this test.

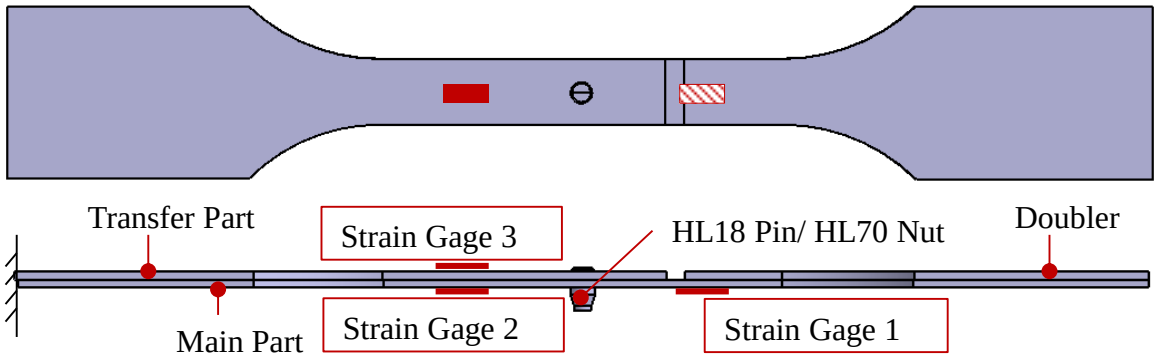

Figure 32. Strain Gage Locations

2.3.3 Load Transfer Test Results

Strain gage data and percentage load transfer from three tests is presented in Figure 33. The data is compared against remote stress, which is evaluated using equation (2.6) where *F* is the force from the load cell, *SG1* are strains are strain gage 1, *SG2* are strains at strain gage 2 and *A* is the cross sectional area of the main part. The strain gage locations are illustrated in Figure 32. The load transfer was estimated by using strain gage measurements at location 1 and location 2, as shown in equation (2.8). The data presented is plotted until failure was reached.

$$\%\ \text{Load Transfer} = \left(1 - \frac{SG2}{SG1}\right) * 100\% \tag{2.8}$$

Based on the test results, it can be noted that location at strain gage 1 shows plastic behavior before failure is reached. From the material characterization tests, the yield strain can be estimated to 0.004733 in/in and the results for strain gage 1 show that the strains are well above the calculated material yield strain value. As a result, using equation (2.8), an increase in load transfer is obtained beyond that point. For test 3, the strain gage 1 location reaches yield sooner than test 1 and 2. This can be attributed to the variability in the material properties and errors induced during test setup as this setup was complex with many components.

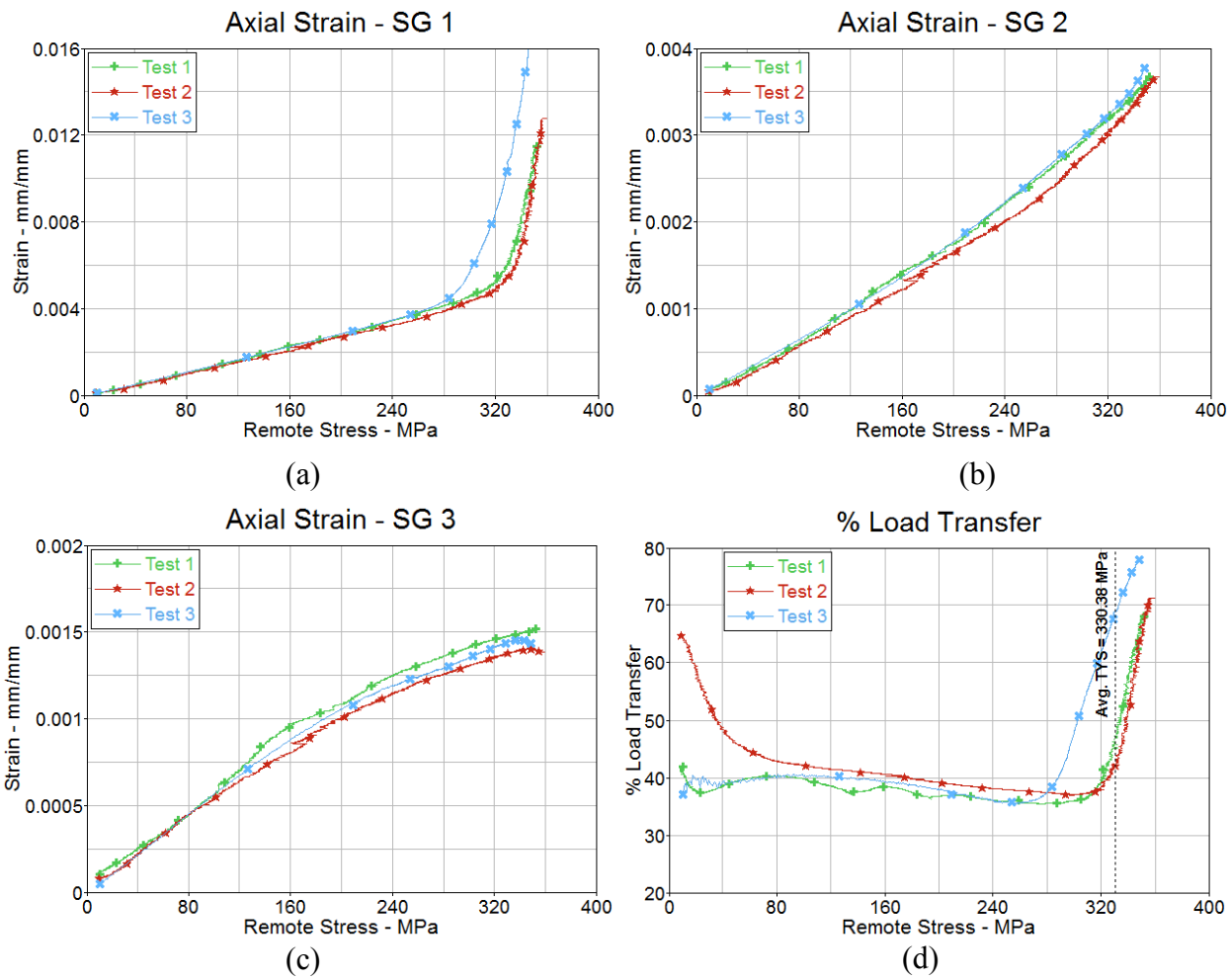

Figure 33. Load Transfer Test Results: (a) Strain Gage 1 (b) Strain Gage 2 (c) Strain Gage 3 and (d) % Load Transfer

The percentage load transfer for the tests remains at a similar average value of around 40%. This value is consistent with the load transfer of a similar configuration reported in [15]. Although the strains are similar for all three tests, the %LT values for test 2 show rather higher values at very low remote stress. At such low loading, the strain values are very small in magnitude and hence even a slight change in the strain will result in a high percentage change. Figure 34 shows the failure location for the three tests. Failure observed was a tear out of the plate material at the net section. Plastic deformations are observed at the boundary of the hole

due to bearing loads. Necking and thinning is also observed on the main part at approximately the mid-plane of the hole or the net section. The necking and thinning of the material at the failure location, along with the 45 degree, to the tensile load, failure plane are properties of a ductile failure which is expected from the material.

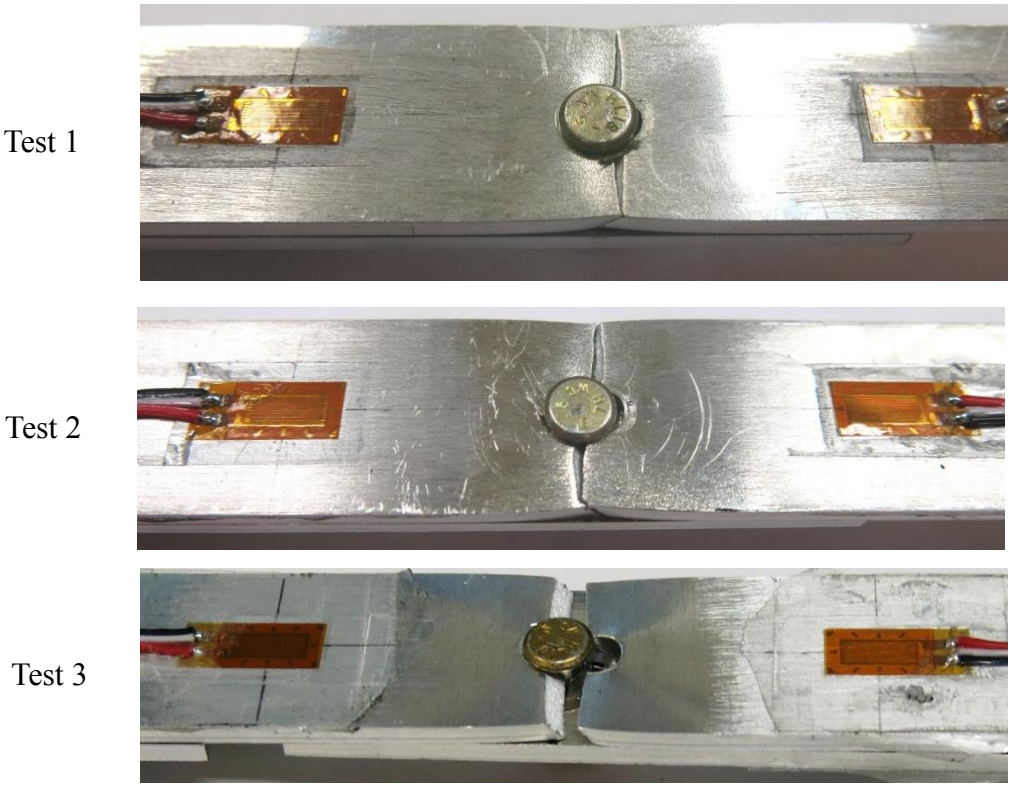

Figure 34. Failure on Specimen for the Load Transfer Test

CHAPTER 3

FINITE ELEMENT MODELING – DESCRIPTION OF MODELS AND METHODS

This chapter describes the FE modeling practices used for this study. The setup of the models, boundary conditions, contact modeling, material definitions and modeling of bolt preload have been summarized in this chapter. Also, since there are several different simplified bolt modeling techniques generated for this study, a nomenclature system is specified to the FE models. In addition, the parameters studied for each FE analysis and the calculations performed are detailed in this chapter.

The FEM solver used for this study is LS-DYNA, a powerful general-purpose FE program capable of simulating complex real world problems [6][7]. LS DYNA offers several solving options, but for this study the non-linear explicit method was used to solve the FE models.

3.1 FE Model Setup

A description of the FE models generated for this study is provided in this section. Five main FE models were generated, one detailed FE Model and four simplified bolt models. The simplified models were selected based on their applicability to large structural FE crash models as described in section 1.7.2. The selected simplified models are: 1) Rigid Body Element bolt model, 2) RBE bolt model with no hole, 3) Mesh Independent Spotweld Beam Model and 4) Mesh Independent Spotweld Beam with elastic patch model. Brief details of these models can be found in Table 1, entry number 5 to 8. For each simplified model, several different variations were also generated.

As described in section 1.7.1, the specimen assembly consists of the main part, transfer part, doubler and Hi-Lok® bolt and nut. To accurately capture the behavior of the specimen, the

anti-buckling fixture used in the test was also modeled for the simulations. Although the purpose of the anti-buckling fixture is to constrain the specimen from bending, a simple boundary constraint cannot be used in the FE model to represent this because the interaction the specimen with the anti-buckling fixture is complex. For all the FE models generated, one inch long patch of elements around the fastener hole of the main part and transfer part were put into separate components for extracting information such as energy and stresses only in the vicinity of the hole. Table 4 summarizes the quality criteria used for all the FE models for consistency and good results [46][47].

TABLE 4
MESH QUALITY CRITERIA

Parameter	Allowable	Parameter	Allowable
Jacobian	> 0.7	Skew	< 60
Warpage	< 5.0	Min Angle	> 45
Aspect Ratio	< 10	Max Angle	< 135

3.1.1 Detailed FE Model

To validate the modeling techniques used for this study, a detailed FE model of the specimen assembly was generated using 3D elements. In terms of capturing the fine details of the geometry, this model most closely represents the test coupon and hence the results of this model have been compared to the test data. Once validated, the detailed FE model can provide useful data such as stress concentrations, stress distributions, strain energy and more that cannot be obtained from the test data. Thus the results from the detailed FE model were used as a baseline for comparing the performance of the simplified bolt modeling techniques. A schematic of the detailed FE model is shown in Figure 35.

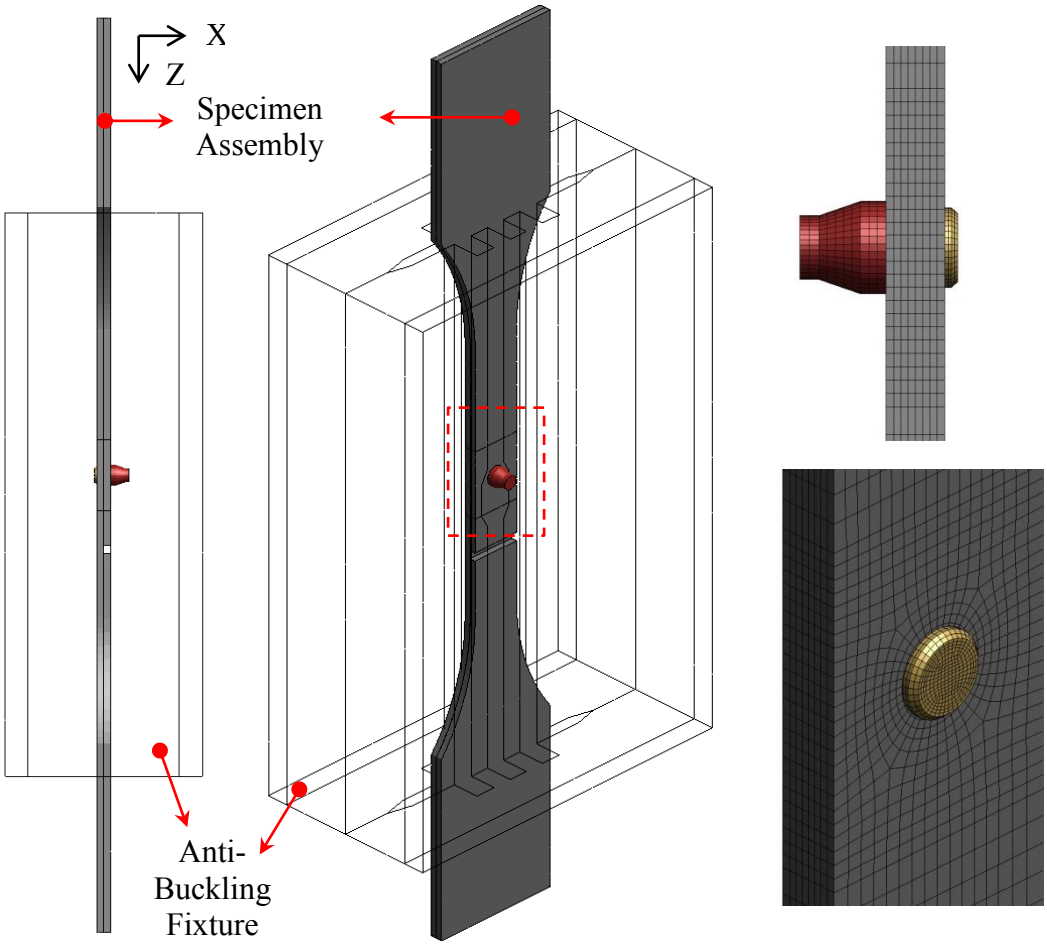

Figure 35. Detailed 3D FE Model Setup

The cost of simulation was disregarded for this model and hence a very fine discretization, with a minimum element length of 0.206 mm, was applied to critical areas of the specimen geometry. This mesh is considered fine because to control time step in large models, the minimum element length used is 3mm [47]. These include the area around the hole on main part and transfer part as shown in Figure 38, and the bolt and nut as shown in Figure 36. The threads of the bolt were not modeled for this study therefore, although the nut was modeled as a separate component, the nodes of the nut are shared with the bolt. The doubler and the anti-buckling fixture were meshed with larger elements, as shown in Figure 37, since these are not parts of interest. As illustrated in Figure 38, one inch long patch of elements around the fastener

hole of the main part and transfer part were put into separate components. In addition, at least four elements were placed across the thickness on the main part and the load transfer part. Due to similarities in the geometry, the same mesh was used for the main part and the transfer part. Note that detailed FE model is also referred to as *solid model* when presenting the FEM results.

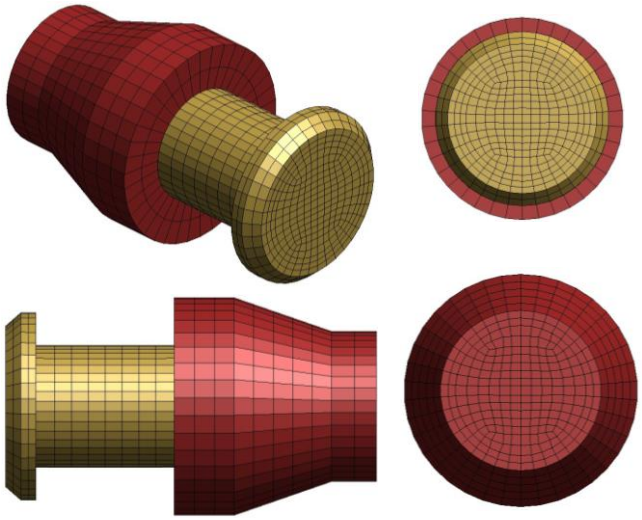

Figure 36. FE Discretization of Hi-Lok® Bolt and Nut

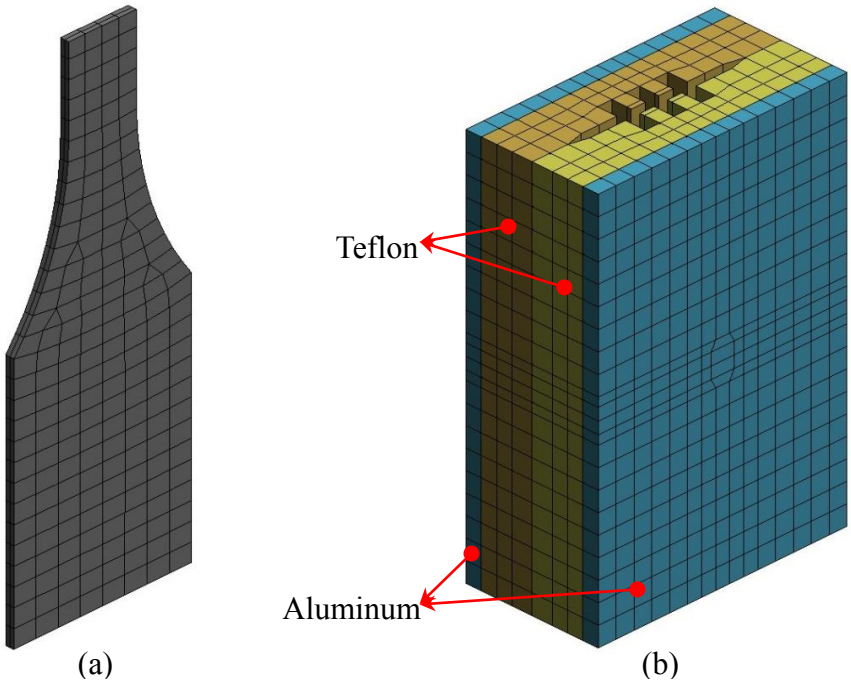

Figure 37. FE Discretization of (a) Doubler and (b) Anti-buckling Fixture

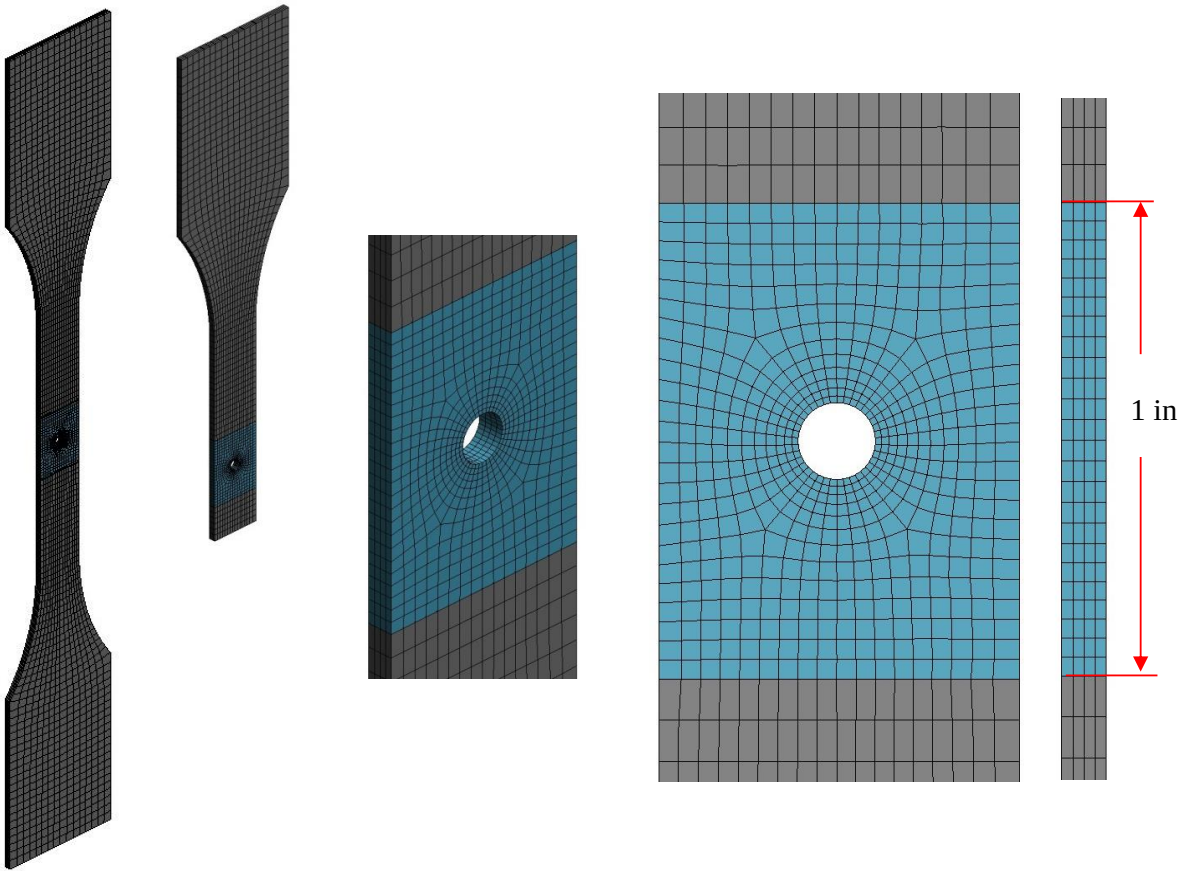

Figure 38. FE Discretization of Main Part and Load Transfer Part

3.1.2 Simplified Technique – RBE Bolt Model

In this technique, the bolt is idealized with a beam element and ends of the beam are connected to the boundary of the bolt hole using rigid body elements as shown in Figure 39. These rigid body elements are known as nodal rigid bodies in LS DYNA [48] and can be modeled using the card *CONSTRAINED_NODAL_RIGID_BODY [48]. The bolt is idealized using beam element formulation type 9 and *MAT_SPOTWELD [48]. Details of the beam element formulation and the material model can be found in section 3.2 and 3.6 respectively.

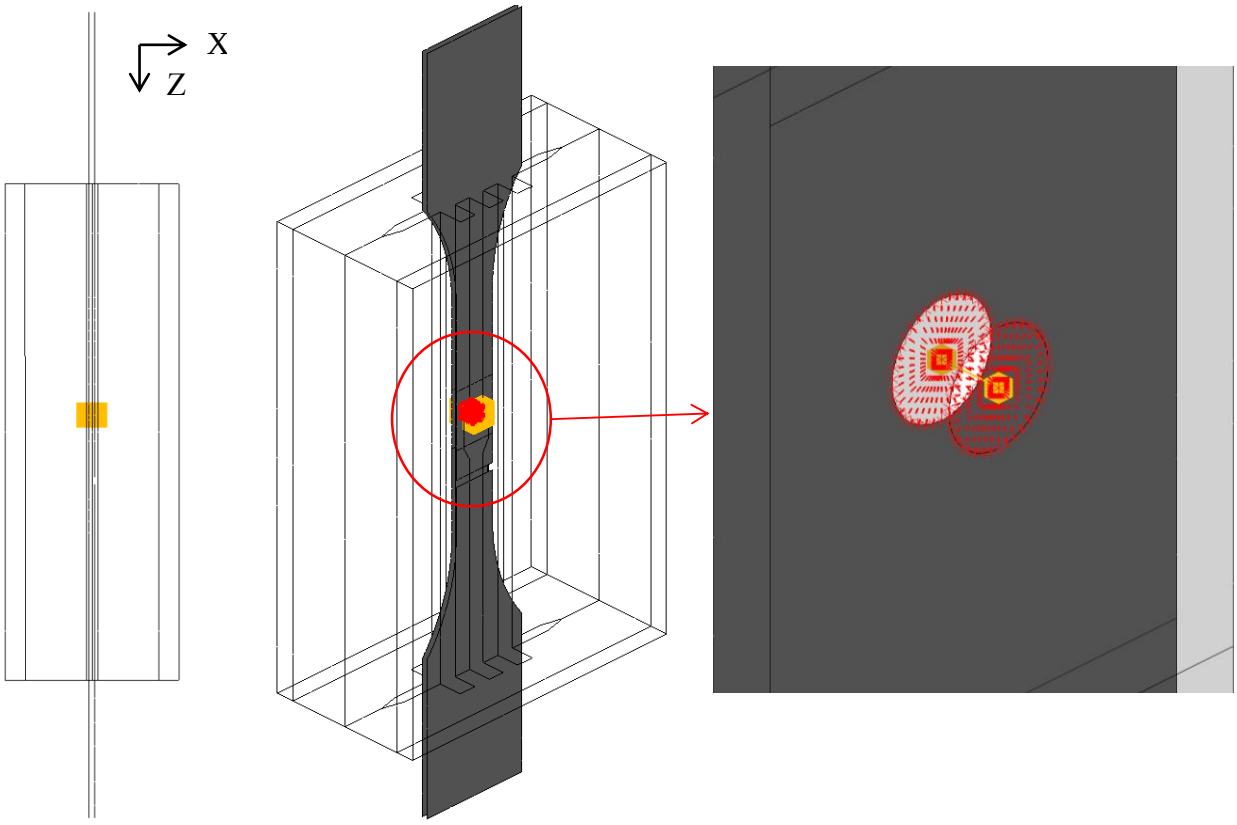

Figure 39. Model Setup of RBE Bolt Model

Since the RBE Bolt model uses rigid body elements, the boundary of the hole is essentially rigid. Therefore the possible variations for this type of simplified modeling exist in the mesh size. For this study, three different models with RBE Bolt model are generated as shown in Figure 40. Configuration 1 is a very fine mesh RBE Bolt Model with minimum element length of 0.331 mm. In this configuration, the number of elements on the edge of the hole is same as the elements on the detailed 3D model. In configuration 1A, a coarser mesh, with minimum element length of 3mm, is used to represent the specimen. Four nodes are placed on the boundary of the hole and thus a square hole is formed. Minimum element length of 3mm is appropriate and has been used in the past for FE models of large structures [7][13][50]. In configuration 1B, 8 nodes are maintained around the edge of the hole and the minimum element

length is 2 mm. Note that the main part and the transfer part both have the same setup unless otherwise stated.

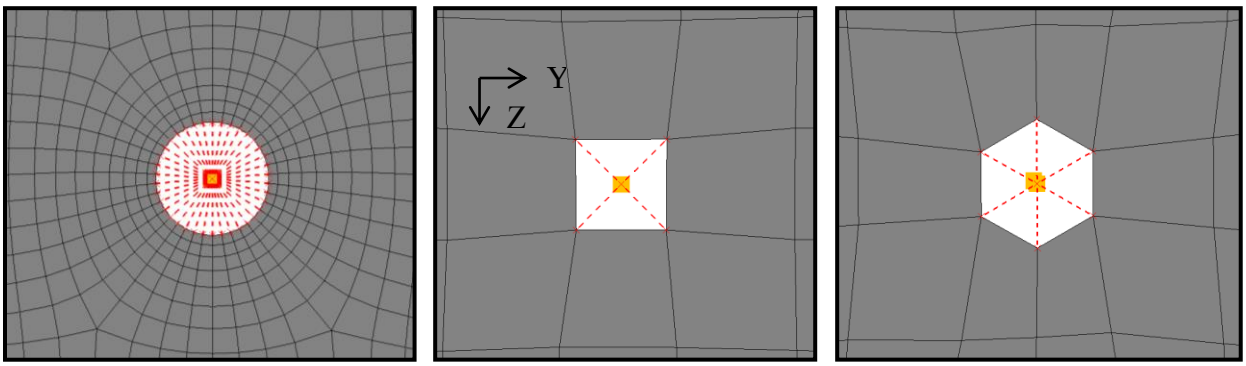

(a) Config (b) Config (c) Config

Figure 40. Variations of RBE Bolt Models

3.1.3 Simplified Technique – Mesh Independent Spotweld Beam Model

In this method the bolt shank is idealized using beam element formulation type 9 and *MAT_SPOTWELD is used for the material definition. The head and nut of the bolt are not modeled. The beam is connected to the parts using a tied contact formulation, *CONTACT_SPOTWELD [48]. The setup of this FE model is shown in Figure 41.

The tied contact mechanism, *CONTACT_SPOTWELD, is explained in detail in section 3.4.1. In summary, forces at the nodes of an element in contact change based on the location of the beam (slave node) with respect to the element (see section 3.4.1). When large models are meshed, it is a laborious process to align elements of joining parts to ensure that the beam is placed at an ideal location with respect to the contact surface. Thus for this study several possible variations of the beam location with respect to the element are explored as shown in Figure 42.

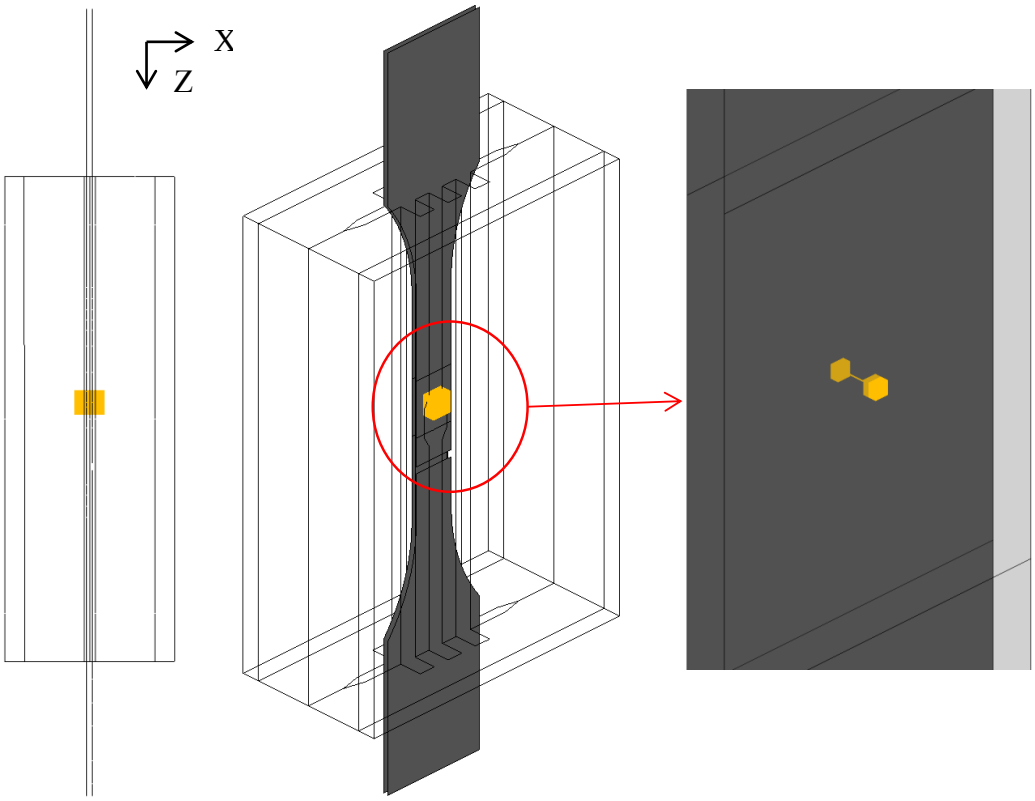

Figure 41. FE Model Setup of Mesh Independent Spotweld Beam Bolt Model

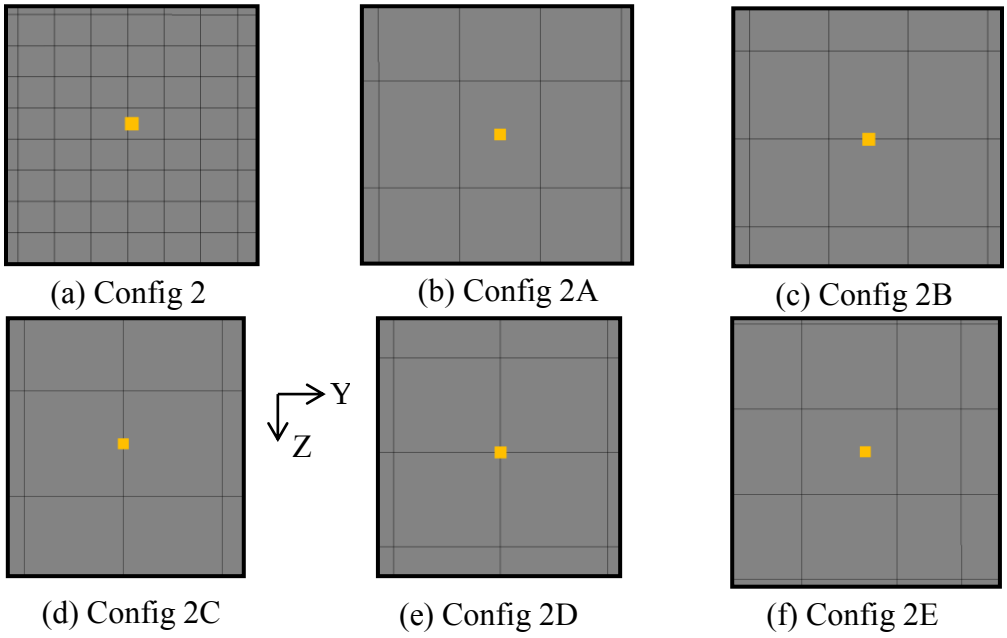

Figure 42. Variations of Mesh Independent Spotweld Beam Bolt Model – Same mesh on Main Part and Transfer Part

As seen in Figure 42, configuration 2 is a fine mesh model with the beam placed at an arbitrary location with respect to the element. The fine mesh model has a minimum element length of 0.3 mm. For the rest of the configurations, the minimum element length is 3 mm. Note that for variations shown in Figure 42 the main part and the transfer part both have the same mesh setups. Variations shown in Figure 42 rarely occur in large models, where parts are meshed independently, and for that reason a few combinations of different mesh on main part and transfer part are also studied as shown in Figure 43.

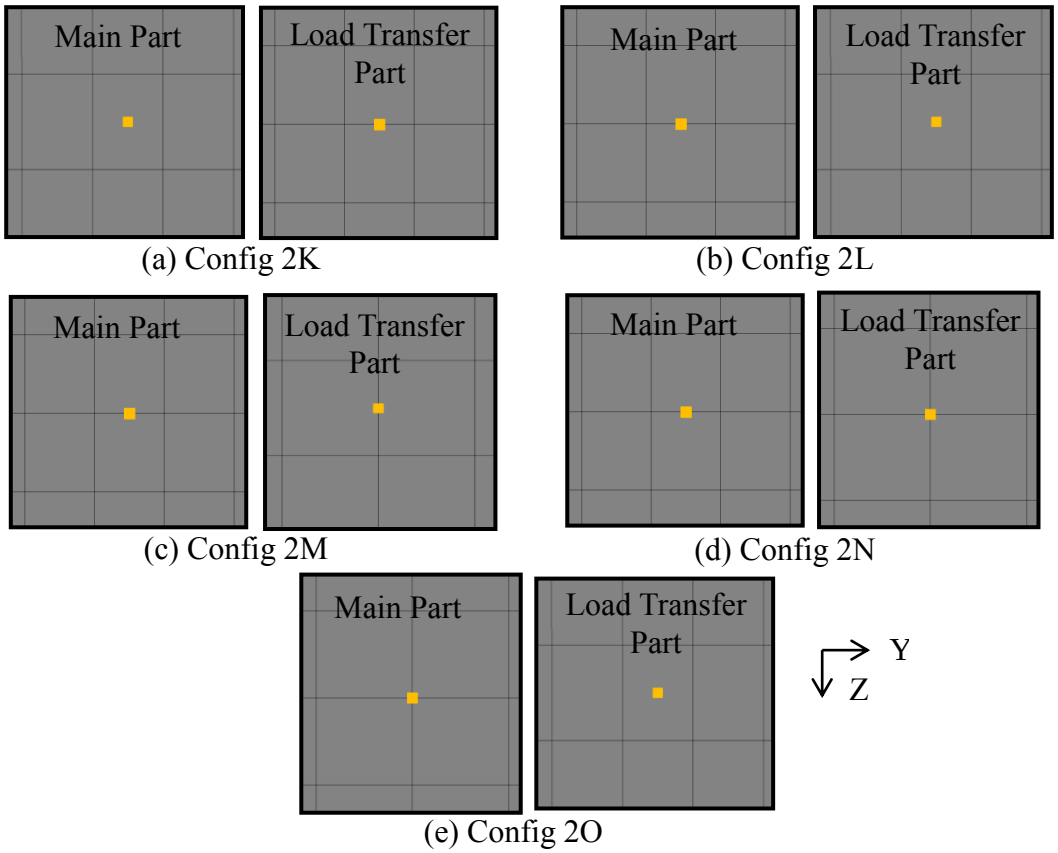

Figure 43. Variations of Mesh Independent Spotweld Beam Bolt Model – Different mesh on Main Part and Transfer Part

3.1.4 Simplified Technique – Mesh Independent Spotweld Beam with Elastic Patch Model

This method is an extension to Configuration 2. This modeling method follows the same setup as described in section 3.1.3 for the bolt shank. The difference in this method is that the elements to which the bolt connects are modeled using an elastic material model (no failure) to simulate the presence of a fastener hole. By controlling the Young's modulus of the elastic elements, stress concentrations develop in the surrounding elements which are representative of the scenario experienced with a fastener hole. In this model, the group of elements with elastic material properties is referred to as an elastic patch. Figure 44 shows the setup for this simplified bolt modeling technique where the red represents the elastic patch. The elastic patch is modeled as steel which is the same material for the bolt head and nut. A stiff material will facilitate load transfer and will not store high amounts of energy thus representing a hole (no energy since no material)

Some variations of this model have been generated as shown in Figure 45. Configuration 3 is a fine mesh model with the same mesh as the detailed 3D model except the hole is filled with elements with elastic material properties. In configuration 3A and 3B, a coarse mesh with minimum element length of 3mm is used. In configuration 3A, the elastic patch is only maintained on the main part which is likely to fail while in configuration 3B, both the main part and the load transfer have an elastic patch. It should be noted that even though this method follows the same setup as described in section 3.1.3, the influence of the beam model with respect to the location on the contact segment is not explored since the patch is intended to represent the fastener hole and the bolt is supposed to be placed at the center of the hole.

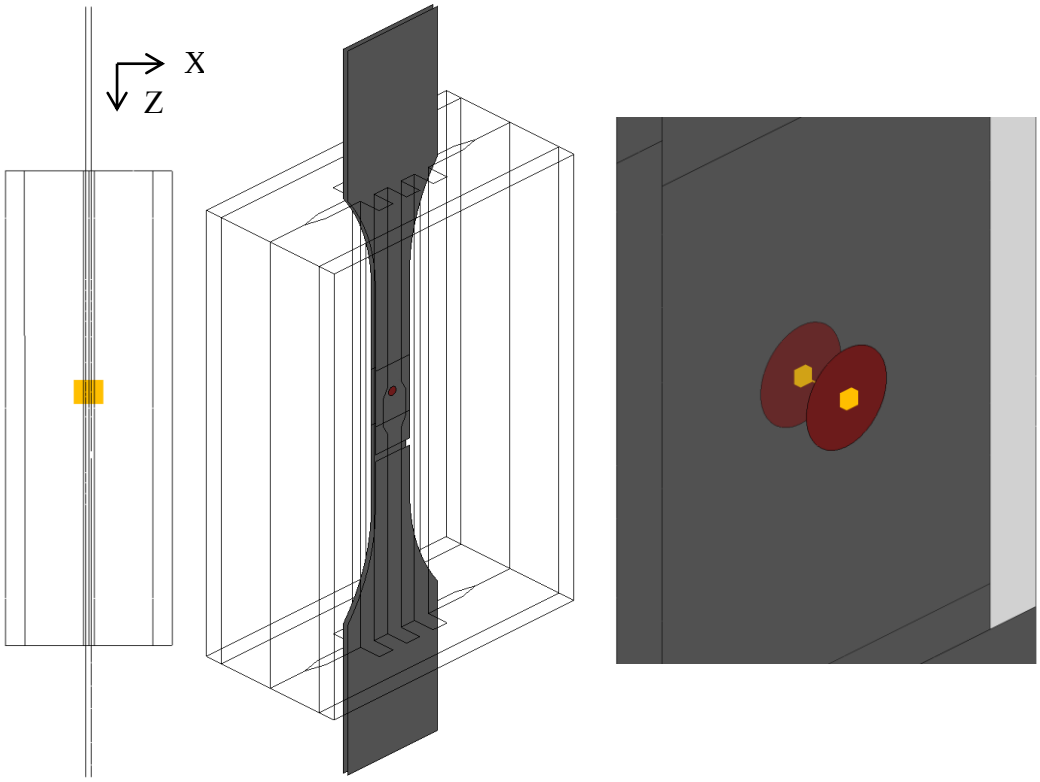

Figure 44. FE Model Setup of Mesh Independent Spotweld Beam with Elastic Patch Model

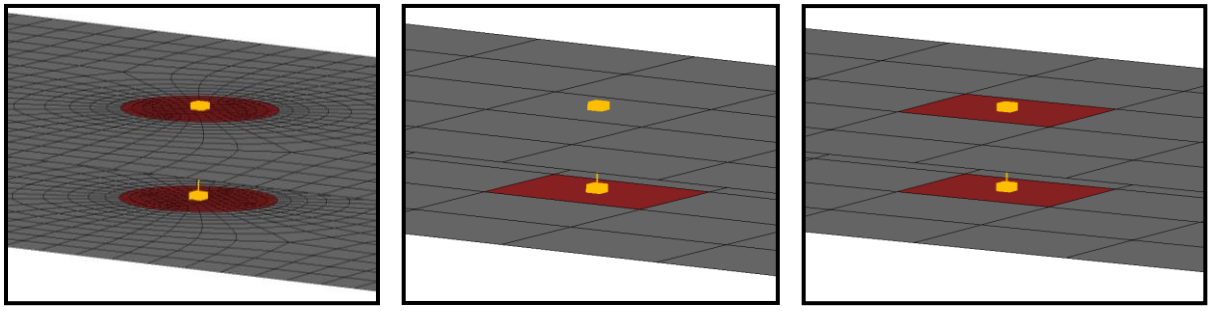

(a) Config 3 (b) Config 3A (c) Config 3B

Figure 45. Variations of Mesh Independent Spotweld Beam with Elastic Patch

3.1.5 Simplified Technique – RBE Bolt Model with No Hole

This simplified technique is an extension to the technique shown in section 3.1.2. As shown in Figure 46, this technique uses the same setup as the technique described in section 3.1.2 except the hole on the main part and the transfer part is not modeled. Due to this, the nodes of the nodal rigid body are connected to the main part and transfer part using a tied contact

option *CONTACT_TIED_NODES_TO_SURFACE [48]. This method allows the nodal rigid bodies to be connected to the parts at any location desired. Note that the beam which represents the bolt shank is not connected to any of the parts. The beam is only connected to the nodal rigid body. Therefore this method allows us to have more connection points on an element rather than a single point as the methods described in 3.1.3 and 3.1.4.

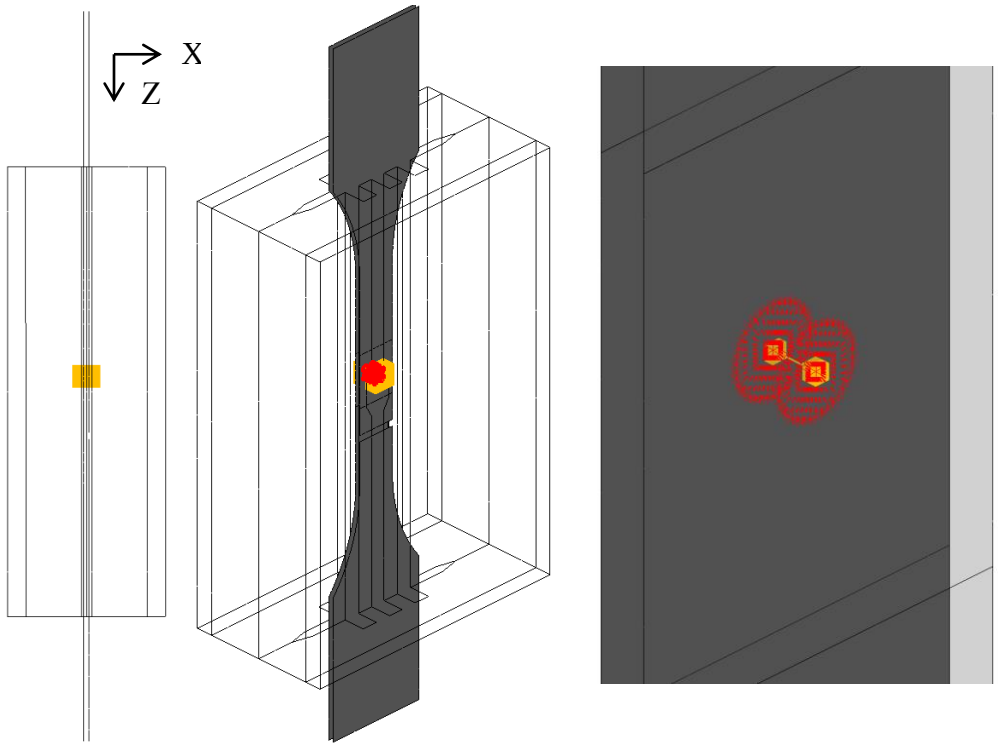

Figure 46. FE Model Setup of RBE Bolt Model with No Hole

Number of nodes in a nodal rigid body and the position of those nodes can be controlled and hence this allows for several variations in this method of bolt modeling. The variations studied are shown in Figure 47. Configuration 4 is a model with a very fine mesh (0.3 mm minimum element length) and about 38 nodes to represent the nodal rigid body. These are the same number of nodes around the hole of the detailed FE model. From configuration 4A to 4D, four nodes have been used to represent the nodal rigid body and the nodes have been rotated by 15 degrees for each configuration. In configuration 4E, the nodal rigid body consists of 8 nodes.

While maintaining the same nodal rigid body, the mesh is changed in configurations 4F to 4H. A coarser mesh with minimum element length of 3 mm is used for the main part and transfer part from configurations 4A to 4H. Note that the nodes of the nodal rigid bodies represent the diameter of the bolt hole.

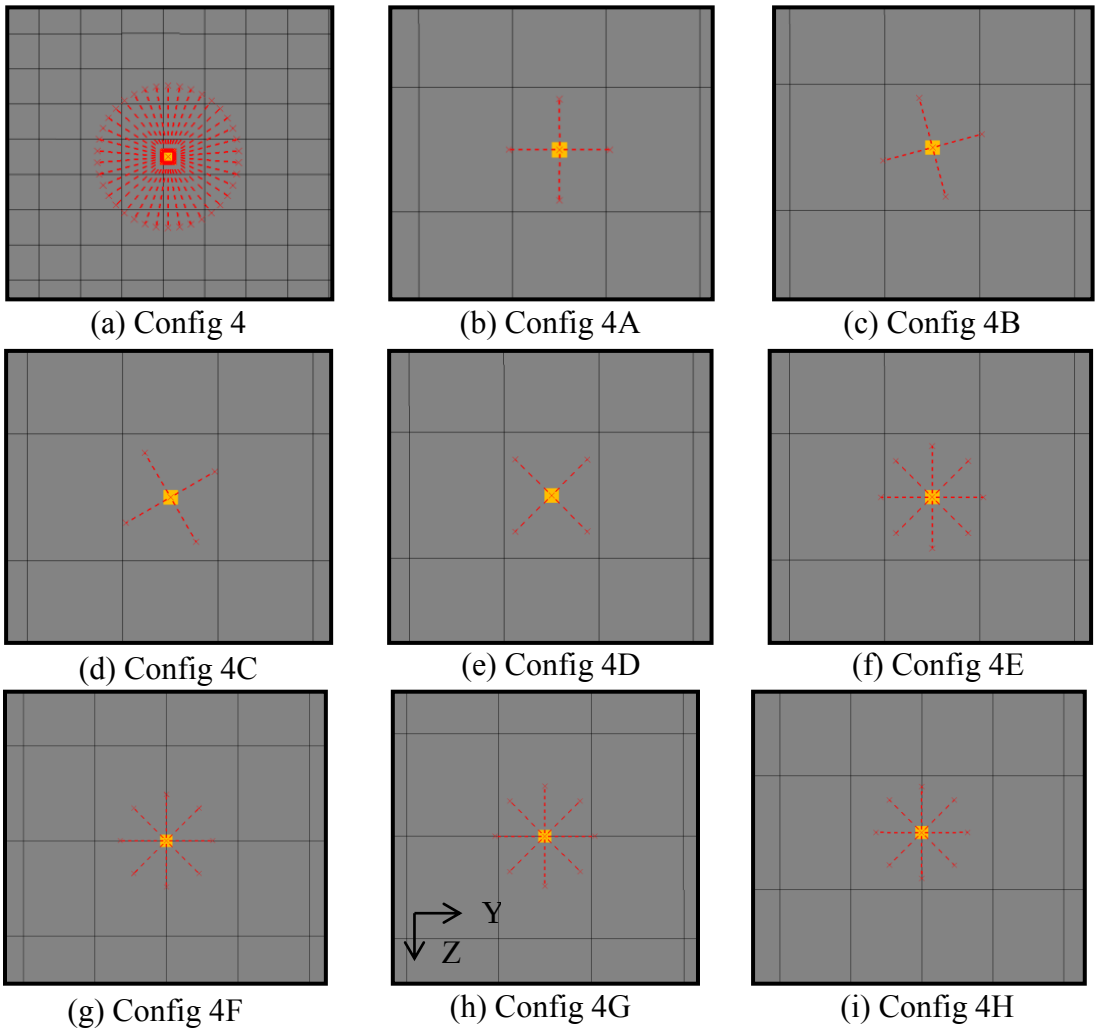

Figure 47. Variations of RBE Bolt Model with No Hole

3.2 **Element Definitions**

Overall, the FE models were discretized using 3D solid elements, 2D shell elements or 1D beam elements or a combination of all. LS DYNA provided the used with many different

formulations for each of these elements. The selection of section properties and element formulation was based on efficiency and use in large structural models.

3.2.1 3D Solid Elements

As shown in Figure 48, solid elements include tetrahedrons, pentahedrons and hexahedrons where hexahedrons are desirable while the others may cause problems in certain situations. A given geometry can be most accurately discretized using solid elements. Based on the LS DYNA user's guide [49], the following is known about solid elements. The hexahedron solid element, which is a 8-noded element uses one point integration scheme by default. This default option is known as the constant stress solid element in LS DYNA. This is the most efficient solid element formulation in terms of computational cost, but can experience zero-energy modes (hourglassing) and thus requires hourglassing control. Another option available is the fully-integrated scheme which eliminates the zero-energy modes but is 4 times more costly.

For this study the default solid element formulation is used by ensuring that the added hourglassing energy is significantly lower than the total energy. In addition, since this option only consists of one integration point, at least four elements were used through the thickness of the main part, bolt and the load transfer part of the specimen to accurately capture bending.

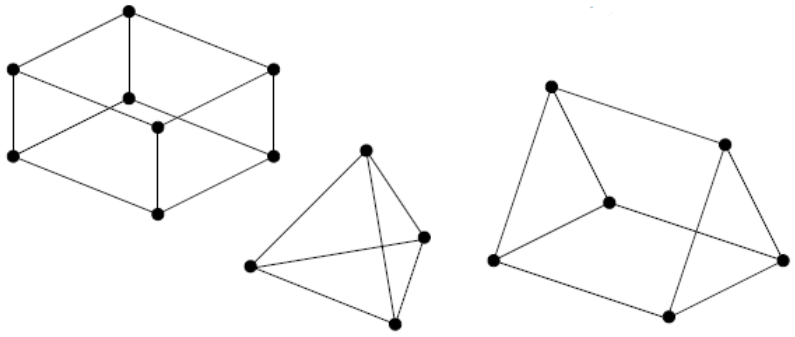

Figure 48. 3D Solid Elements [49]

3.2.2 2D Shell Elements

Shell elements 2D elements generally used to represent sheet metals or parts with small thicknesses. As shown in Figure 49, shell elements include quadrilateral or triangular elements where the triangular elements exhibit a stiffer behavior and hence quadrilateral elements are preferred [50]. For all the FE models and for large structural models, the shell element formulation of choice is the BELYTSCHKO-LIN-TSAY shell due to its computational efficiency compared to other models [47]. This element formulation also requires hourglass control [48].

For non-linear material models, it is recommended to use more than two integration points through the thickness. For this study, three integration points through thickness are used similar to the setup used in a study performed by NIAR [13]. The computational cost increases with higher number of integration points [45].

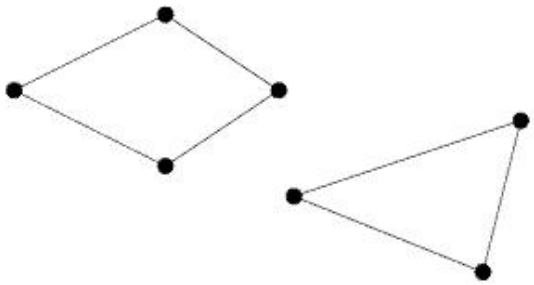

Figure 49. 2D Shell Elements [49]

3.2.3 1D Beam Elements

Beam elements are 1-D elements with two nodes, as shown in Figure 50, and can be used as truss, beams, discrete springs or dampers. For this study a beam element, specifically type-9 beam element formulation which is a spotweld beam, is used a simplified technique to model bolts. Type-9 beam element formulation is a Hughes-Liu Beam type which means it is incrementally objective (rigid body rotations do not generate strains) [51]. Hughes-Liu beam

types are known to be simple which translates into robustness and computational efficiency [49]. The element variables for this beam type are integrated at the midpoint of the reference axis with multiple points on the cross-sectional area [51]. The beam element formulation requires special treatment for torsion and ignores Poisson's effect [51]. Only *MAT_SPOTWELD material definition can be used to define the material properties for the beam. This beam element formulation has been used to model bolts for many studies involving large structural models [13], [50].

Figure 50. 1D Beam Element [49]

3.3 **Boundary Conditions and Constraints**

Boundary conditions for all the FE models were specified as per the load transfer tests described in section 2.3. The test equipment, that is the grips, slack-inducer system and the MTS machine were not modeled in the FE models and thus similar boundary conditions were applied by selecting the nodes of the tab area. As a result, the effect of test machine compliance cannot be captured by the FE models. Boundary conditions applied to the FE models are shown in Figure 51. Note that all the boundary conditions are applied in global coordinate system. For the fixed boundary, both the translations and rotations in the global X, Y and Z coordinates are constrained *BOUNDARY_SPC card in LS DYNA [48]. The anti-buckling fixture is constrained on one end only, similar to the test setup shown in Figure 28.

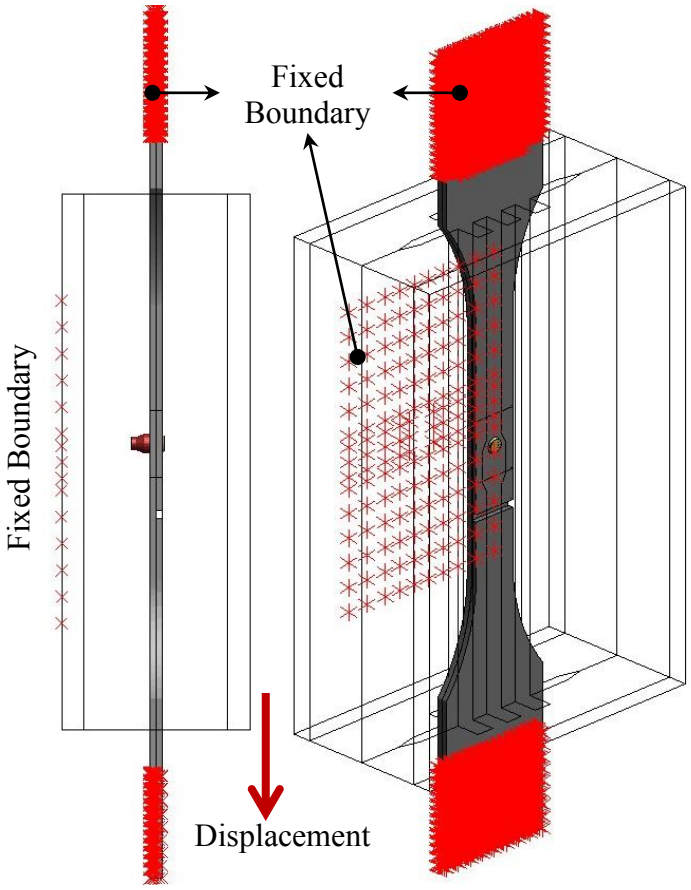

Figure 51. FE Model Boundary Conditions

The tests were conducted at quasi-static rate of 0.05 in/min and failure was attained after approximately 4 minutes of loading. Since all the FE analyses were conducted using the explicit LS DYNA solver, it would be very costly to run a FE simulation for 4 minutes. Hence, the displacement used for all the quasi-static FE analysis is 0.5 in/s and is applied using *BOUNDARY_PRESCRIBED_MOTION.

A constraint type used for the FE models is a nodal rigid body. This option is available in LS DYNA using the card *CONSTRAINED_NODAL_RIGID_BODY. By using this option, the selected nodes get constrained and behave as a rigid body. The loads experienced by the first selected node are transferred to the rest of the nodes of the nodal rigid body. For the FE models

of this study, nodal rigid bodies are used to constrain the anti-buckling fixture as shown in Figure 52and are also used for the RBE Bolt models described in sections 3.1.2 and 3.1.5.

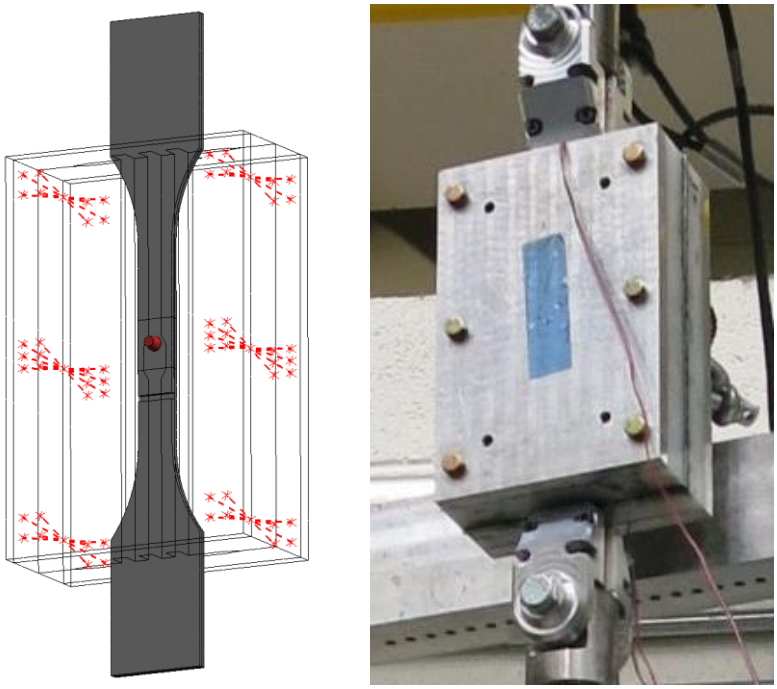

Figure 52. Constraint on the Anti-Buckling Fixture

3.4 **Contact Modeling**

LS DYNA provides several methods for contact modeling with automatic options or manual options. With automatic options, nodes are checked for contact in both directions of the normal vector while in manual options, the check is only performed in the direction of the normal [49]. Several options for modifying the contact performance are available for each contact and can be found in [48]. Note that for this study, the default options were used to model the contacts.

Friction parameters are also defined in the contact card. The parameters available to define friction in contacts are *FS*, static coefficient of friction, *FD*, dynamic coefficient of friction, *DC*, the decay constant and *VC*, coefficient of viscous friction [48]. The coefficient of friction (μc) is evaluated using *FS, FD, DC* and the relative velocity of surfaces in contact (*Vrel*)

as shown in equation (3.1) [48]. Equation (3.1) is an exponential equation where the curve is dictated by *DC* and the friction coefficient (μc) ranges from *FS* to *FD* [48].

$$\mu_c = \mathrm{FD} + (\mathrm{FS} - \mathrm{FD})e^{-DC|Vrel|} \quad [48] \tag{3.1}$$

For this study, the values of *FS, FD* or *DC* were not quantified by any experiments and hence remain unknown. Therefore, for all the simulations, FS is set equal to *FD* and *DC* is set to zero. A study with different values of *FS* or *FD* was conducted to understand the effect of friction (see section 4.3.3) and a value of 0.1was used for FS and FD for validation with test data.

For the detailed FE model, *AUTOMATIC_SINGLE_SURFACE [48] and the *AUTOMATIC_SURFACE_TO_SURFACE [48] options were used for modeling contact. Two contact definitions were required for defining contact because the coefficient of friction between the specimen and the anti-buckling fixture was zero, compared to 0.1 used for friction within the specimen itself.

Similarly for shell element models two *AUTOMATIC_SURFACE_TO_SURFACE contacts were used, one for the specimen itself and one between the specimen and anti-buckling fixture. For shell element models, *AUTOMATIC_SINGLE_SURFACE was not used because it resulted in penetrations on the application of bolt preload. In addition, a tied contact, *CONTACT_SPOTWELD was used to connect the beam element to the shell elements in simplified techniques described in section 3.1.3 and 3.1.4. *CONTACT_TIED_NODES_TO_SURFACE_OFFSET was used for connecting nodes of the nodal rigid body to the shell elements for the simplified technique described in section 3.1.5.

3.4.1 *CONTACT_SPOTWELD

It is crucial to understand the tied contact, *CONTACT_SPOTWELD as it is the primary entity forming the joint on some of the simplified joint methods. The description of this contact below is summarized from [14] and [51].

This contact is a constraint based contact which means no sliding is allowed between the components. It enables coupling of both translational and rotational degrees of freedom. The components in contact are defined as slave, which are the nodes of the beam and master, which are the segments of the shell elements. The components of this contact are shown in Figure 53.

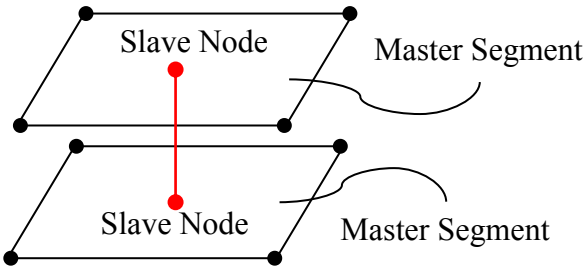

Figure 53. Components of *CONTACT_SPOTWELD [51]

On initialization, the contact point is established by searched for the closest master segment to the slave node. Once the contact point is established, constraints are developed based on shape functions as shown in Figure 54.

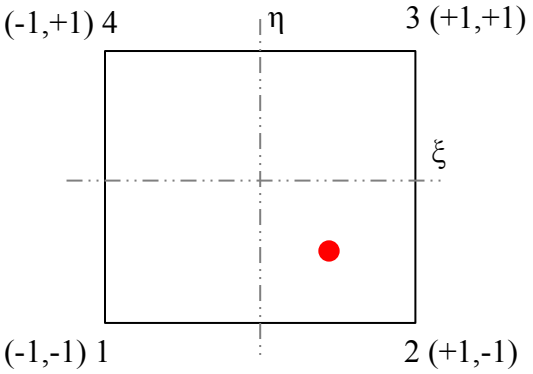

$$N_1=\frac{1}{4}(1-\xi)(1-\eta) \qquad N_3=\frac{1}{4}(1+\xi)(1+\eta)$$

$$N_2=\frac{1}{4}(1+\xi)(1-\eta) \qquad N_4=\frac{1}{4}(1-\xi)(1+\eta)$$

Figure 54. Shape Functions [51]

Thus the incremental master segment nodal force Δf_m^i and mass Δm_m^i are calculated using the shape functions as shown by equations (3.2) and (3.3) respectively [51]. The forces on the slave node f_s are computed as the weighted average of the master segment nodes as shown by equation (3.4). For instance, if the contact point is at the center of the element shown in Figure 54, all the four nodes will get 25% of the slave nodal force and mass.

$$\Delta f_m^i = \sum_{i=1}^{4} N_i(\xi,\eta) * f_s \quad [51] \tag{3.2}$$

$$\Delta m_m^i = \sum_{i=1}^{4} N_i(\xi,\eta) * m_s \quad [51] \tag{3.3}$$

$$f_s = \sum_{i=1}^{4} N(\xi,\eta) * f_i^j \quad [51] \tag{3.4}$$

As a result, this contact is highly affected by the location of the contact point on the master segment. It is noted in the LS-DYNA keyword manual that failure forces change with respect to the contact point location and scaling factors and options for failure force are also available in the manual [48].

3.4.2 *CONTACT_TIED_NODES_TO_SURFACE_OFFSET

This contact is similar to *CONTACT_SPOTWELD except it couples only translational degrees of freedom. The offset option was used because it is required for contact between rigid body and deformable body.

3.5 **Preload Modeling**

A key question to be answered in this study is the importance of preload application for simplified bolt models. The physics and mechanics of bolt preload, and the factors that affect bolt preload are many and have been studied at length by [10][11]. For this study, a Hi-Lok® fastener is used which comes with a pre-existing preload as described in section 2.1. From the load transfer tests conducted, the average measured bolt preload was 2296 N as shown in Table 3. Several options are available for the application of preload in LS DYNA and two different methods, one for solid element bolt model and one for beam element bolt model, were used for this study.

3.5.1 Preload in Solid Bolt Model

Six different preload application methods can be used for a solid bolt model as presented by Nakalswamy [52]. A detailed study was performed using four of the six methods and is presented in APENDIX A. From the preload study, *INITIAL_STRESS_SECTION option was used for the FE models in this study. In brief, to use this method of preload application, a cross-section plane is defined through the center of the bolt shank and a curve defining the desired stress in the bolt shank is also defined. A pseudo-simulation, called the dynamic relaxation phase, is used for the preload application. Once convergence is achieved, the model with the preloaded final state is used as the initial point for the transient simulation (actual simulation) [48].

This preload application method requires the input of stress which was evaluated using equation (2.6), where F is 2296 N (Table 3) and A is the cross-sectional area of the bolt, which was calculated using the bolt diameter of 4.1275 mm. As a result, the equivalent stress required

for preload was evaluated to be approximately 172 MPa. The result of preload application is shown in Figure 55.

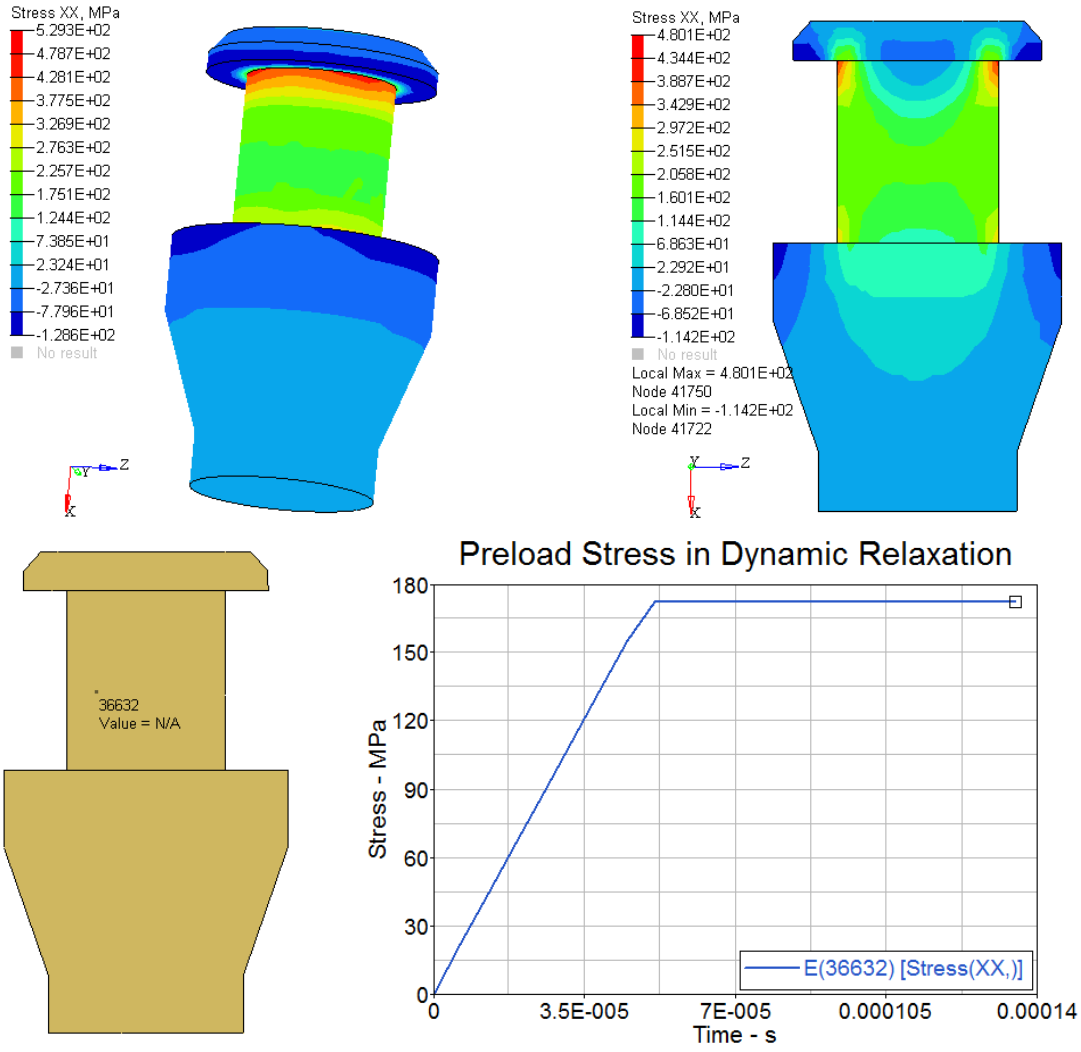

Figure 55. Preload on Solid Bolt Model

3.5.2 Preload in Beam Bolt Model

For the remaining simplified models, beam element is used for representing the bolt shank. To introduce a preload on the beams, the *INITIAL_AXIAL_FORCE_BEAM card was used. This card only works with beam element formulation type 9 and is used to initialize axial force resultants in the beam [48]. Similar to the preload application in solid model, the dynamic relaxation phase was used to achieve the desired force. Once convergence was attained, the

actual tensile loading of the specimen begins. Figure 56 shows that the desired preload of 2296 N was attained by this method.

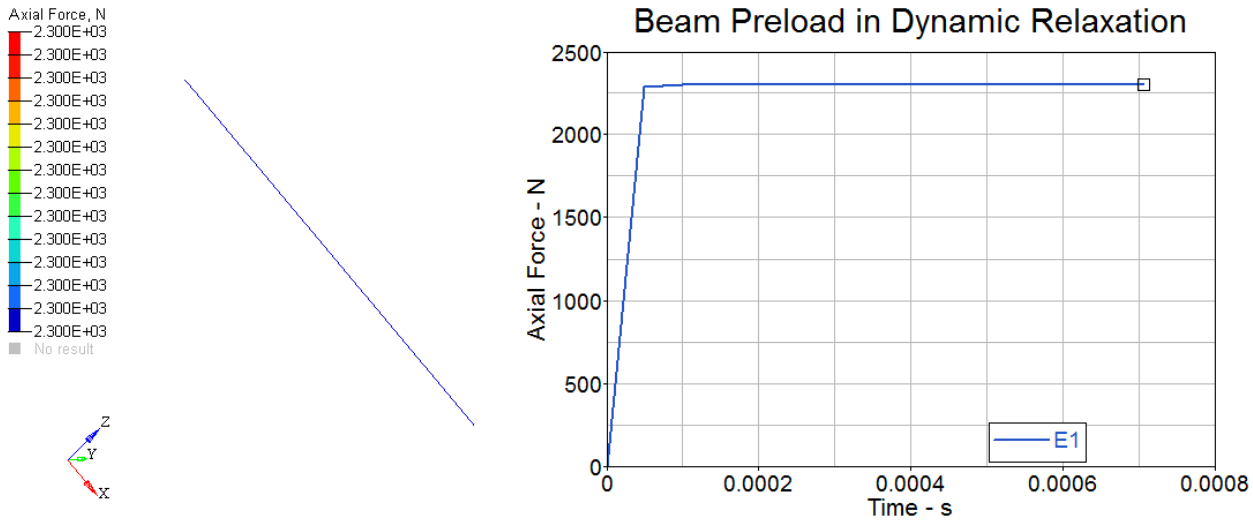

Figure 56. Preload on Beam Bolt Model

3.6 **Material Modeling**

Accurate modeling of materials in FEM is very important to capture the behavior of a system. Based on the specimen assembly, the main part, the transfer part and the doubler are constructed from clad aluminum 2024-T3, the bolt consists of a steel pin and aluminum nut, and the anti-buckling fixture consists of Teflon material and Aluminum backing. It can be noted that since the bolt consists of a steel pin, which is much stiffer than the aluminum parts it joins, failure is expected to occur on the aluminum parts. Therefore, an elasto-plastic material definition with the stress-strain profile is necessary for the main part and transfer part to study plasticity effects and to model failure. For the other parts, since failure or plastic strains are not expected, the elastic material model is sufficient for capturing the material stiffness. To ensure FE models accurately represent the tests material characterization tests were conducted, as documented in section 2.2, to extract the material properties for clad aluminum 2024-T3 and generic properties were used for other materials [53], TEFLON. The mechanical properties,

along with the LS DYNA material card used for different parts, of the specimen assembly are listed in Table 5.

TABLE 5
MECHANICAL PROPERTIES OF MATERIALS USED IN FE MODEL

Part	LS DYNA MAT [55]	Density ($tonne/mm^3$)	Youngs Modulus (MPa)	Poisson's ratio	Yield Strength (MPa)	Failure Strain	REF
Main Part	*MAT_024	2.768e-9	69806	0.33	330.38	0.199	Sec 2.2
Transfer Part							
Doubler							
Bolt Pin (solid)	*MAT_001	2.768e-8	199948	0.27	-	-	[53]
Bolt Pin (beam)	*MAT_100	2.768e-8	199948	0.27	-	-	[53]
Bolt Nut (solid)	*MAT_001	2.768e-9	72395	0.33	-	-	[53]
ABF Aluminum	*MAT_001	2.768e-9	72395	0.33	-	-	[53]
ABF Teflon	*MAT_001	2.16e-9	7239.5	0.33*	-	-	[54]

**Assumed*

The elasto-plastic material properties are defined using the LS DYNA material card *MAT_024 [55]. This material card is a piecewise linear plasticity elasto-plastic material model with an arbitraty stress versus strain curve and where arbitrary strain rate dependency can be defined [55]. Failure in the material model is defined based on plastic strains. A study performed at NIAR [45], has shown that this material model provides good performance and correlation to test data.

For *MAT-024, along with the mechanical properties listed in Table 5, the stress strain profile extracted from the test (section 2.2) was used to define the behavior of the material after yielding occurs. This material card requires the stress versus strain curve to be input in the form of effective stress versus effective plastic strain. As a result, additional adjustments (using

equations found in [45]) were made to convert the test data, which is presented in the form of engineering stress versus engineering strain, to the required format. Figure 57 below shows the effective stress versus effective plastic strain curve.

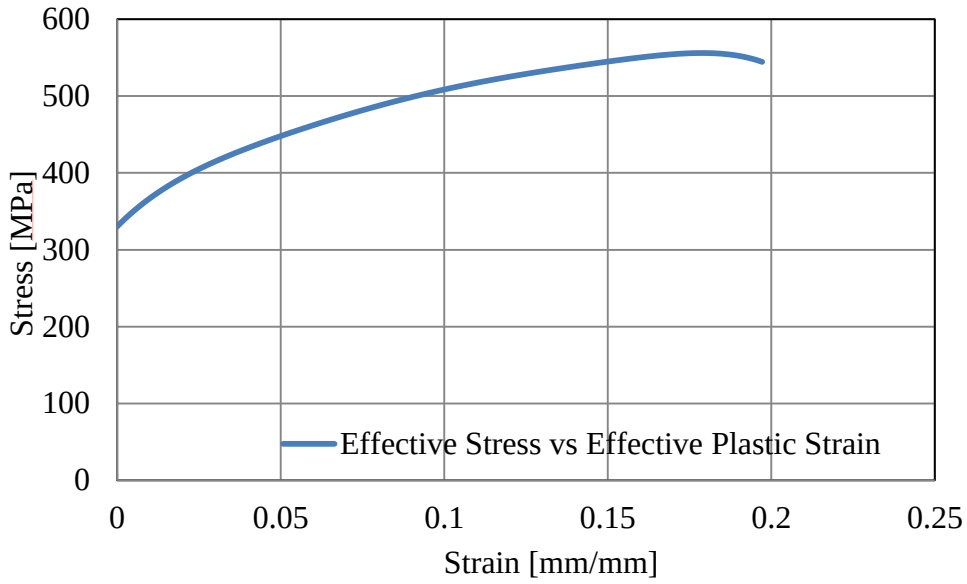

Figure 57. Comparison of Engineering Stress-Strain to Effective Stress vs. Effective Plastic Strain for Clad Aluminum 2024-T3 at Quasi-static Rate

For parts where failure is not expected, *MAT_001 [48], a linearly elastic material model is used where the only parameters defined are the materials Young's modulus, density and Poisson's ratio. For representing the bolt as a type 9 beam, *MAT_100 is the only material model that can be used [48]. Although failure can be described in this model, for this study bolt failure was out of the question since the bolt is fabricated from Steel while the parts it connects are Aluminum.

3.6.1 Material Strain Rate Dependency

Mechanical properties of certain materials such as yield stress, ultimate stress and failure strain are known to change when different strain rates are applied. A part of this study involves exploring the effect of high strain rates (common in a crash scenario) on the load

transfer characteristics of the detailed and simplified bolt modeling techniques. To perform this study via FEM, strain rate sensitive material data is required. *MAT_024 material model allows the user to define a table with stress versus strain curves for different strain rates [55]. If strain rates fall within the curves for the specified rates, LS DYNA extrapolates the provided curves for that strain rate. If the strain rate exceeds the specified rate, LS DYNA uses the stress-strain curve for the maximum rate specified [55].

In a Round Robin exercise performed by NIAR [56], bare Aluminum 2024-T3 was tested at different strain rates. The data from bare Aluminum was used to scale the test data documented in section 2.2 to obtain the rate sensitive stress versus strain curves for Clad Aluminum 2024-T3 for this study. As specified in the standard ASTM B209-10 [57], the difference between Clad Aluminum and Bare Aluminum is that the Clad Aluminum consists of a very thin layer (approx. 0.2% thickness) of pure aluminum on the surface. The strain rate dependent material data used for this study is shown in Figure 58.

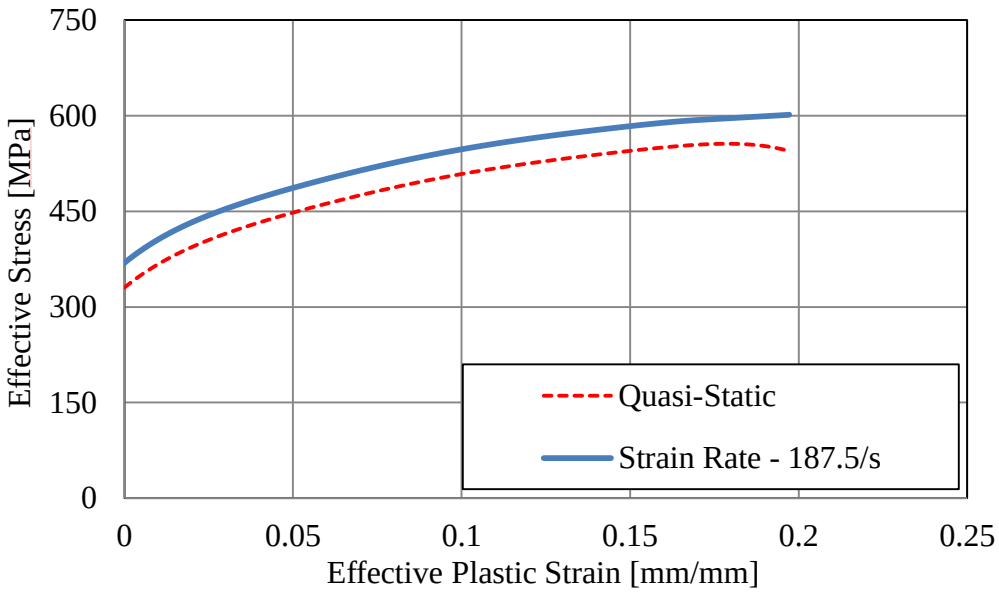

Figure 58. Clad Aluminum 2024-T3 Material Data for Quasistatic and Strain Rate 187.5/s

3.7 FE Simulation Parameters Studied

First, the study is performed at quasi-static strain rates where four different simplified bolt modeling techniques (each has more variations) are compared to the detailed 3D FE bolt model (ideal representation). For each comparison, the load transfer (%LT), energy stored in the bolt, energy stored in 1 inch long patch around the bolt (in both main part and load transfer part), overall energy distribution, stress/strain fields around the joint, shear and normal force on bolt and failure modes are investigated. Further the strain rates, friction and preload were varied on the detailed FE model and a selected simplified model. The effect of these variables on the simplified bolt model is studied

3.8 Calculations

For presenting the FE simulation results, some of the parameters were calculated as explained in subsequent sections.

3.8.1 Load Transfer

The load transfer calculation for the simulations differs slightly from that used in the test. In the test, strain gages were only used on the surface and due to that, the effect of secondary bending on load transfer was not captured by the test. Secondary bending is explained in section 1.3.4. Therefore, to account for secondary bending, the load transfer for all the simulations was evaluated using cross sectional forces. The cross sections were located at the same locations as the strain gages as shown in Figure 59. Equation 3.5 is used to evaluate the percentage load transfer. *CS 1* is cross section 1 and *CS 2* is cross section 2

$$\% \text{ Load Transfer} = \left(\frac{Z\ Force\ on\ CS\ 1}{Z\ Force\ on\ CS\ 2}\right) \text{ x } 100\% \tag{3.5}$$

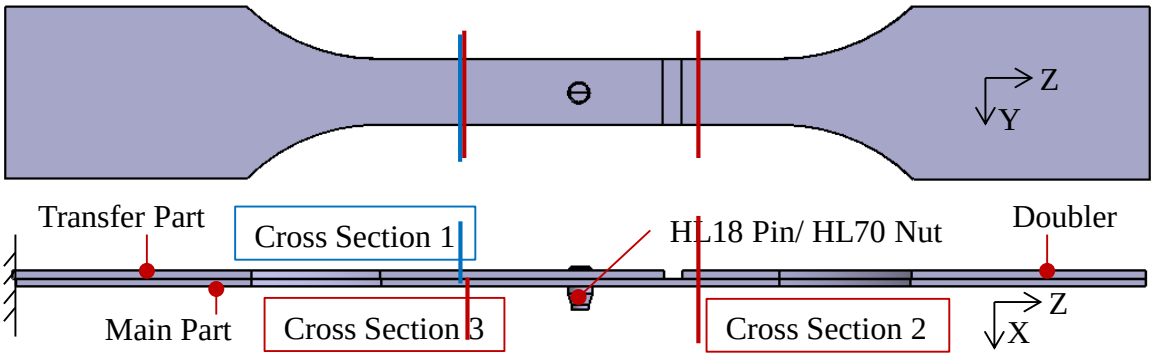

Figure 59. Cross Section Plane Locations on Single Shear Specimen

3.8.2 Load Transfer by Bolt and by Friction

The % load transfer by bolt and by friction was also evaluated. To accomplish this, a cross section plane was placed through the center of the bolt shank for both the solid model and the simplified models as shown in Figure 60. The load transfer by bolt was then evaluated using equation where CS 1 is the cross section plane that measures the load on the transfer part as shown in Figure 59. The remainder of the load is transferred by friction.

$$\%\ Load\ Transfer\ by\ Bolt = \left(\frac{Z\ Force\ on\ CS\ 4}{Z\ Force\ on\ CS\ 1}\right) x\ 100\% \qquad (3.6)$$

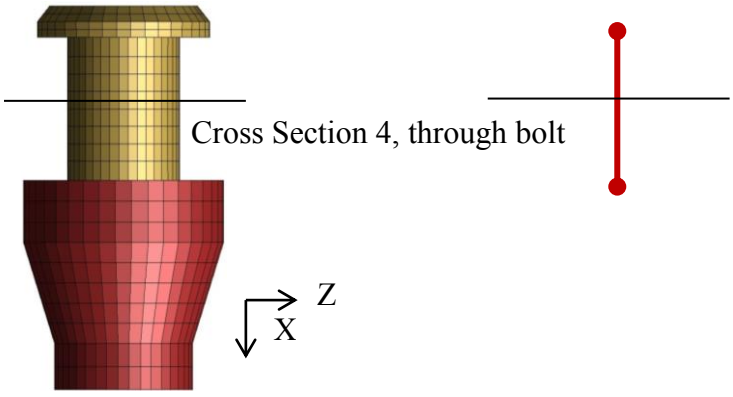

Figure 60. Cross Section Plane Location on Bolt

CHAPTER 4

FINITE ELEMENT MODELING - RESULTS

Detailed and simplified numerical models of the one half dog bone specimen assembly were generated to study the behavior of mechanical joints under single lap shear loading. In section 4.1, the analysis of the detailed FE model is presented and validated against test results presented in section 2.3. This is done to validate the FE modeling practices used in this study. In section 4.2 simplified FE models are generated and compared to the detailed FE model. For parametric studies, the material rate sensitivity, preload and friction are varied for the detailed FE model and a selected simplified model. Although the effect of friction and preload in the 3D model has been highlighted by Ghods [19], the effect of such parameters on simplified joint modeling is yet to be explored. The parametric study is documented in section 4.3.

4.1 Detailed FE Bolt Model

There are two main reasons for creating a 3D FE model for this study: 1) to validate the FE modeling methods (since 3D modeling is the most ideal way to represent the test) and 2) to extract data that cannot be collected from the test (such as energies, stress distribution and more) for evaluating the simplified bolt modeling techniques.

It should be noted that for the FE simulations, assumptions were made to simplify the models and reduce the computational cost. These assumptions are as follows:

1. The slack-inducer system, the grips and the test machine were not modeled in the simulations, and hence the compliance of these parts is not taken into account.
2. The friction value of 0.1 between the aluminum parts was used based on the study presented in section 4.3.3 and the friction value of 0 was used between the anti-buckling fixture and the specimen.

3. In the test, bolts were used to clamp the anti-buckling fixture with 10 in-lb torque on each bolt. In the simulation, the anti-buckling fixture was clamped using nodal rigid body elements (RBE).
4. In the test, the ABF was held in place using brackets and a bar attached to the MTS machine post while in the simulation a SPC constraint was utilized to represent this.
5. Average preload of all three tests was used for the simulations.

4.1.1 Validation of FE Model and FE Modeling Methods

Prior to presenting the comparison of the test and simulation data, it is important to understand the basic forces in the system as shown by the free body diagram in Figure 61. Force (F) is generated on the application of displacement and due to the displacement compatibility between the main part and transfer part [12], F is divided into load transfer force ($F_{transfer)}$ and bypass force (F_{bypass}). F_{bypass} is the load that remains in the main part and $F_{transfer}$ is the load that is transmitted to the load transfer part. $F_{transfer}$ is generated from a bearing force ($F_{bearing}$) resulting from pressure exerted by the bolt shank on the hole surface and a friction force ($F_{friction}$) resulting from mating of the sheets. Due to bolt preload, friction effect is localized under the bolt head and nut surface where maximum clamping occurs.

Figure 61 presents only a basic force distribution encountered by the specimen setup. It should be noted that load transfer is a rather complex phenomenon and factors such as the deformation of the hole, rotation of the joint, fastener bending, bolt clamp-up, hole preparation and friction level affect the load transfer as described in section 1.3.

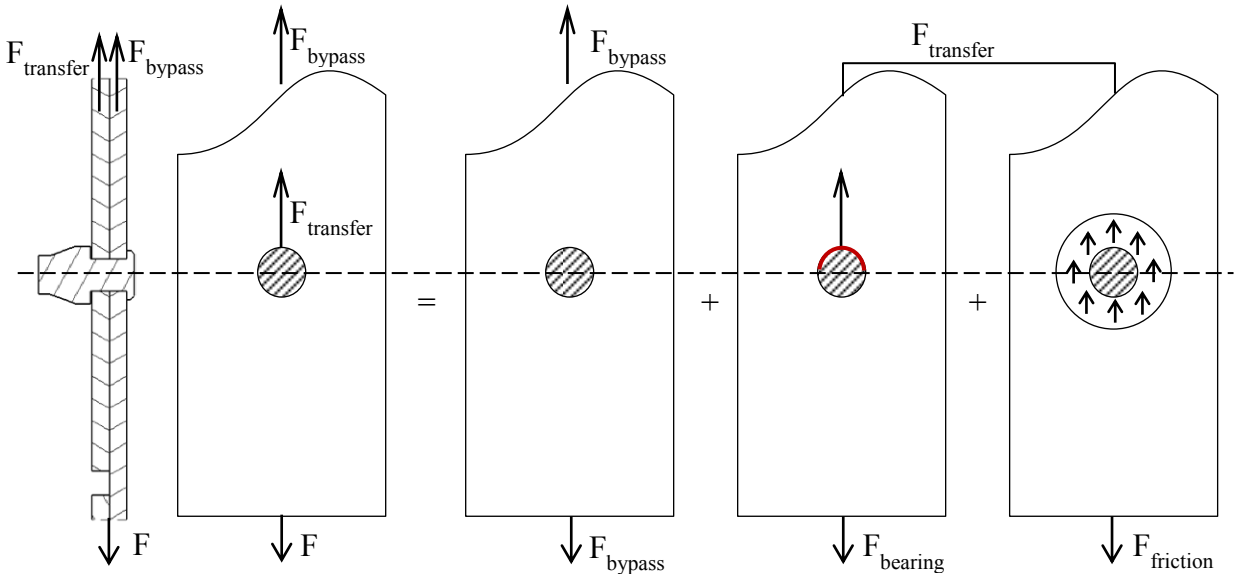

Figure 61. Static Force Distribution in Detailed FE Model

Figure 62 presents the comparison of simulation results to test data. Results from simulation were obtained in the same manner as the test was conducted that is the average strains were used for evaluating the %LT using equation (2.8). Strains were averaged from elements over the area and location of the strain gages (Figure 32).

The comparison presented in Figure 62 shows that the strains at the three strain gage locations and the %LT from the detailed FE model are in good correlation to the test data. For majority of the elastic portion, the %LT is in good agreement to the test data. It can be noted that at the beginning, when remote loads are very low the %LT for the simulation is different from the test. It should be noted that the simulation is not able to match 100% of the test data due to several unknown factors such as friction on faying surfaces and bolt preload which will vary for each test. In addition, the test specimens carry imperfections from manufacturing and specimen handling and such imperfections are not accounted for in the simulation. Also, simulation requires assumptions due to several limitations posed by the FE tool, time and cost constraints (section 4.1). Further, the %LT is evaluated using strains (equation (2.8)), and at very low remote

loads, the strains are very low hence even a small change in strains will result in a large change in % LT.

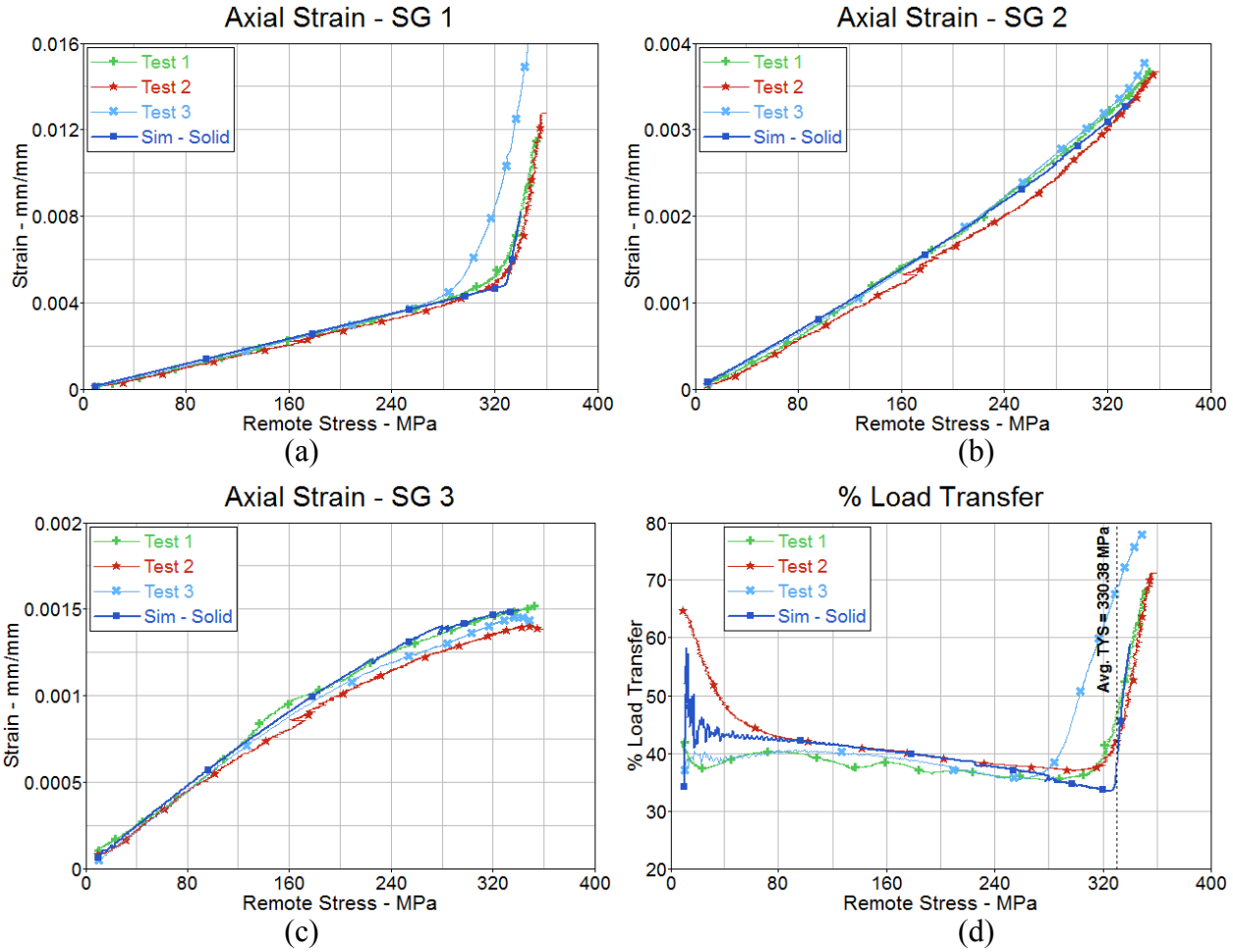

Figure 62. Detailed FE model (sim-solid) vs Load Transfer Test Results: (a) Axial Strain at Strain Gage 1 (b) Axial Strain at Strain Gage 2 (c) Axial Strain at Strain Gage 1 and (d) % LT

Comparison of the simulation results to the test data validates the FE modeling methods and hence the detailed FE model can be used to compare and evaluate the simplified bolt modeling techniques.

4.1.2 Kinematic Frames

Due to the presence of a hole, stress concentrations and hence failure are expected along the center line of the hole perpendicular to the direction of loading as shown in Figure 63. The

expected necking and failure, as seen on the test, is attained through the simulation model as shown in Figure 64.

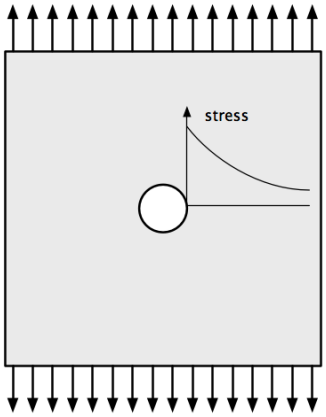

Figure 63. Stress Concentration in Plates with Hole

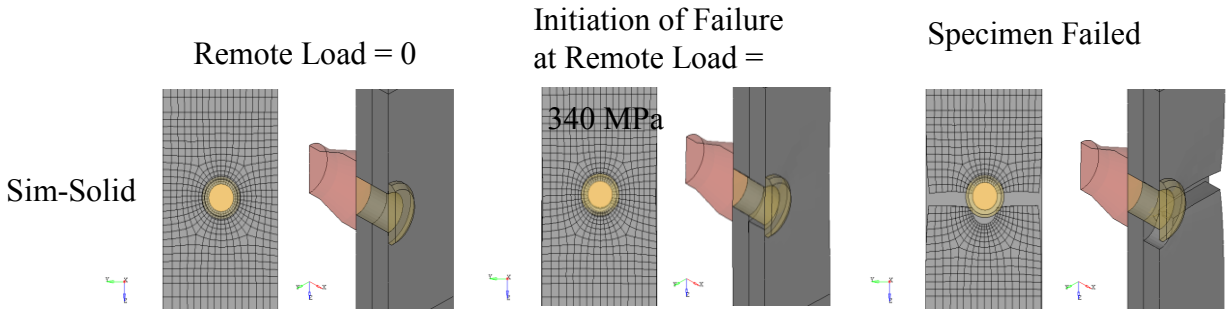

Figure 64. Kinematic Frames for Solid Model

4.1.3 Stress and Strain Profiles

Figure 65 shows the stresses developed on the plates from the application of bolt preload. High compressive stresses, in the magnitude of 30 to 160 MPa, occur in a localized area beneath the head and the nut. As a result, friction forces are higher in that region. These friction forces affect the load transfer within the joint system.

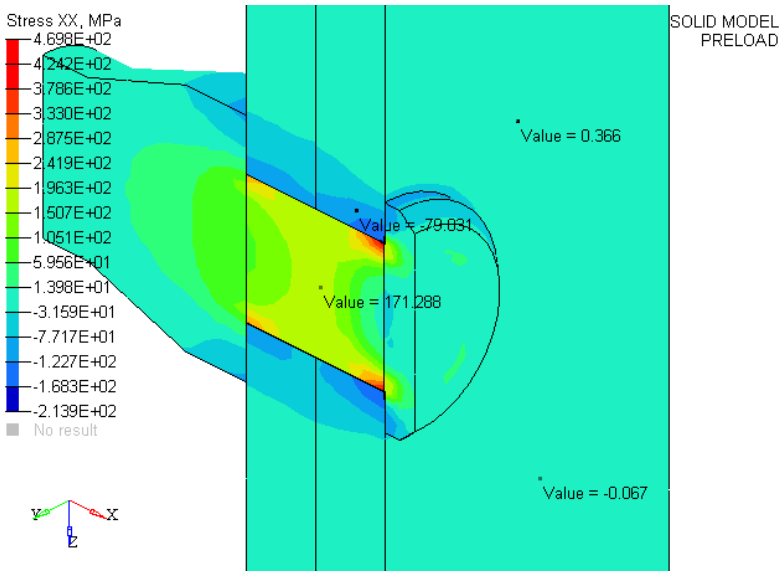

Figure 65. Clamping Stresses Due to Preload Application on Detailed FE Joint Model

The state of stress at the initiation of failure on the main part is shown in Figure 66. The stresses at the edge of hole agree with the expected state of stress as shown in Figure 63.

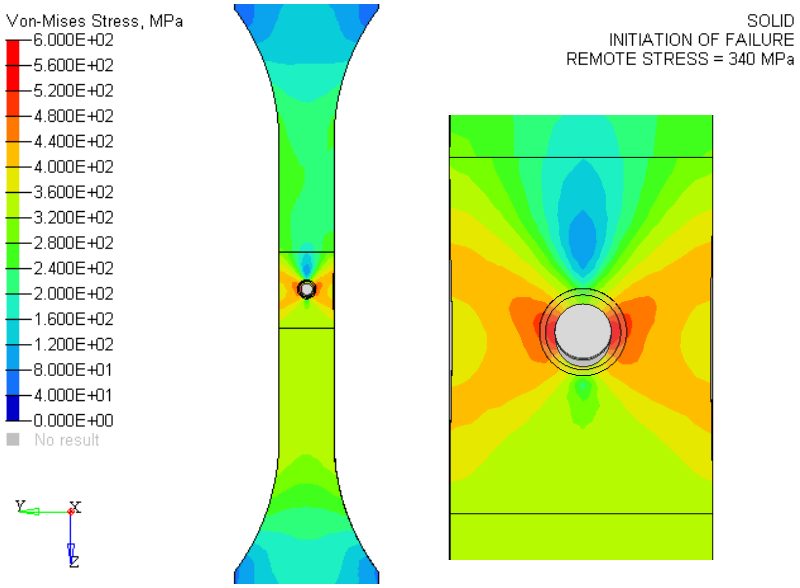

Figure 66. VonMises Stress on Main Part: Solid Model

4.1.4 Bolt Loads

Figure 67 shows the load transferred to the transfer part, the shear force on bolt and the % LT by the bolt. The %LT can be divided into bearing force and friction force. The bearing

load translates into shear force in the bolt, while the friction force is dictated by the clamp-up of the bolt. Based on the clamp-up stress distribution shown in Figure 65, high friction forces are expected in the vicinity of the joint. As loading begins, load is transferred only through friction until the bolt comes in contact with the hole surface. At this point, the bearing loads kick in and end fixity of the bolt head and nut occurs due to fastener rotation which results in fastener bending and higher shear force on the fastener. As a result, the %LT shifts dependency from friction to the bolt. Thus based on Figure 67, it can be noted that at the beginning of the simulation, majority of the load is transferred by friction and towards the end of the simulation only up to 20% of work is done by friction.

Figure 68 shows the axial force on the bolt of the solid model. The decrease of axial load can be attributed to the following mechanisms occurring in the joint system. On continued application of loading, the specimen length increases and the thickness at the gage section (in this case, the area around the hole) decreases due to Poisson's ratio effect. As a result the preload applied to the bolt, which is a tensile load, relaxes and thus the axial load decreases. On the other hand, continued application of axial load to the specimen results in bearing loads acting on the hole of the plates. The bearing loads result in compressive forces on the surface of the hole which causes the thickness to bulge up, thus adding to the axial load. In addition to these mechanisms, due to the end fixity condition of the fastener the bolt shank experiences bending which also adds to the change in axial loads.

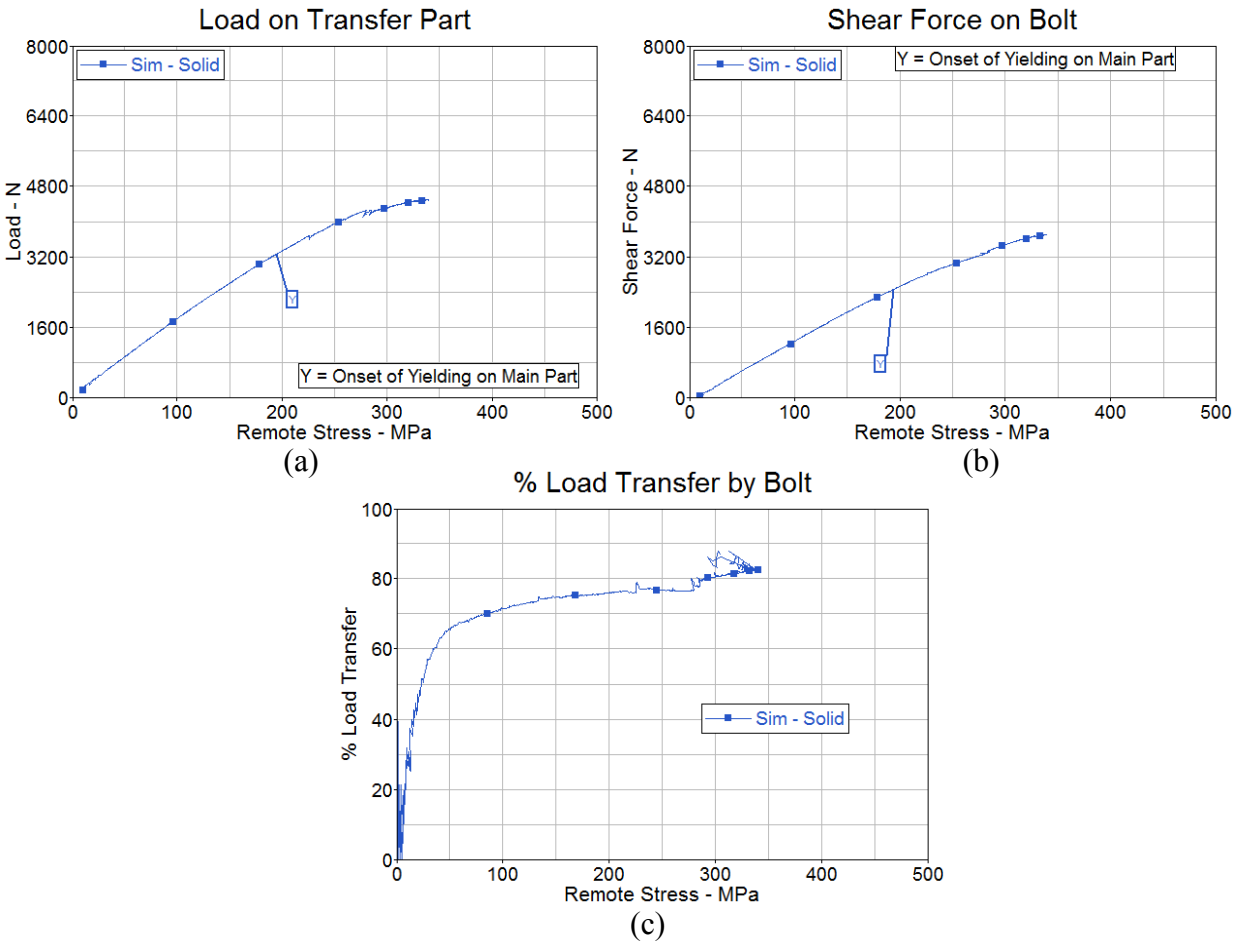

Figure 67. Load Transferred by bolt on Solid Model (a) Load on transfer part, (b) Shear force on bolt and (c) %LT by bolt

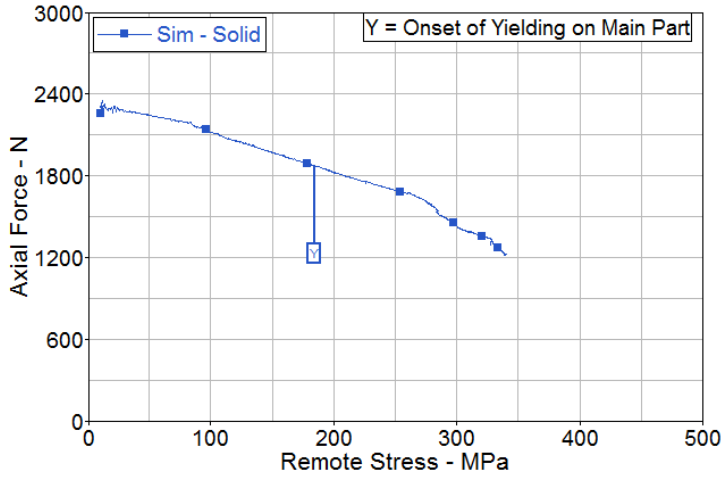

Figure 68. Axial Force on Bolt Solid Model

4.1.5 Energy

The energy levels seen on the solid model simulation are summarized in Figure 69. It can be noted that majority of the total energy is translated into internal energy and some into interface energy. The eroded internal energy is the energy stored in the deleted elements and is already included within the internal energy plot shown in Figure 69(a).

Figure 69(b) shows a comparison of internal energy versus remote stress. It can be noted that the total internal energy level in the system amounts to approximately 18 J. For the solid model up to 16 J (approx. 88 %) of internal energy is stored in the joint, which is comprised of the 1 in patch on the main part and load transfer part and the bolt. It can be noted that most of the energy within the joint is stored in the 1 in patch on the main part where failure occurs.

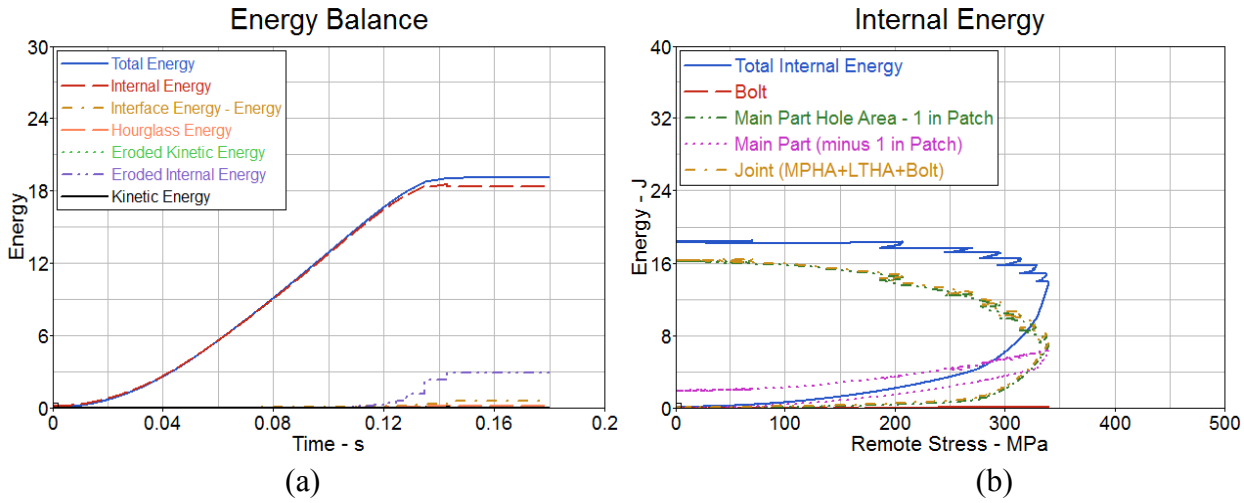

Figure 69. Energy levels from Solid Model (a) Energy Balance (b) Internal Energy Distribution

4.2 Simplified FE Bolt Models

The assumptions specified in section 4.1, for the detailed FE model, also apply to the simplified bolt FE models.

4.2.1 Configuration 1 – RBE Bolt Model

Three different variations, one a fine mesh and two coarse mesh models, of the RBE Bolt Model are compared to the detailed FE model. The RBE bolt models have been described in detail in section 3.1.2. To obtain a better understanding of this setup, the static forces related to the RBE bolt model are shown in Figure 70.

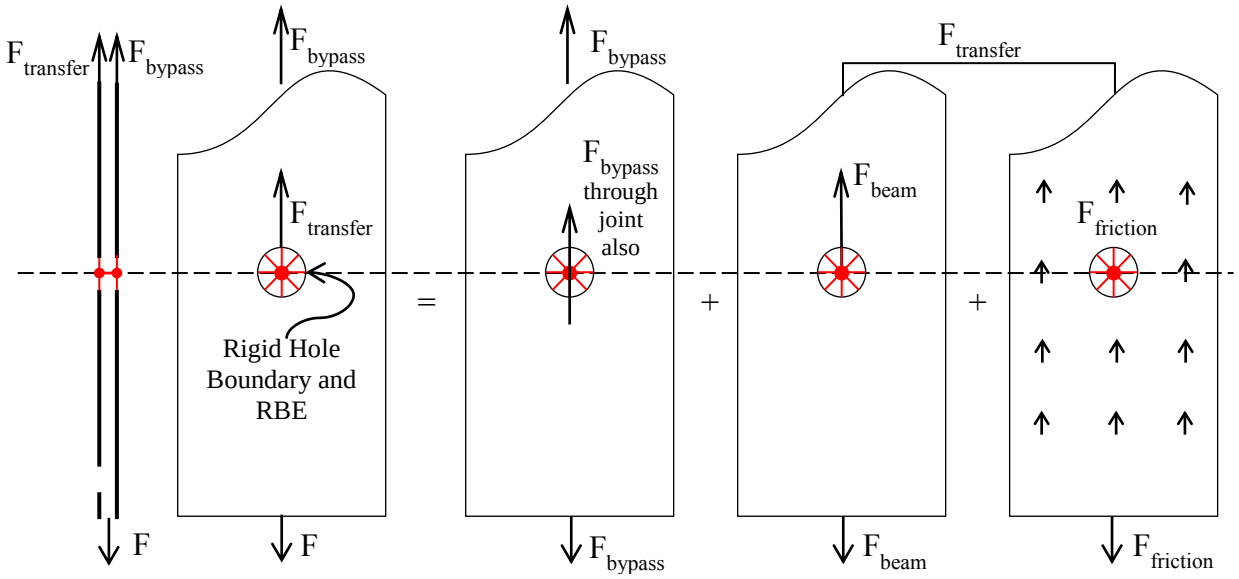

Figure 70. Static Force Distribution in RBE Bolt Model

The force (F) introduced in the system is split into transfer force ($F_{transfer}$) and bypass force (F_{bypass}) due to displacement compatibility enforced by the presence of the bolt [12]. F_{bypass} is the load that remains in the main part and $F_{transfer}$ is the load that is transmitted to the load transfer part. The bolt shank in the RBE bolt model is represented by beam element and the nodes of the beam are connected to the respective side fastener hole boundary using rigid body elements (RBE). Thus all the RBE share a common node, which is the node of a beam. As a result, the RBE also play a part in F_{bypass}. Since the hole boundary is rigid, and moves with the beam node, there are no bearing loads in this model. $F_{transfer}$ is via the shear loads (F_{beam}) registered in the bolt and friction force between the plates ($F_{friction}$). The bolt head and nut are not

modeled in this setup and hence the clamp-up loads on the plates are no longer localized as is the case in the solid model. In addition, since the plates are a continuum the clamping forces will be distributed throughout the plate and the localized effect of friction due to clamping won't be present. Thus the contribution of $F_{friction}$ to $F_{transfer}$ will be less than in the Solid model.

4.2.1.1 Load Transfer

The percentage load transfer for this comparison was evaluated using equation (3.5). The following points can be deduced from the comparison of %LT between the detailed solid model and the RBE bolt model as shown in Figure 71.

The load transfer comparison indicates that the three variations of configuration 1 have very similar %LT. As described in section 4.2.1 this simplified bolt modeling techniques uses rigid body elements to connect the bolt (modeled as a beam) to the bolt hole. As a result, the nodes on the boundary of the hole are rigid and do not undergo any deformations (only rigid body motion). This indicates that the load transfer is not sensitive to mesh size.

The %LT is higher for all the RBE bolt models when compared to the detailed solid model. Since the nodes of hole are coupled with the beam using RBE, all those nodes undergo similar displacements. As a result, the fastener does not undergo bending and the fastener hole will not deform. In addition, friction does not play a major role in the load transfer process since the clamp-up loads are not localized. Due to these events the %LT in RBE models is higher than solid model.

It can also be noted from Figure 71 that failure on the RBE bolt models occurs at a higher remote stress compared to the solid model. Due to the rigid hole and use of RBE, stress concentrations occur at different locations in the models. The stress concentrations are dependent on the orientation of the RBE elements (generally occurs at the first rigid node on the load

introduction side). In the solid model, the net section area is smaller due to the fastener hole while in the RBE models even though there is a hole it behaves as a continuum due to the rigid links and thus the net section is larger. As a result, RBE models require larger remote load to fail.

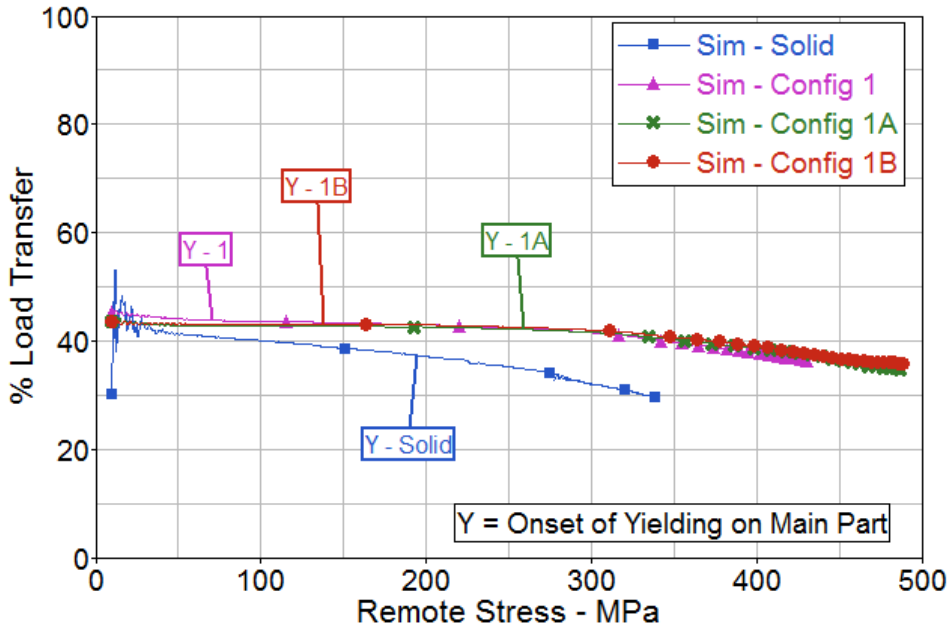

Figure 71. Load Transfer Comparison of Configuration 1 – RBE Bolt Model to Solid Bolt Model

4.2.1.2 Kinematic Frames and Failure Modes

The kinematics for the solid model and simplified RBE bolt models is shown in Figure 72. In comparison to the Solid Model the failure mode for configurations 1, 1A and 1B is also tear-out of the main part, but this occurs on the load introduction side of the main part, in front of the bolt hole. Also necking on the main part occurs on the load introduction side of the main part. In comparison to the solid model, this simplified technique is quite different in terms of failure mode and remote stress at failure.

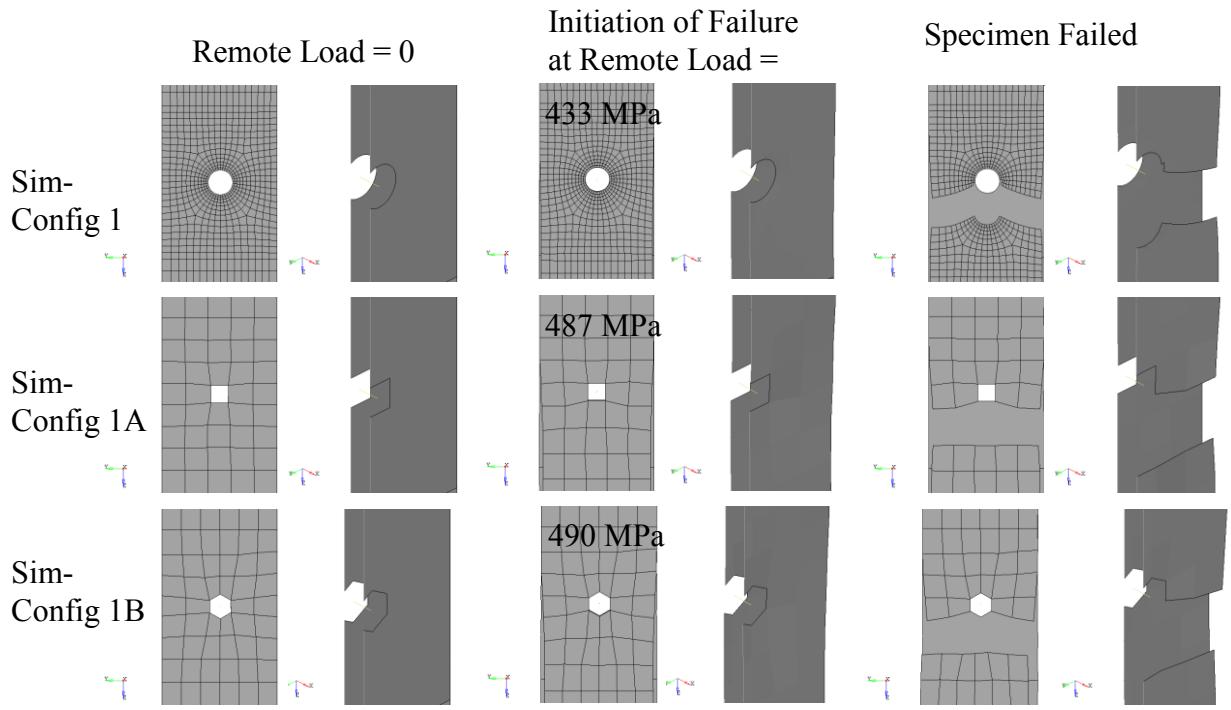

Figure 72. Kinematic Frames Comparing Solid model to RBE Bolt Models

4.2.1.3 Stress and Strain Profiles

The preload measured in the test was applied to all the FE models. For different bolt modeling techniques the stresses that develop in the vicinity of the bolt hole, as a result of the application of preload, are quite different. The stresses developed on the main part and transfer part of the solid model due to preload are shown in Figure 65. Since the bolt head and nut are not modeled for the simplified techniques, on the application of preload, the localized compressive stresses (seen in solid model) are not present in such models as shown in Figure 73. Therefore, although preload is applied to this simplified model, the localized effect of preload are not captured by this technique and thus preload may not have an effect on the overall performance of the specimen. On the other hand, the preload on the bolt itself is sustained which may improve the performance of the beam itself.

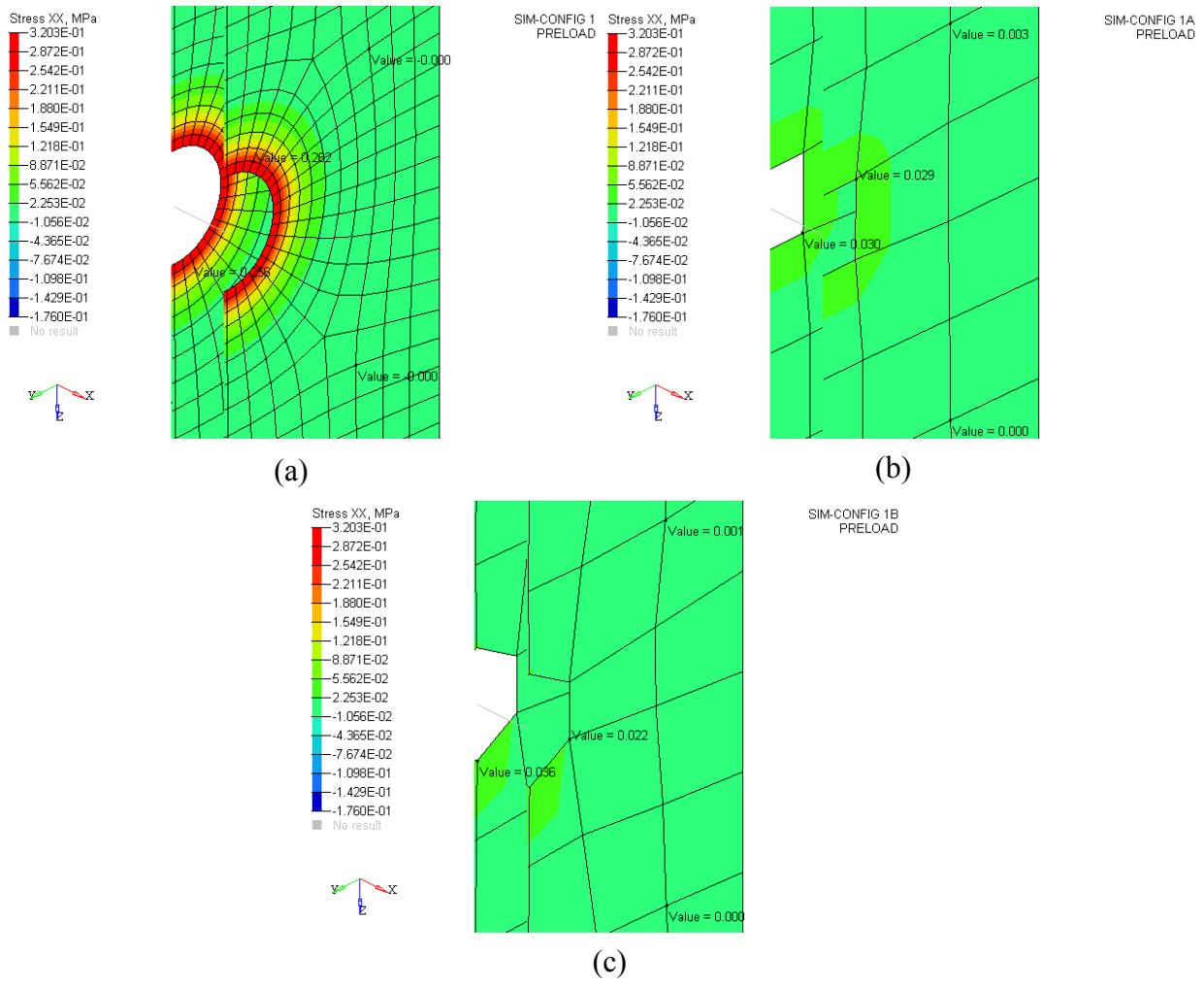

Figure 73. Stresses due to Preload Application (a) Sim-Config 1 (b) Sim-Config 1A and (c) Sim-Config 1B

Figure 66 shows the state of stress (vonMises stress) at the initiation of failure on the main part of the Solid model and Figure 74 shows the comparison of the state of stress on the main part of simplified RBE bolt models. These provide an indication of the location of stress concentrations. It can be noted that when the mesh is changed, the location of the first rigid node on the load introduction side also changes thus the stress distribution in the vicinity of the bolt is different for each case. In addition, stress concentrations occur at different locations for the

simplified models which indicate that failure will occur at a different location compared to the Solid model (this is shown in Figure 72).

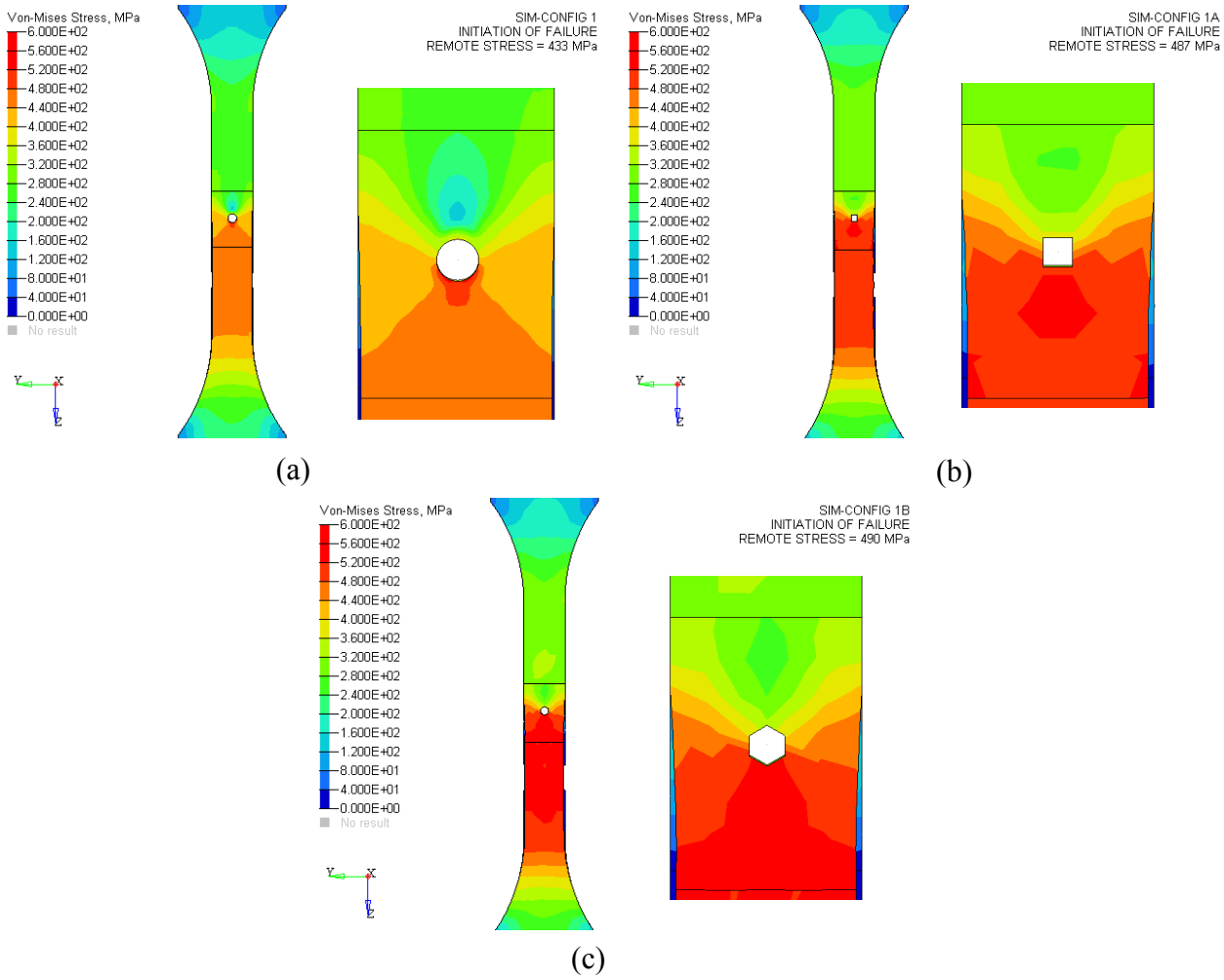

Figure 74. VonMises Stress Comparison on Main Part (a) Sim-Config 1 (b) Sim-Config 1A and (c) Sim-Config 1B

Strains, at the strain gage locations shown in Figure 32, are compared in Figure 75. These strains provide an indication of the state of loading at locations further away from the fastener hole. For all the simplified RBE bolt models, strains at strain gage 1 location are in good correlation to the solid model. This indicates that the use of shell elements in simplified models

is sufficient to capture the stress-strain distribution. On the other hand, strains at strain gage 2 and strain gage 3 are similar to the solid model only at low remote loads (less than 150 MPa). Deviations in strains between the solid and simplified models are seen after this point. This can be attributed to the differences in load transfer for the different models. As shown in Figure 71, load transfer is higher for simplified models, and higher transferred loads result in higher strains on transfer part as seen on Figure 75 (d).

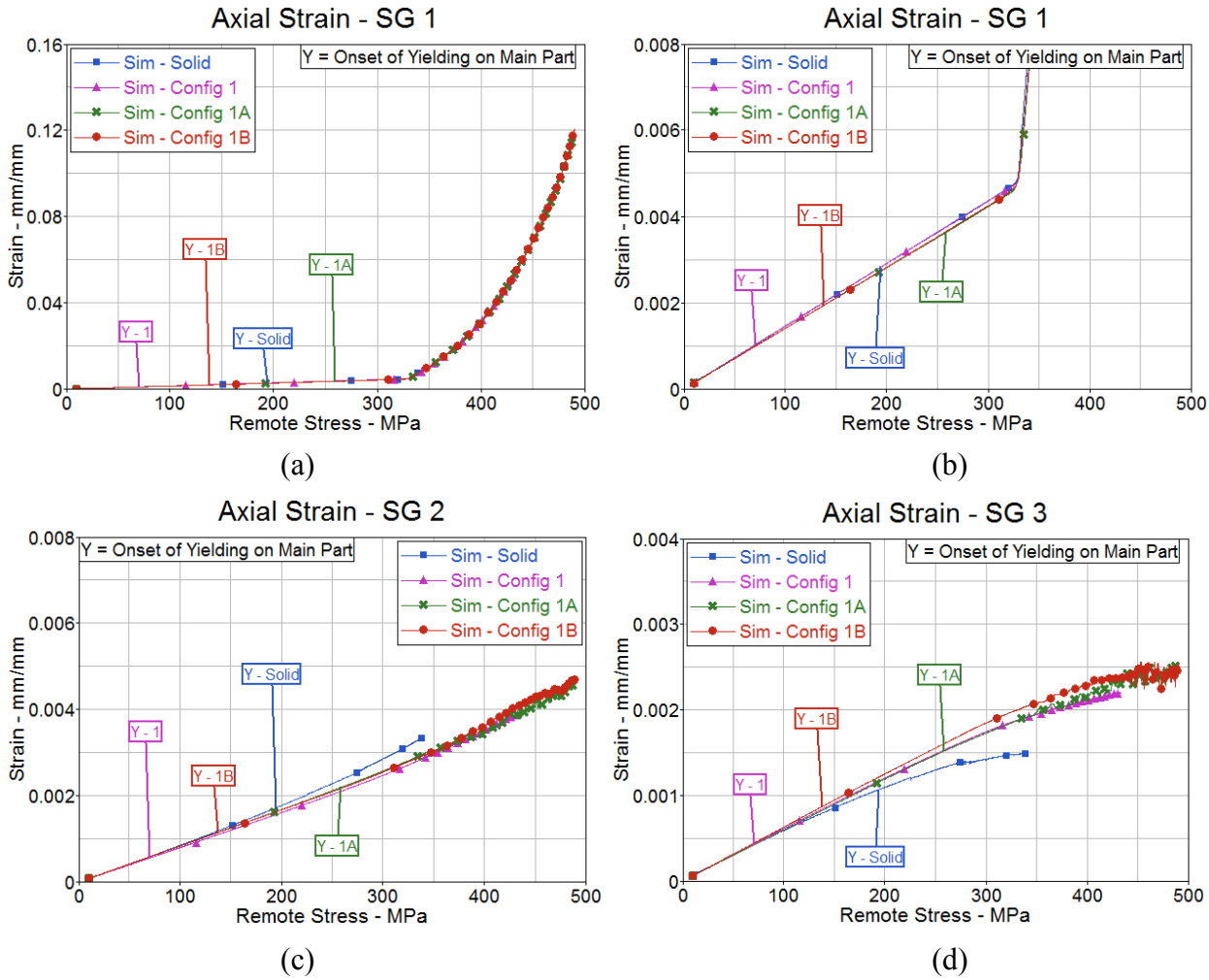

Figure 75. Axial Strain vs Remote Stress for RBE Bolt Models (a) Strain gage 1 (b) Strain Gage 1 (close-up) (c) Strain Gage 2 and (d) Strain Gage 3

4.2.1.4 Bolt Loads

In addition to the %LT, it is interesting to understand what percentage of load is transferred by the bolt versus the percentage of load transferred by friction. This can be deduced by comparing the shear force on the bolt and the load recorded in the cross-section plane on the load transfer part as shown in Figure 76. For the simplified RBE bolt models, the boundary of the hole is rigid and connected to the bolt and thus majority of the load passing through that region gets transferred to the bolt. Thus higher percentages of loads are transferred through the bolt in the RBE bolt models. In addition, Figure 73 indicates that the compressive stresses due to bolt preload are negligible on the simplified models and thus resulting in lower load transferred through friction. The effect of this can be seen on Figure 76 (c), where the load transfer by friction lasts for very low remote loads on the simplified models compared to the solid model.

For the solid model, the load transferred by the bolt is around 75% on average compared to 96% in the RBE Bolt models. The remaining load is transferred by friction. From Figure 76 (c) it can be noted that for all the models %LT by the bolt starts from zero and increases with increasing remote stress. When the loading begins, the bolt is not engaged, at low remote loads, and the load transfer is carried out purely by friction. As the bolt gets engaged, bearing loads kick in and the bolt starts picking up load.

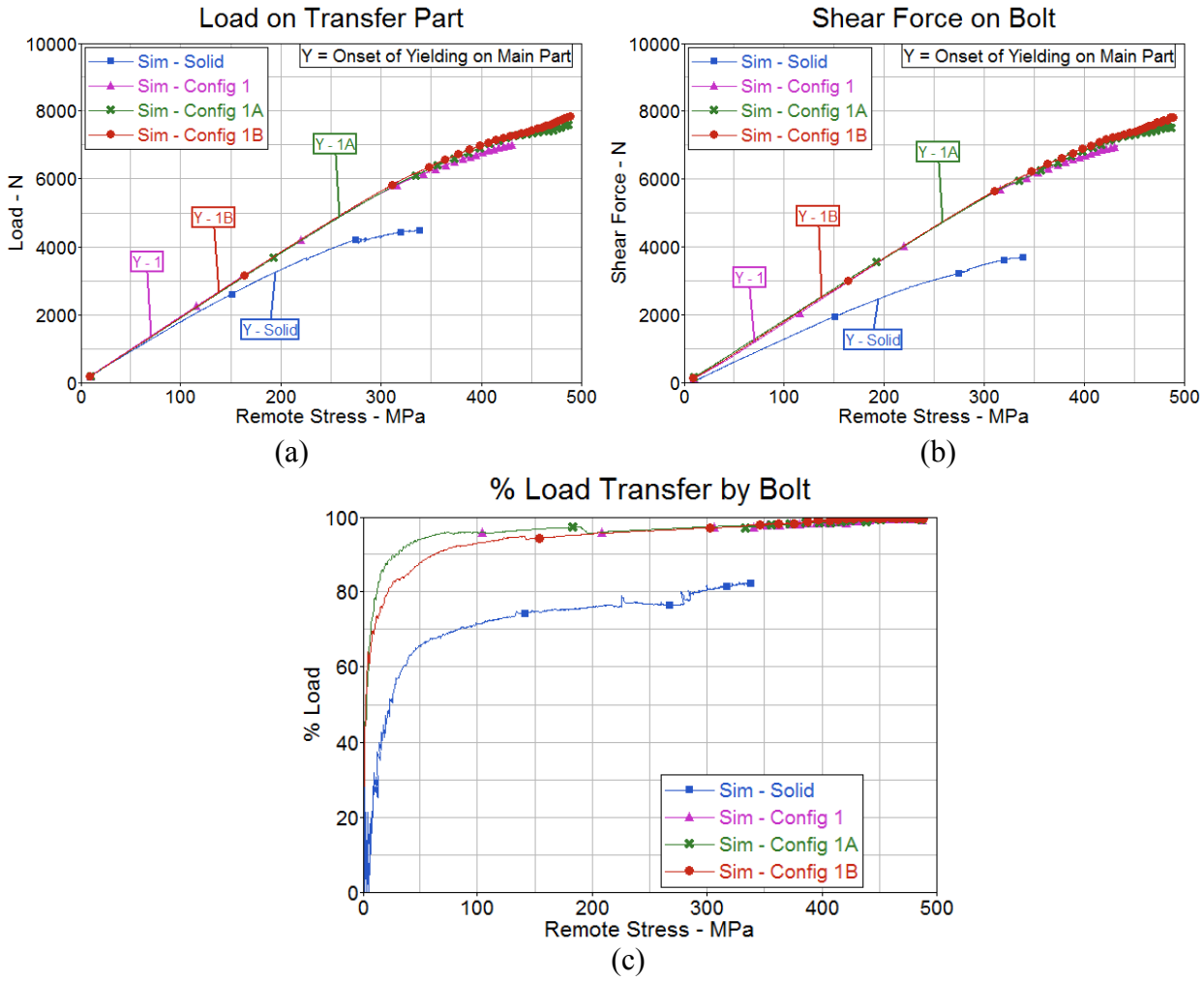

Figure 76. Comparison of Loads transferred by bolt (a) Load on Transfer Part (b) Shear Force on Bolt and (c) % LT by Bolt

Figure 77 shows the comparison of axial loads on the bolt. As expected, the initial axial load for all the models is approximately 2300 N, which is the preload applied to all the models. Configurations 1 and 1B show good correlation to the solid model, especially at low remote loads. The RBE bolt models also exhibit a drop in axial load as the solid model. The orientation of the RBE to the direction of loading is different on configuration 1A and 1B and that seems to affect the axial loads.

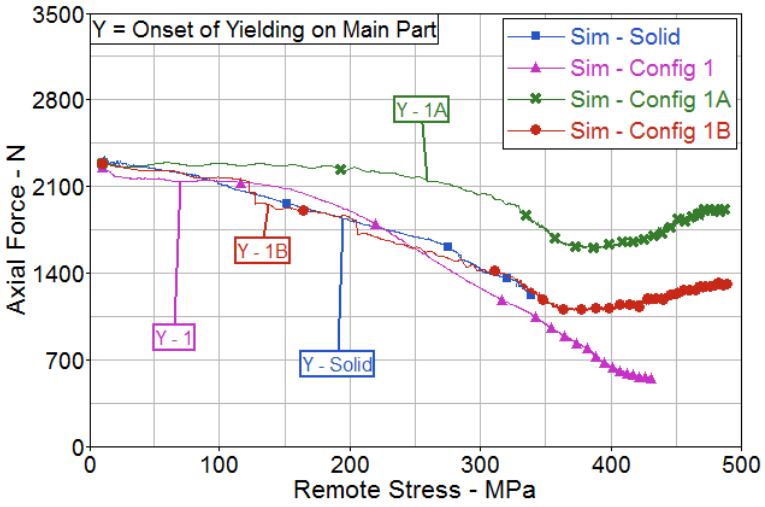

Figure 77. Comparion of Axial Force on Bolt – Solid vs Simplified Config 1

4.2.1.5 Energy Comparison

Figure 78 presents the energy distribution for configuration 1B to represent the energy distribution seen for this technique. As described in section 3.1, one inch long patch of elements in the vicinity of the bolt, on the main part and transfer part, were placed in separate components. The strain energy in these areas and the strain energy in the bolt shank, at different remote loads, is compared to the solid model in Figure 79 and Figure 80 respectively.

In comparison to the energy distribution in the solid model (total energy ~ 19 J), this simplified technique shows a total energy of approximately 170 J. The energy levels are higher for the simplified model because the simplified models reach failure at much higher remote stress thus inputting more energy into the structure. In addition, for this simplified model, majority of the internal energy (approx. 120 J or 71%) is stored in the main part and not within the joint. The joint which is comprised of 1 in patch on the main part and load transfer part and the bolt only stores 29 % of total internal energy at failure. This can be attributed to the shift in stress concentrations, towards load introduction side, created by the simplified joint. In addition, large amounts of plastic strains are also seen at the strain gage 1 location on the main part (see

Figure 75) which is a contributing factor to the internal energy. Note that the energy distribution shown in Figure 78 may not apply to the fine mesh model (Config 1) but since the focus of this study is crashworthiness, larger mesh models are focused on.

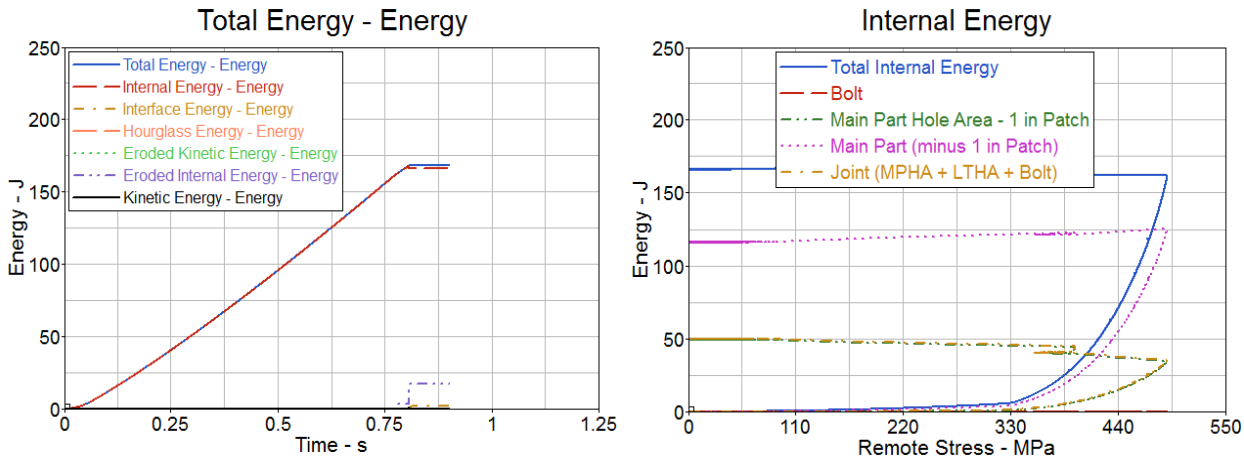

Figure 78. Energy Distribution in Configuration 1B (a) Energy Balance (b) Internal Energy

Based on Figure 79 the energy in the Solid model is higher than the simplified because the Solid model consists of a deformable hole where stress concentrations are found and thus high strains are found in that region for both the main part and transfer part. High clamp-up stresses present in the solid model explain the high initial strain energy. The use of RBE's in the simplified models results into a rigid hole boundary and thus deformations are mitigated away from that region through higher load transfer therefore lower strains are recorded in the 1 in patch of the main part and transfer part.

The energy in the bolt shank, shown in Figure 80 is higher in the RBE Bolt models compared to the solid model. This result is expected since the shear force on the bolt shank of the simplified models is much higher than the solid model, as shown in Figure 76 (b).

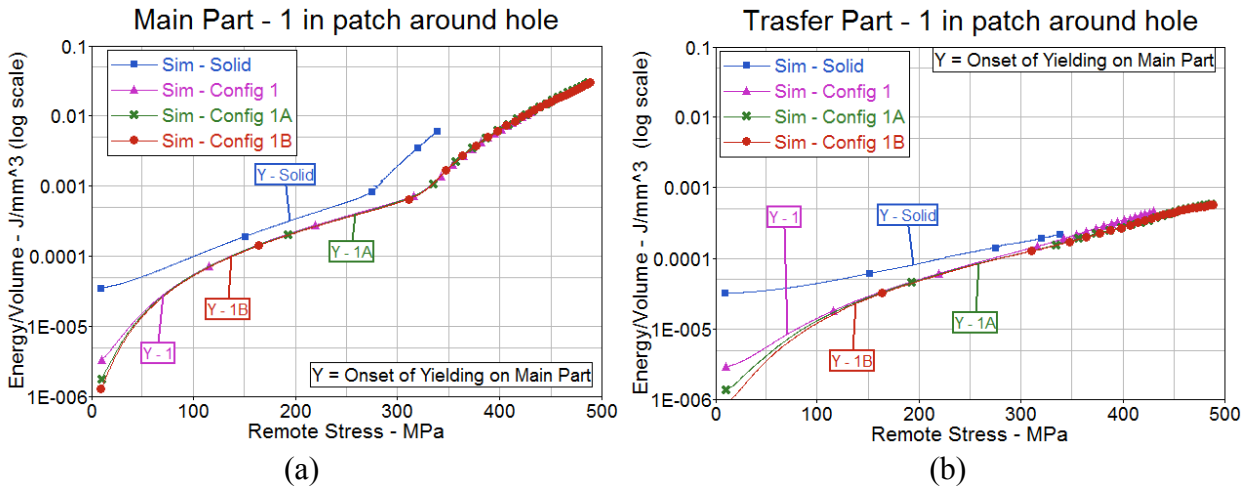

Figure 79. Comparison of Strain Energy per Volume in 1 in. long patch (a) Main Part (b) Transfer Part

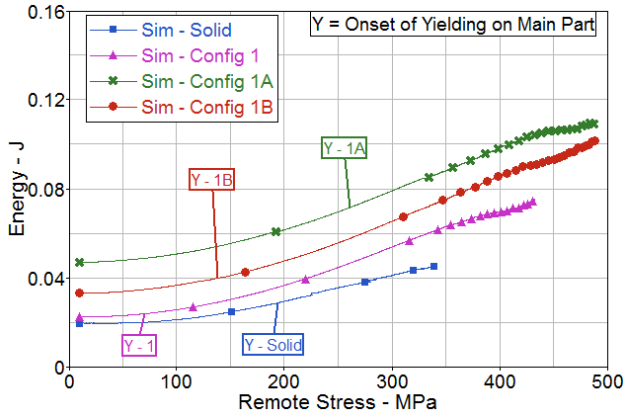

Figure 80. Comparison of Strain Energy in Bolt Shank versus Remote Stress – Configuration 1

4.2.2 Configuration 2 – Mesh Independent Spotweld Beam

Many different configurations exist for this type of simplified connection, but selected 11 configurations are compared in this study. Six of the configurations (2 – 2E) are such that the location of the node of the bolt (modeled as beam), with respect to the element, is the same on both the main part and load transfer part while on the remaining five configurations (2K – 2O), the locations vary. Detailed explanation of the setup of this simplified bolt modeling technique is

provided in section 3.1.3. To obtain a better understanding of this setup, the static forces related to this simplified technique are shown in Figure 81.

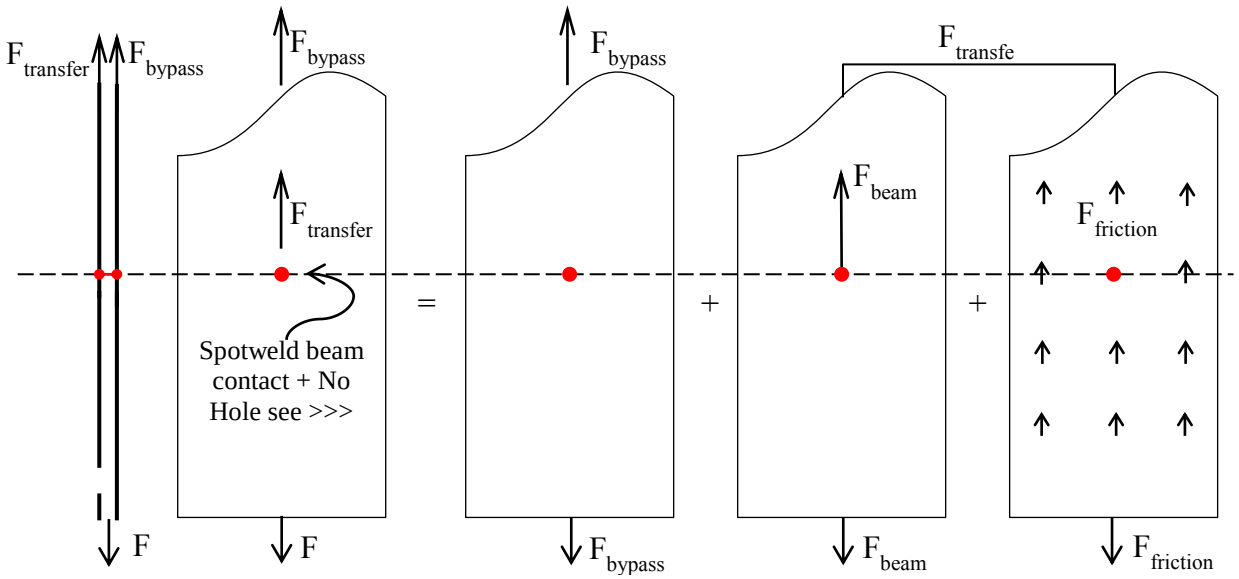

Figure 81. Static Force Distribution in Mesh Independent Spotweld Beam Model

The force (F) introduced in the system is split into transfer force ($F_{transfer}$) and bypass force (F_{bypass}) due to displacement compatibility enforced by the presence of the bolt [12]. F_{bypass} is the load that remains in the main part and $F_{transfer}$ is the load that is transmitted to the load transfer part. The bolt shank is represented by beam element and the nodes of the beam are connected to the plates by a tied contact, *CONTACT_SPOTWELD. Tied contact couples the nodes of the connected segment to the bolt node, as detailed in section 3.4.1, thus there are no bearing loads in this model. Since there is no fastener hole in this modeling technique, the joint is a continuum and thus facilitates some F_{bypass} load to pass through. $F_{transfer}$ is via the shear loads (F_{beam}) registered in the bolt and friction force between the plates ($F_{friction}$). The bolt head and nut are not modeled in this setup and hence the clamp-up loads on the plates are no longer localized as is the case of the solid model. In addition, since the plates are a continuum the clamping forces will be distributed throughout the plate and the localized effect of friction due to clamping won't

be present. Thus the contribution of $F_{friction}$ to $F_{transfer}$ will be significantly less compared to the solid model.

4.2.2.1 Load Transfer

The %LT of the different configurations of mesh independent spotweld beam model is compared to the detailed FE model in Figure 82 and Figure 83. Based on the comparison, a lot of scatter is observed in the %LT results. Less scatter is observed in the models where the beam contact point is different on main part and transfer part as seen on Figure 83. An attempt is made to understand the underlying factor affecting the %LT.

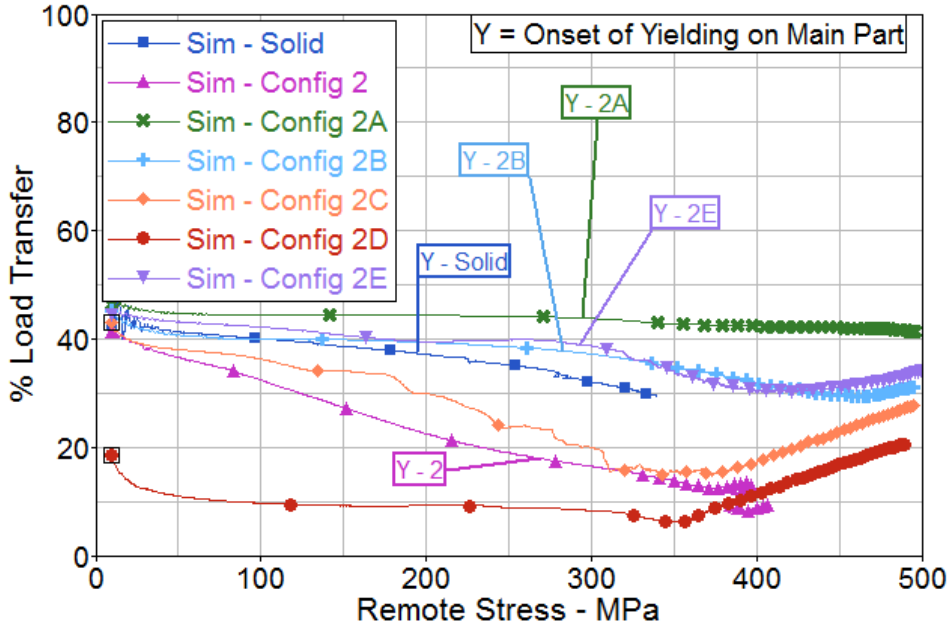

Figure 82. Load Transfer Comparison of Config 2 Mesh Independent Spotweld Beam - Similar mesh on Main Part and Transfer Part

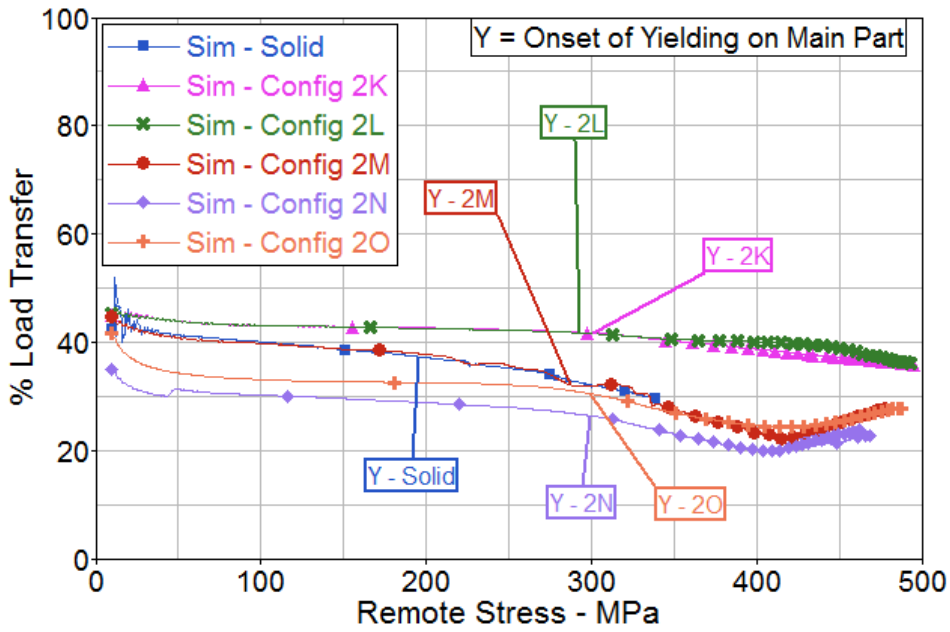

Figure 83. Load Transfer Comparison of Config 2 Mesh Independent Spotweld - Beam Mesh different on Main Part and Transfer part

From the explanation of the how *CONTACT_SPOTWELD works, detailed in section 3.4.1, it is understood that the constraints change based on the location of contact point. It is speculated that the change in constraints affects the bending stiffness of the contact region which in turn affects the load transfer. It can be said that the higher the bending stiffness, the higher the load transferred. To prove this point four configurations, configurations 2B, 2L, 2M and 2N, are compared. These configurations are chosen because they all they have same contact point on the main part and different contact points on the load transfer part as shown in Figure 84. Thus the bending stiffness of the load transfer part will be analyzed for these models and correlated to the load transfer.

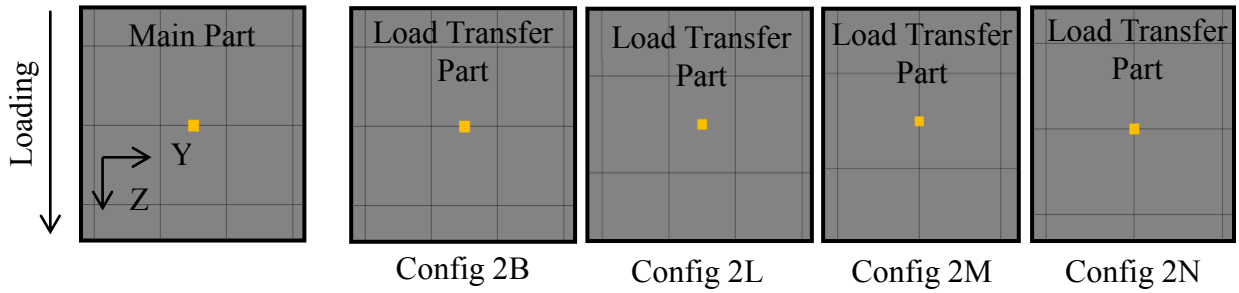

Figure 84. Configurations chosen for Further Analysis

In order to understand how the bending stiffness changes, the nodes and elements affected by the contact point have been highlighted in Figure 85. Therefore just by analyzing Figure 85, one can deduce that Config 2L will have the highest bending stiffness on the load transfer part followed by Config 2B, Config 2M and Config 2N with the least. This is also reflected in the comparison of %LT of these four configurations shown in Figure 86.

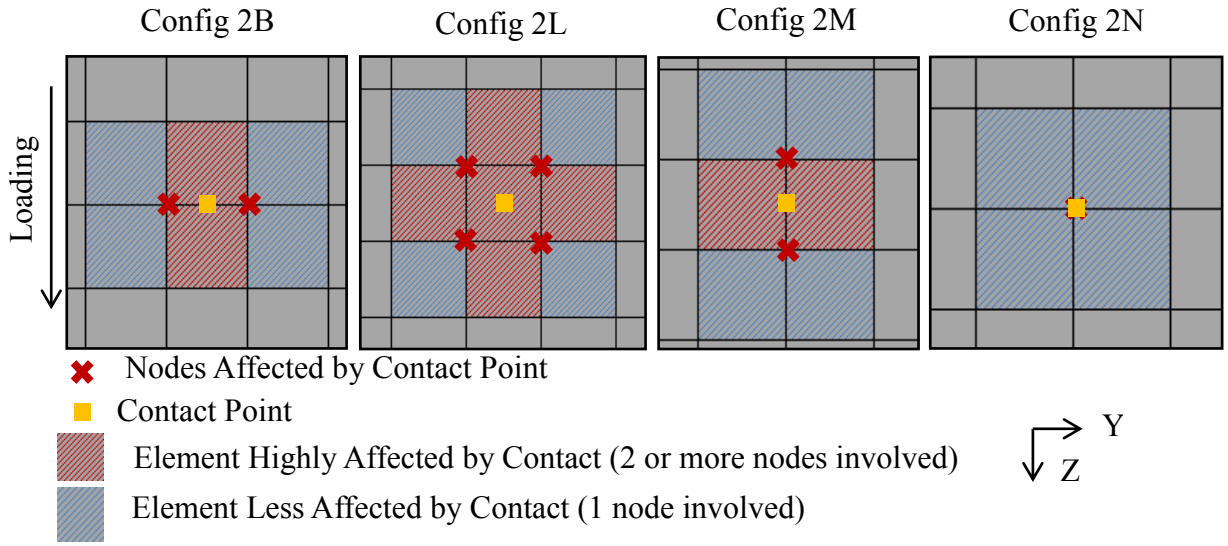

Figure 85. Nodes and Elements affected by Contact Point on Load Transfer Part

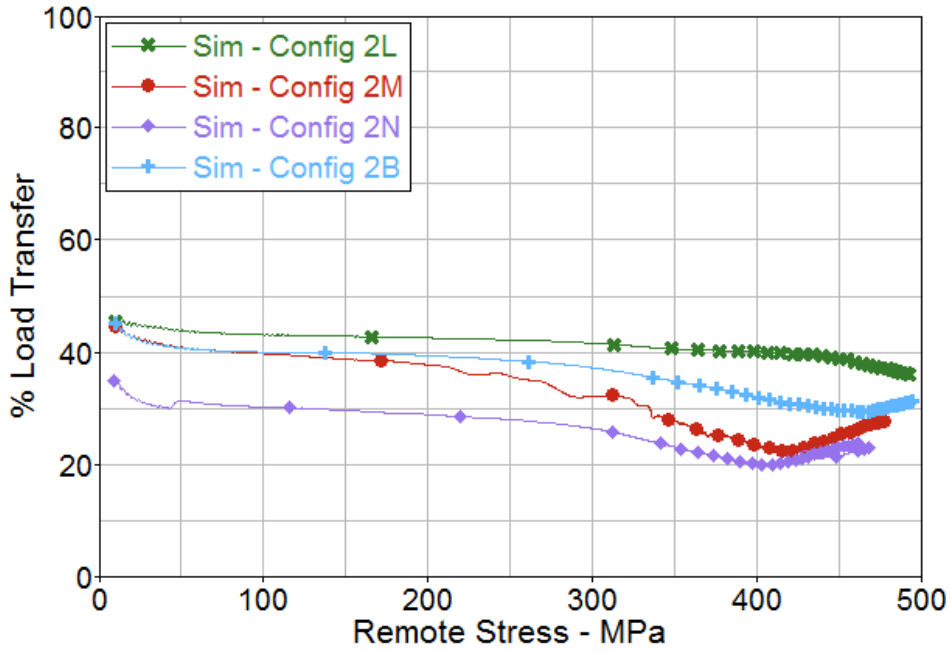

Figure 86. %LT Comparison for Config 2B, 2L, 2M and 2N

To further support the point, the bending stiffness for each of the models is analyzed by plotting the out of place displacement of the contact region as shown in. The configuration with the highest bending stiffness is expected to have the lowest out of plane deformations. Figure 87 shows that Config 2L has the lowest out of place displacements, as expected, followed by Config 2B, Config 2M and Config 2N. The net out of plane displacement on Config 2L is 0.206 mm, 0.278 mm on Config 2B, 0.294 on Config 2M and 0.322mm on Config 2B. These displacement values are calculated using highest and lowest values in front and aft of the connection point as shown in Figure 87. Thus it can be concluded that the load transfer in Mesh independent spotweld beam model is affected by the bending stiffness of the localized area of the plates which changes based on the contact point.

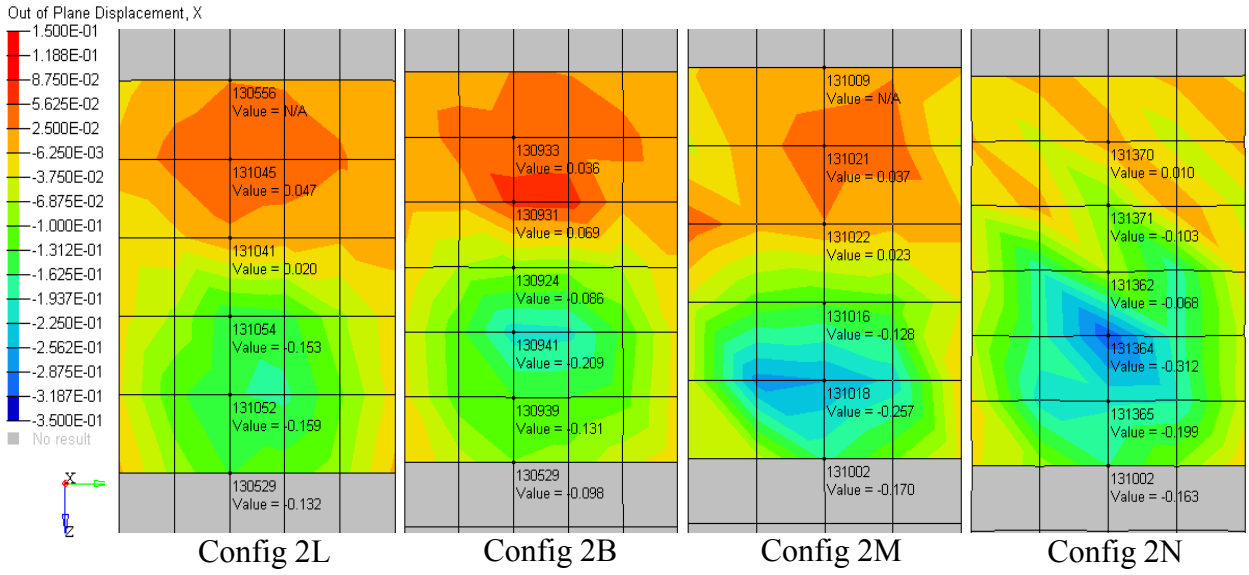

Figure 87. Out of Plane displacements (mm) on Load Transfer Part of Config 2B, 2L, 2M & 2N

Looking back at Figure 82, it can be noted that Config 2A, 2E, 2K and 2L show higher load transfer compared to solid model. Config 2B has good correlation to solid model at low remote loads after which the load transfer remains high. Config 2M shows very good correlation to the solid model. To simplify further analysis of this method, Config 2C, 2D and 2N are dropped due to poor load transfer performance in comparison to the solid model. In the solid model, the net section area is smaller due to the fastener hole while in this simplified model the plates are a continuum and thus the net section is larger. As a result, failure occurs at larger remote stress for all the configurations.

4.2.2.2 Kinematic Frames and Failure Modes

Based on the kinematic frames shown in Figure 88 and Figure 89, failure modes on all the models is tear-out of the loading side of the main part due to the constraints created by *CONTACT_SPOTWELD. Also necking on the main part occurs on the load introduction side of the main part. For all the models, the initiation of failure occurs at different remote stresses. This can be attributed to the differences in stiffness induced by the contact which affects the load

carrying capabilities within that region. In comparison to the solid model, this simplified technique is quite different in terms of failure mode and remote stress at failure. This indicates that a new technique is required for modeling failure of the simplified joint systems where shear failure of the joined plates is expected.

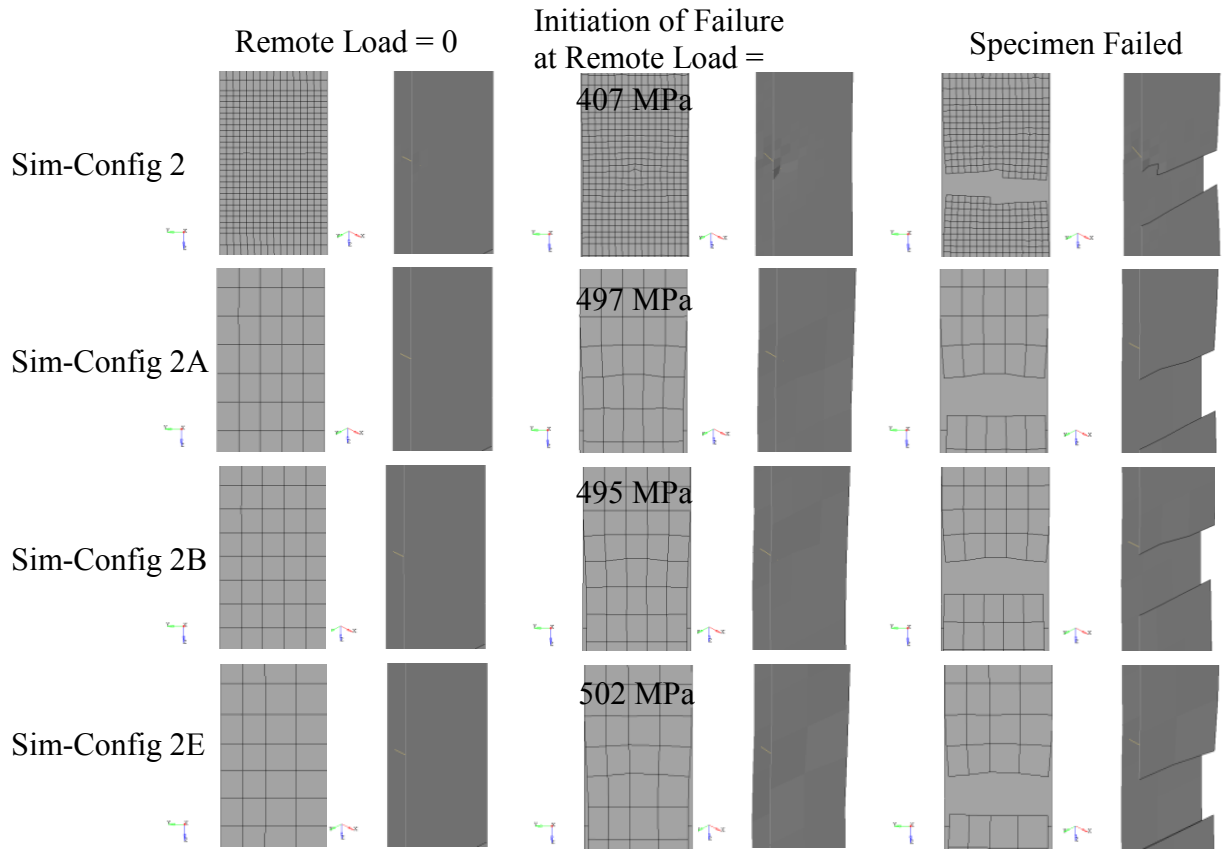

Figure 88. Kinematic Frames Comparison of Mesh Independent Spotweld Beam Config 2-2E

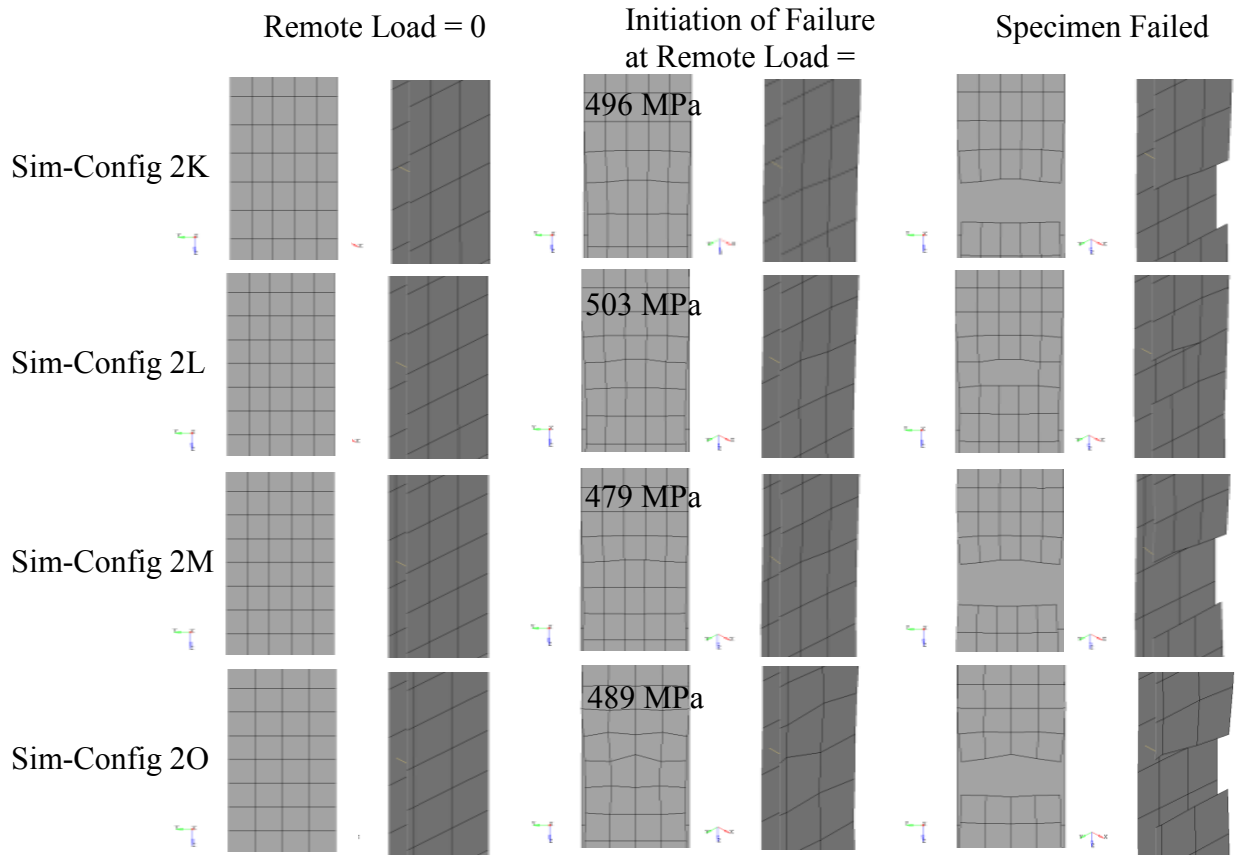

Figure 89. Kinematic Frames Comparison of Mesh Independent Spotweld Beam Config 2L-2O

4.2.2.3 Stress and Strain Profiles

The preload measured in the test was applied to all the FE models. Due to different bolt modeling techniques the stresses that develop in the vicinity of the bolt hole, as a result of the application of preload, are quite different. The stresses developed on the main part and transfer part of the solid model due to preload are shown in Figure 65. Since the bolt head and nut are not modeled in the simplified techniques, on the application of preload, the localized compressive stresses (seen in solid model) are not present in such models and thus the stress levels seen on the models of this simplified technique are close to 0 MPa as shown in Figure 90 and Figure 91. Therefore, although preload is applied to this simplified model, the localized effect of preload are not captured by this technique and thus preload may not have an effect on the overall

performance of the specimen. On the other hand, the preload on the bolt itself is sustained which may improve the performance of the beam itself.

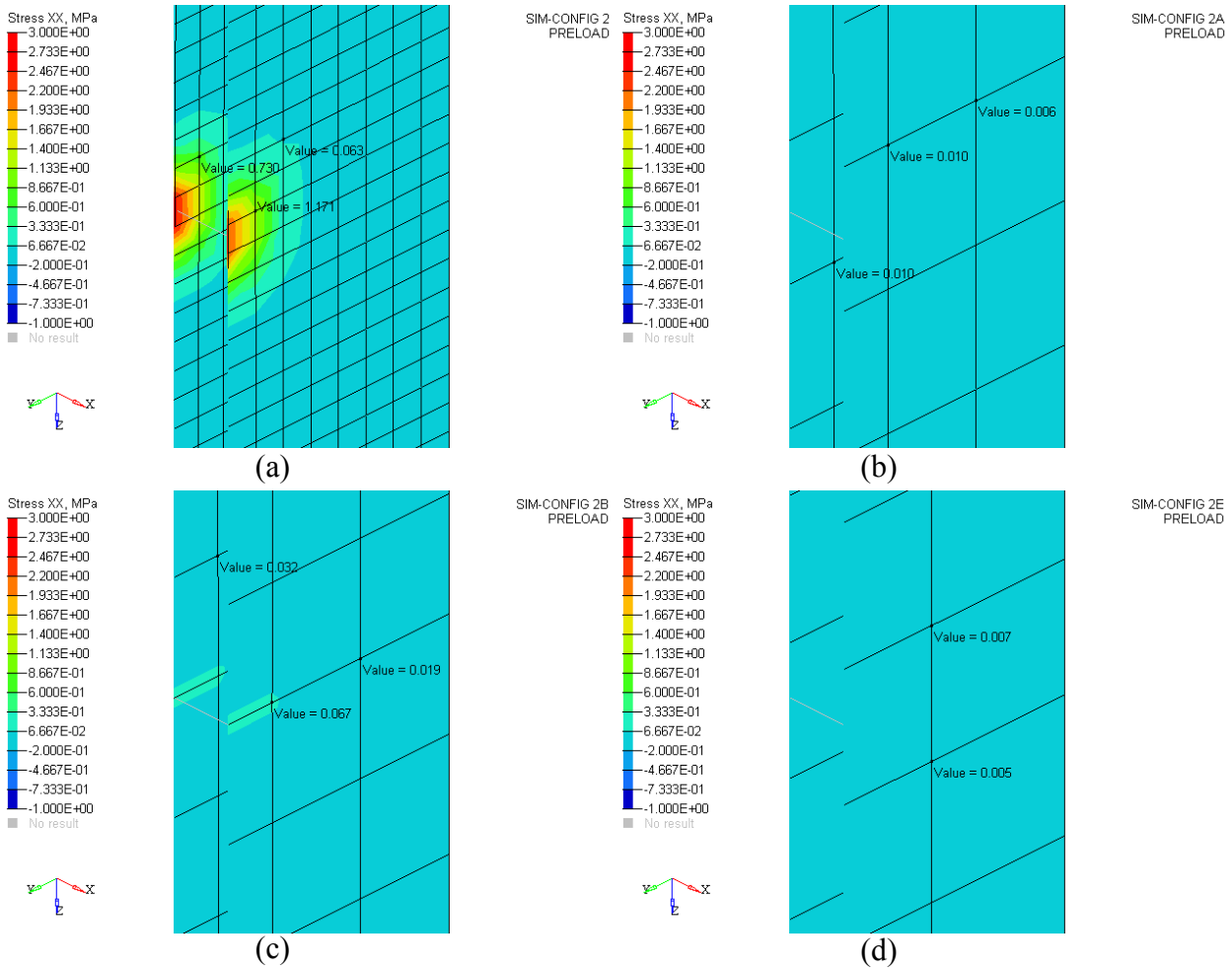

Figure 90. Stresses due to Bolt Preload (a) Sim-Config 2, (b) Sim-Config 2A, (c) Sim-Config 2B and (d) Sim-Config 2E

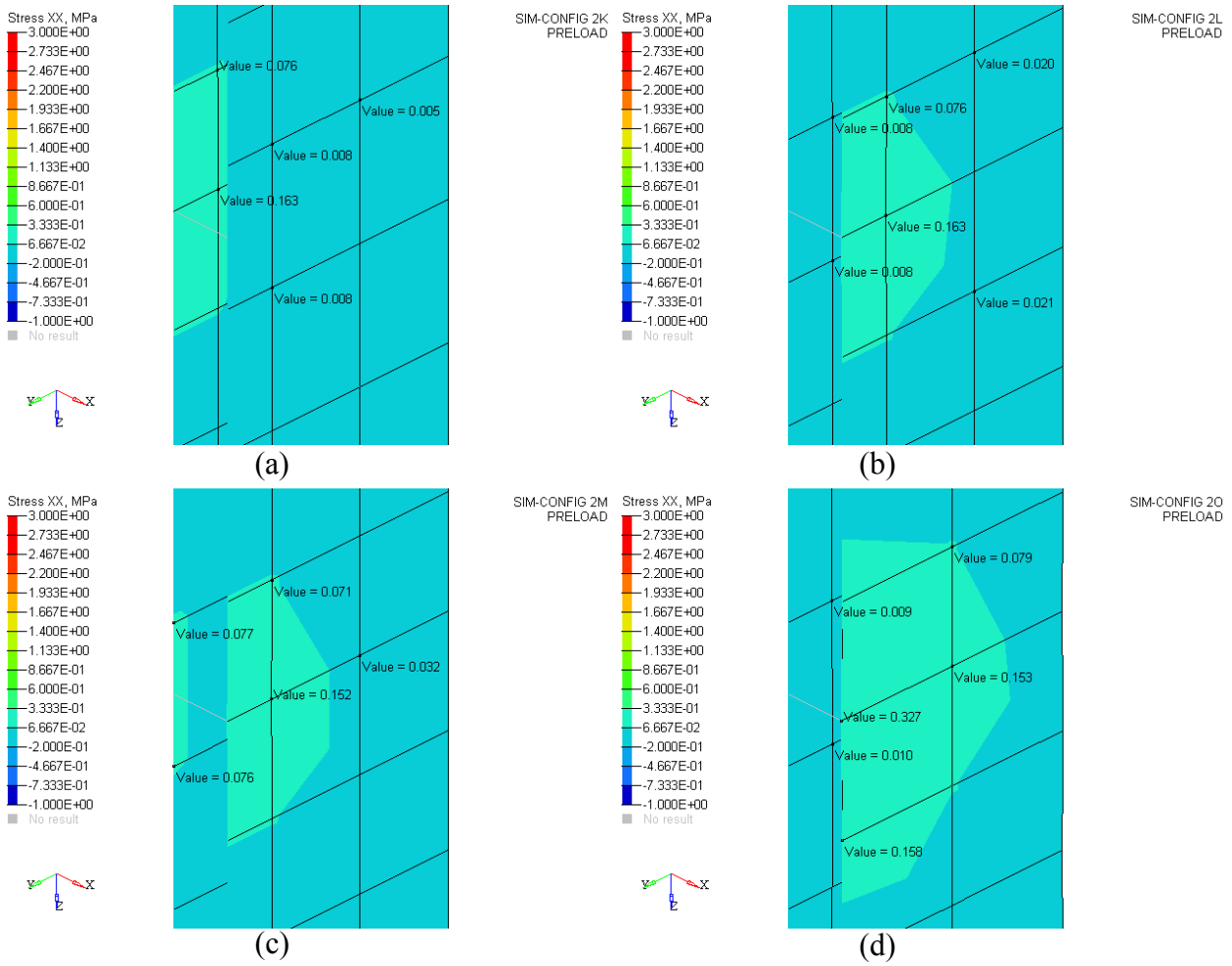

Figure 91. Stresses due to Bolt Preload (a) Sim-Config 2K, (b) Sim-Config 2L, (c) Sim-Config 2M and (d) Sim-Config 2O

The state of stress (vonMises stress) at the initiation of failure on the main part of the Solid model is presented Figure 66 and for the Mesh Independent spotweld beam model is presented in Figure 92 and Figure 93. The fine mesh model, configuration 2, shows slightly better comparison to the solid model while the rest of the configurations do not compare well with the solid model. Although the fine mesh configuration exhibits a better stress distribution, it should be noted that the minimum element size used for that model is 0.3 mm which makes it impractical for use in large FE models. For this simplified technique, the stresses are highly concentrated on the load introduction side of the main part which is where necking and

ultimately failure occurs. Changing the contact point location does not drastically affect the stress concentrations in the simplified models.

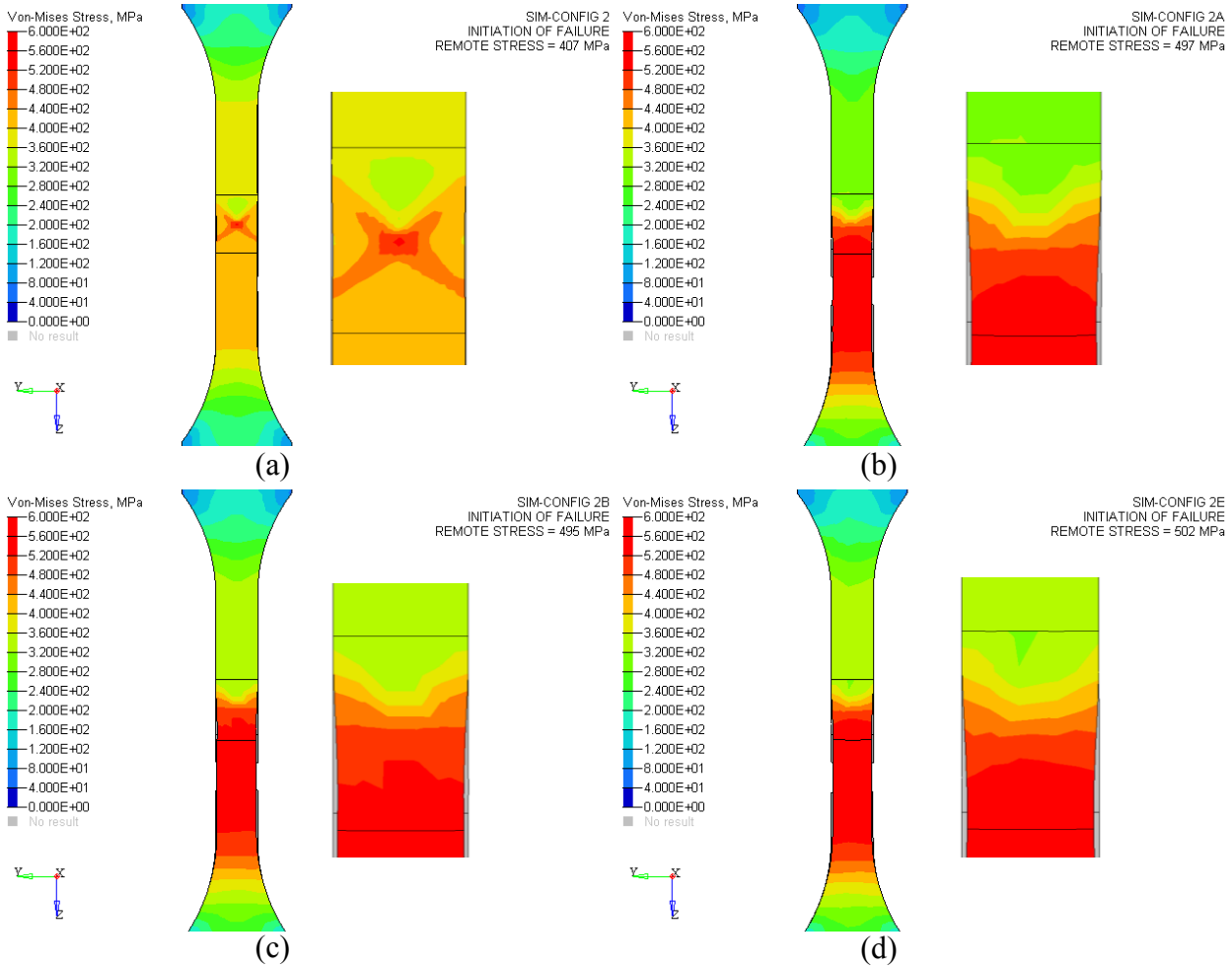

Figure 92. Von-Mises Stresses on Main Part at Initiation of Failure (a) Sim-Config 2, (b) Sim-Config 2A, (c) Sim-Config 2B and (d) Sim-Config 2E

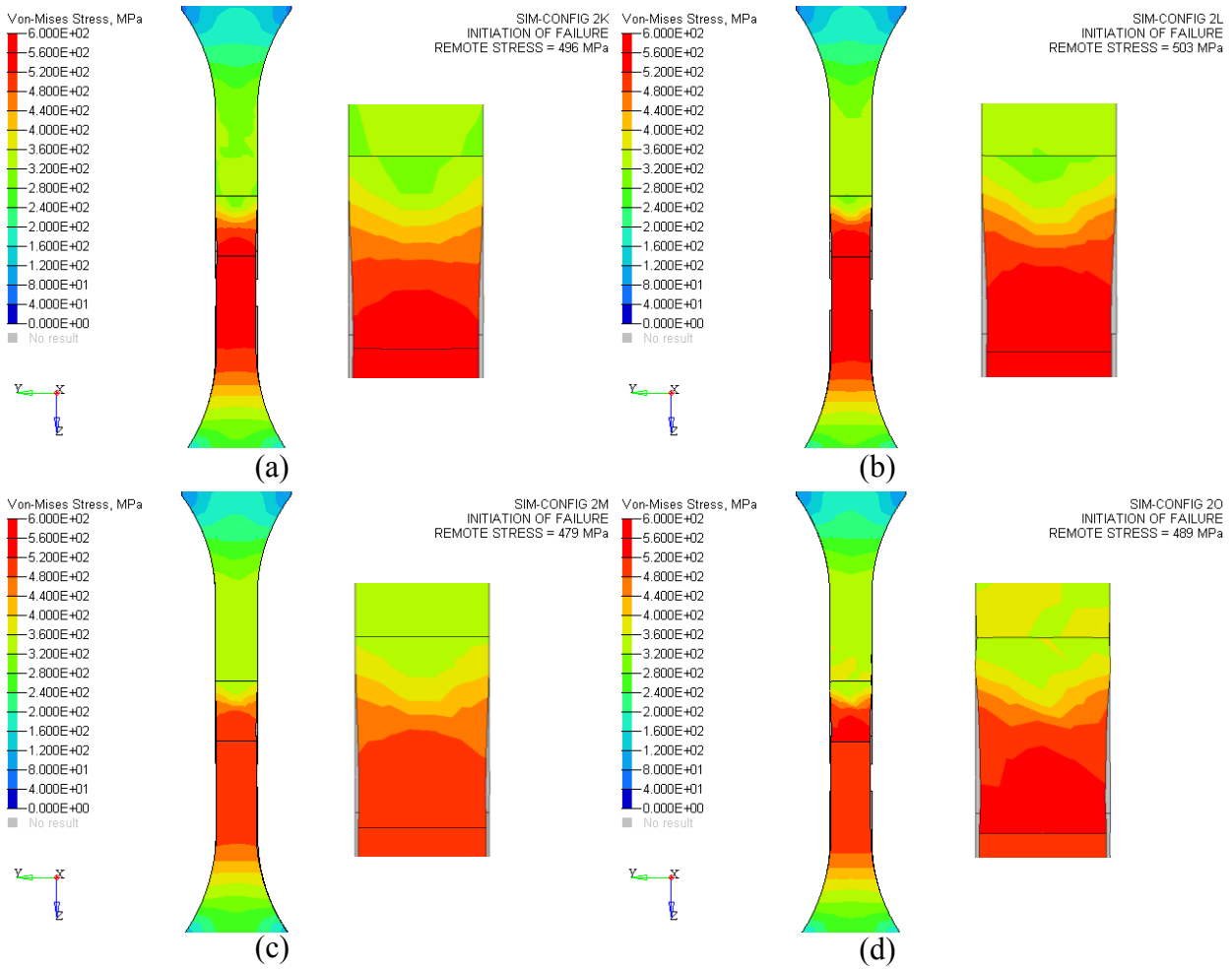

Figure 93. Von-Mises Stresses on Main Part at Initiation of Failure (a) Sim-Config 2K, (b) Sim-Config 2L, (c) Sim-Config 2M and (d) Sim-Config 2O

Strains, at the strain gage locations shown in Figure 32, are compared in Figure 94 and Figure 95. These strains provide an indication of the state of loading at locations further away from the fastener hole. For all the models of this simplified technique, strains at strain gage 1 location are in good correlation to the solid model. This indicates that the use of shell elements in simplified models is sufficient to capture the stress-strain distribution. On the other hand, strains at strain gage 2 and strain gage 3 have large deviations between the solid and simplified models. This can be attributed to the differences in load transfer for the different models. As shown in Figure 82, the load transfer is scattered for the simplified models with some showing higher

%LT than the solid model, while the others showing less load transfer. It can be noted from Figure 94 (d) and Figure 95 (d) that the configurations with higher %LT show higher strains.

Configuration 2M and 2B, which showed good correlation of %LT to the solid model, also show very good correlation of strains to the solid model.

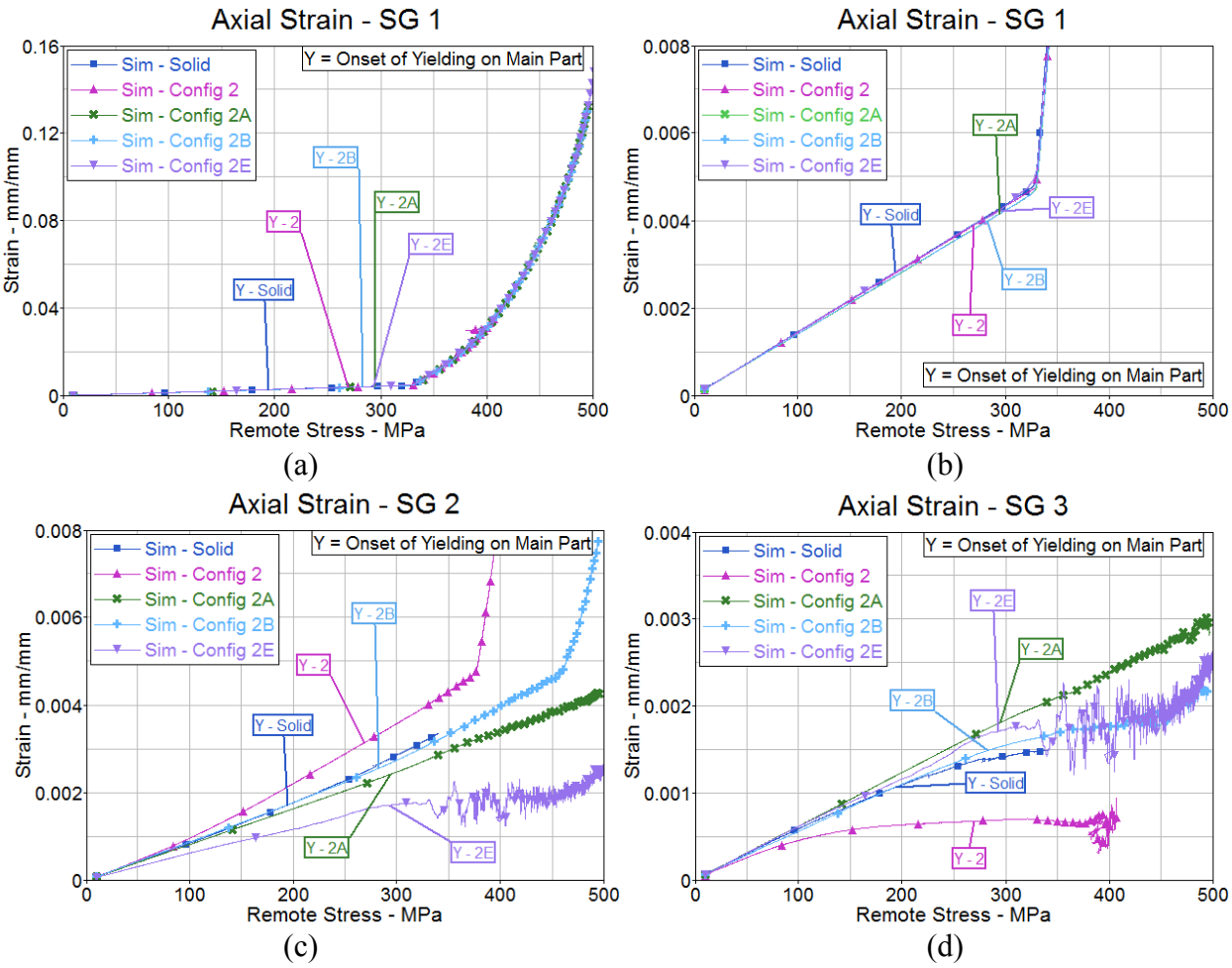

Figure 94. Axial Strain vs Remote Stress for Mesh Independent Spotweld Models Config 2-2E

(a) Strain gage 1 (b) Strain Gage 1 (close-up) (c) Strain Gage 2 and (d) Strain Gage 3

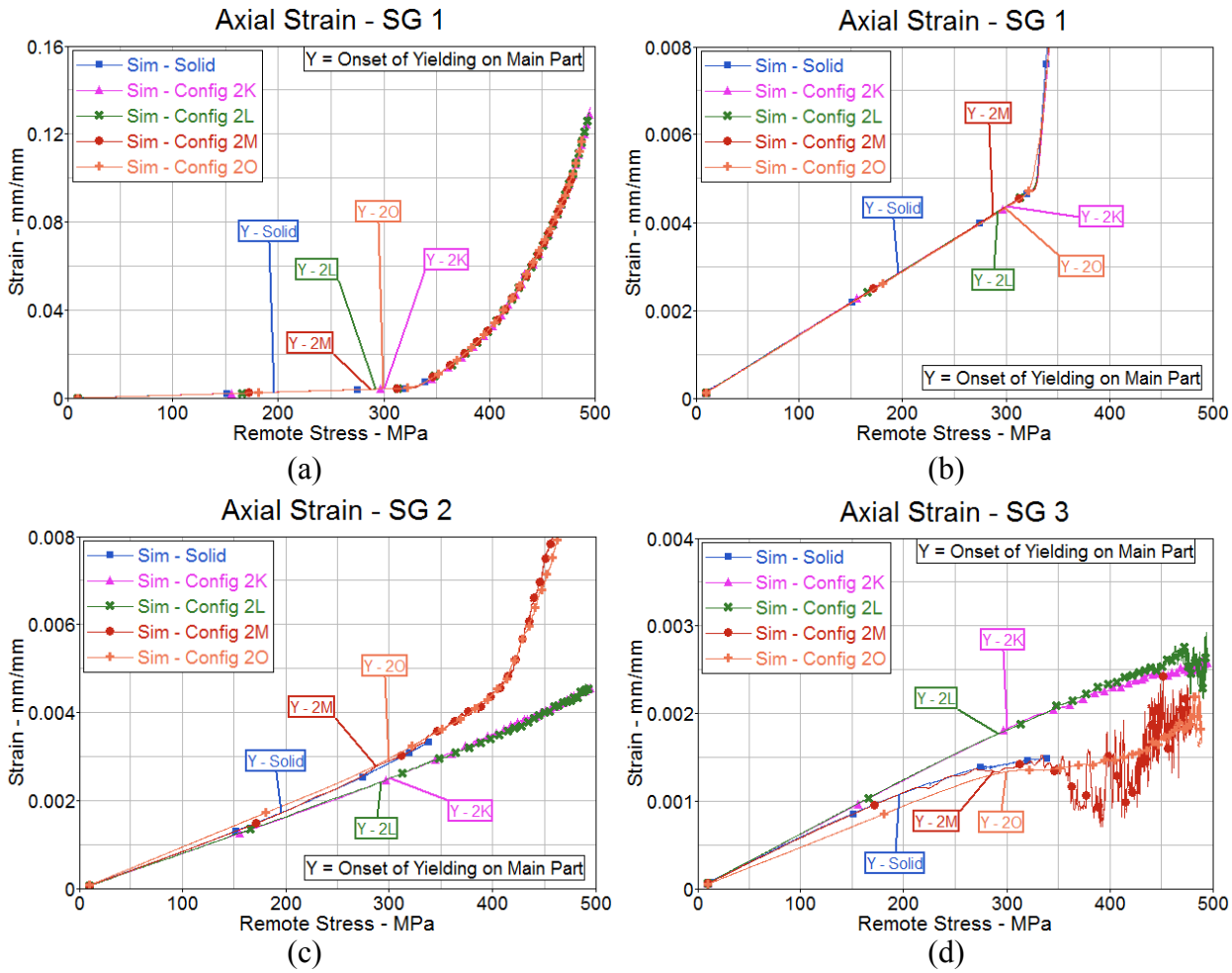

Figure 95. Axial Strain vs Remote Stress for Mesh Independent Spotweld Models Config 2K-2O

(a) Strain gage 1 (b) Strain Gage 1 (close-up) (c) Strain Gage 2 and (d) Strain Gage 3

4.2.2.4 Bolt Loads

The shear force on the bolt and the load recorded in the cross-section plane on the load transfer part are compared to deduce the percentage of load transferred by the bolt and that transferred by friction as shown in Figure 96 and Figure 97. For the simplified bolt model configurations the compressive stresses due to bolt preload are negligible and thus results in lower load transferred through friction and higher through the bolt. The effect of this can be seen on Figure 96 (c) and Figure 97 (c), where the load transfer by friction lasts for very low remote loads on the simplified models compared to the solid model.

For the solid model, the load transferred by the bolt is around 75% on average compared to 96% in the simplified bolt model configurations. The remaining load is transferred by friction. From Figure 96 (c) and Figure 97 (c) it can be noted that for all the models %LT by the bolt starts from zero and increases with increasing remote stress. When the loading begins, the bolt is not engaged, at low remote loads, and the load transfer is carried out purely by friction. As the bolt gets engaged, bearing loads kick in and the bolt starts picking up load.

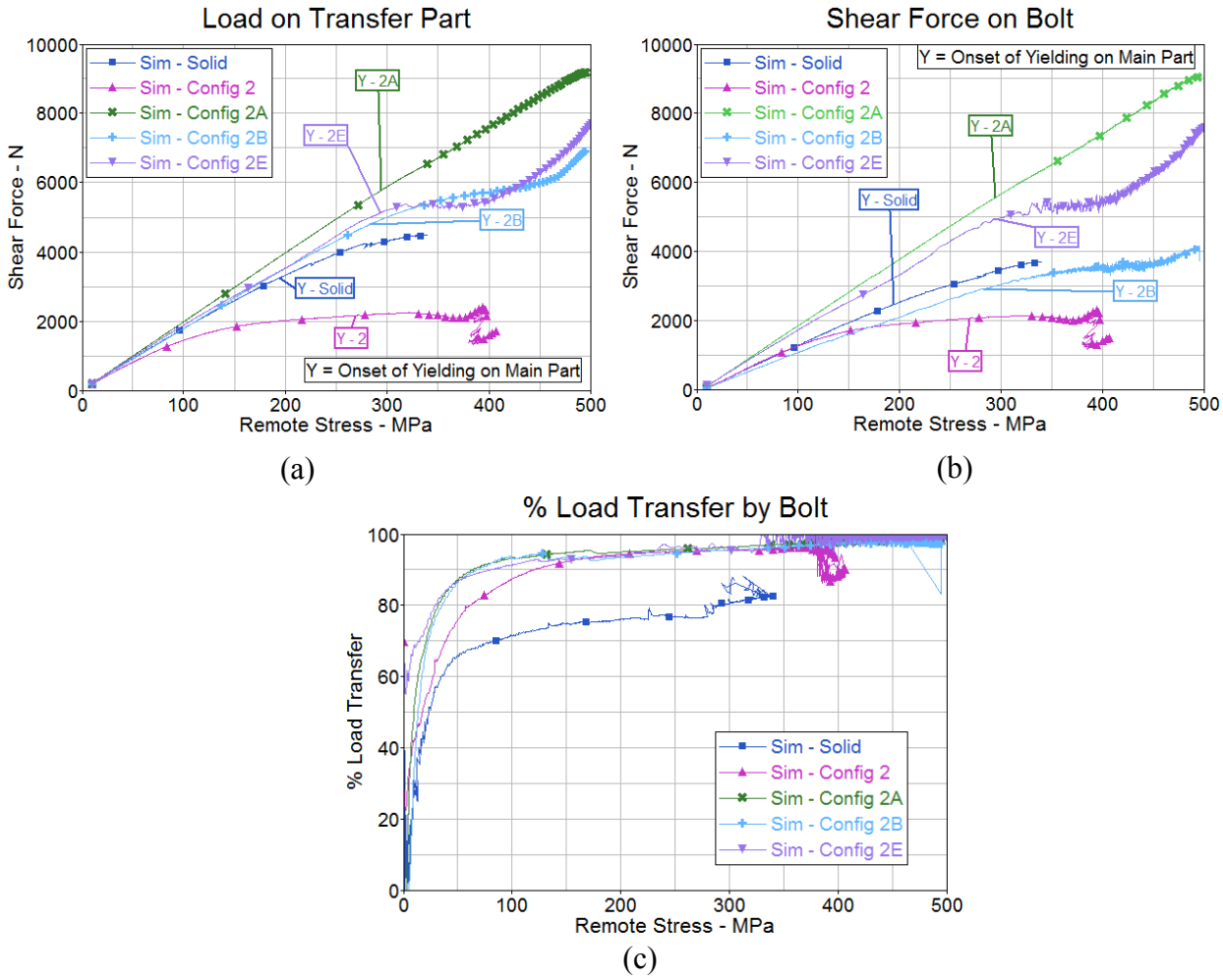

Figure 96. Comparison of Loads transferred by bolt (a) Load on Transfer Part (b) Shear Force on Bolt and (c) % LT by Bolt

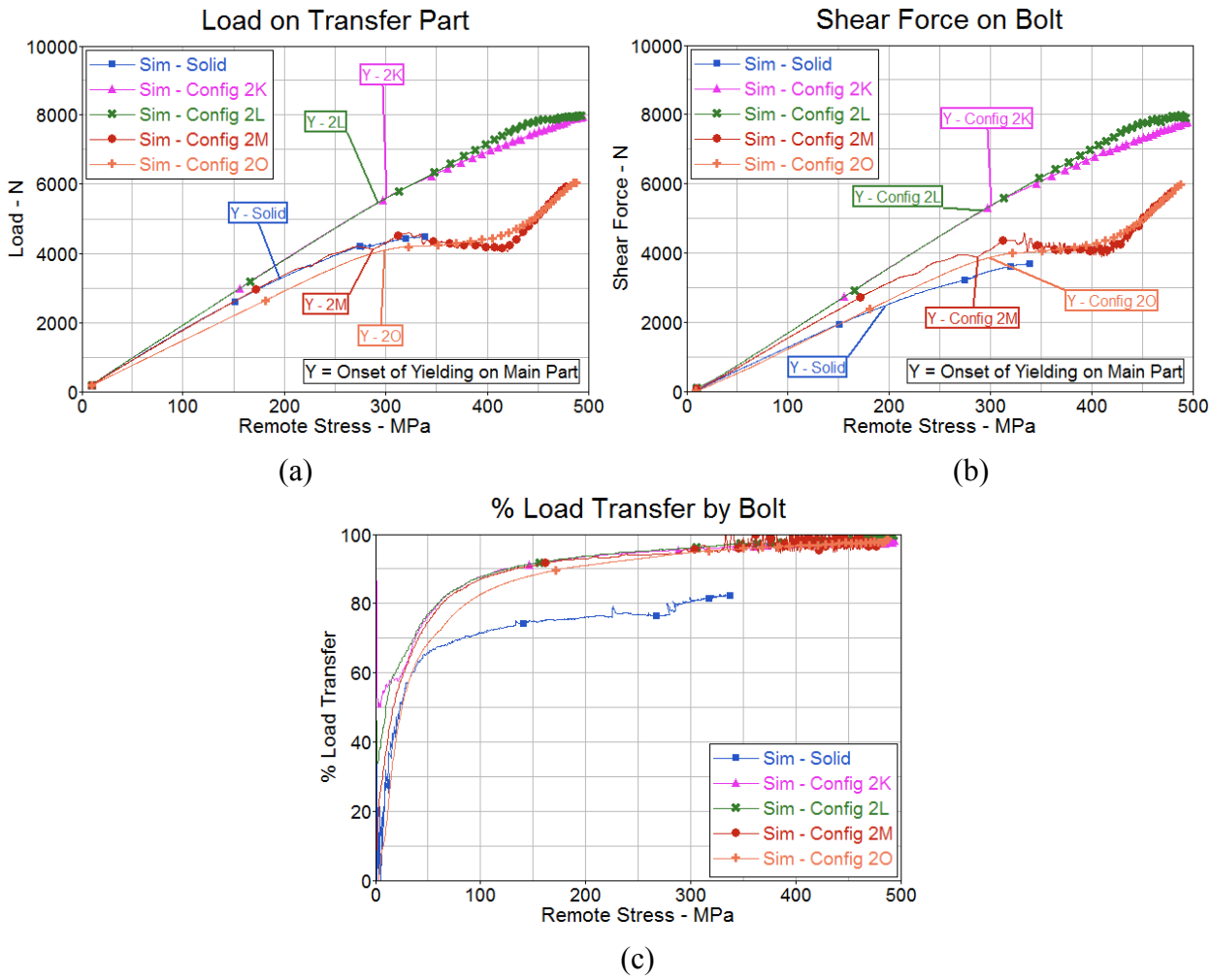

Figure 97. Comparison of Loads transferred by bolt (a) Load on Transfer Part (b) Shear Force on Bolt and (c) % LT by Bolt

Figure 98 shows the comparison of axial loads on the bolt. As expected, the initial axial load for all the models is approximately 2300 N, which is the preload applied to all the models. For all the simplified models except Configuration 2 (fine mesh), it can be noted that the axial load is sustained or drops very slightly up to 300 MPa of remote stress after which there is a drop and rise in the axial load. The levels of drop and rise vary between different simplified configurations. Due to different contact points and contact constraints in the simplified configurations, the localized bending is different for all the models as discussed in section 4.2.2.1

and thus the rotation of the bolt is also different. As a result, the axial loads are also affected. The correlation of axial loads to the solid model, of this simplified technique, is not good. In the detailed model, the bolt undergoes complex loading due to the end fixity of head and nut, bearing loads and high friction on faying surfaces. None of these phenomena are observed in the simplified model.

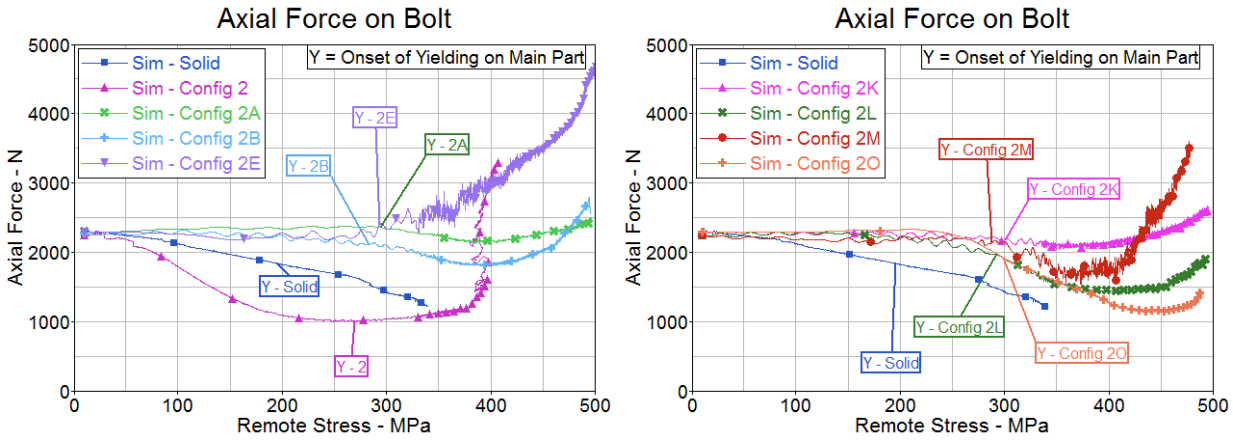

Figure 98. Comparison of Axial Force on bolt (a) Config 2-2E (b) Config 2K-2O

4.2.2.5 Energy Comparison

The distribution of energy and internal energy in Configuration 2B is shown in Figure 99. Configuration 2B is used to represent the energy distribution for this simplified technique. As described in section 3.1, one inch long patch of elements in the vicinity of the bolt, on the main part and transfer part, were placed in separate components. The strain energy in these areas is presented in Figure 101 and Figure 102, and the strain energy in the bolt shank is presented in Figure 103.

In comparison to the energy distribution in the solid model (total energy ~ 19 J), this simplified technique shows a total energy of approximately 185 J. The energy levels are higher for the simplified model because the simplified models reach failure at much higher remote

stress thus inputting more energy into the structure. In addition, for this simplified model, majority of the internal energy (approx. 130 J or 68%) is stored in the main part and not within the joint. The joint which is comprised of 1 in patch on the main part and load transfer part and the bolt only stores 32 % of total internal energy at failure. This can be attributed to the shift in stress concentrations, towards load introduction side, created by the simplified joint. In addition, large amounts of plastic strains are also seen at the strain gage 1 location on the main part (see Figure 94) which is a contributing factor to the internal energy. Note that the energy distribution shown in Figure 99 may not apply to the fine mesh model (Configuration 2) but since the focus of this study is crashworthiness, larger mesh models are concentrated on.

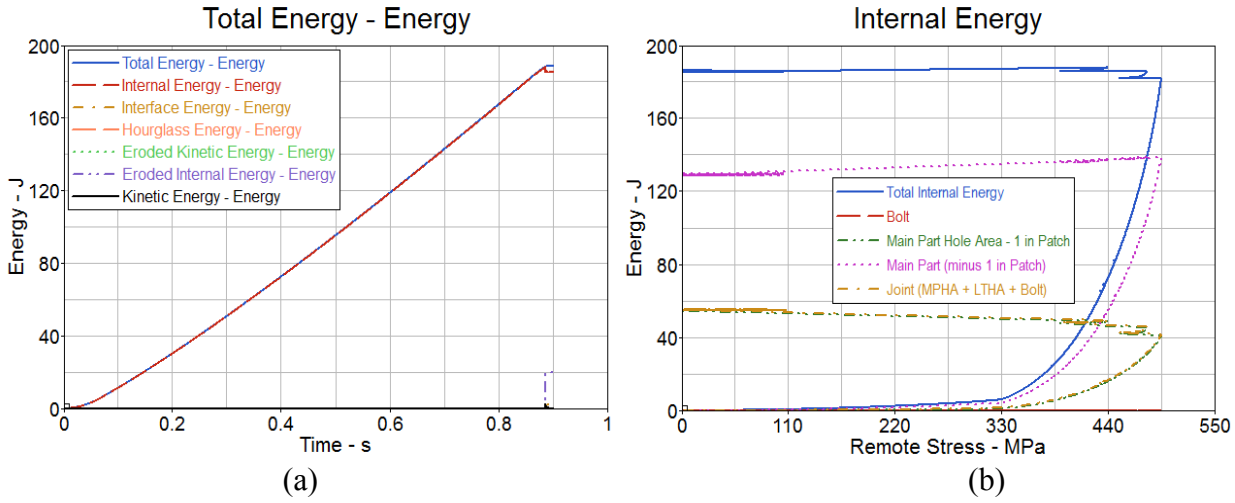

Figure 99. Energy Distribution in Config 2B (a) Energy Balance (b) Internal Energy

Although the energy levels for this simplified method are high in comparison to the solid model, it is noted from Figure 100 that for low remote loads the energy levels compare well. The total internal energy, main part internal energy and joint internal energy compare well from remote stress of 50 MPa to 250 MPa. On the simplified model the energy is low before loading begins because the stresses due to preload are not significant.

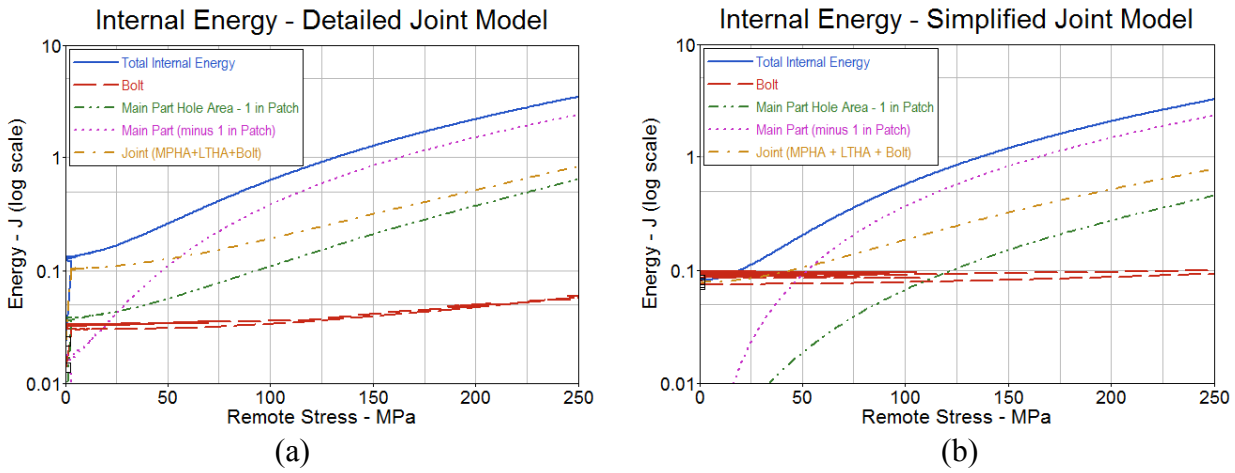

Figure 100. Energy at Low Remote Loads (a) Detailed Model (b) Simplified Model Config 2B

Based on Figure 101 and Figure 102 on the main part and transfer part, at low remote stress, the energy on the solid model is much higher than on the simplified configurations. This is due to the presence of high clamp-up stresses in the solid model. At higher remote stress the energies of the simplified configurations are closer to that of the solid model especially for the mixed configurations (Configurations 2K – 2O).

The energy in the bolt shank, shown in Figure 103, is higher in the simplified configurations compared to the solid model. This result is expected since the shear force on the bolt shank of the simplified models is much higher than the solid model, as shown in Figure 96 (b) and Figure 97 (b).

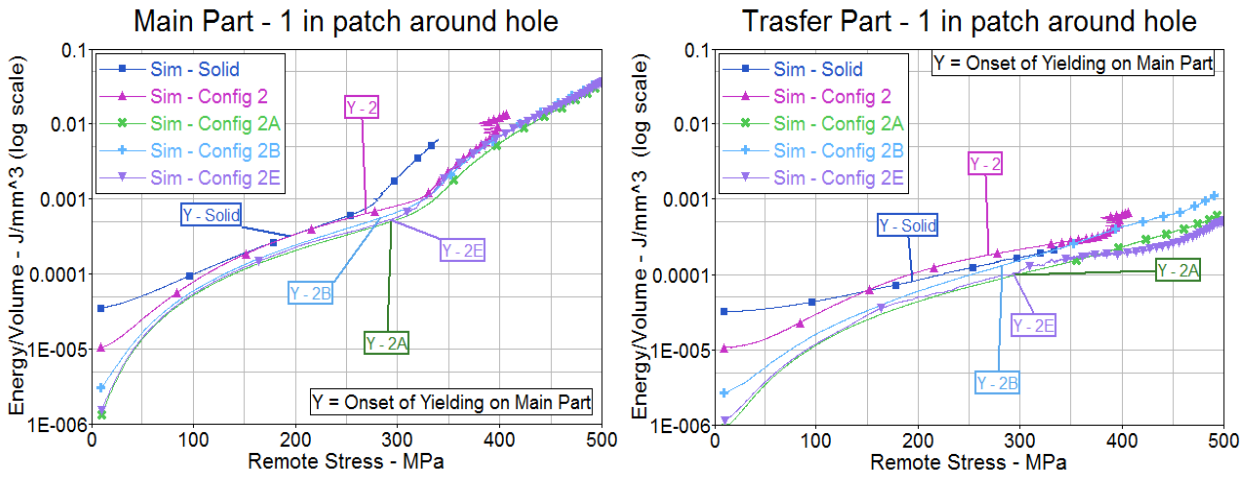

Figure 101. Strain Energy per Volume in 1 in. long patch, 2 -2E (a) Main Part (b) Transfer Part

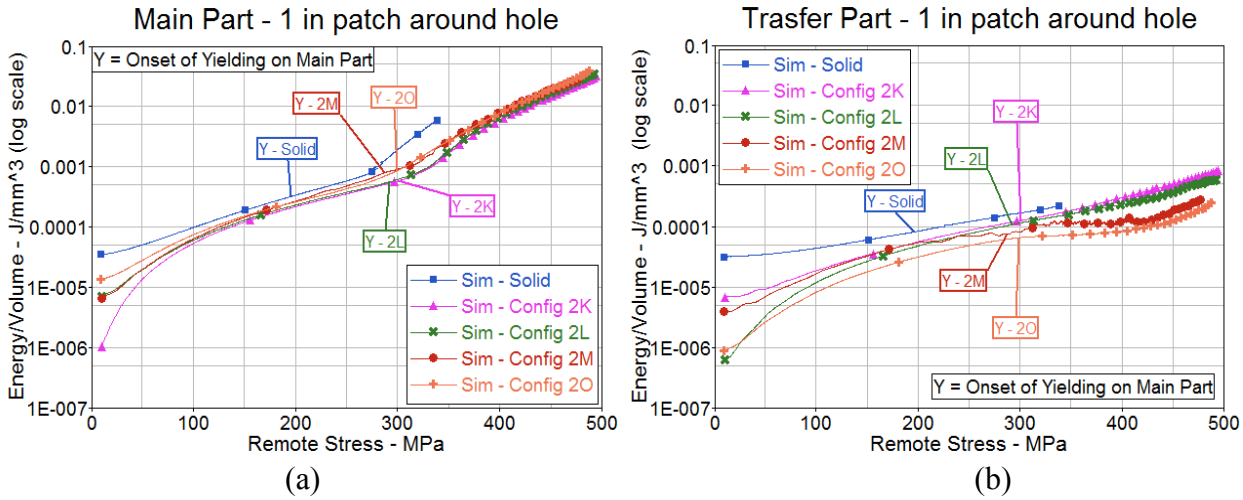

Figure 102. Strain Energy per Volume in 1 in. long patch, 2K-2O (a) Main Part (b) Transfer Part

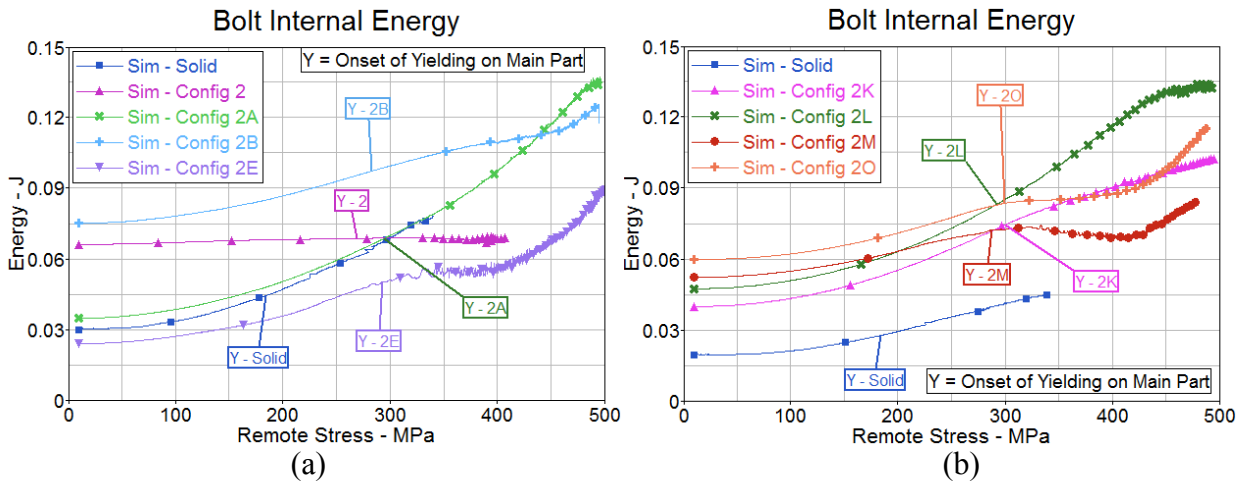

Figure 103. Comparison of Bolt Internal Energy (a) Config 2-2E (b) Config 2K-2O

4.2.3 Configuration 3 – Mesh Independent Spotweld Beam with Patch

For this simplified technique, three different variations are compared to the solid model. The primary entity of this joint definition, that is *CONTACT_SPOTWELD, is the same as that used in Configuration 2. Detailed explanation of the setup of this simplified bolt modeling technique is provided in section 3.1.4. To obtain a better understanding of this setup, the static forces related to the RBE bolt model are shown in Figure 104.

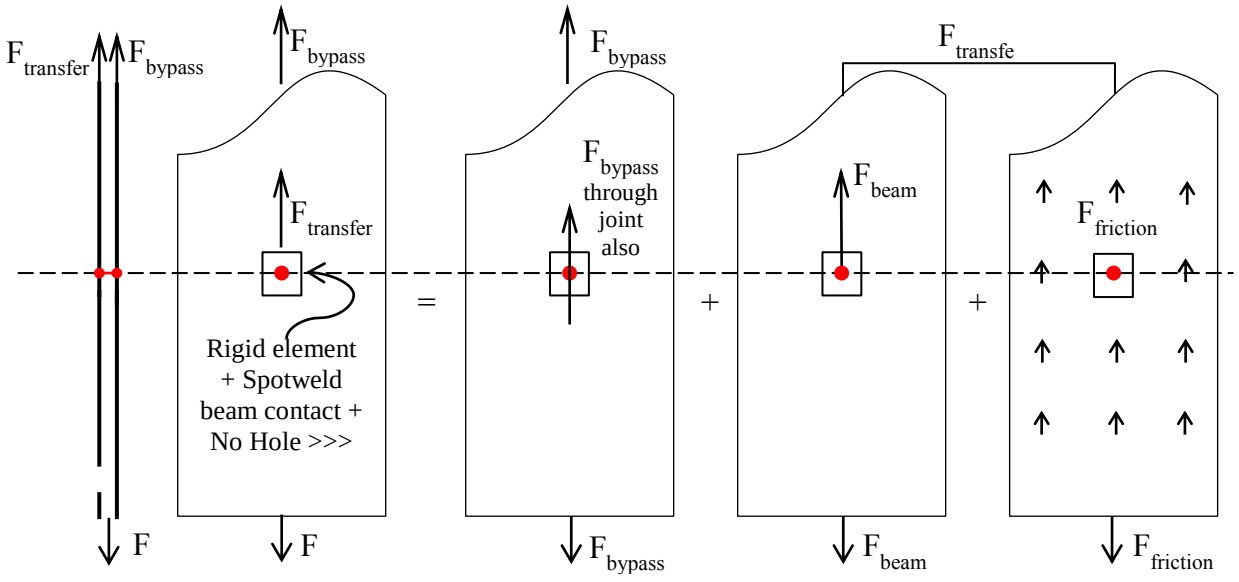

Figure 104. Free Body Diagram for Config 3

The force (F) introduced in the system is split into transfer force ($F_{transfer}$) and bypass force (F_{bypass}) due to displacement compatibility enforced by the presence of the bolt [12]. F_{bypass} is the load that remains in the main part and $F_{transfer}$ is the load that is transmitted to the load transfer part. The bolt shank is represented by beam element and the nodes of the beam are connected to the plates by a tied contact, *CONTACT_SPOTWELD. Tied contact couples the nodes of the connected segment to the bolt node, as detailed in section 3.4.1, thus there are no bearing loads in this model. Since there is no fastener hole in this modeling technique, the joint is a continuum and thus facilitates some F_{bypass} load to pass through. $F_{transfer}$ is via the shear loads (F_{beam}) registered in the bolt and friction force between the plates ($F_{friction}$). The bolt head and nut are represented by applying a stiff material to the connected element or elements (for the fine mesh model). Thus the clamping forces developed may be slightly higher than that seen in Config 2, but may still be less than the solid model where the bolt head and nut provide high clamping loads. Since the plates are a continuum the clamping forces will be distributed throughout the plate and the localized effect of friction due to clamping won't be present.

4.2.3.1 Load Transfer

The comparison of %LT is shown in Figure 105. Since the joining mechanism is the same as that in Configuration 2, the load transfer behaves in the same was as described in section 4.2.2.1. The %LT results of configurations 3A and 3B are similar to configuration 2A which indicates that increasing the stiffness of one element forming the joint does not affect the load transfer. The load transfer is more dependent on the contact. Similar to the results obtained in configuration 2, the fine mesh model of configuration 3 also shows less load transfer than the solid model. Nevertheless, the fine mesh model in configuration 3 does show some improvement in %LT compare to the fine mesh model of configuration 2.

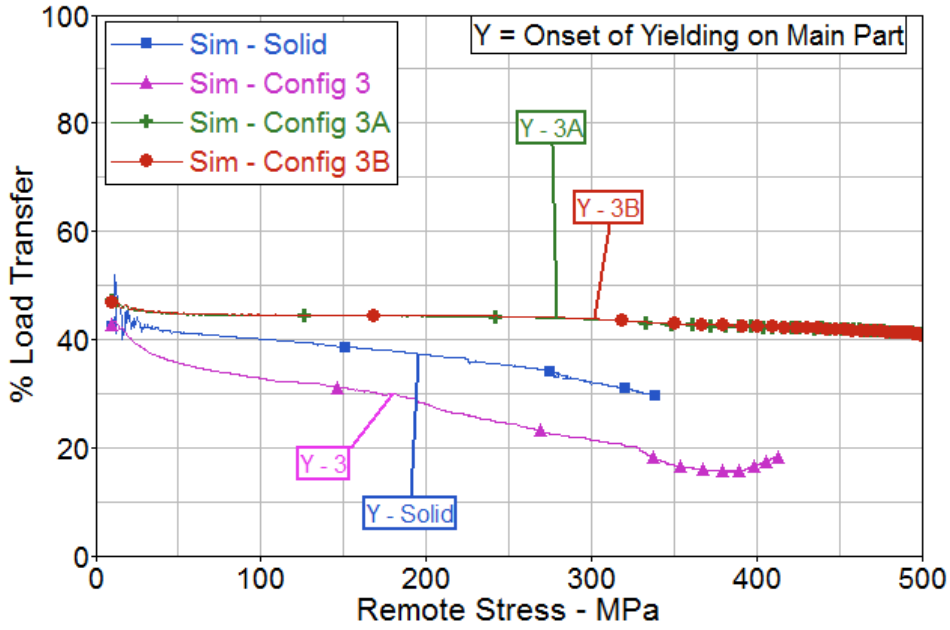

Figure 105. % Load Transfer Comparison

4.2.3.2 Kinematic Frames and Failure Modes

Based on the kinematic frames shown in Figure 106, failure modes on all the models is tear-out of the loading side of the main part due to the presence of contact and/ or stiffer element. Also necking on the main part occurs on the load introduction side of the main part. The initiation of failure for the fine mesh model occurs at a lower remote stress compared to the models with larger mesh size. This can be attributed to the differences in mesh size and stiffness induced by the contact which affects the load carrying capabilities within that region. It can be noted that failure on the fine mesh model occurs on the boundary of the stiffer material while the failure for configuration 3A is due to contact. In comparison to the solid model, this simplified technique is quite different in terms of failure mode and remote stress at failure. This indicates that a new technique is required for modeling failure of the simplified joint systems where shear failure of the joined plates is expected.

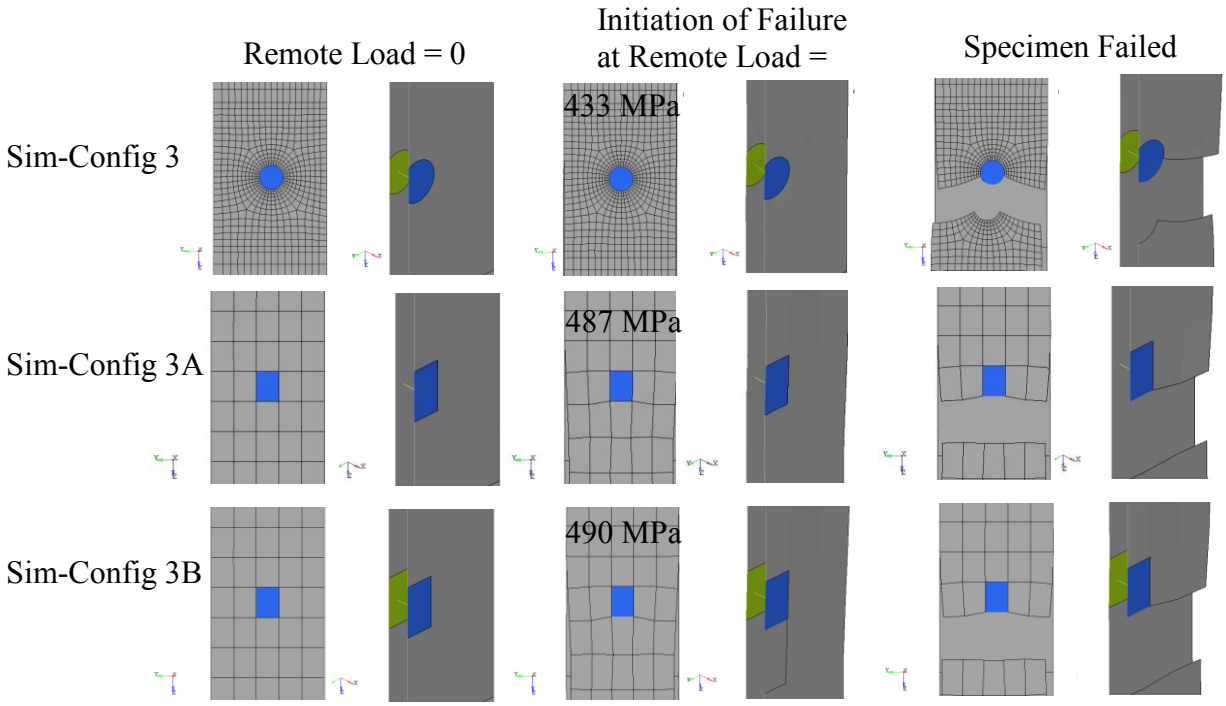

Figure 106. Kinematic Frames for Config 3

4.2.3.3 Stress and Strain Profiles

The preload measured in the test was applied to all the FE models. Due to different bolt modeling techniques the stresses that develop in the vicinity of the bolt hole, as a result of the application of preload, are quite different. The stresses developed on the main part and transfer part of the solid model due to preload are shown in Figure 65. Since the bolt head and nut are not modeled in the simplified techniques, on the application of preload, the localized compressive stresses (seen in solid model) are not present in such models and thus the stress levels seen on this simplified technique are close to 0 MPa as shown in Figure 107. Therefore, although preload is applied to this simplified model, the localized effect of preload are not captured by this technique and thus preload may not have an effect on the overall performance of the specimen. On the other hand, the preload on the bolt itself is sustained which may improve the performance of the beam itself.

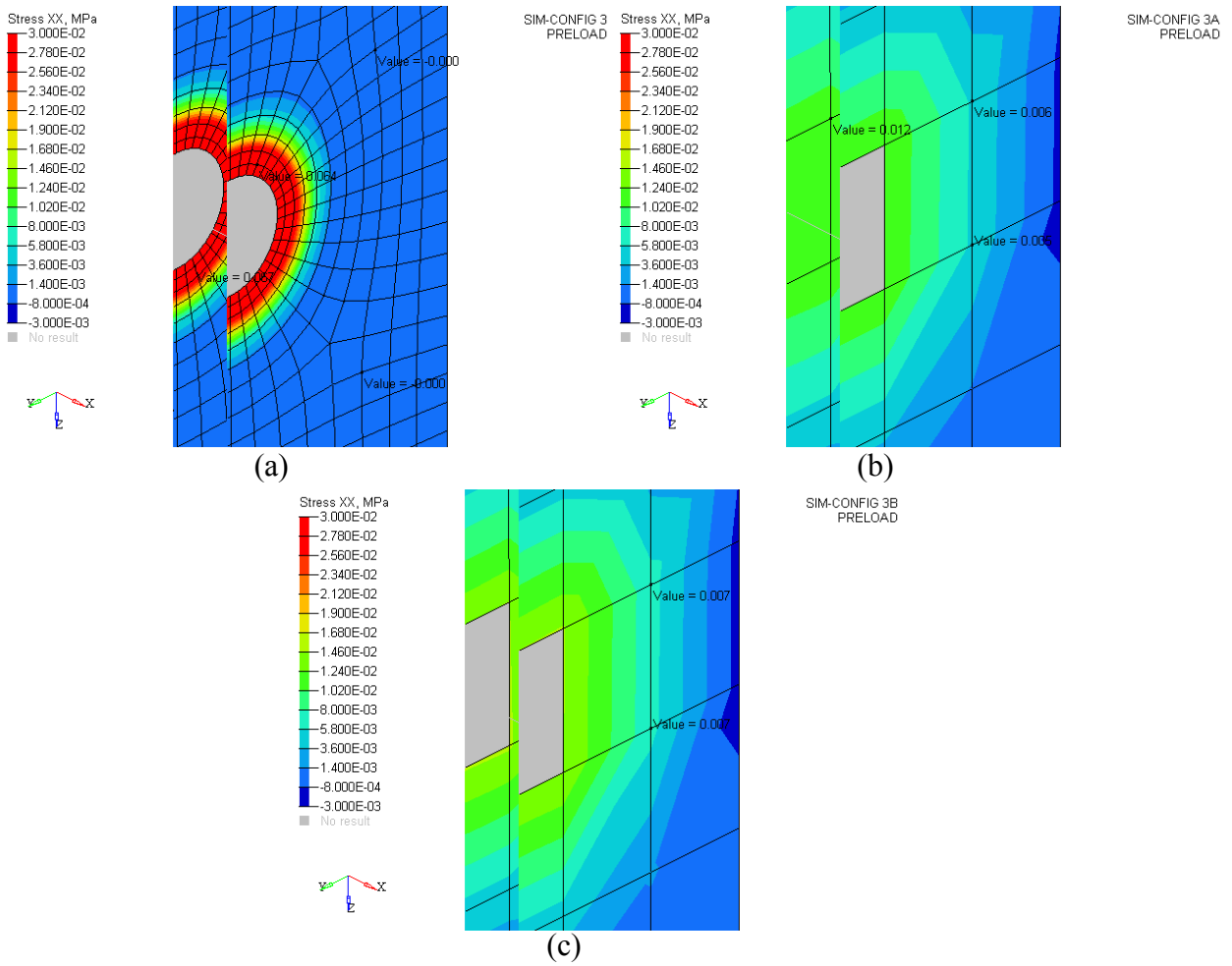

Figure 107. Stresses due to Preload (a) Config 3 (b) Config 3A and (c) Config 3B

The state of stress (vonMises stress) at the initiation of failure on the main part of the Solid model is presented Figure 66 and for this simplified technique is presented in Figure 108. Overall the configurations do not compare well with the solid model. Although the fine mesh configuration, configuration 3, exhibits a better stress distribution, it should be noted that the minimum element size used for that model is 0.3 mm which makes it impractical for use in large FE models. For this simplified technique, the stresses are highly concentrated on the load introduction side of the main part which is where necking and ultimately failure occurs. Adding stiffer material on the main part (configuration 3B) versus not having it (configuration 3A) does not create any significant differences in the stress concentrations.

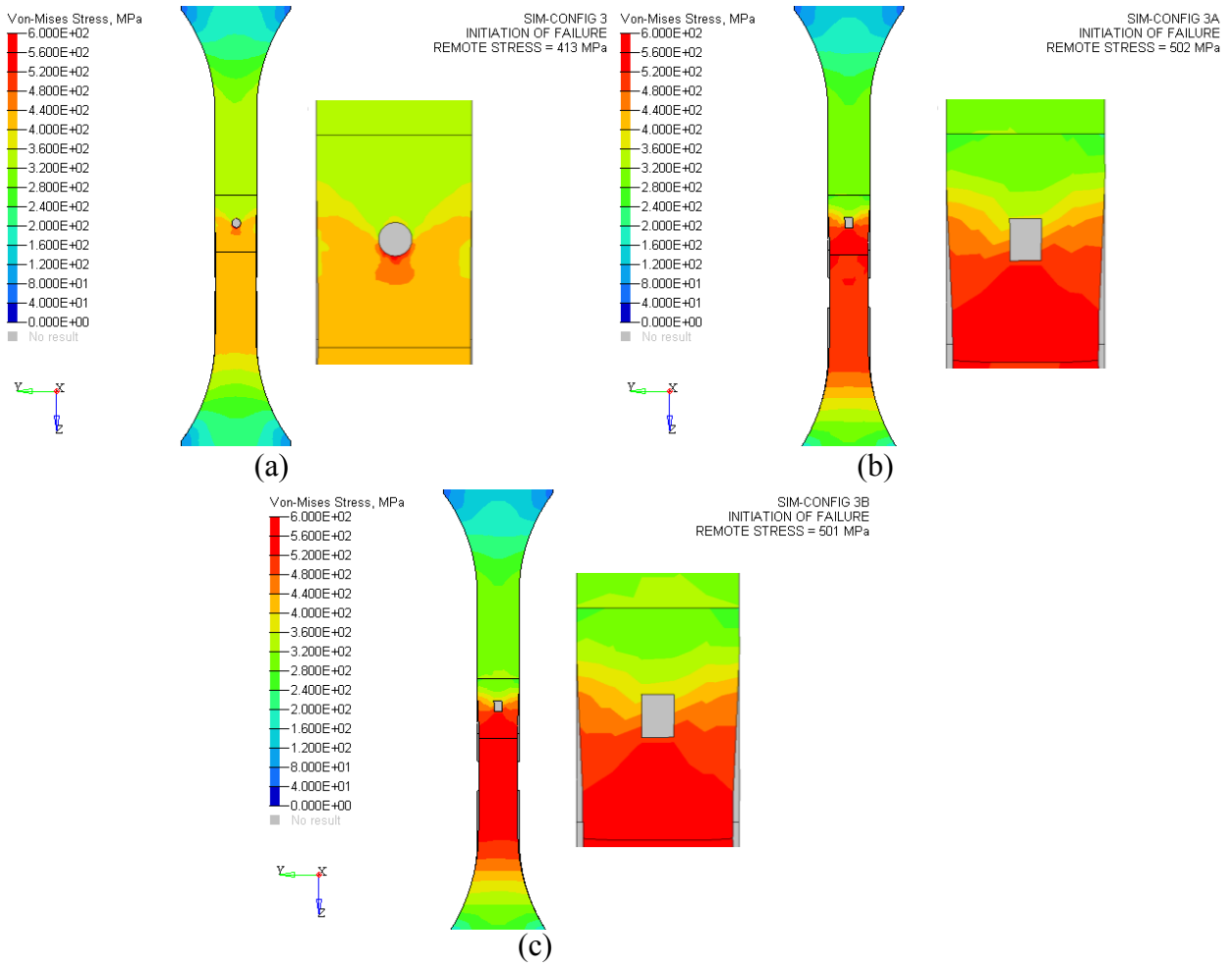

Figure 108. Von Mises Stresses on Main Part (a) Config 3 (b) Config 3A and (c) Config 3B

Strains, at the strain gage locations shown in Figure 32, are compared in Figure 109. These strains provide an indication of the state of loading at locations further away from the fastener hole. For this simplified technique, strains at strain gage 1 location are in good correlation to the solid model. This indicates that the use of shell elements in simplified models is sufficient to capture the stress-strain distribution. On the other hand, strains at strain gage 2 and strain gage 3 have deviations between the solid and simplified models. This can be attributed to the differences in load transfer for the different models.

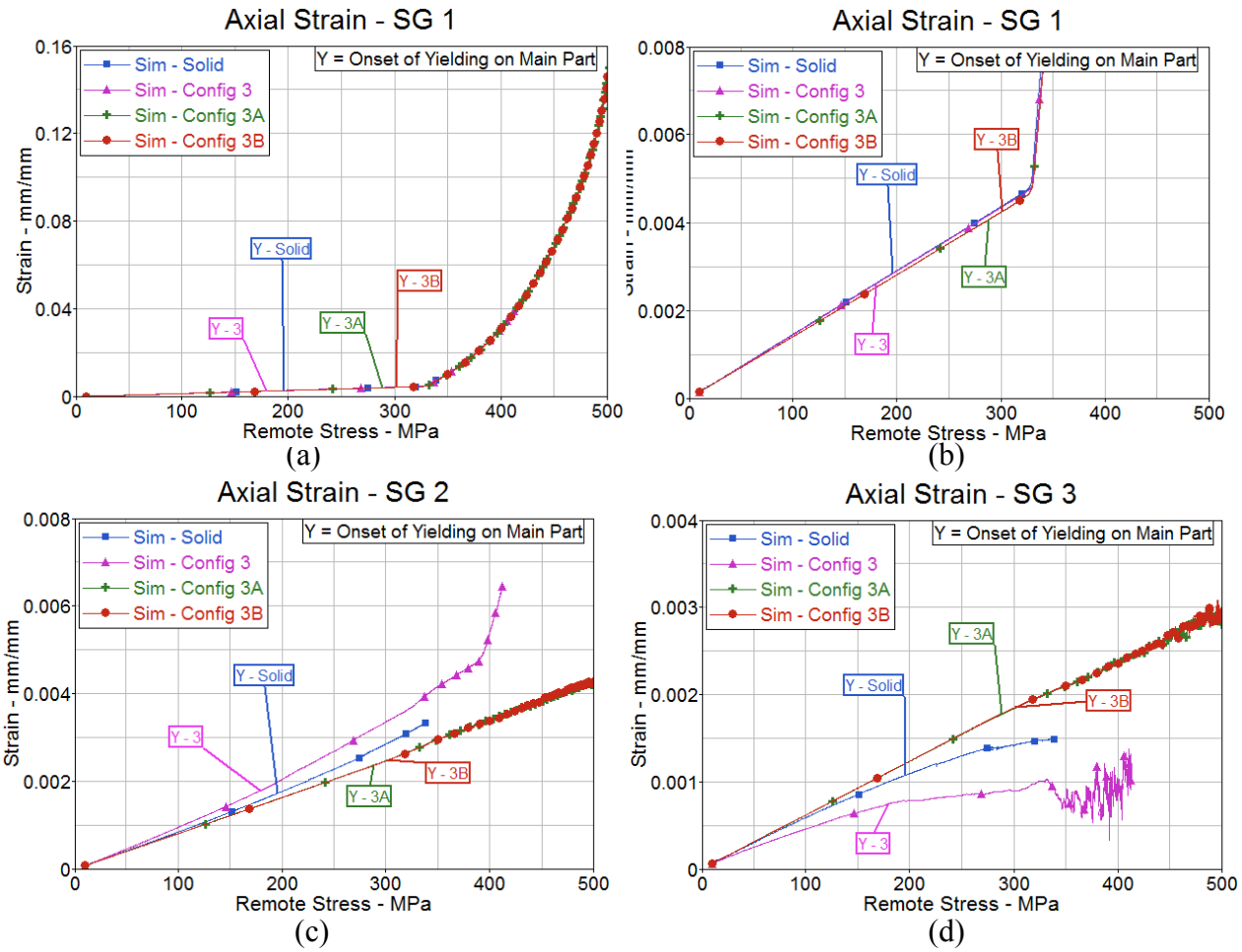

Figure 109. Axial Strain vs Remote Stress for Mesh Independent Spotweld with Elastic Patch Model (a) Strain gage 1 (b) Strain Gage 1 (close-up) (c) Strain Gage 2 and (d) Strain Gage 3

4.2.3.4 Bolt Loads

The shear force on the bolt and the load recorded in the cross-section plane on the load transfer part are compared to deduce the percentage of load transferred by the bolt and that transferred by friction as shown in Figure 110. For the simplified bolt model configurations the compressive stresses due to bolt preload are negligible and thus results in lower load transferred through friction and higher through the bolt. The effect of this can be seen on Figure 110 (c), where the load transfer by friction lasts for very low remote loads on the simplified models compared to the solid model.

For the solid model, the load transferred by the bolt is around 75% on average compared to 96% in the simplified bolt model configurations. The remaining load is transferred by friction. From Figure 110 (c) it can be noted that for all the models %LT by the bolt starts from zero and increases with increasing remote stress. When the loading begins, the bolt is not engaged, at low remote loads, and the load transfer is carried out purely by friction. As the bolt gets engaged, bearing loads kick in and the bolt starts picking up load.

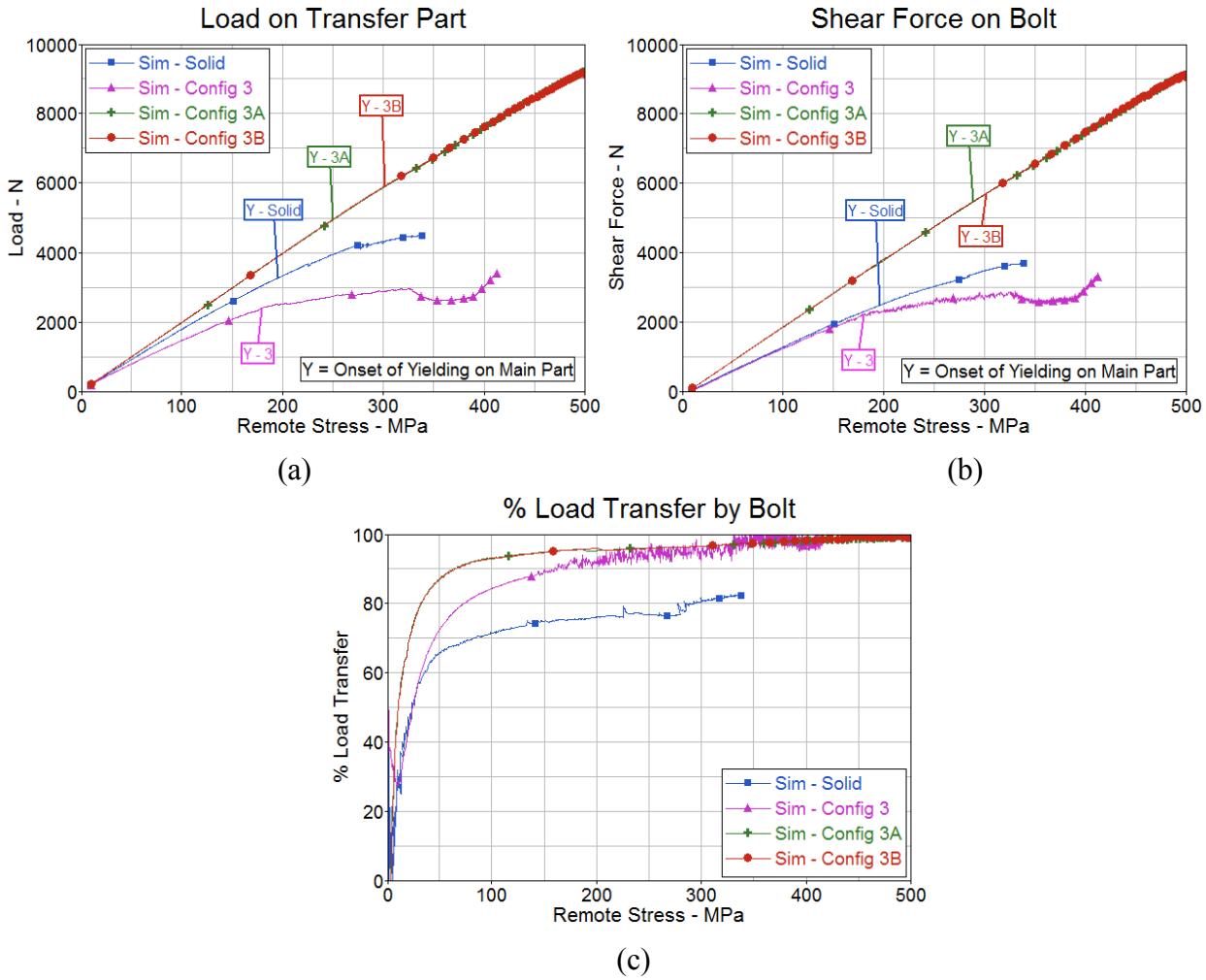

Figure 110. Comparison of Loads transferred by bolt (a) Load on Transfer Part (b) Shear Force on Bolt and (c) % LT by Bolt

Figure 111 shows the comparison of axial loads on the bolt. As expected, the initial axial load for all the models is approximately 2300 N, which is the preload applied to all the models. For all the simplified models except configuration 3 (fine mesh), it can be noted that the axial load is sustained or drops very slightly up to 300 MPa of remote stress after which there is a drop and rise in the axial load. The correlation of axial loads to the solid model, of this simplified technique, is not good. In the detailed model, the bolt undergoes complex loading due to the end fixity of head and nut, bearing loads and high friction on faying surfaces. None of these phenomena are observed in the simplified model.

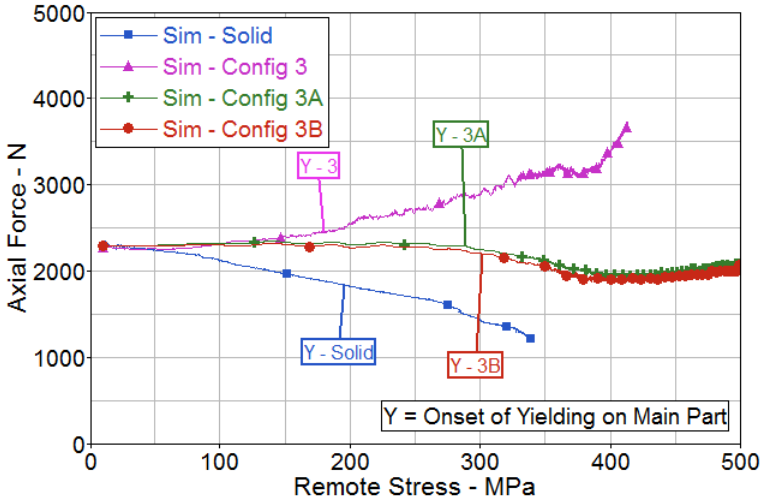

Figure 111. Comparison of Axial Force on bolt

4.2.3.5 Energy Comparison

The energy distribution for configuration 3B is shown in Figure 112. As described in section 3.1, one inch long patch of elements in the vicinity of the bolt, on the main part and transfer part, were placed in separate components. The strain energy in these areas is presented in Figure 113 and the strain energy in the bolt shank is presented in Figure 114.

In comparison to the energy distribution in the solid model (total energy = 19 J), this simplified technique shows a total energy of approximately 205 J. The energy levels are higher

for the simplified model because the simplified models reach failure at much higher remote stress thus inputting more energy into the structure. In addition, for this simplified model, majority of the internal energy (approx. 150 J or 75%) is stored in the main part and not within the joint. The joint which is comprised of 1 in patch on the main part and load transfer part and the bolt only stores 25 % of total internal energy at failure. This can be attributed to the shift in stress concentrations, towards load introduction side, created by the simplified joint. In addition, large amounts of plastic strains are also seen at the strain gage 1 location on the main part (see Figure 120) which is a contributing factor to the internal energy. Note that the energy distribution shown in Figure 99 may not apply to the fine mesh model (configuration 3) but since the focus of this study is crashworthiness, larger mesh models are focused on.

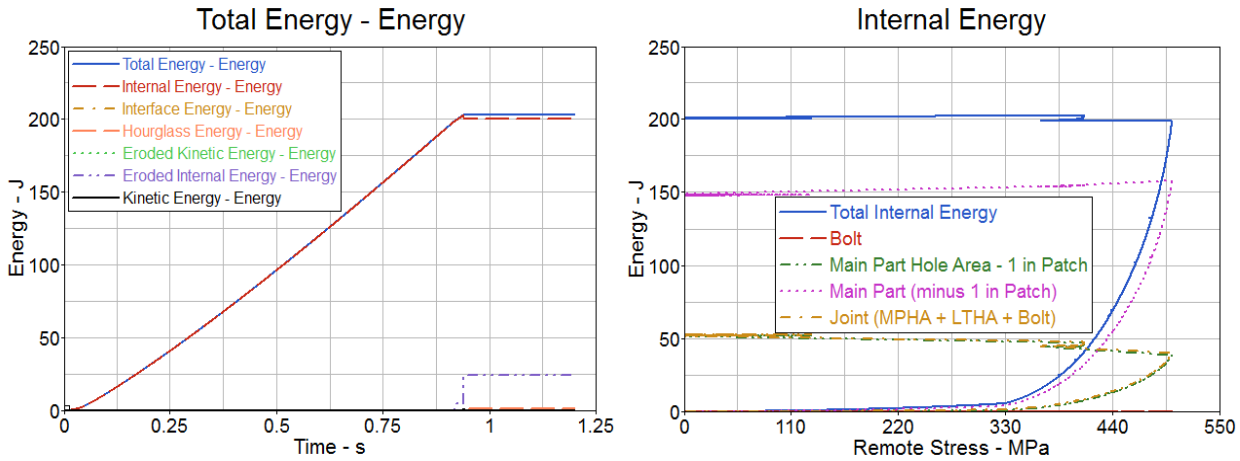

Figure 112. Energy Distribution in Config 3B (a) Energy Balance (b) Internal Energy

Based on Figure 113 on the main part and transfer part, at low remote stress, the energy on the solid model is much higher than on the simplified configurations because of the presence of high clamp-up stresses in the solid model. At higher remote stress the energies of the simplified configurations get closer to that of the solid model.

The energy in the bolt shank, shown in Figure 114, is higher in the simplified configurations compared to the solid model. This result is expected since the shear force on the bolt shank of the simplified models is higher than the solid model, as shown in Figure 110 (b).

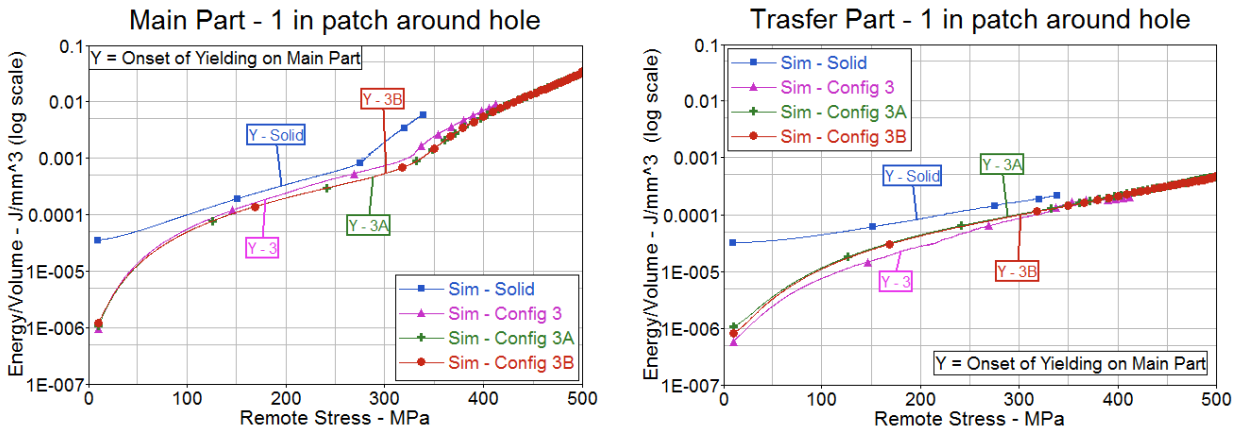

Figure 113. Comparison of Strain Energy per Volume in 1 in. long patch (a) Main Part (b) Transfer Part

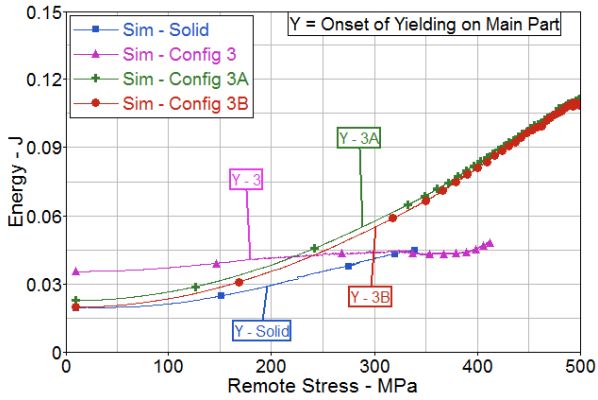

Figure 114. Comparison of Bolt Internal Energy

4.2.4 Configuration 4 – RBE Bolt Model No Hole

Many different configurations exist for this type of simplified connection, but selected few are compared in this study. RBE elements are used in different quantities and orientations to make up the different configurations. Detailed explanation of the setup of this simplified bolt

modeling technique is provided in section 3.1.5. To obtain a better understanding of this setup, the static forces related to this simplified technique are shown in Figure 115.

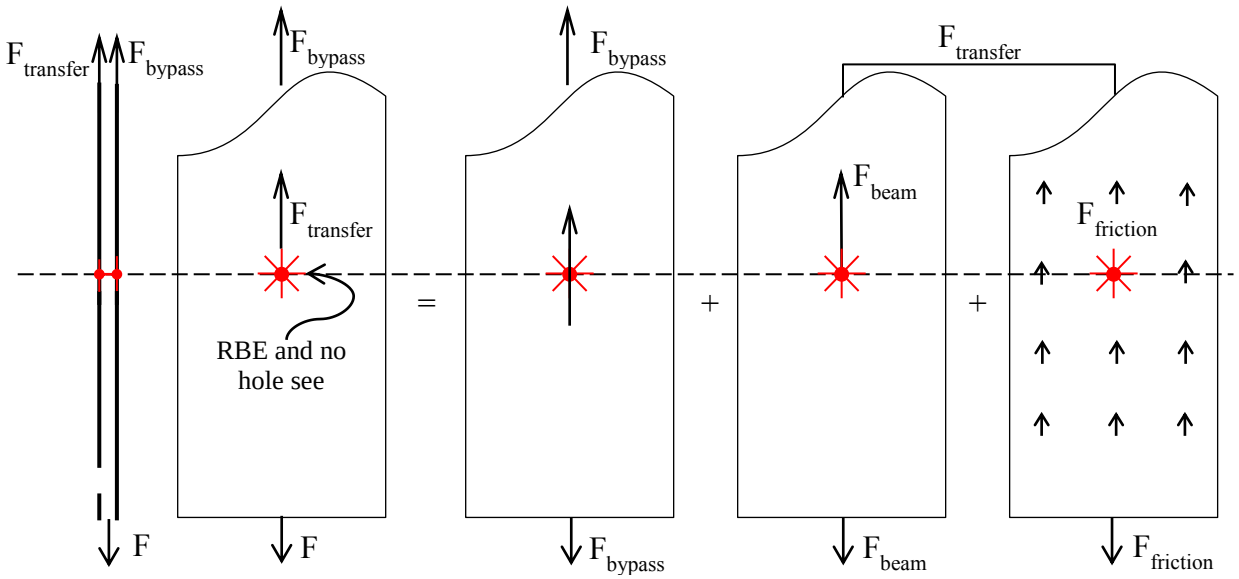

Figure 115. Free Body Diagram Config 4

The force (F) introduced in the system is split into transfer force ($F_{transfer}$) and bypass force (F_{bypass}) due to displacement compatibility enforced by the presence of the bolt [12]. F_{bypass} is the load that remains in the main part and $F_{transfer}$ is the load that is transmitted to the load transfer part. The bolt shank is represented by beam element and the nodes of the beam are connected to a nodal rigid body. The nodes of the NRB are then connected to the plates by a tied contact, *CONTACT_NODES_TO_SURFACE. The tied contact couples the nodes of the connected segment to the contact node, as detailed in section 3.4.2. The NRB distributes the loads through RBE since more nodes are used for contact and these nodes couple different elements. Since there is no fastener hole in this modeling technique, the joint is a continuum and thus facilitates some F_{bypass} load to pass through. $F_{transfer}$ is via the shear loads (F_{beam}) registered in the bolt and friction force between the plates ($F_{friction}$). The bolt head and nut are not modeled in this setup but instead are represented by NRB's. Since the plates are a continuum the clamping

forces will be distributed throughout the plate and the localized effect of friction due to clamping won't be present. Thus the contribution of $F_{friction}$ to $F_{transfer}$ will be significantly less compared to the solid model.

4.2.4.1 Load Transfer

Based on the comparison of %LT shown in Figure 116 all the configurations of this simplified technique, except Config 4H show a similar trend in %LT. The %LT for this simplified technique drops at a fast rate at low remote stress and is then sustained throughout the loading compared to the solid model where the %LT has a gentle drop throughout the loading. The load transfer behaves in the same was as described in section 4.2.2.1 except that a larger area within the plate is constrained to the bolt through the various nodes of the NRB. As a result, the bending stiffness within the localized area of the joint is low and thus the % LT is low.

Config 4A through 4D exhibits the lowest %LT and are equal to each other. Note that Config 4A through 4D are similar with only a change in the orientation of the NRB. This indicates that if the mesh is the same, the orientation of the NRB does not affect the %LT. For Config 4E through 4H, the NRB has 8 nodes, but the location of the NRB nodes with respect to the mesh is changes as shown in Figure 47. These configurations show a change in %LT which indicates that this method is mesh sensitive. Config 4B, 4C and 4D are omitted in further analysis as they show poor performance of %LT and are similar to Config 4A. In addition, Config 4F and 4H are also omitted from further analysis.

All the configurations of this simplified technique reach failure at higher remote stress than the solid model. In the solid model, the net section area is smaller due to the fastener hole while in this simplified model the plates are a continuum and thus the net section is larger. As a result, failure occurs at larger remote stress for all the configurations.

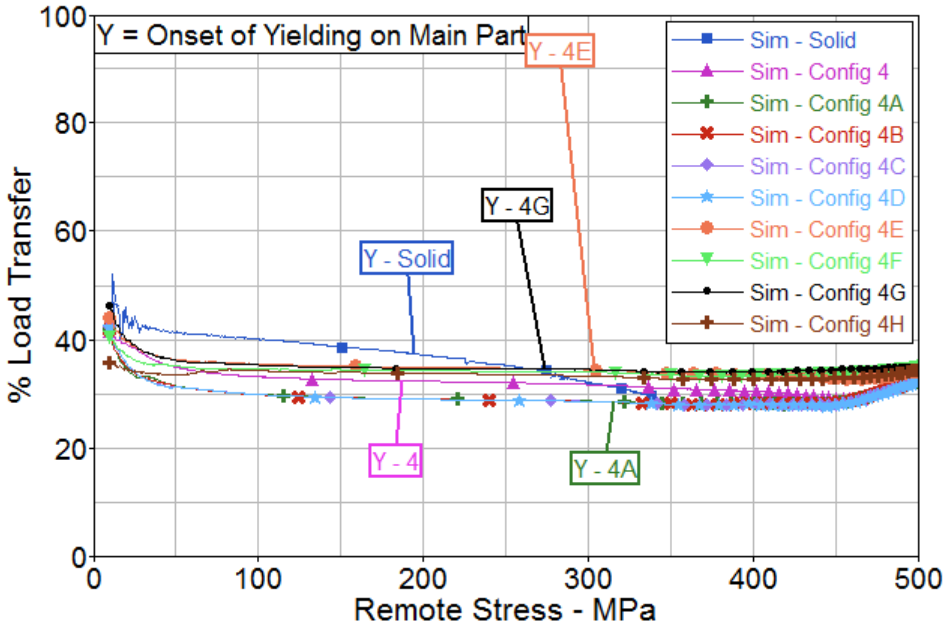

Figure 116. % Load Transfer Comparison

4.2.4.2 Kinematic Frames and Failure Modes

Based on the kinematic frames shown in Figure 117, failure modes on all the models is tear-out of the loading side of the main part due to the constraints created by the tied contact. Also necking on the main part occurs on the load introduction side of the main part. For all the models except the fine mesh model configuration 4, the initiation of failure occurs at similar remote stress. In comparison to the solid model, this simplified technique is quite different in terms of failure mode and remote stress at failure (lower compare to this simplified technique).

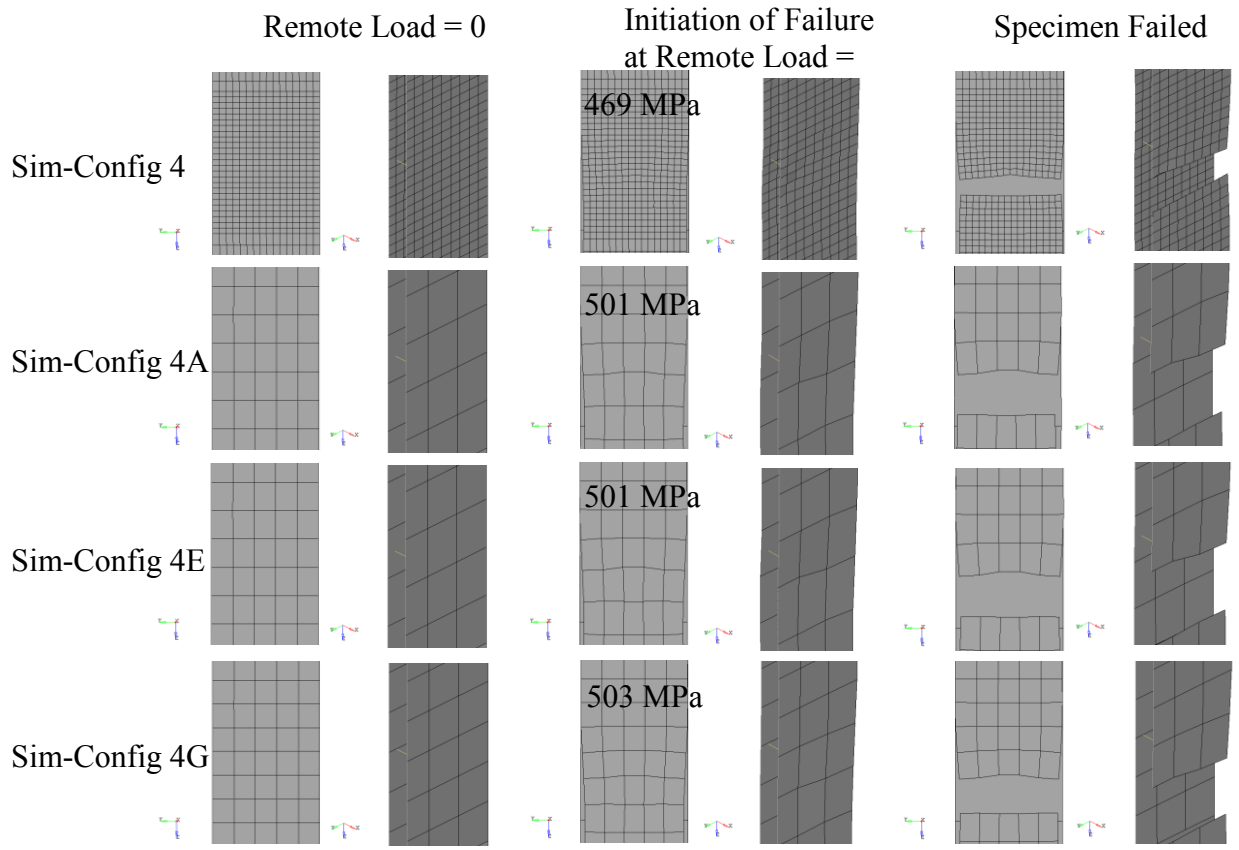

Figure 117. Kinematic Frame Comparison for Config 4

4.2.4.3 Stress and Strain Profiles

The preload measured in the test was applied to all the FE models. Due to different bolt modeling techniques the stresses that develop in the vicinity of the bolt hole, as a result of the application of preload, are quite different. The stresses developed on the main part and transfer part of the solid model due to preload are shown in Figure 65. Since the bolt head and nut are not modeled in the simplified techniques, on the application of preload, the localized compressive stresses (seen in solid model) are not present in such models and thus the stress levels seen on the models of this simplified technique are close to 0 MPa as shown in Figure 118. Therefore, although preload is applied to this simplified model, the localized effect of preload are not captured by this technique and thus preload may not have an effect on the overall performance of

the specimen. On the other hand, the preload on the bolt itself is sustained which may improve the performance of the beam itself.

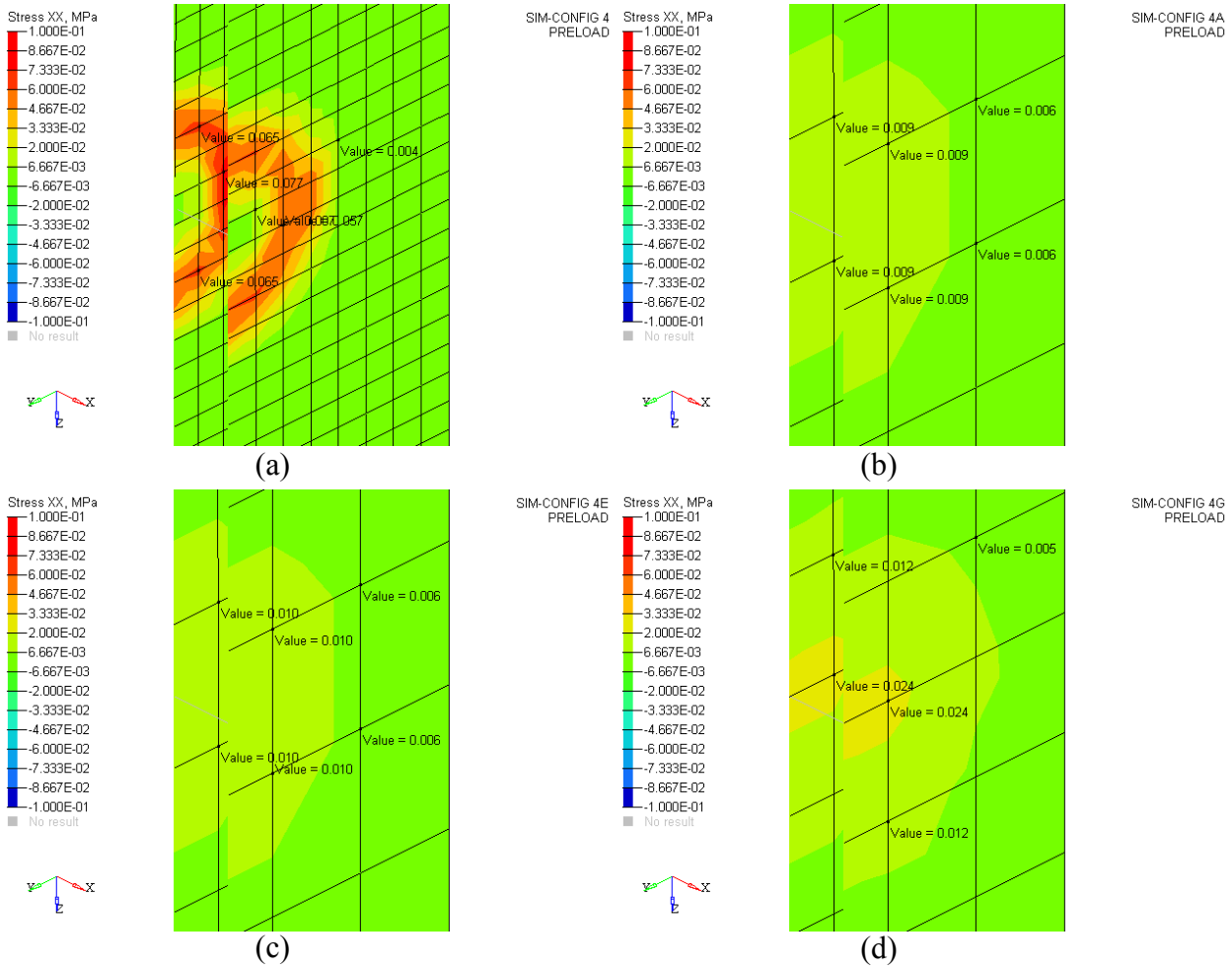

Figure 118. Stresses due to Preload (a) Config 4 (b) Config 4A (c) Config 4E and (d) Config 4G

The state of stress (vonMises stress) at the initiation of failure on the main part of the Solid model and for this simplified technique is presented Figure 66 and Figure 119 respectively. The fine mesh model, configuration 4, shows slightly better comparison to the solid model while the rest of the configurations do not compare well with the solid model. For this simplified technique, the stresses are highly concentrated on the load introduction side of the main part which is where necking and ultimately failure occurs. Changing the contact point location does not drastically affect the stress concentrations in the simplified models.

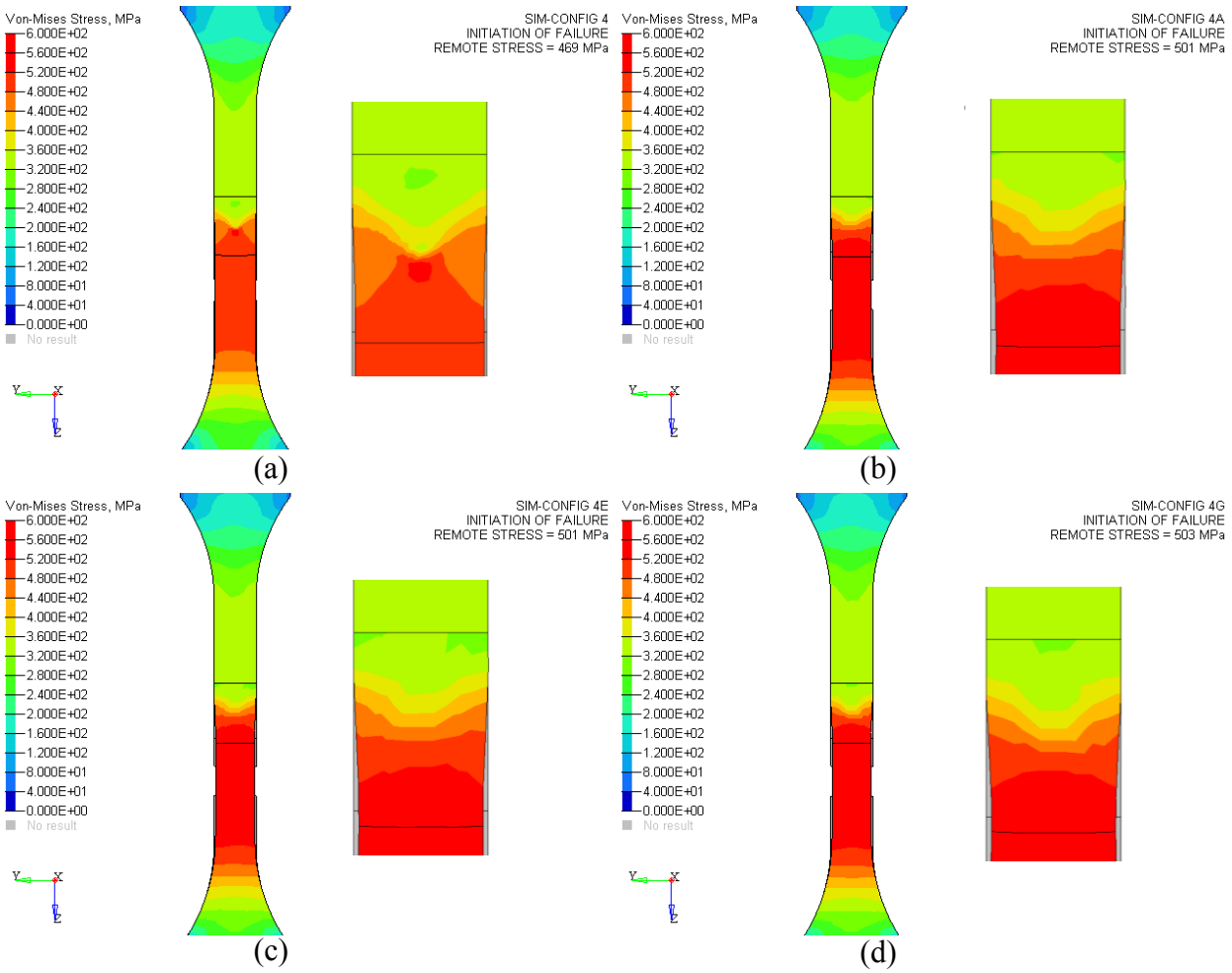

Figure 119. von Mises Stress on Main Part (a) Config 4 (b) Config 4A (c) Config 4E and (d) Config 4G

Strains, at the strain gage locations shown in Figure 32, are compared in Figure 120. These strains provide an indication of the state of loading at locations further away from the fastener hole. For all the models of this simplified technique, strains at strain gage 1 location are in good correlation to the solid model. This indicates that the use of shell elements in simplified models is sufficient to capture the stress-strain distribution. On the other hand, strains at strain gage 2 and strain gage 3 deviate from the solid model. This can be attributed to the differences in load transfer for the different models.

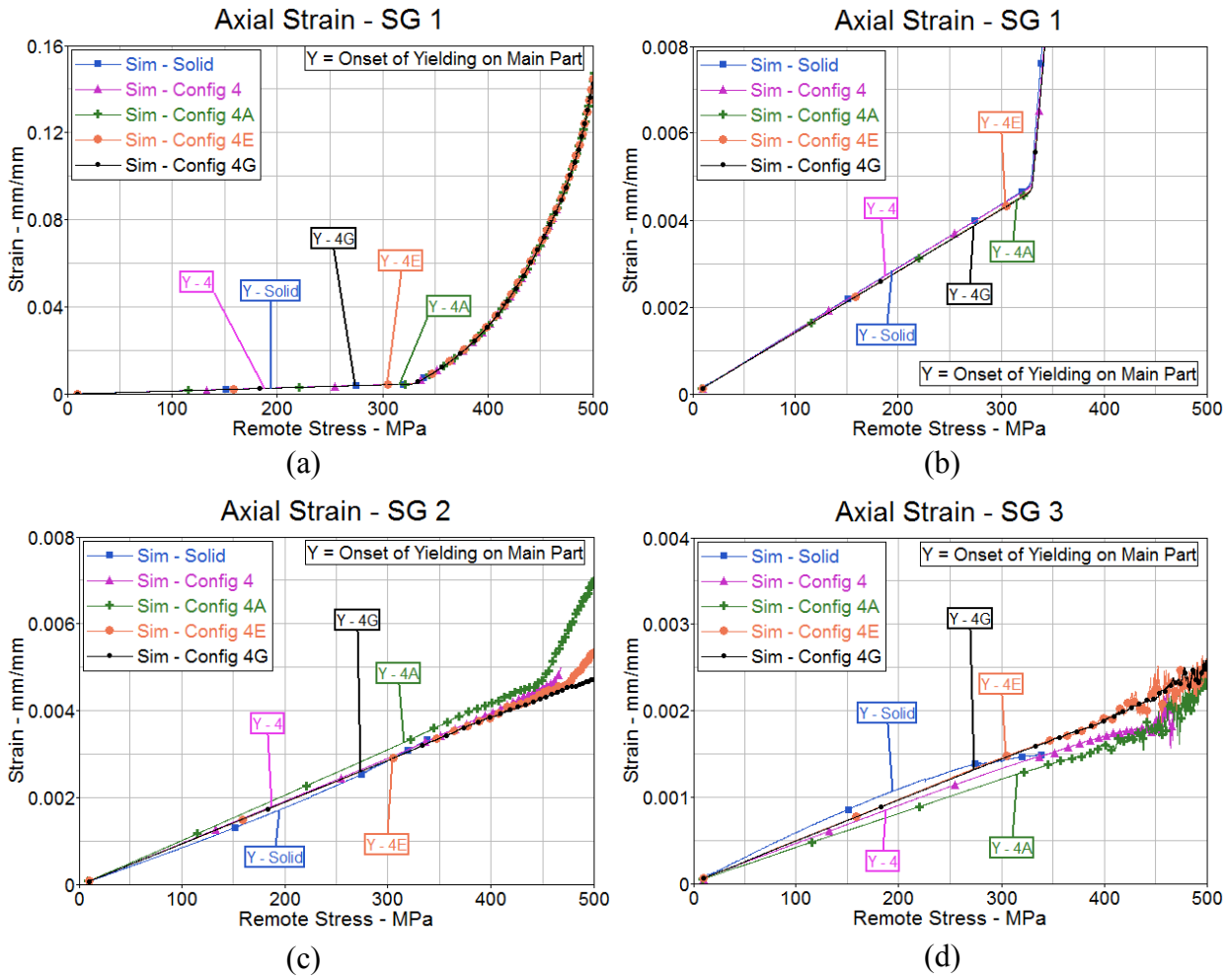

Figure 120. Axial Strain vs Remote Stress for RBE No Hole Model (a) Strain gage 1 (b) Strain Gage 1 (close-up) (c) Strain Gage 2 and (d) Strain Gage 3

4.2.4.4 Bolt Loads

The shear force on the bolt and the load recorded in the cross-section plane on the load transfer part are compared to deduce the percentage of load transferred by the bolt and that transferred by friction as shown in Figure 121. For the simplified bolt model configurations the compressive stresses due to bolt preload are negligible and thus results in lower load transferred through friction and higher through the bolt. The effect of this can be seen on Figure 121 (c),

where the load transfer by friction lasts for very low remote loads on the simplified models compared to the solid model.

For the solid model, the load transferred by the bolt is around 75% on average compared to 96% in the simplified bolt model configurations. The remaining load is transferred by friction. From Figure 121 (c) it can be noted that for all the models %LT by the bolt starts from zero and increases with increasing remote stress. When the loading begins, the bolt is not engaged, at low remote loads, and the load transfer is carried out purely by friction. As the bolt gets engaged, bearing loads kick in and the bolt starts picking up load.

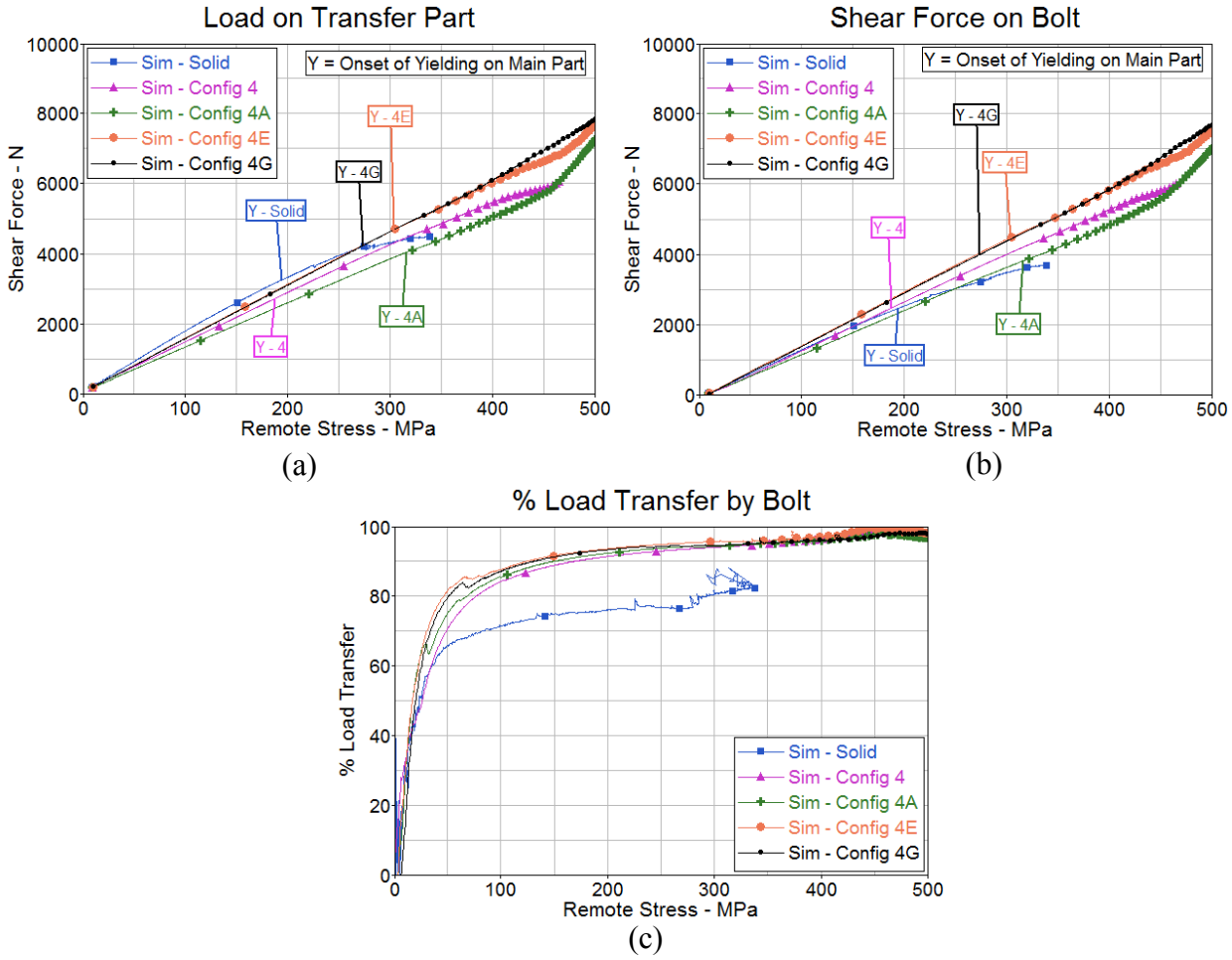

Figure 121. Comparison of Loads transferred by bolt (a) Load on Transfer Part (b) Shear Force on Bolt and (c) % LT by Bolt

Figure 122 shows the comparison of axial loads on the bolt. As expected, the initial axial load for all the models is approximately 2300 N which is the preload applied to all the models. For all the simplified the axial load is sustained up to 300 MPa of remote stress after which there is a rise in the axial load. Overall the axial loads on all the configurations of this simplified technique are very similar. The correlation of axial loads to the solid model, of this simplified technique, is not good. In the detailed model, the bolt undergoes complex loading due to the end fixity of head and nut, bearing loads and high friction on faying surfaces. None of these phenomena are observed in the simplified model.

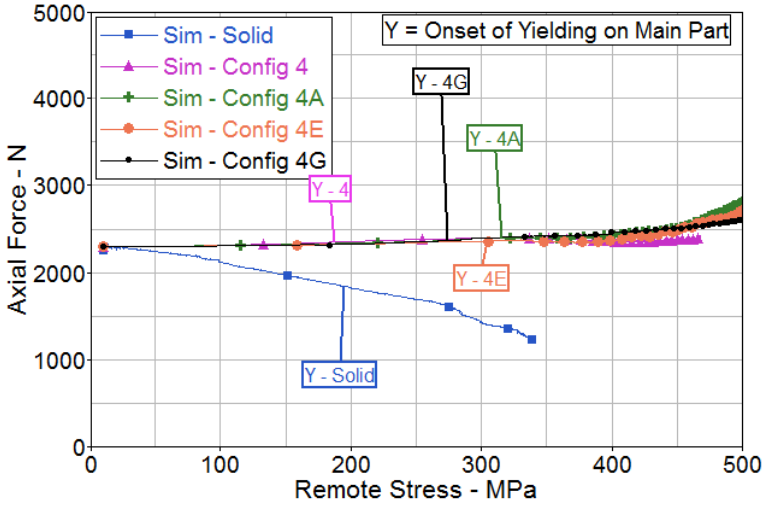

Figure 122. Comparison of Axial Force on bolt

4.2.4.5 Energy Comparison

The energy distribution for Config 4G is shown in Figure 123. As described in section 3.1, one inch long patch of elements in the vicinity of the bolt, on the main part and transfer part, were placed in separate components. The strain energy in these areas is presented in Figure 124 and the strain energy in the bolt shank is presented in Figure 125.

In comparison to the energy distribution in the solid model (total energy ~ 19 J), this simplified technique shows a total energy of approximately 210 J. The energy levels are higher

for the simplified model because the simplified models reach failure at much higher remote stress thus inputting more energy into the structure. In addition, for this simplified model, majority of the internal energy (approx. 160 J or 76%) is stored in the main part and not within the joint. The joint which is comprised of 1 in patch on the main part and load transfer part and the bolt only stores 24 % of total internal energy at failure. This can be attributed to the shift in stress concentrations, towards load introduction side, created by the simplified joint. In addition, large amounts of plastic strains are also seen at the strain gage 1 location on the main part (see Figure 120) which is a contributing factor to the internal energy. Note that the energy distribution shown in Figure 99 may not apply to the fine mesh model (Config 3) but since the focus of this study is crashworthiness, larger mesh models are focused on.

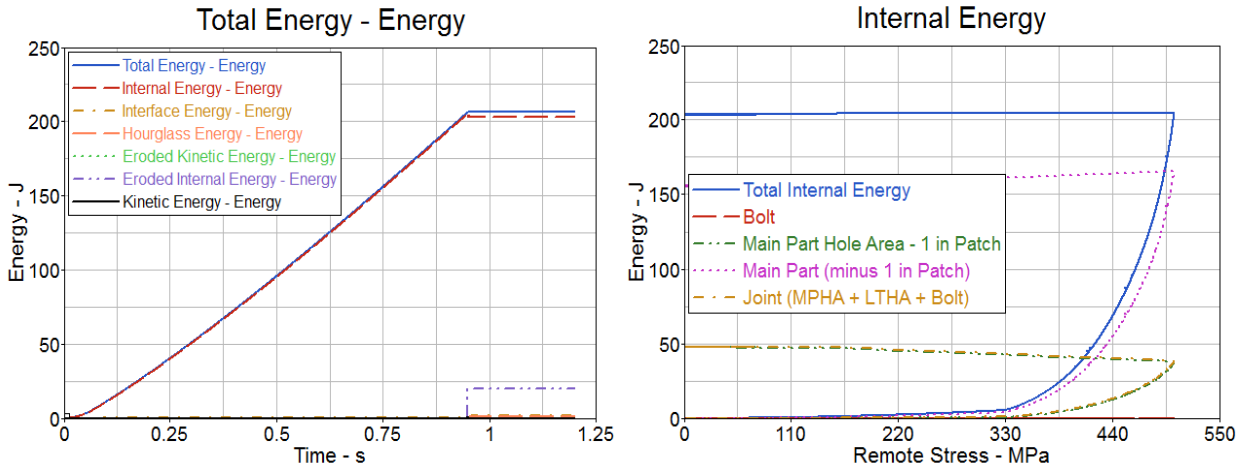

Figure 123. Energy Distribution in Config 4G (a) Energy Balance (b) Internal Energy

Based on Figure 124 on the main part and transfer part, at low remote stress, the energy on the solid model is much higher than on the simplified configurations because of the presence of high clamp-up stresses in the solid model. Overall the energy on the main part and transfer part of this simplified technique configurations does not compare well with the solid model.

The energy in the bolt shank, shown in Figure 125, is higher in the simplified configurations compared to the solid model. This result is expected since the shear and axial force on the bolt shank of the simplified models is much higher than the solid model, as shown in Figure 121 (b) and Figure 122.

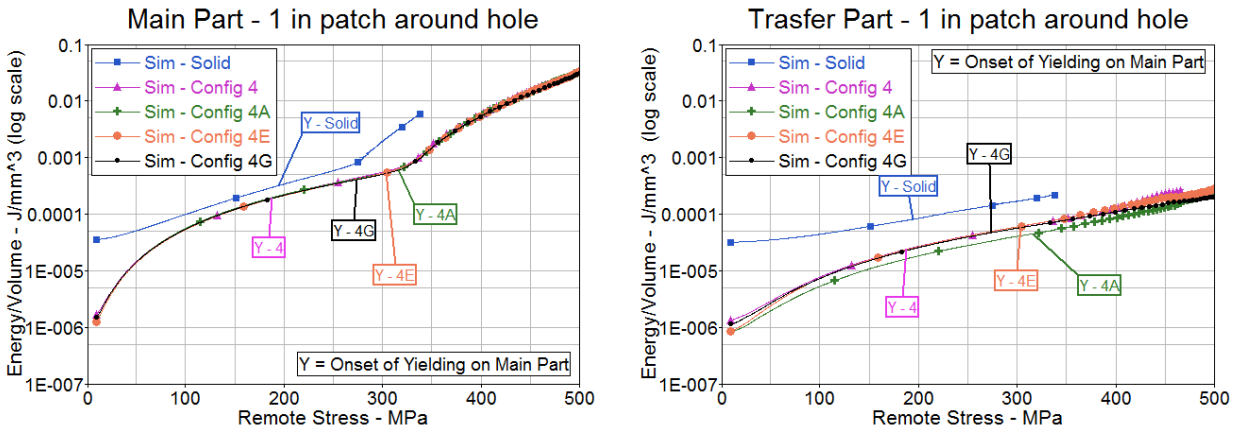

Figure 124. Comparison of Strain Energy per Volume in 1 in. long patch (a) Main Part (b) Transfer Part

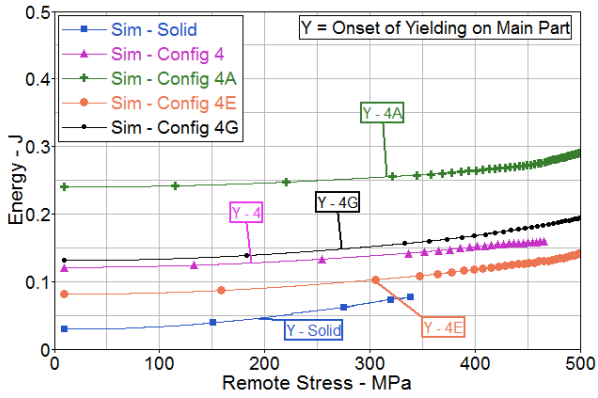

Figure 125. Comparison of Bolt Internal Energy

4.3 **Parametric Analysis of Selected Simplified Model**

High loading rates and strain rates are associated with crashworthiness analysis. Thus it is critical to understand the influence of material strain rate sensitivity on both detailed and simplified bolt models. In addition the effect of preload and friction on the performance of the

joint is also highlighted. The effects of these parameters on the performance of detailed and simplified joints is presented in subsequent sections

4.3.1 Strain Rates Effect

In a study performed at NIAR [13], the loading rates at fastener joints were estimated and it was found that loading the specimen at 20 in/s resulted in similar loading rates at the joint. Thus, for studying the effect of strain rates, the detailed 3D model and the simplified model Config 2B were loaded at 10 in/s, 20 in/s, 50 in/s and 100 in/s.

4.3.1.1 Detailed FE Model

In this study, specimen failure occurs on the plates since the plate stiffness is significantly lower than that of the bolt. Therefore, the strain rates were measured at SG 1 location and the strain rate at the hole area where failure occurs as shown in Figure 126.

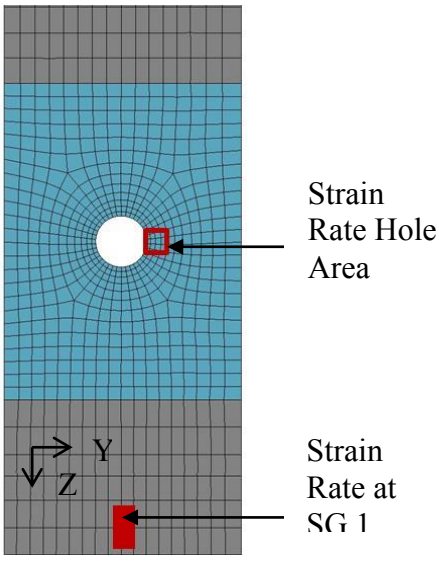

Figure 126. Strain Rate Measuring Locations on Detailed FE Model

The strain rates measured at these locations are presented in Figure 127. As expected, the strain rates increase with increasing loading rates. Rate sensitivity in the model is captured using stress-strain curves as described in section 3.6.1. Strain rates at these locations provide an indication of the material behavior at that location.

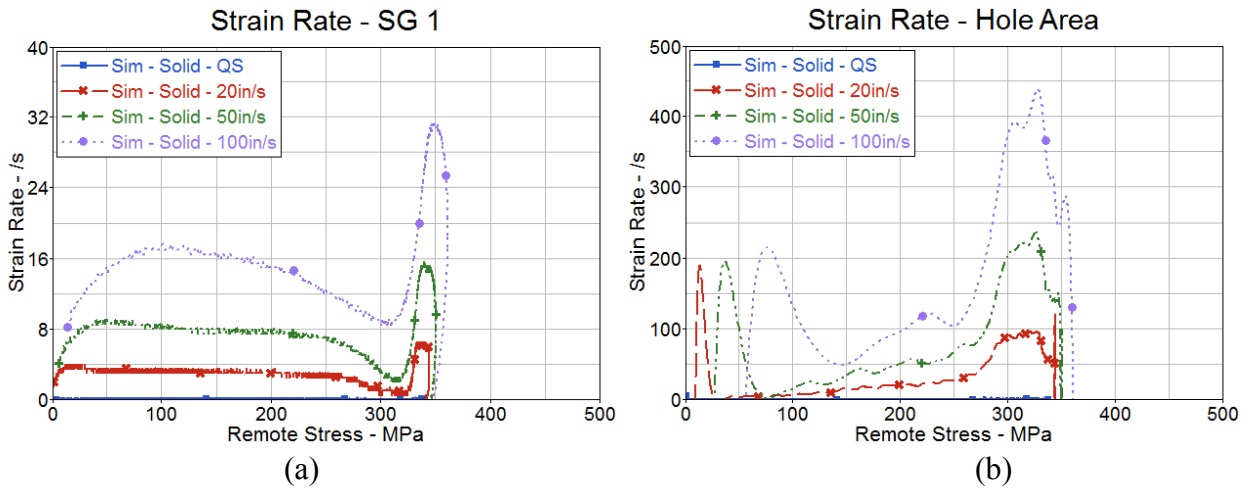

Figure 127. Strain Rates on Main Part of Detailed FE Model (a) SG 1 (b) Hole Area

Figure 128 shows a comparison of strains at the three strain gage locations specified in Figure 32 and the % load transfer for loading rates 10 in/s, 20 in/s, 100 in/s and quasi-static. It can be noted, from Figure 128(d), that for higher loading rates the % load transfer is not affected. Due to higher strain rates, the properties of the material change and thus a higher remote stress is required to initiate failure. This is reflected in the strain plots where it can be noted that the strains measured increase with an increase in loading rates.

Due to increased load carrying capacity induced by higher loading rates, it can be noted from Figure C-1 in APPENDIX C that the total energy within the system and hence the total internal energy increase with higher loading rates. A 26% increase in total internal energy is observed from quasi-static to a loading rate of 100 in/s. It can also be noted that with higher loading rates, the percentage of total internal energy in the joint (1 in patch on main part + 1 in patch on transfer part + bolt) decreases. Due to high loading rates, higher strain rates are experienced within the joint and thus the joint exhibits a stiffer behavior and more energy is stored outside the 1 in patch when loading rate is increased. A summary of the percentage of energy stored is shown in Table 6.

TABLE 6
ENERGY DISTRIBUTION FOR HIGH STRAIN RATE – DETAILED MODEL

Loading (in/sec)	Total Internal Energy (J)	Joint Internal Energy (J)	Main Part Internal Energy (J)	% Energy stored in Joint	% Energy stored in Main Part
QS	18.3	16.3	1.8	89 %	10 %
20	20.5	17.7	2.6	86 %	13 %
50	22.1	18.1	3.7	82 %	17 %
100	23.5	18.5	4.8	78 %	20 %

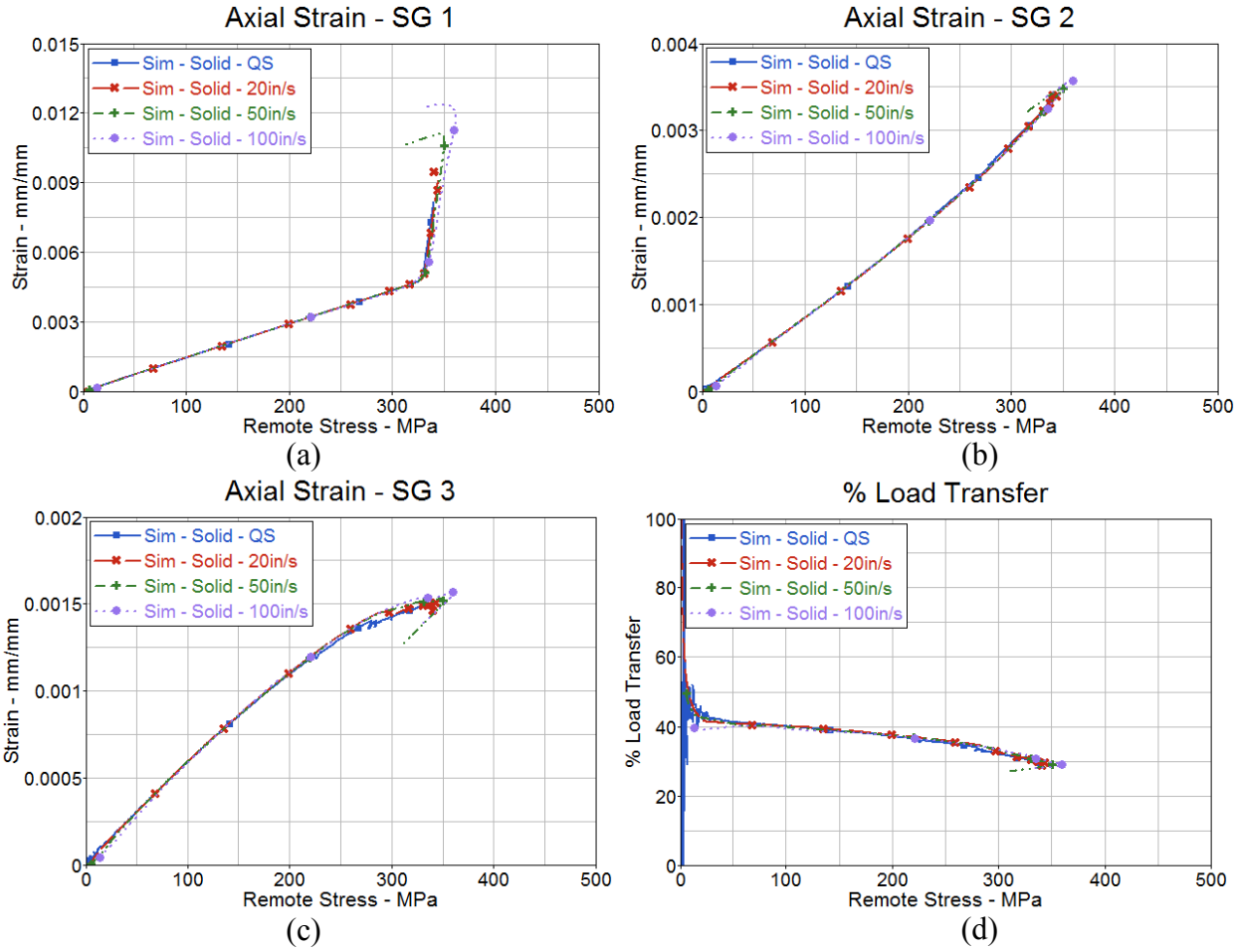

Figure 128. Comparion of High Loading Rate on Detailed FE Model (a) Strain at SG 1 (b) Strain at SG 2 (c) Strain at SG 3 and (d) % Load Transfer

4.3.1.2 Simplified FE Joint Model

Figure 129 presents the locations where strain rates are measured for the simplified FE model and Figure 130 shows the strain rates at these locations. Strain gage hole area is the location where failure initiates and the rate at SG 1 location is also measured. Based on Figure 130, it can be noted that the strain rates at SG 1 are similar to the detailed model. On the other hand, the strain rates at the hole are lower for the simplified model.

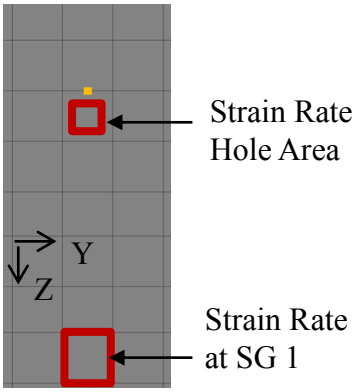

Figure 129. Strain Rate Measuring location on Simplified FE Model

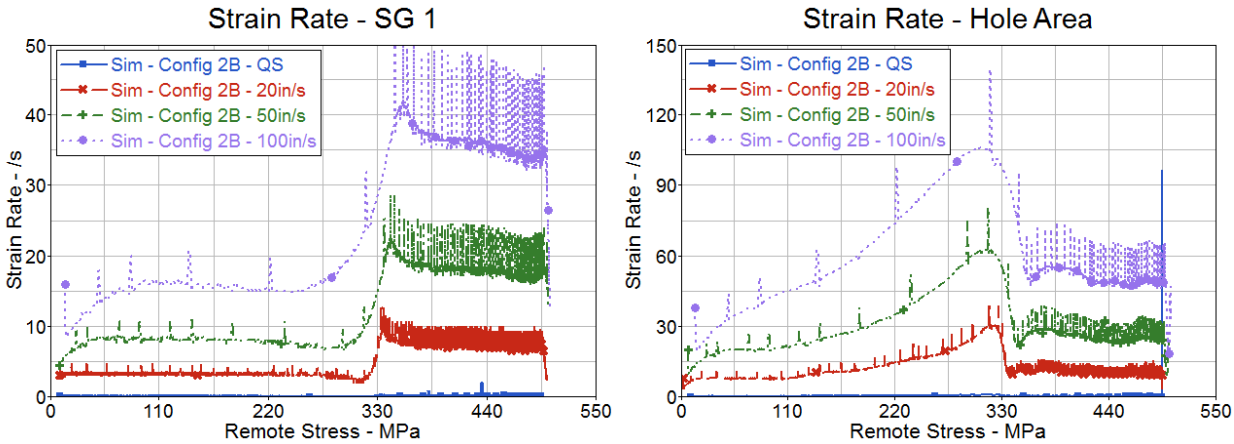

Figure 130. Strain Rates on Main Part of Detailed FE Model (a) SG 1 (b) Hole Area

Based on Figure 131, higher loading rate does not have any effect on the % load transfer or the strains for the simplified FE model. The only difference noted is that failure

occurs at higher remote stress which is expected due to stiffer material behavior induced by higher strain rates.

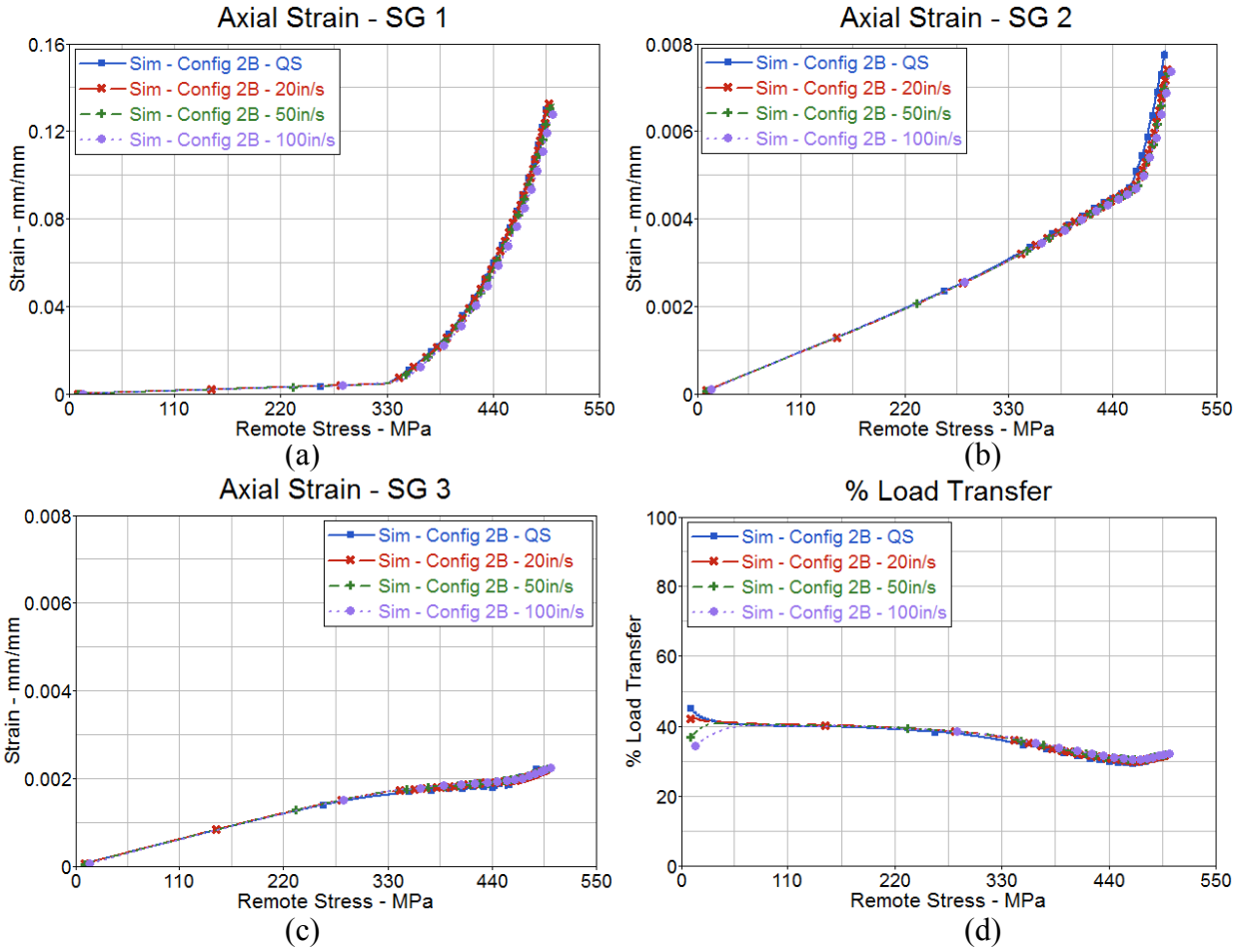

Figure 131. Comparion of High Loading Rate on Simplified FE Model (a) Strain at SG 1 (b) Strain at SG 2 (c) Strain at SG 3 and (d) % Load Transfer

From Figure C-2 in APPENDIX C, it can be noted that the total energy of the system and the total internal energy increase with an increase in loading rates. A 5% increase in total internal energy is observed from quasi-static to a loading rate of 100 in/s. It can also be noted that the internal energy of the joint (consists of 1 in patch on main part and transfer part and the bolt) does not change with increasing loading rates but the internal energy of the main part only increases. This can be attributed to the constraints imposed by the bolt of the simplified model

which results in stress concentrations occurring closer to the main part of the system as described in section 4.2.2. The energy levels for the four loading rates are presented in Table 7

TABLE 7
ENERGY DISTRIBUTION FOR HIGH STRAIN RATE – SIMPLIFIED MODEL

Loading (in/sec)	Total Internal Energy (J)	Joint Internal Energy (J)	Main Part Internal Energy (J)	% Energy stored in Joint	% Energy stored in Main Part
QS	185	55	128.4	29.7 %	69 %
20	189	55.2	132.5	29.2 %	70 %
50	194	56.2	136.2	28.9 %	70 %
100	194	56.3	135.4	28.9 %	70 %

4.3.2 Effect of Preload

In a study performed by Ghods [19], it was concluded that preload had an effect of the load transfer and hence the performance of the joint. For this study, the effect of preload is extended to simplified bolt models to understand if modeling preload is critical. For comparison purposes, the detailed model used in this study was also exposed to the no preload condition. In section 4.1.3 it has been shown that in the detailed model preload creates large compressive stresses which translate into high friction on faying surfaces, in the vicinity of the joint. This friction plays a vital role in load transfer in the detailed 3D model. As shown in Figure 132, higher percentage of load is transferred by the bolt in the no preload model and thus less work is done by friction in load transfer.

As shown in Figure 133, when no preload is applied to the model the load transfer for the detailed model drops by approximately 3%. The strains at SG 1, which is the load introduction side, is the same for the case of preload and no preload meanwhile the strains at SG 2 and SG 3 vary due to the change in load transferred.

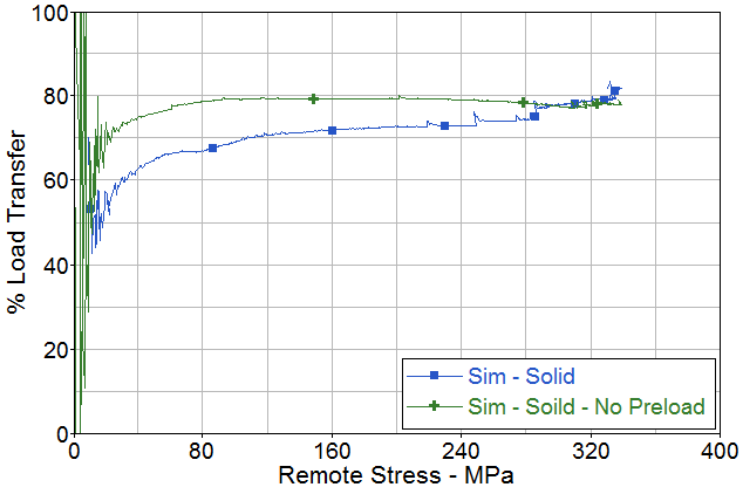

Figure 132. % Load Transfer by Bolt on Detailed FE Model

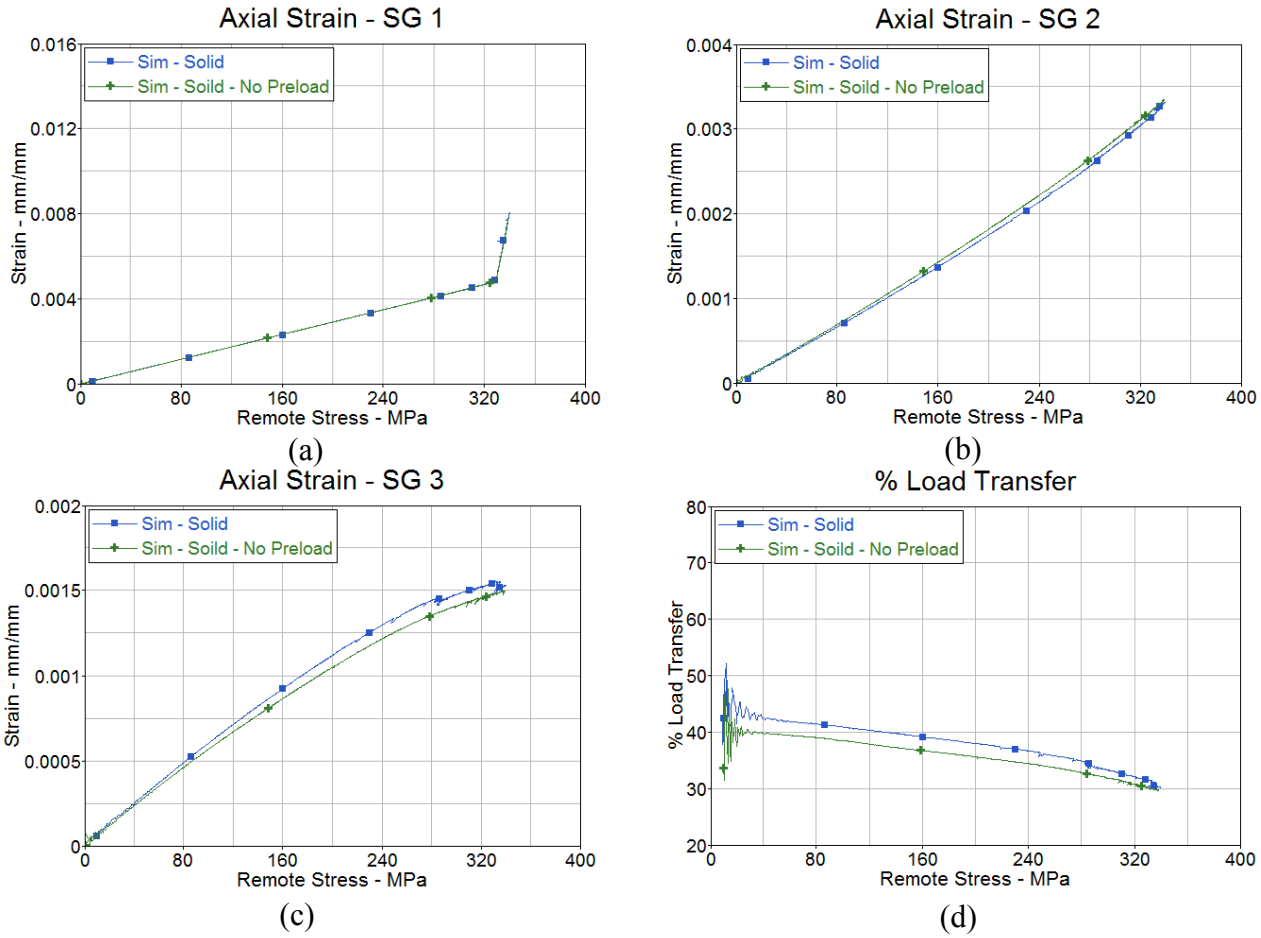

Figure 133. Comparison of Preload in Detailed FE Model (a) Strain at SG 1 (b) Strain at SG 2 (c) Strain at SG 3 and (d) % Load Transfer

For the case of simplified model Config 2B is used and preload is removed in the simulation. It can be noted in the comparison shown in Figure 134 that preload does not have a significant effect on load transfer for the simplified models. For majority of the loading, the % load transfer remains the same and a change in load transfer is observed after a remote stress of 350 MPa.

In section 4.2.2, it has been shown that the load transfer for the simplified technique Config 2 varies with the position of the beam on the element segment. Not only the load transfer, but the performance of the bolt (axial and shear loads) and the remote stress at failure are also affected. Thus the effect on preload for Config 2A is also studied and shown in Figure 135. No change in % Load transfer is observed when zero preload is applied to the bolt.

For the simplified technique in the case of no preload almost 100% of the load is transferred by the bolt in comparison to 80% in case of detailed FE model with no preload. This is shown in Figure 136.

It should be noted that although load transfer is not affected, the axial loads on the bolt will not be the same as shown in Figure 137, and thus the energy stored in the bolt will also decrease.

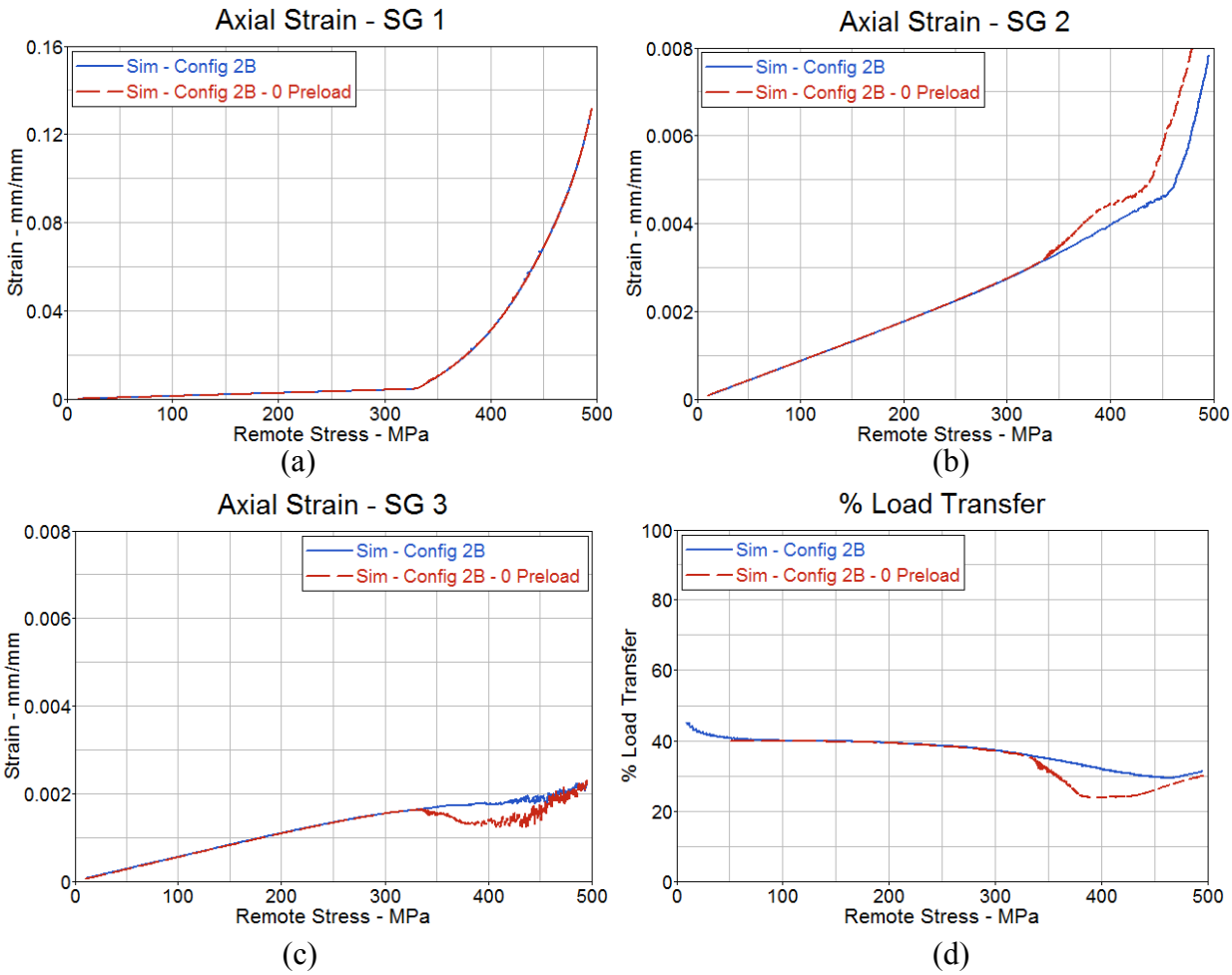

Figure 134. Effect of Preload in Simplified FE Model Config 2B (a) Strain at SG 1 (b) Strain at SG 2 (c) Strain at SG 3 and (d) % Load Transfer

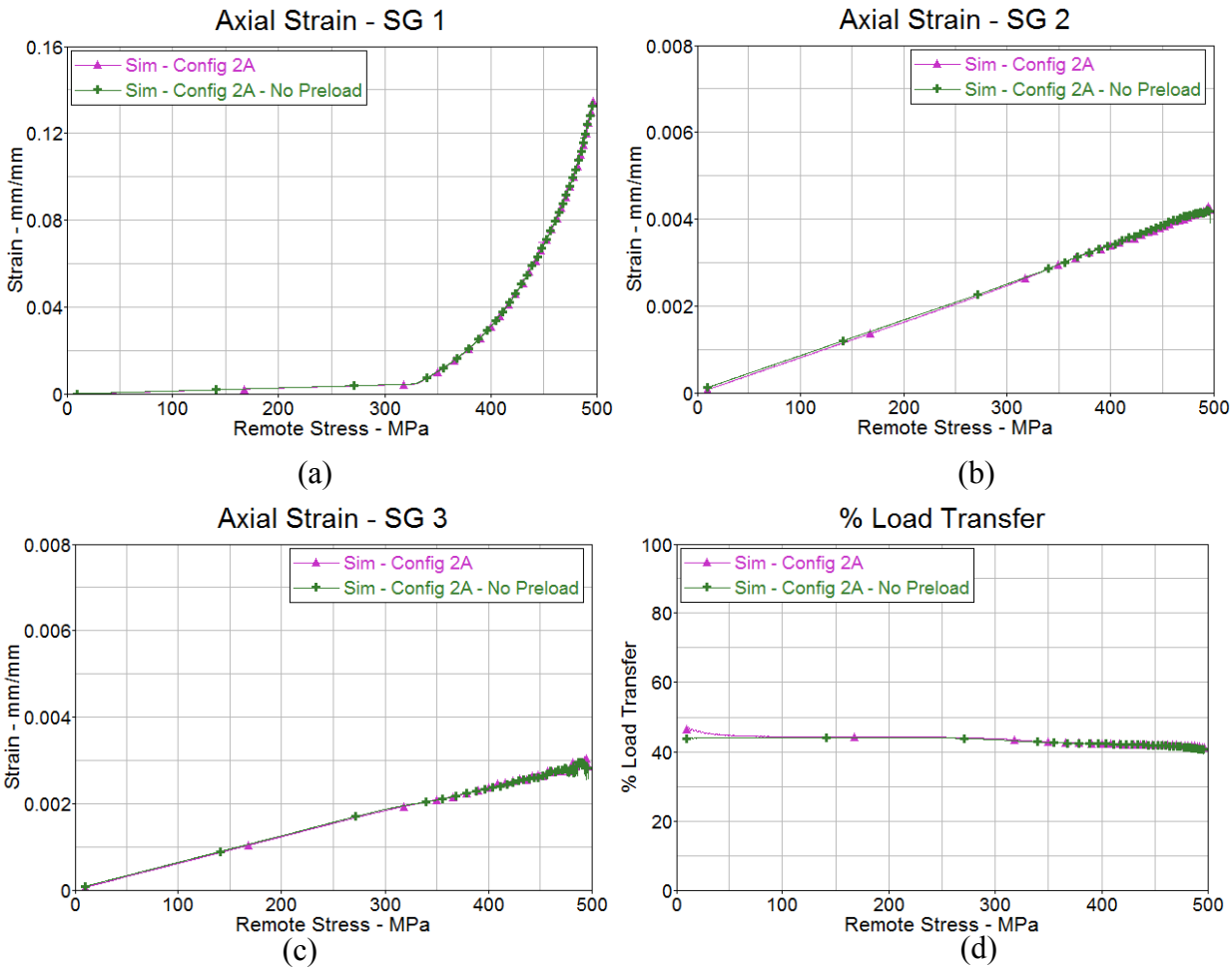

Figure 135. Effect of Preload in Simplified FE Model Config 2A (a) Strain at SG 1 (b) Strain at SG 2 (c) Strain at SG 3 and (d) % Load Transfer

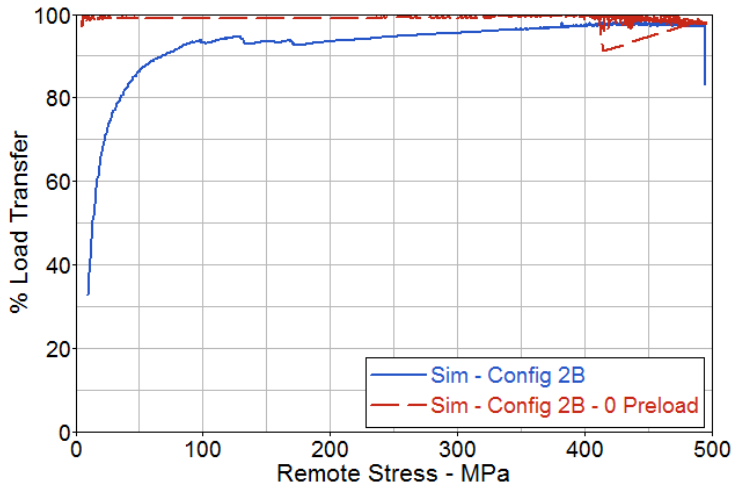

Figure 136. % Load Transfer by Bolt for Simplified FE Model Config 2B

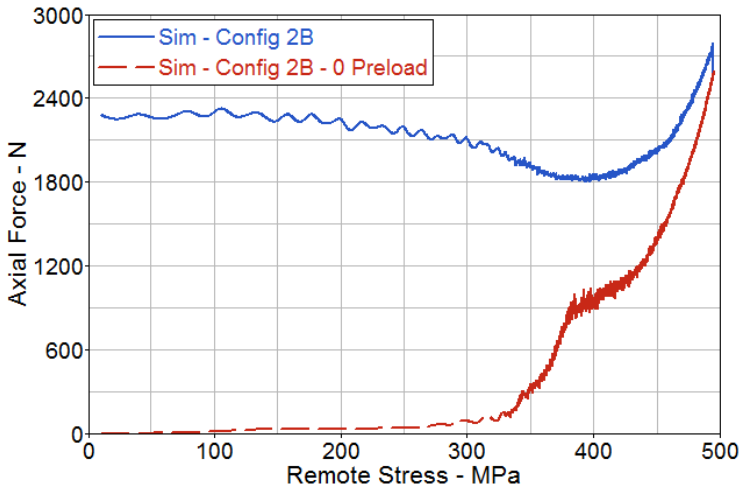

Figure 137. Axial force in Bolt for Simplified FE Model Config 2B

4.3.3 Effect of Friction

In the study performed by Ghods [19], it was also noted that coefficient of friction between faying surfaces of the single shear lap joint specimen had a major effect on percentage load transfer. For this study, friction was an unknown and was not determined by any form of testing. Thus the friction was varied and the results were compared against test data to identify a friction for comparison of simplified techniques to detailed model. As shown in Figure 138, it was deduced that a coefficient of friction of 0.1 was required for best comparison to test data. Thus this value was used for the study as described in section 3.4. In addition, Figure 138 shows that friction has a major effect on the % load transfer for the detailed model. Note that since the % load transfer shown in Figure 138 is compared to the test data, it is evaluated using the load transfer equation (2.8).

To expand on the effect of friction, the simplified FE model was also subjected to different friction values to understand how the load transfer varied. This comparison is shown in Figure 139. It can be noted that friction does have an effect on load transfer for the simplified technique but the effect does not carry the same weight as the solid model. For example in can be

noted that a change in coefficient of friction from 0.1 to 0.4 results in approximately 4% increase in load transfer for the solid model while the load transfer for the simplified model only changes by approximately 1%.

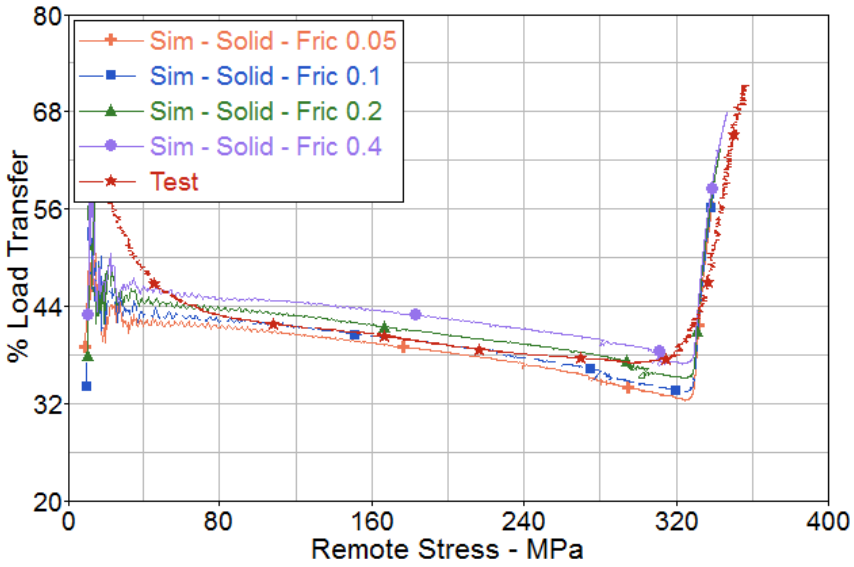

Figure 138. Effect of Friction of Detailed FE Model

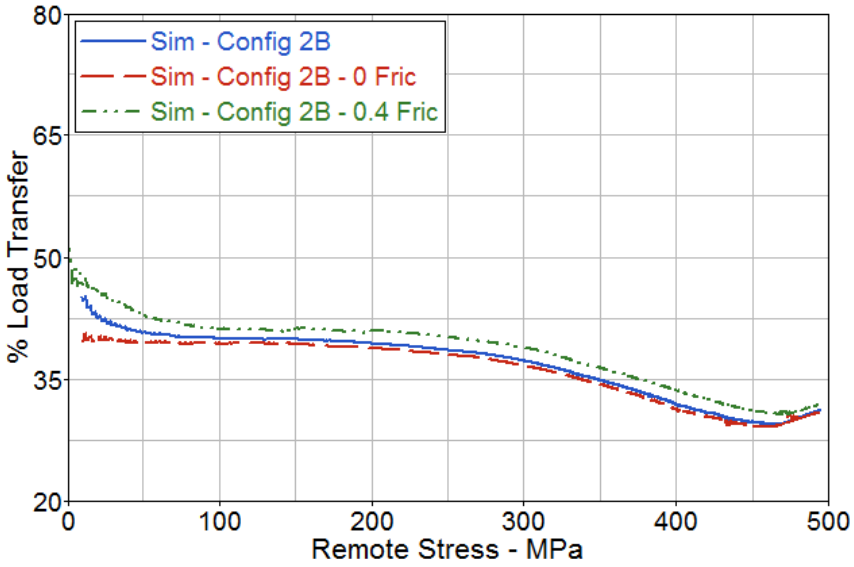

Figure 139. Effect of Friction of Simplified FE model Config 2B

CHAPTER 5

SUMMARY AND CONCLUSIONS

A one half dog bone single shear lap joint specimen was used for this study. The specimen assembly consists of the main part, load transfer part and the bolt. The main part and transfer part are constructed from aluminum 2024-T3 Clad and the bolt used in this study is a Hi-Lok® 18 bolt. Details of the specimen geometry are provided in 1.7.1. This study was performed using the FEM tool LS DYNA.

In this study, the performance of simplified joint modeling methods was explored in detail. A detailed 3D FE model was created using solid elements to validate the FE modeling methods, by comparing it to experimental testing. The detailed model was also used as a baseline model for comparing different simplified techniques. The effect of friction, preload and high strain rates on the simplified joint models was also studied. A summary of the results and conclusions drawn by analyzing the results are presented in subsequent sections. It should be noted that due to the specimen assembly, this setup only constitutes a single point load transfer and the conclusions may vary in cases of multiple point load transfer or different loading conditions.

5.1 Experimental Testing

Three experimental tests were performed for this study: test for preload characterization, test for characterization of material properties and the single shear fastener joint test to characterize the load transfer. The test setup, procedure used and results are published in detail in Chapter 2.

From the testing the preload versus torque curve was characterized to identify the preload on the specimen used for single shear joint testing. In average, the preload value found from the three joint tests was 2300 N as detailed in Table 3.

Correct material properties are critical for good FE simulations thus characterization of the plate material was also performed via testing. Five specimens were tested and the coefficient of variation for the extracted properties was within 10% which indicates that good repeatability was obtained. The data extracted from these tests is summarized in Table 2.

The setup for the single shear joint tests was complex and involved many different components such as the slack inducer system and the anti-buckling fixture. Strain histories and load transfer characterized for three specimens are presented in Figure 33. Overall good repeatability was obtained for the three specimens. The variability obtained in the test results could be due to differences in preload for each model and any errors induced in specimen preparation and setup. From the tests, the average load transfer found was 40% which is similar to the load transfer reported by previous researchers (see section 1.5). Note that load transfer is sensitive to friction, preload, specimen geometry and hole finish (see section 1.3).

5.2 **Validation of FE Modeling Methods**

A detailed joint model was created to validate the FE modeling methods and to use as baseline for comparison of simplified joint FE models. The specimen assembly of the detailed 3D model consists of 21,980 solid elements with a minimum element size of 0.206 mm. The element size was driven by the hole and bolt diameter (4.1275 mm). In addition at least four elements were maintained through the thickness of the plates which also drove the number of elements high. Three or more elements through thickness are required for solid elements to

accurately capture bending (solid elements in LS DYNA have 1 integration point at the center [14]).

The definition of material properties, boundary conditions, element formulations and contact is critical to obtain good results from the FE model. As noted, the preload and material properties were extracted from experiments and applied to the FE model. The stress strain curve extracted from the test was used in the FE model to accurately capture the material behavior. The definition of the FE model is documented in detail in Chapter 3.

Overall very good correlation of results was obtained for the detailed FE model and experimental data as shown in Figure 62. The strains at the three strain gage location, shown in Figure 32, and the percentage load transfer were in very good agreement to the test data. The comparison validates the FE modeling methods and thus the detailed FE model is used to compare to other simplified joint models.

5.3 Comparison of Detailed Joint Model to Simplified Joint Models

For this study, the fastener of choice was a bolt (HL-18) which is much stiffer than the plates it connects, which means that failure of the structure occurs at the plates. Such joints are also common in aircraft structures [12]. It should be noted that the conclusions drawn only apply to such cases.

The simplified joint models compared in this study were selected based on the criteria specified in section 1.7.2. In depth analysis and comparison of each simplified technique to the detailed FE model is provided in section 4.2. One of the most important reasons for utilizing simplified joints is the savings in computational cost. As explained in section 1.1, the computational cost in explicit time integration methods is controlled by the minimum element length. A summary of the total number of elements, the minimum element length and the run

time for detailed and selected simplified FE models is provided in Table 8. Based on Table 8 it can be concluded that using simplified models do indeed provide significant savings in simulation cost.

TABLE 8
ELEMENT SIZE AND RUN TIME SUMMARY OF DETAILED AND SELECTED SIMPLIFIED FE MODELS

	Number of Elements	Min Element Length (mm)	Run Time (min)	% Computational Time Savings
Solid Model	21980 Solid Elements	0.206	595	
Config 1 (1B)	1076 Shell and 1 Beam	2.038 shell, 2.286 beam	99	83.4 %
Config 2 (2B)	957 Shell and 1 Beam	3.644 shell, 2.286 beam	61	89.7 %
Config 3 (3B)	947 Shell and 1 Beam	3.644 shell, 2.286 beam	76	88.1 %
Config 4 (4G)	957 Shell and 1 Beam	3.644 shell, 2.286 beam	65	89.1 %

Although significant time savings are achieved, it is more important to analyze the performance and accuracy of these simplified models. A critical flaw identified in all the simplified models is the load required to reach failure. As shown in Table 9, for all the simplified joint models, approximately 40% to 45% more load is required to induce failure. In the solid model, the fastener hole is a weak point where stress concentrations are created and thus failure is initiated (net section failure). On the other hand, due to the absence of the fastener hole and the nature of constraints imposed by the simplified joints (see Chapter 3), the joint is no longer a weak point and in fact becomes more stiff. Thus stress concentrations are mitigated away from the joint (the 1 inch area, Figure 38) and the net section now has a larger width. As a result the simplified models require a larger load to initiate failure as compared to the solid model. Therefore, on application the simplified models may show higher load carrying capabilities which is not conservative.

Since the simplified models require larger loads to reach failure, naturally the total energy in the system and the total internal energy are also higher. The energy levels for detailed and simplified models after failure occurs are also compared in Table 9. Considering the joint (Figure 38) to be comprised of the 1 inch patch on the main part and transfer part plus the bolt, it has been found that approximately 88% of the total internal energy is stored there for the solid model meanwhile only about 24 % to 30 % for the simplified bolt models. This indicates that using simplified models certainly makes the joint stiffer than the actual joint. Also the importance of the fastener hole is highlighted by this analysis. Incorporating the effects of the fastener hole is critical to obtain correct energy distribution when a structure with joints is subjected to loading up to failure.

Although the energy levels after specimen failure do not compare well between detailed and simplified models, it is found that the energy levels are in good agreement for low remote loads as shown in Figure 100.

TABLE 9
COMPARISON OF REMOTE STRESS AT FAILURE AND ENERGY AFTER FAILURE

	Remote Stress at Failure (MPa)	Excess Load for Failure Compared to Solid (%)	Total Energy (J)	Total Internal Energy (J)	Internal Energy in Joint* (J)	% Internal Energy in Joint
Solid Model	348		19	18	16	**88.9 %**
Config 1 (1B)	490	40.8 %	170	169	50	**29.6 %**
Config 2 (2B)	495	42.2 %	185	188	55	**29.7 %**
Config 3 (3B)	490	40.8 %	205	200	50	**25 %**
Config 4 (4G)	503	44.5 %	210	205	50	**24.4 %**
* *Note: Joint Consists of 1 in patch on Main Part and Transfer Part + Bolt (* Figure 38*)*						

Table 10 shows the comparison of percentage load transfer before and after the initiation of yield on the specimen. The remote stress at which yielding begins on the specimen is

also documented in Table 10. Note that yielding on detailed and simplified models begins at different remote stresses. This can be attributed to the different constraints imposed by the simplified joints and hence different structural response. From Table 10 it is found that many simplified joint configurations show less than or equal to 5% difference in load transfer below yield. The differences in load transfer increase beyond yield. It is also noted that for simplified joints that involve contacts (configuration 2, 3 and 4) the % load transfer is mesh sensitive. For the fine mesh models, the % load transfer for these three configurations is lower than for the coarse mesh models. Configurations 2B and 2M show very good correlation in terms of % load transfer.

Table 10 enables the user to select the appropriate simplified model on the basis of load transfer, but it should be noted that although the load transfer may be in good agreement other parameters such as bolt loads may not compare well. It is recommended that the user understand the overall behavior of the simplified joint model. Also note that the results presented are for single point load transfer obtained from single shear lap joint tests.

In addition, it has been found that the contribution of the bolt to the %LT is always higher in the simplified model (80 - 97%) compared to the solid model (60% - 80%). This implies that the %LT by friction is lower for the simplified joint models. It is known that the bolt head and nut and the fastener hole are not modeled in the simplified techniques. As a result the compressive forces induced by the bolt head and nut, due to preload, are lower and thus the effect of friction on faying surfaces is minimized. Thus majority of the load transfer is carried out by the bolt in simplified models.

TABLE 10
COMPARISON OF % LOAD TRANSFER

	Configurations	Remote Stress at Initiation of Yield (MPa)	% Difference in Load Transfer Before Yield (Compared to Solid)	% Difference in Load Transfer After Yield (Compared to Solid)
Solid	Solid	194	-	-
RBE Bolt Model with Hole	1	75	0% - 4% Higher	4% - 10% Higher
	1A	259	0% - 7% Higher	5% - 7% Higher
	1B	138	0% - 4% Higher	4% - 5% Higher
Mesh Independent Spotweld Beam Model	2	269	0% - 17% Lower	16% - 17% Lower
	2A	294	0% - 11% Higher	11% - 12% Higher
	2B	282	0% - 3% Higher	1% - 3% Higher
	2E	293	0% - 5% Higher	1% - 5% Higher
	2K	301	0% - 9% Higher	6% - 9% Higher
	2L	292	0% - 9% Higher	6% - 9% Higher
	2M	288	0% - 0.5% High/Low	0% - 7% Lower
	2O	299	1% - 7% Lower	2% - 9% Lower
Mesh Independent Spotweld Beam with Patch	3	180	0% - 8% Lower	8% - 14% Lower
	3A	288	0% - 11% Higher	11% - 12% Higher
	3B	302	0% - 11% Higher	11% - 12% Higher
RBE Bolt Model with No Hole	4	188	5% - 7% Lower	5% Low - 2% High
	4A	316	3% - 10% Lower	3% Low - 3% High
	4E	304	5% Low - 3% High	3% - 5% High
	4G	274	5% Low - 0.5% High	0.5% - 6% Higher

In terms of the axial loads on the bolt, as expected, the solid model shows a drop in axial loads from the initial preload. All the simplified models except configuration 4 also exhibit a drop in axial loads from the initial preload (configurations 1-1B, 2-2O and 3-3B). But the drop in axial loads for the simplified models occurs at different remote loads. Also in most simplified

models (except configuration 4), the axial loads rise after the initial drop. Only for a few simplified models, the axial loads surpass the initial preload and this occurs close to reaching failure (configuration 3, 2E, 2M). Configuration 1 and 1B show good correlation to solid in terms on axial loads but not configuration 1A. Thus overall it can be concluded that for simplified configurations 1, 2 and 3 the axial loads are mesh sensitive. For configuration 4, the axial loads show an increasing behavior and the loads are similar for all the different variations of configuration 4.

The shear forces show scatter in data for all the configurations. For some cases the shear forces in the bolt are higher than the detailed model while for some cases the shear forces are lower. For all variations in configuration 4, the shear forces show good correlation to the solid model at low remote loads. It can be concluded that bolt shear forces are sensitive to mesh and the constraints imposed by the simplified joints.

The strain gage locations are reported in Figure 32. From a comparison of axial strains, it is found that the strain at SG 1, which is on the load introduction side of the main part, shows very good correlation to the solid model. This indicates that the use of shell elements is sufficient to capture the axial strains. On the other hand, since the % load transfer changes in the simplified models, the strains at SG 2 and SG 3 vary when compared to the solid model. The strains at SG 2 and SG 3 are in good agreement to the solid model only for configurations 2B and 2M which show good correlation of %LT. The stresses and strains at preload do not compare well to the solid model due to the absence of the bolt hole and the bolt head and nut. The stress distribution at the initiation of failure is also different for the simplified models due to change in location of stress concentrations.

Therefore, for the case of single point load transfer where the bolt is much stiffer than the joining plates and failure is expected on the plates, it can be concluded that simplified joint models can be used for low loading conditions. Beyond yield, the difference in the results increases and a thorough understanding of the limitations and behavior of the selected simplified method is important. Overall, the simplified methods successfully captured the load transfer mechanism of the joint but due to the absence of a fastener hole and bolt head and nut the failure modes and energy levels differ. The use of simplified joints does result in significant savings in computational cost and thus may be employed for a quick evaluation of design concepts or for preliminary studies. For areas where detailed information is required, it is recommended to use detailed joint modeling methods. It is rather difficult to decipher if the simplified models suffice as replacement for detailed joint models as it is subjective to the end use and purpose of the model.

5.4 Effect of Strain Rates, Friction and Preload

From the parametric study documented in 4.3, it is found that higher strain rates do not affect the load transfer on both the detailed and simplified joint models. For both cases, the remote stress at failure increases with higher strain rate since the material response changes. Thus, as expected, higher strain rates (higher material strength) allows for higher load carrying capacity. As a result, the total energy and total internal energy also increase for both detailed and simplified joint models. The strain rates developed in the vicinity of the bolt differ for the detailed and simplified models. As a result, the amount of change in energy due to high loading rates is also different for detailed and simplified joint model. For example when the loading rates change from quasi-static to 100 in/s the maximum strain rate in the detailed joint model is approximately 400 /s and the total internal energy increases by approximately 26%. Similarly for

the simplified joint model the maximum strain rate for loading rate of 100 in/s is approximately 110 /s and the total internal energy increases by approximately 5%. Therefore in comparison to detailed joint model, the simplified models underperform when subjected to high loading rates.

The effect of preload is high for detailed joint model where the % LT decreases by about 3% when preload is removed from the simulation. In addition, the amount of load transferred by bolt also increases. This goes on to prove that preload increases the effect of friction and thus facilitates higher load transfer by friction. The %LT for the simplified joint model did not change when preload was removed from the model but the amount of load transferred by bolt does increase.

When friction values are changed, the %LT changes for both detailed and simplified joint models. It is found that the effect of friction is more pronounced in the detailed model. For instance when the coefficient of friction is changed from 0.1 to 0.4, approximately 4% increase in load transfer is seen on the solid model while the load transfer for the simplified model only changes by about 1%.

5.5 **Recommendations and Future Work**

Based on the summary of results and conclusions drawn from the study, simplified joint models for single point load transfer (single shear applications) should be used with extreme caution as they tend to be highly mesh sensitive and alter the load carrying characteristics of the structure enabling it to carry large amount of loading. Thus it is recommended to use simplified models within the lower elastic range of the joined plates.

In addition, the selection of the simplified joint should be based on the end result expected. For example if the goal of the study is only to achieve the correct load transfer

(example aircraft seat structures) and not to analyze failure or bolt loads, certain simplified models may be sufficient.

From the results of the parametric study, it is recommended to use correct friction values as the load transfer is sensitive to friction even in simplified joints. If bolt loads are being monitored and studied, the application of preload is also important for simplified joint models.

It was also observed that the overall energy levels in simplified models are significantly larger for simplified joint models. To improve the correlation of energy, a new failure criterion for the joint is required. From the comparison of internal energy on the main part hole area (Chapter 4) where failure occurs for all models, the internal energy for some simplified joint models is similar to the detailed model when failure of detailed model occurs. Thus a failure criteria based on internal energy of the main part may be used to initiate failure within the joint. The drawback of this would be that in a large model each joint would have to be grouped as a separate component to apply the suggested failure criteria. This would result in a laborious pre-processing effort.

By comparing the percentage load transfer, it was found that for configurations 2, 3 and 4 the fine mesh models (0.3mm minimum element length) had low load transfer compared to the coarse mesh models (3mm minimum element length). Therefore, by doing a mesh sensitivity study, it may be possible to identify a mesh size suitable for matching the load transfer.

Clearly ignoring the fastener hole in simplified models creates many problems. Therefore if the effect of fastener hole can be incorporated in the simplified techniques the overall joint performance, energy levels and failure modes can improve.

In addition, the bolt head and nut also play a critical role to capture effect of friction and in load transfer as well. Therefore incorporating the bolt head and nut in simplified models may also improve the load transfer.

Overall it can be concluded that at the specimen level, simplified joint models perform poorly compared to the detailed joint model. It is recommended that simplified joint models should only be used once all limitations are understood and the risks are assessed.

5.5.1 Future Work

To obtain a more complete understanding for joint behavior especially simplified joint modeling and how it can be translated for use in large FE models to support crashworthiness simulations, the following are some areas that require in depth analysis.

1. Study joints under axial loading and combined loadings. In a crash analysis, the joints are generally subjected to combined loading hence it is trivial to expand the research to different modes of loading.
2. Expand the study to multiple fastener connections. This study involved a single shear lap joint with a single bolted connection. It is important to understand if the results obtained from this study extrapolate to cases with multiple fastener joints.
3. Further analyzing real structural components (components from aircraft or sizeable aircraft section) to compare detailed and simplified joint models will add great value to this area of research and provide evidence of how simplified joint models fare when subjected to such structures..
4. To round up the research on joints, scenarios where bolt failure is more likely than the failure of joined plates, such as riveted joints or where the fastener stiffness is equivalent or less than the stiffness of joined plates should be looked into. Also how such joints compare to

simplified joint modeling techniques is an important area for improving crashworthiness simulations. In addition looking into joints in composite materials (Carbon Fiber Composites) is also a great area of interest with the recent advancement in use of composites in both aircraft and automotive structures. Composite material tends to have a more brittle failure compared to metals hence the use of simplified bolt models may work for such materials. In addition, FE modeling of composites heavily relies on the use of Shell Elements and thus simplified joint models would be preferred.

REFERENCES

REFERENCES

[1] LSTC. "LS-DYNA," Livermore Software Technology Corp., 2011. <http://www.lstc.com/products/ls-dyna>.

[2] Ostergaard, M. G., Ibbotson, A. R., Le Roux, O., and Prior, A.M., "Virtual testing of aircraft structures," *CEAS Aeronautical Journal*, Vol. 1, No. 1-4, 2011, pp. 83-103.

[3] Fasanella, E. L., and Jackson, K. E. "Crash simulation of a vertical drop test of a B737 fuselage section with auxiliary fuel tank," *Third Triennial International Fire & Cabin Safety Research Conference*, 2001.

[4] Fasanella, E. L., Jackson, K. E. and Lyle, K. H., "Finite Element Simulation of a Full-Scale Crash Test of a Composite Helicopter," *Journal of the American Helicopter Society*, Vol. 47, No. 3, 2002, pp. 156-168.

[5] Olivares, G., and Yadav, V., "Mass transit bus-vehicle compatibility evaluations during frontal and rear collisions," *Proc. 20th Int. Technical Conf. Enhanced Safety of Vehicles*, 2007.

[6] Dhole, N., Yadav, V., and Olivares, G., "Certification by Analysis of a Typical Aircraft Seat," *12th International LS-DYNA Users Conference*, Dearborn, Michigan, 3-5 June 2012.

[7] Olivares, G., "Transit bus crashworthiness: Finite Element modeling and validation." *International Crashworthiness Conference,* Athens, Greece. 2006.

[8] Byar, A., "A crashworthiness study of a Boeing 737 fuselage section," Ph.D. diss., Drexel University, Philadelphia, 2003.

[9] Advisory Circular 20-146, "Methodology for Dynamic Seat Certification by Analysis for Use in Parts 23, 25, 27 and 29 Airplanes and Rotorcraft," Federal Aviation Administration, 2003.

[10] Bickford, J. H., *Introduction to the design and behavior of bolted joints: non-gasketed joints*, CRC Press, 2007.

[11] Fisher, J. W., Struik, J. and Kulak, G., *Guide to design criteria for bolted and riveted joints*, Wiley, 1974.

[12] Skorupa, A., and Skorupa, M., *Riveted lap joints in aircraft fuselage: design, analysis and properties*, Vol. 189, Springer, 2012.

[13] Olivares, G., Dhole, N., Zinzuwadia, C., and Acosta, J. F., "Crashworthiness Analysis of Generic Narrow Body Aircraft," DOT/FAA/(AR)-XX/XX.

[14] LS-DYNA Theory Manual, Livermore Software Technology Corporation, Livermore, CA, 2014.

[15] Keshavanarayana, S., Smith, B. L., Gomez, C., Caido, F., "Fatigue-based severity factors for shear-loaded fastener joints," *Journal of Aircraft,* vol. 47, pp. 181-191, 2010.

[16] Barrios, W., "Stresses and Displacements due to Load Transfer by Fasteners in Structural Assemblies," Engineering Fracture Mechanics, Vol. 10, No. 1, 1978, pp. 115–176.

[17] Jarfall, L., "Fatigue Cycling of Riveted or Bolted joints," FFA report HF-1239, The Aeronautical Research Institute of Sweden, 1969.

[18] Narkhede, S., Lokhande, N., Gangani, B., and Gadekar, G., "Bolted Joint Representation in LS-DYNA® to Model Bolt Pre-Stress and Bolt Failure Characteristics in Crash Simulations," *International LS-DYNA Users Conference,* USA, 2010.

[19] Ghods, F., "Finite element modeling of single shear fastener joint specimens: a study of clamp-up, friction and plasticity effects," Thesis, Wichita State University, 2011.

[20] Wang, G. S., "Computational Method for Evaluating the Fatigue Life of Mechanical Joints," 2001.

[21] Zeng, L., Haylock, L., Zonker, H., Goodman, J., and Burg, J., "Effects of Coating Tribology on Fastener Single and Double Shear Strength," No. 2006-01-3155, SAE Technical Paper, 2006.

[22] Oskouei, R. H., Keikhosravy, M., and Soutis, C., "A finite element stress analysis of aircraft bolted joints loaded in tension," *Aeronautical JournaL,* Vol. 114, No. 1155, 2010, pp. 315.

[23] Birch, R. S., and Alves, M., "Dynamic failure of structural joint systems." *Thin-walled structures* 36.2 (2000): 137-154.

[24] Young, W. C., and Budynas, R. G., *Roark's formulas for stress and strain*, Vol. 7, New York, McGraw-Hill, 2002.

[25] Starikov, R. "Mechanically fastened joints: critical testing of single overlap joints," FOI-R-0441-SE, FOI Swedish Defence Research Agency, 2002.

[26] Ireman T., "Three-dimensional Stress Analysis of Bolted Single-lap Composite Joints", *Composite Structures,* Vol. 43, No. 3, 1998, pp. 195-216.

[27] Schijve, J., "Fatigue damage in aircraft structures, not wanted, but tolerated?," *International Journal of Fatigue,* Vol. 31, pp. 998-1011, 2009.

[28] Jarfall, L., "Shear Loaded Fastener Installations," *International Journal of Vehicle Design*, Vol. 7, pp. 337-380, 1986.

[29] Ekh,J., Schon, J., and Melin, L. G., "Secondary bending in multi fastener, composite-to-aluminium single shear lap joints," *Composites Part B: Engineering*, Vol. 36, pp. 195-208, 2005.

[30] van der Linden, H. H., "Fatigue Rated Fastener Systems - An AGARD Coordinated Testing Program," 1985.

[31] Reddy, J. N., *An introduction to the finite element method*, Vol. 2, New York, McGraw-Hill, 1993.

[32] Soo Kim, T., and Kuwamura, H., "Finite element modeling of bolted connections in thin-walled stainless steel plates under static shear," *Thin-Walled Structures*, Vol. 45, No. 4, 2007, pp. 407-421.

[33] Kim, J., Yoon, J., and Kang, B., "Finite element analysis and modeling of structure with bolted joints," *Applied Mathematical Modelling*, Vol.31, No.5, 2007, pp. 895-911.

[34] Montgomery, J., "Methods for modeling bolts in the bolted joint," *ANSYS user's conference*, Vol. 5, 2002.

[35] Marzenmiller, A., Schweizerhof, K., and Rust, W., "Joint Failure Modeling in Crashworthiness Analysis", Second International LS-DYNA3D Conference, San Francisco, California, September 20 and 21, 1994.

[36] Tanlak N., Sonmez, F.O., and Talay, E., "Detailed and simplified models of bolted joints under impact loading," *The Journal of Strain Analysis and Engineering Design*, Vol. 46, No. 3, 2011, pp. 213-225.

[37] Sonnenschein, U. "Modelling of bolts under dynamic loads." *LS-Dyna Anwenderforum*, Bamberg, 2008.

[38] Vand, E., Hemmati, R., Oskouei, H., and Chakherlou, T. N., "An experimental method for measuring clamping force in bolted connections and effect of bolt threads lubrication on its value," *Proc. of World Academy of Science: Engineering & Technology*, Vol. 48, 2008, pp. 457-460.

[39] Hi-shear Corporation, "Product Specification hi-lok/ hi-tigue and hi-lok fastening systems hi-lok/ hi-tigue and hi-lok collars," Spec. No. 345, July, 2004.

[40] Hi-shear Corporation, 2600 Skypark Drive, Torrance, CA 90509

[41] Transducer Techniques, LLC., 42480 Rio Nedo Temecula, CA 92590.

[42] Tohnichi America Corporation, 1303 Barclay Blvd., Buffalo Grove, IL 60089.

[43] MTS Systems Corporation, 1400 Technology Drive, Eden Prairie, MN 55344.

[44] Micro-Measurements, 951 Wendell Blvd., Wendell, NC 27591

[45] Olivares, G., Raju, K. S. and Acosta, J. F., "Crashworthiness of Composite Fuselage Structures Material Dynamic Properties (Phase-I)," DOT/FAA/(AR)-XX/XX.

[46] Du Bois, P. A. "Crashworthiness engineering with LS-DYNA." *Daimler-Chrysler AG* (2000).

[47] Day, J., Bala, S., "General Guidelines for Crash Analysis in LS-DYNA", Copyright Livemore Software Technology Corporation.

[48] LS-DYNA Keyword User's Manual Volume I, Livermore Software Technology Corporation, Livermore, CA, 2014.

[49] LS-DYNA user's guide, Livermore Software Technology Corporation, accessed 06 June, 2014, at: http://www.dynasupport.com/tutorial/ls-dyna-users-guide.

[50] Yadav, V., "Finite element modeling and side impact study of a low-floor mass transit bus," Thesis, Wichita State University, 2006.

[51] Bala, S., "Deformable Spotwelds in LS-DYNA for Impact and NVH Applications", Copyright Livemore Software Technology Corporation.

[52] Nakalswamy, K. K., "Experimental and numerical analysis of structures with bolted joints subjected to impact load," UNLV Theses/Dissertations/Professional Papers/Capstones, Paper 227, 2010, http://digitalscholarship.unlv.edu/thesesdissertations/227

[53] Metallic Material Properties Development and Standardization (MMPDS-01), U.S. Dept. of Transportation, 2003.

[54] W.S. Hampshire Inc., "Teflon-Typical Properties of PTFE," 365 Keyes Ave., Hampshire, IL, 60140, 10 March, 2014, http://catalog.wshampshire.com/Asset/psg_teflon_ptfe.pdf

[55] LS-DYNA Keyword User's Manual Volume II, Livermore Software Technology Corporation, Livermore, CA, 2014.

[56] Olivares, G., Raju, K. S. and Acosta, J. F., "Round Robin Exercise For Tension Testing Of Laminated Composites at Different Strain/Stroke Rates", DOT/FAA/(AR)-XX/XX.

[57] ASTM B209 - 10, “Standard Specification for Aluminum and Aluminum-Alloy Sheet and Plate,” ASTM International, 100 Barr Harbor Drive, PO Box C700, West Conshohocken, PA 19428-2959.

APPENDICES

STANDARDS COMMITTEE FOR HI-LOK® PRODUCTS

2600 SKYPARK DRIVE, TORRANCE, CALIFORNIA 90509 U.S.A.

HI-SHEAR CORPORATION, U.S.A. ——(Patent Holder)—— CAGE No. 73197
a LISI AEROSPACE Company
AIR INDUSTRIES CO., INC., U.S.A. ——(Licensee - U.S.A & Canada)—— CAGE No. 06725
HUCK INTERNATIONAL, INC., U.S.A. ——(Licensee)—— CAGE No. 97928
SPS TECHNOLOGIES, U.S.A. ——(Licensee)—— CAGE No. 96818
FAIRCHILD Aerospace Fastener Division ——(Licensee)—— CAGE No. 99215
WEST COAST AEROSPACE INC., U.S.A. ——(Licensee)—— CAGE No. 60516
(Pins & Steel Collars)

BLANC AERO INDUSTRIES UK LIMITED ——(Licensee)—— CAGE No. 0LB66
a LISI AEROSPACE Company
HUCK S.A. Francs ——(Licensee - ECC Countries)
BLANC AERO S.A. Francs ——(Licensee - ECC Countries)
a LISI AEROSPACE Company
TOKYO SCREW COMPANY, Japan ——(Licensee - Japan)

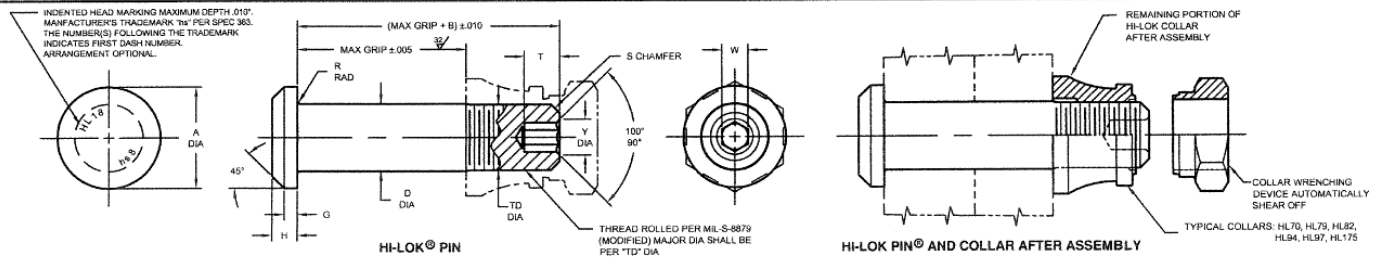

FIRST DASH NO.	PIN NOM DIA	A DIA	B REF	D DIA	TD DIA	G REF	H	R RAD	S CHAMFER REF	THREAD	SOCKET W HEX	SOCKET T DEPTH	SOCKET Y DIA	DOUBLE SHEAR POUNDS MINIMUM	TENSION POUNDS MINIMUM
5	5/32	.262 .242	.312	.1635 .1625	.1595 .1570	.020	.047 .037	.025 .015	1/32" x 45°	8-32UNJC-3A Modified	.0801 .0791	.135 .115	[6]	4,010	1,940
6	3/16	.315 .295	.325	.1895 .1885	.1840 .1810	.025	.055 .045	.025 .015	1/32" x 45°	10-32UNJF-3A Modified	.0806 .0791	.135 .115	.119 .104	5,380	2,500
8	1/4	.412 .387	.395	.2495 .2485	.2440 .2410	.030	.069 .059	.025 .015	1/32" x 45°	1/4-28UNJF-3A Modified	.0967 .0947	.150 .130	.142 .122	9,300	4,300
10	5/16	.505 .475	.500	.3120 .3110	.3060 .3020	.035	.078 .068	.030 .020	3/64" x 45°	5/16-24UNJF-3A Modified	.1295 .1270	.170 .150	.180 .160	14,600	6,300
12	3/8	.600 .565	.545	.3745 .3735	.3680 .3640	.040	.088 .078	.030 .020	3/64" x 45°	3/8-24UNJF-3A Modified	.1617 .1582	.200 .180	.217 .197	21,000	8,700
14	7/16	.676 .641	.635	.4370 .4360	.4310 .4260	.045	.105 .093	.030 .020	3/64" x 45°	7/16-20UNJF-3A Modified	.1930 .1895	.230 .210	.253 .233	28,600	12,100
16	1/2	.770 .735	.685	.4995 .4985	.4930 .4880	.050	.115 .103	.030 .020	3/64" x 45°	1/2-20UNJF-3A Modified	.2242 .2207	.260 .240	.289 .269	37,300	15,300
18	9/16	.864 .829	.770	.5615 .5605	.5550 .5500	.055	.127 .112	.040 .025	1/16" x 45°	9/16-18UNJF-3A Modified	.2555 .2520	.290 .270	.326 .306	47,200	19,000
20	5/8	.953 .918	.825	.6240 .6230	.6180 .6120	.060	.137 .122	.040 .025	1/16" x 45°	5/8-18UNJF-3A Modified	.2555 .2520	.330 .305	.326 .306	58,300	23,000
24	3/4	1.108 1.066	1.050	.7490 .7480	.7430 .7370	.070	.151 .136	.045 .030	1/16" x 45°	3/4-16UNJF-3A Modified	.3185 .3150	.395 .365	.398 .378	83,900	30,700
28	7/8	1.285 1.241	1.210	.8740 .8730	.8680 .8610	.090	.187 .172	.050 .035	5/64" x 45°	7/8-14UNJF-3A Modified	.3820 .3780	.455 .425	.471 .451	114,000	45,000
32	1	1.468 1.424	1.390	.9990 .9960	.9930 .9860	.110	.218 .203	.060 .045	5/64" x 45°	1-12UNJF-3A Modified	.5100 .5040	.580 .550	.618 .598	149,000	60,900

SEE COLLAR STANDARDS FOR COLLAR STRENGTHS. LOWER STRENGTH (PIN OR COLLAR) DETERMINES SYSTEM STRENGTH.

GENERAL NOTES:
1. Concentricity: "A" to "D" diameter within .010 FIM.
2. Dimensions to be met after finish.
3. Surface texture per ANSI B46.1.
4. Hole preparation per NAS618.
5. Non-lubed pins must be used with sealant or lubed collars.
6. Evidence of broken edge across points.
7. Use HL62 for oversize replacement.

MATERIAL: Alloy steel per AMS6415, AMS6349 or AMS-S-6049.

HEAT TREAT: 95,000 psi shear (160,000 - 180,000 psi tensile per AMS-H-6875).

(25) FINISH:
- HL18-( )-( ) = Cadmium plate per AMS-QQ-P-416, Type I, Class 2, and cetyl alcohol lube per Hi-Shear Spec. 305.
- HL18PB( )-( ) = Cadmium plate per AMS-QQ-P-416, Type II, Class 2, and cetyl alcohol lube per Hi-Shear Spec. 305.
- HL18TF( )-( ) = Cadmium plate per AMS-QQ-P-416, Type III, Class 2, and Hi-Kote 2 solid film lube per Hi-Shear Spec. 292.
- [5] HL18PN( )-( ) = Cadmium plate per AMS-QQ-P-416, Type II, Class 2.

SPECIFICATION: Hi-Lok Product Specification 342.

CODE: First dash number indicates nominal diameter in 1/32nds
Second dash number indicates maximum grip in 1/16ths.
See Finish note for explanation of code letters.

HOW TO ORDER EXAMPLE:

Pin Part Number Only (25)
HL18PB8-8
- 8/16 or 1/2 Maximum Grip Length
- 8/32 or 1/4 Nominal Diameter Pin
- Type II Cadmium Plate
- Pin Basic Part Number

Pin and Collar Assembly Part Number Combination
HL18PB70-8-8
- Size and Grip Length, See Above Example
- Collar Part Number
- Pin Finish
- Pin Basic Part Number

"Hi-Lok" and "HL" are internationally registered trademark of Hi-Shear Corporation.

DRAWN	DATE	TITLE
J.C.S.	7-19-82	**HI-LOK© PIN** PROTRUDING SHEAR HEAD ALLOY STEEL 1/16 GRIP VARIATION
APPROVED	DATE	
Cessna	7-24-62	
REVISION (25)	DATE J.F.O. 10-17-02	DRAWING NUMBER **HL18**

JFO-STD/HLPIN

© 2002 Hi-Shear Corporation

STANDARDS COMMITTEE FOR HI-LOK® PRODUCTS

2600 SKYPARK DRIVE, TORRANCE, CALIFORNIA 90509 U.S.A.

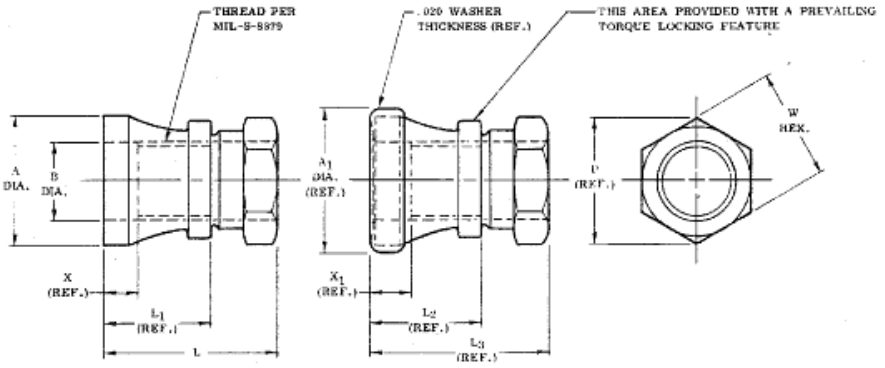

DASH NO.	PIN NOM. DIA.	THREAD	A DIA.	A_1 DIA (REF)	B DIA.	L LENGTH	L_1 (REF)	L_2 (REF)	L_3 (REF)	P (REF.)	W HEX.	X (REF.)	X_1 (REF)	UTS POUNDS MIN.	TORQUE OFF IN. LBS.
5	5/32	5-32UNJC-3B	.292 .288	.337	.173 .166	.447 .427	.270	.300	.467	.344	.314 .302	.107	.137	1,400	15-25
6	3/16	10-32UNJF-3B	.307 .303	.360	.200 .192	.457 .437	.280	.310	.477	.344	.314 .302	.107	.137	1,600	25-35
8	1/4	1/4-28UNJF-3B	.412 .408	.462	.261 .252	.552 .532	.340	.370	.572	.380	.346 .332	.112	.142	3,000	60-80
10	5/16	5/16-24UNJF-3B	.518 .512	.575	.325 .314	.672 .652	.430	.460	.692	.484	.440 .425	.122	.152	5,000	130-160
12	3/8	3/8-24UNJF-3B	.628 .622	.690	.388 .376	.744 .724	.470	.500	.764	.557	.503 .488	.122	.152	7,000	200-240
14	7/16	7/16-20UNJF-3B	.713 .707	.770	.450 .442	.662 .642	.560	.590	.882	.624	.565 .550	.137	.167	9,500	270-330
16	1/2	1/2-20UNJF-3B	.815 .809	.872	.513 .501	.942 .922	.610	.640	.962	.763	.690 .675	.137	.167	12,500	370-430
18	9/16	9/16-18UNJF-3B	NOTE: USE HL79-18												
20	5/8	5/8-18UNJF-3B	NOTE: USE HL79-20												
24	3/4	3/4-16UNJF-3B	NOTE: USE HL79-24												
28	7/8	7/8-14UNJF-3B	NOTE: USE HL79-28												
32	1	1-12UNJF-3B	NOTE: USE HL79-32												

NOTES:
1. Go thread penetration shall be 3/4 of one revolution minimum.
2. Dimensions apply after finish.
3. Use HL79 for oversize replacement.

MATERIAL: Collar - 2024 aluminum alloy per QQ-A-430 or QQ-A-225/6.
Washer - "NW" = 300 series stainless steel.
"TW" = 5052 aluminum alloy per QQ-A-250/8, or 2024 aluminum alloy per QQ-A-250/4 OR QQ-A-250/5.

HEAT TREAT: Collar - Age to T6 condition per MIL-H-6088.
Washer - "NW" = None.
"TW" = Age to T6 condition per MIL-H-6088 (for 2024 only).

FINISH: Collar -
HL70-( ) = Anodize per MIL-A-8625, dye color red, and cetyl alcohol lube per Hi-Shear Spec. 305.
HL70CM-( ) = Chemical conversion coat per MIL-C-5541, Class 1A, and cetyl alcohol lube per Hi-Shear Spec. 305.
HL70D-( ) = Anodize per MIL-A-8625 and solid film lube per MIL-L-46010, Type I.
HL70K-( ) = Anodize per MIL-A-8625 and solid film lube per "Lubeco" 905.
(31) HL70TF-( ) = Anodize per MIL-A-8625 and Hi-Kote 2 solid film lube per Hi-Shear Spec. 292.
HL70TT-( ) = Anodize per MIL-A-8625, dye color red and translube.
Collar & Washer -
HL70DTW-( ) = Collar finish is the same as HL70D-( ). Washer finish is anodize per MIL-A-8625, dye color grey, or blue (for 2024 only).
HL70NW-( ) = Collar finish is the same as HL70-( ). Washer is passivated.
HL70TW-( ) = Collar finish same as HL70-( ). Washer finish is anodize per MIL-A-8625, dye color grey, or blue (for 2024 only).

SPECIFICATION: Hi-Lok Product Specification 345.

CODE: Dash number indicates nominal thread size in 1/32nds.
See Finish note for explanation of code letters.

EXAMPLE: HL70-8 = 1/4-28 Hi-Lok collar only.
HL70TW-8 = 1/4-28 Hi-Lok collar with aluminum washer.

U.S. patents 3,390,906; and foreign patents.
"Hi-Lok" and "HL" are Registered Trademarks of Hi-Shear Corporation.

	DATE	BY
DRAWN	7-27-60	VAN
APPROVED	7-27-60	MEC
(31) REVISION	11-28-95	J.F.Obispo

TITLE
HI-LOK® COLLAR
2024 - T6 ALUMINUM ALLOY
1/16" GRIP VARIATION - SHEAR APPLICATION

DRAWING NUMBER
HL70

©1994 Hi-Shear Corporation

APPENDIX B

PRELOAD APPLICATION IN A SOLID BOLT

Six different bolt preload techniques available in LS DYNA have been discussed and compared by Kumarswamy in a dissertation. To get a deeper understanding on how the different preload methods affect the results of the simulations in this study, four methods were selected from the six and have been compared below.

a) Initial Stress Section

This method uses the *INITIAL_STRESS_SECTION card available in LS DYNA to for preloading a bolt. A cross-section plane is created at the center of the shank and a stress is defined, which is applied through the section to preload the bolt. An optional analysis that takes place before regular transient analysis, known as dynamic relaxation (DR), is used to preload the bolt. The preload stresses applied in this phase are typically elastic and the deformations are small. In explicit DR, the nodal velocities are reduced by a DR factor for each timestep, thus the solution undergoes a form of damping. DR phase ends when the distortional kinetic energy is sufficiently reduced, that is the convergence factor has become sufficiently small. Once the DR phase terminates, the analysis automatically proceeds to the next phase. The load is required to be ramped and then held constant for the DR phase. This is done to ensure that the model converges after full application of the preload. DR phase is typically invoked by setting the parameter SIDR in the load curve to 1 or 2.

The main advantage of using this method for applying a preload is that it is very easy to set up, and the targeted preload is accurately achieved. A disadvantage to this method is that the row of elements, through which the cross-section plane passes, show very high compressive

strains and therefore the strain distribution in the bolt shank cannot be obtained. The rest of the elements around it show the expected strain values.

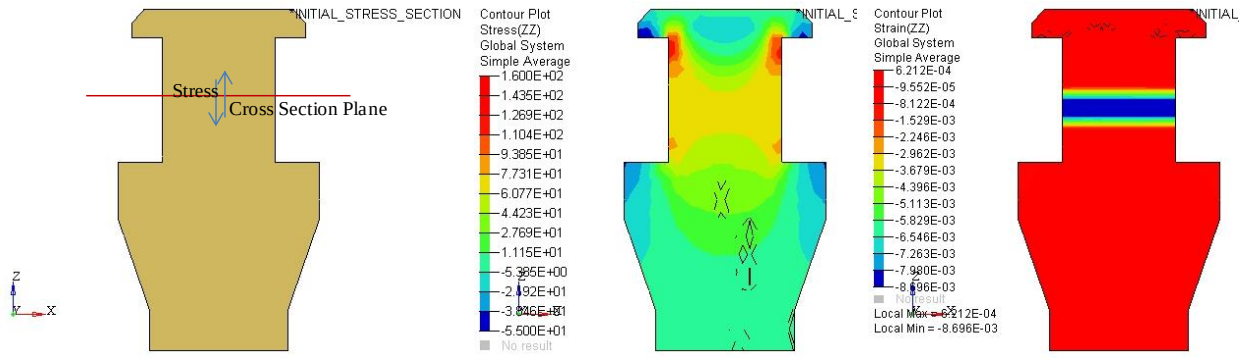

b) Initial Stress Solid

All the solid elements in the bolt shank are selected and an initial stress is applied to the selected elements. The initial stresses are applied first and the stress application is terminated when a new card is read. DR phase is run to damp out the resulting kinetic energies.

The advantage of this method is that it is very easy to apply to the model. Some of the disadvantages are as follows:

i) A higher stress needs to be applied to achieve the desired stress value in the bolt. This is because the stress is transmitted to other parts after initial application. A trial and error method needs to be used to get the correct initial stress to apply.

ii) An initial strain cannot be applied with initial stress therefore the strains observed in the model need to be offset by the value of initial strains.

iii) The stresses in the shank drop to almost half the targeted value as you move towards the center of the shank. As a result, the force through the shank is less than the desired preload force.

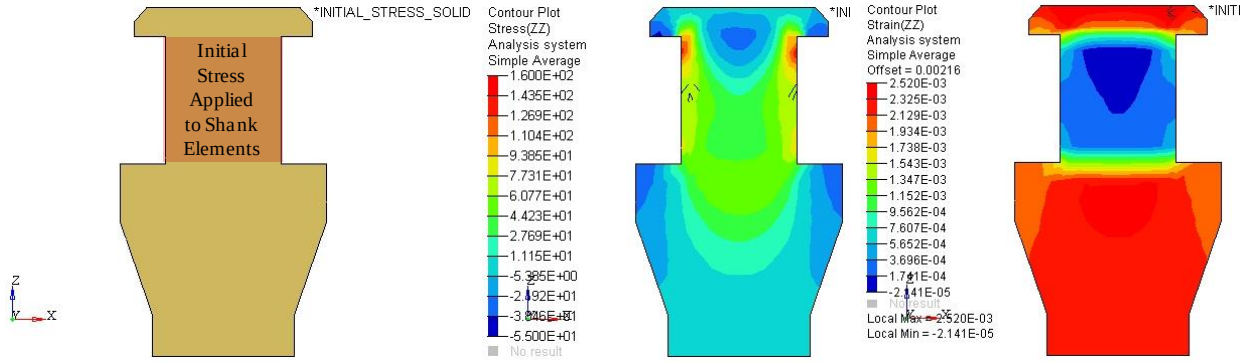

c) Force at the Shank Center

For this method of preloading, the bolt shank was split at the center and the nodes were separated with a small gap. Equal and opposite forces were applied to the two faces of the shank using implicit analysis. *CONTACT_TIED_SURFACE_TO_SURFACE was used to tie the split surfaces once the desired force is reached and the system is in equilibrium. Tying the surfaces would enable to maintain the preload.

A problem with this method of preloading or LS DYNA is that the split surfaces do not join completely, thus leaving a discontinuity in the bolt shank. Also, the gap required between the split surfaces needs to be changed based on the preload applied. Higher preload values will require a bigger gap thus requiring more manual work from the user.

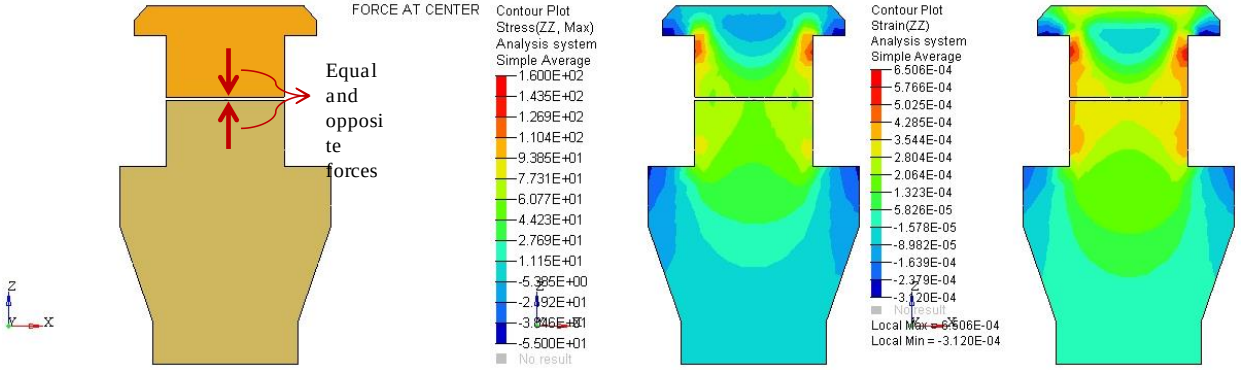

d) Force on Bolt and Nut

This method of preloading requires the bolt and nut to be separate parts. A load is applied on the bolt pulling it down and an equal load is applied on the nut pulling it up. This is done in the implicit phase of the analysis. Once equilibrium is reached, the nut is tied to the bolt at that position and hence the preload is maintained.

One of the issues with this method of preloading is that it requires many contact definitions for accurate modeling and thus will cost more.

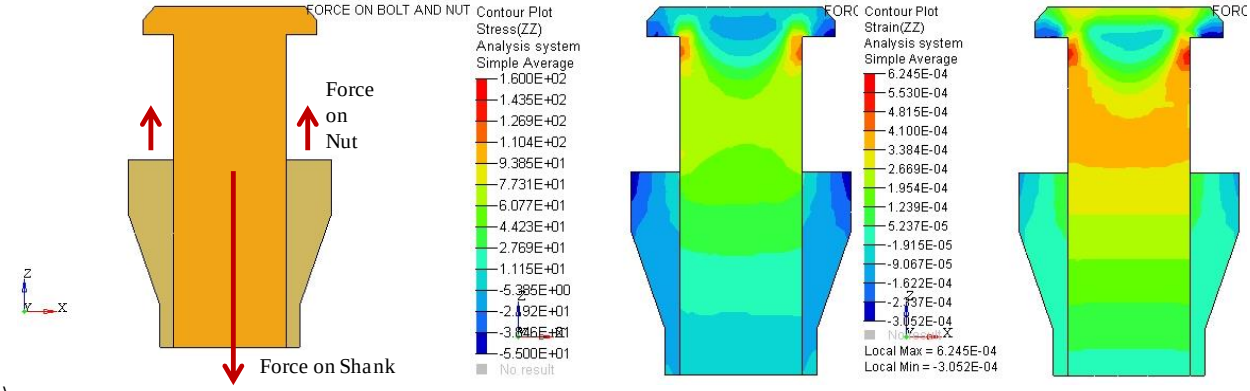

\

Comparison of Preload Methods

For all these methods, the bolt model was preloaded to 68.95 MPa, the load applied was 1in/s and a friction coefficient of 0.6 was maintained. After applying the preload, the simulation was run for 0.003 sec to monitor the preload. After that, the normal tension loading was introduced.

a) Target Preload (Stress)

In order to compare the four methods discussed above, the stresses after preload application, that is the Z-Stress, have been compared. The figure below shows the stresses on elements at different locations on the preloaded bolt. The same elements have been chosen on all the bolts for comparison. The stresses below have not been averaged compared to the stresses presented in the images above. The target stress for the preload was 68.95 MPa. Based on the

figure, it can be noted that the Initial Stress Section and the Force on Bolt and Nut method shows the least variation compared to the target stress. Initial Stress Solid method shows good correlation around the edge of the bolt, but at the center the value of the prestress is almost half the targeted value. The Force at center method shows varying measurements at all the three elements with large variations compared to the targeted values.

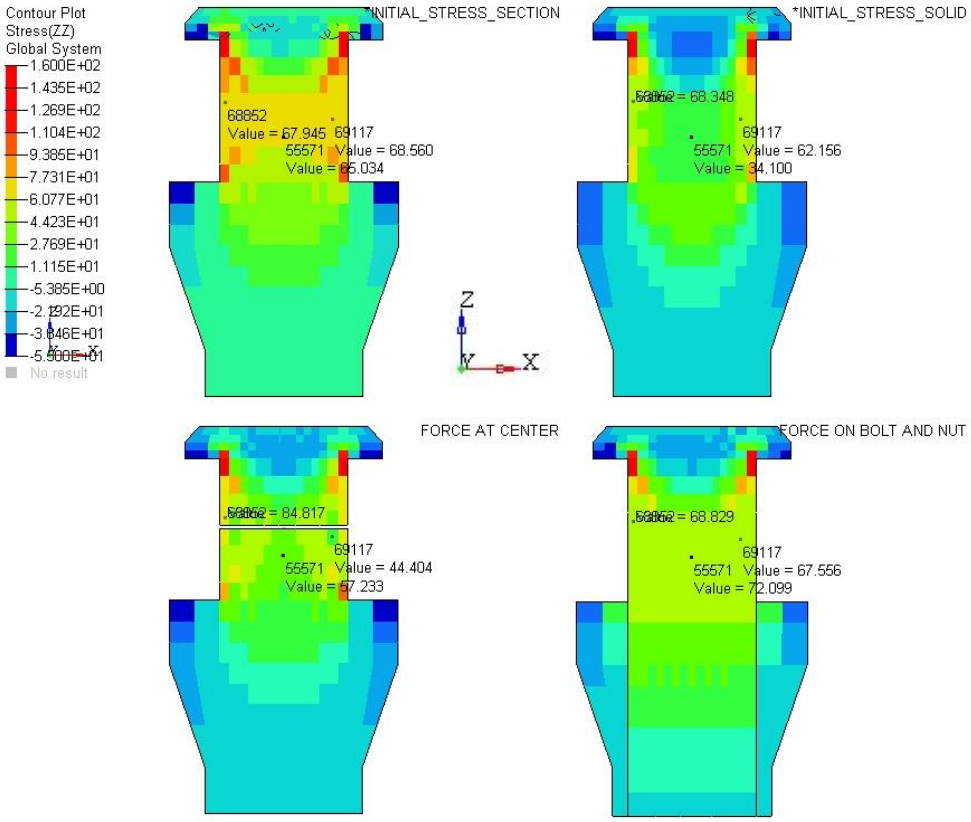

Based on the stress plots in the figure below, it can be noted that similar stress values are observed with the Initial Stress Section method and Force on Bolt and Nut method. Both these methods also correlate well with the expected stress of 68.95 MPa. The other two methods undershoot the stress values.

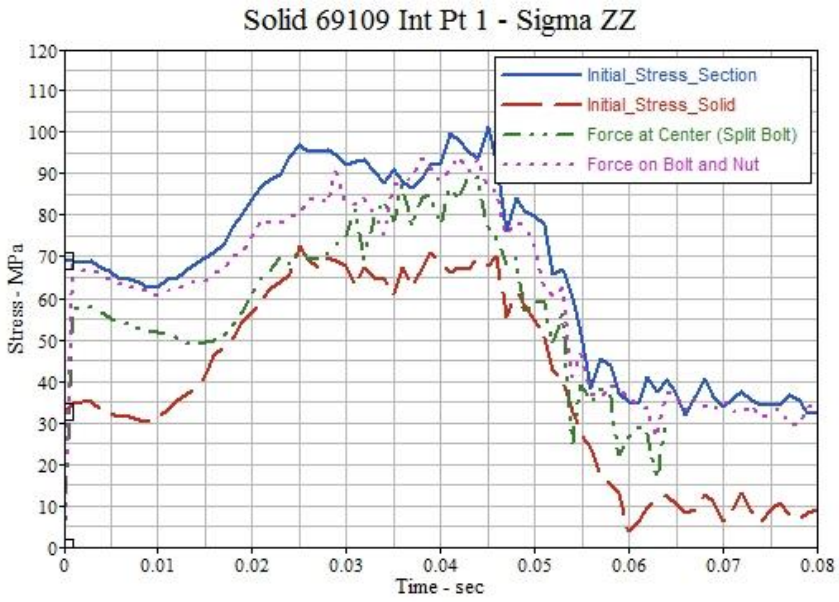

b) Strains

The material used for the bolt is Steel with a youngs modulus of 199948 MPa. *MAT_ELASTIC is used to define the material in LS DYNA, thus the part only exhibits elastic behavior. Based on this, to verify the preload, the expected strain value is strain = Stress/E, that is strain = 68.95/199948, therefore strain = 3.448e-4. This is the expected Z strain. The figure below compares the Z strains for the four methods of preload. As mentioned previously, for Initial Stress Section method, the strains on the elements corresponding to the cross section plane do not reflect the correct strains. This is a limitation in LS DYNA. The Initial Stress Solid method requires a strain offset because an initial stress is applied to the elements, but not an initial strain. Applying both the Initial Stress and Initial Strain on the same elements does not work with LS DYNA. The two methods, where force is applied at the center and on bolt and nut, show good correlation when compared to the expected strain values.

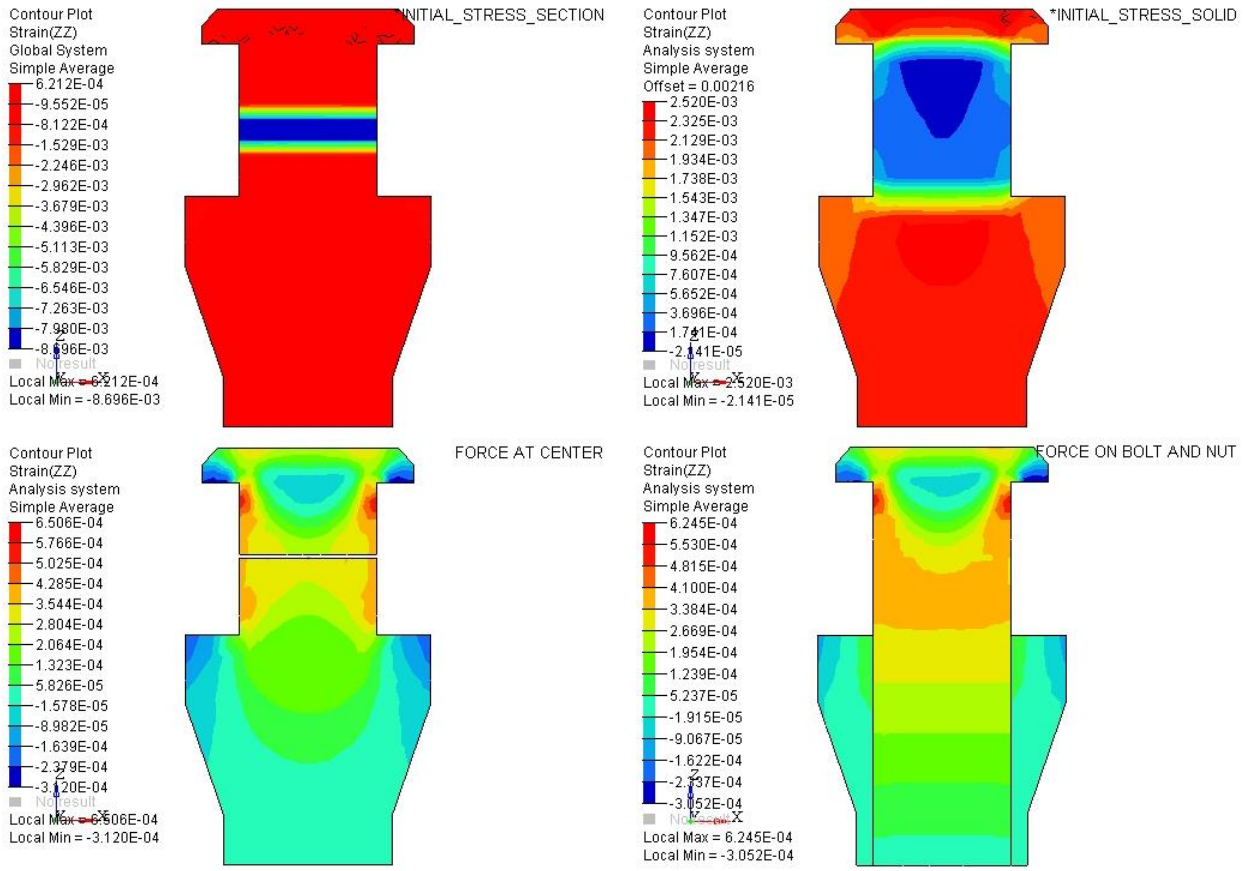

The strain plots for the four different methods are presented in the figure below. Two elements were chosen, 69109 and 69108. Element 69109 shows the compressive strains due to the Initial Stress Section method. This is because that element corresponds to the cross section plane. Thus with that method we get wrong strains for the elements corresponding to the cross section plane. On the other hand, element 69108 shows good results, and this element is the next element above 69109 as shown in the figure.

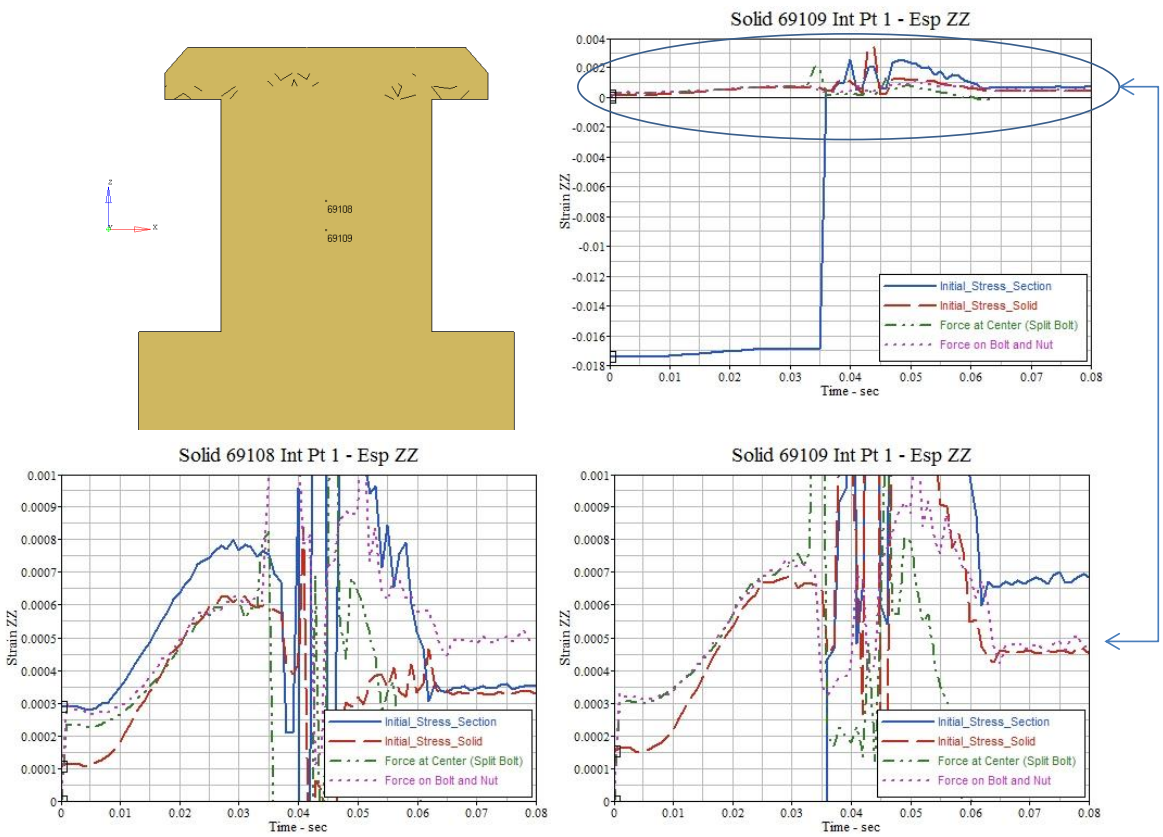

c) Force Comparison

Based on the applied stress of 68.95 MPa, the preload force on the bolt should be 924N. The figure below compares the forces between the four methods from the preload point to 0.003 sec. The preload was applied, and the simulation was run without any other external loads for 0.003 seconds, after which the external loads were applied. All the methods except Initial Stress Solid method show good correlation to the expected force values. This could be attributed to the fact that, in this method, the stresses decrease drastically as you move to the center of the shank. The X force on the bolt, that is the shear force on the bolt, is also compared below. All the four methods show slightly different forces, through the bolt, in shear.

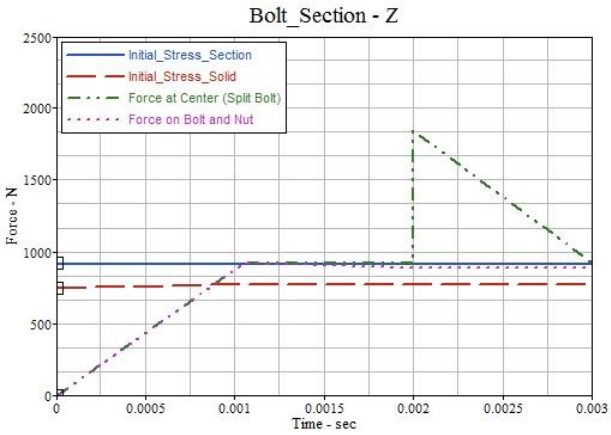

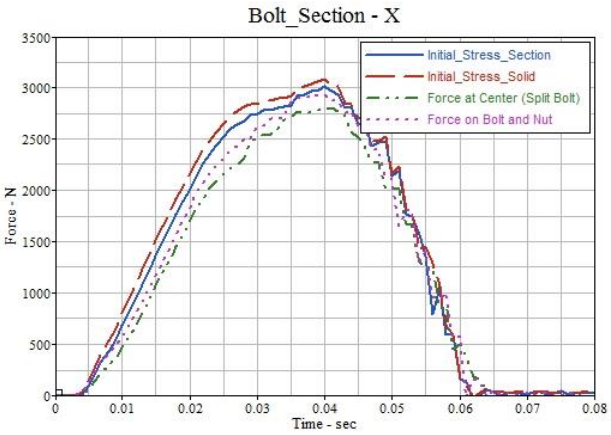

Forces recorded by the cross section planes on the main part and the load transfer part are shown below. Based on the forces below, the same amount of load is recorded in the load transfer part for Initial Stress Section and the Initial Stress Solid method. The load recorded in the load transfer part in the Force on Bolt and Nut method also compares well with these two methods. The Force at Center method shows a low force being transferred compared to the other methods. The same is observed on the forces recorded in the main part.

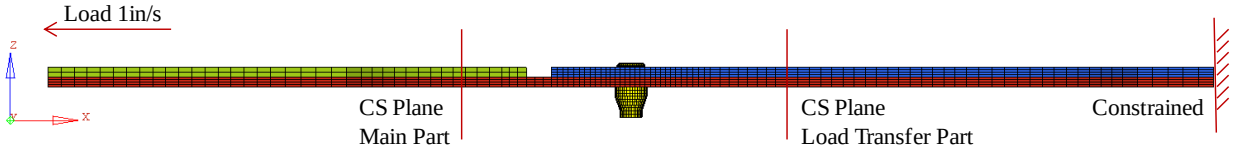

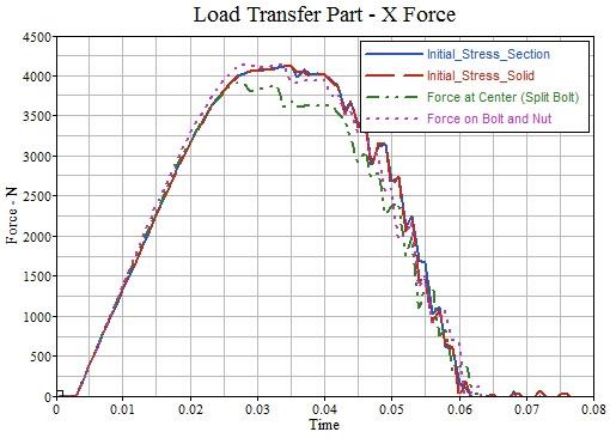

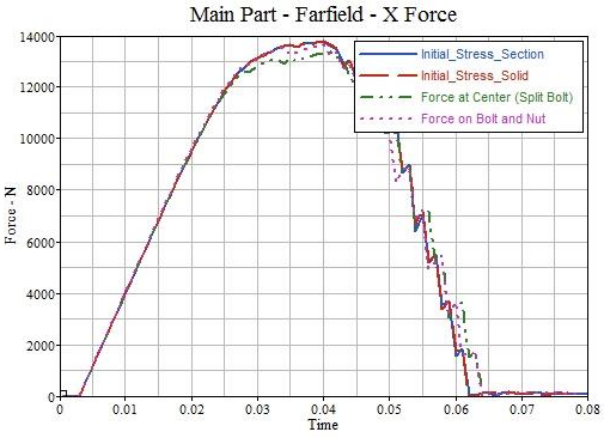

d) Conclusion

Based on the four methods discussed the following conclusions are drawn:

i) The Initial Stress Section method is the easiest to set up and produces consistent stress and force values. The disadvantage for this method is that the presentation of strains is not consistent.

ii) The Force on Bolt and Nut method provides the best overall results for stress, force, and strains. It also results in good load transfer forces when compared to other methods.

iii) The Initial Stress Solid method requires trial and error method to identify the right amount of initial stress that needs to be applied to obtain the desired preload. Once the bolt is preloaded, the stress distribution within the bolt has high variations. The force in the bolt is a lot less than desired.

iv) The Force at center method also shows high variation in stresses within the bolt section. This method provides good force correlation. This method is also tedious as it requires a change in gap every time the preload is changed. Also, it has a disadvantage that the gap cannot be closed and there will be a discontinuity in the bolt. The load transferred to the load transfer part is also less than other methods.

APPENDIX C

ENERGY FOR HIGH RATE STUDY

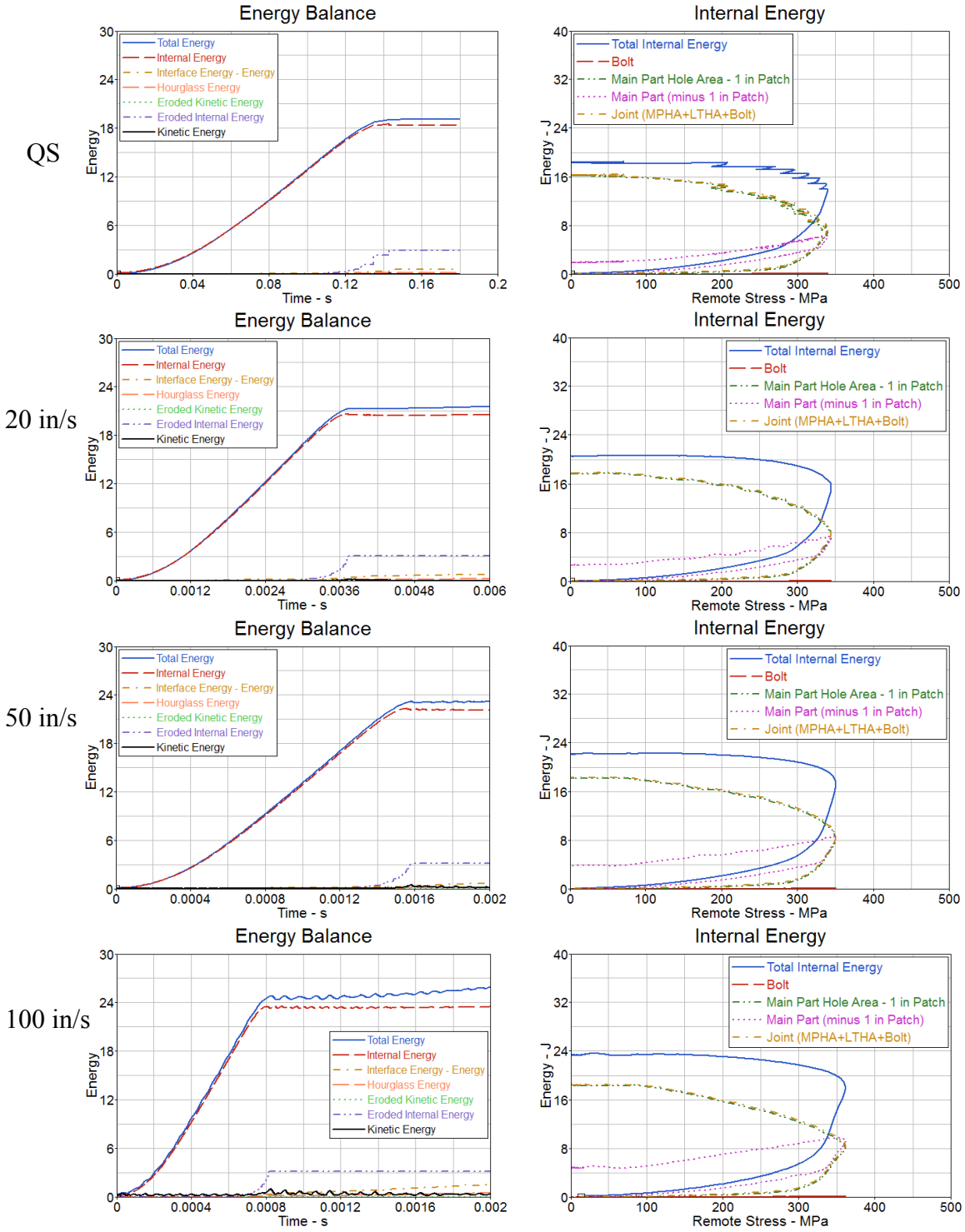

Figure C-1. Comparison of Energy for Detailed FE Model for Different Loading Rates

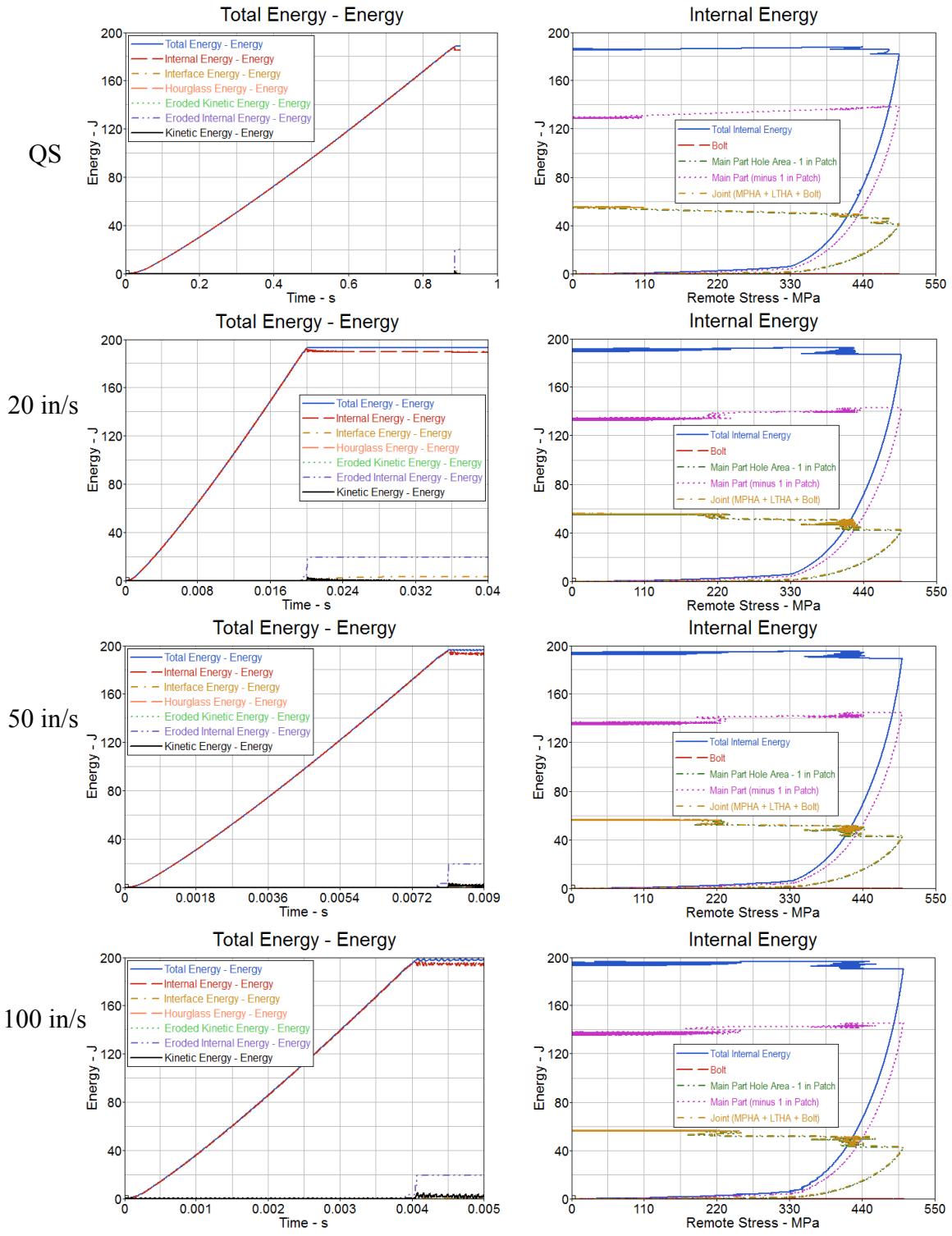

Figure C-2. Comparison of Energy for Simplified FE Model for Different Loading Rates